MULTISCALE MECHANICAL, STRUCTURAL, AND COMPOSITIONAL RESPONSE OF TENDON TO STATIC AND DYNAMIC LOADING DURING HEALING

Benjamin Ross Freedman

A DISSERTATION

in

Bioengineering

Presented to the Faculties of the University of Pennsylvania

in

Partial Fulfillment of the Requirements for the

Degree of Doctor of Philosophy

2017

Supervisor of Dissertation	Graduate Group Chairperson
_____	_____
Louis J. Soslowsky, Ph.D.	Jason A. Burdick, Ph.D.
Fairhill Professor, Orthopaedic Surgery	*Professor, Bioengineering*

Dissertation Committee
Robert L. Mauck, Ph.D. (Committee Chair)
Mary Black Ralston Professor, Orthopaedic Surgery, Bioengineering, University of Pennsylvania
Vivek B. Shenoy, Ph.D.
Professor, Materials Science, Mechanical Engineering and Applied Mechanics, Bioengineering, University of Pennsylvania
Rebecca Wells, M.D.
Associate Professor, Medicine, University of Pennsylvania
Lin Han, Ph.D.
Assistant Professor, Biomedical Engineering, Drexel University

MULTISCALE MECHANICAL, STRUCTURAL, AND COMPOSITIONAL

RESPONSE OF TENDON TO STATIC AND DYNAMIC LOADING

DURING HEALING

DEDICATION

I would like to dedicate my dissertation to my parents, Sheryl and Curt Freedman, whom I would not be here without. They always encouraged me to pursue my dreams and I feel very lucky to have been their son. I always looked up to my dad growing up, as he was an extremely positive role model for me. My mom has been and always will be the wind beneath my wings. Growing up, my mom was a constant source of love and support, and was my number one fan. Her positive persona, funny personality, creativity, and warmth are things I will always remember. My mom taught me many things—most importantly—to not take life too seriously, to be happy with what you have, and to never give up. She often quoted the poem, "*It Couldn't Be Done*," which she would recite endlessly whenever we felt weary. The past six years have had their highs and lows since her diagnosis and passing, and at times have seemed like the challenge of a PhD just *couldn't be done*. But I'm reminded that when things get tough,

…You just buckle right in with the trace of grin,

Just take off your coat and go to it.

Just start to sing, as you tackle the thing, that couldn't be done,

And you'll do it.

ACKNOWLEDGMENT

Words cannot describe how grateful I am for everyone that has supported me throughout my life—before graduate school, during my PhD, and in my next steps ahead as a postdoctoral fellow. Earning an undergraduate degree in Biomedical Engineering is not an easy one, let alone a graduate degree, and I'm so thankful for the incredible individuals I have been able to lean on along the way for guidance, support, and friendship.

I have been so fortunate to have landed in Dr. Lou Soslowsky's laboratory. Lou has been an absolutely stellar mentor, and has given me an extreme sense of freedom and ability to ask interesting and important research questions. Lou has afforded me so many opportunities to work on a diverse set of projects, mentor and train students, and pursue opportunities within Penn that have made my graduate experience extremely rich and fulfilling. I also wish to thank my thesis committee for all of their work in refining my dissertation and providing key feedback. I am extremely grateful for Dr. Rob Mauck for all of his keen insight and wisdom into my project and his help in developing and focusing my initial ideas. I am also grateful for the opportunity to work closely with Dr. Vivek Shenoy, Dr. Becky Wells, and Dr. Lin Han.

My project would not be possible without the support and enthusiasm of many amazing scientists in our lab. In particular, I am most appreciative for the great contributions Ashley Rodriguez, Stephanie Weiss, Dr. Cody Hillin, Ryan Leiphart, and Joseph Newton, have made for this project. I am also thankful for the help of Biao Han for teaching me AFM, Dr. Ehsan Ban for helping me with FE modeling, and Carrie Barnum for help with biological assays.

I will always remember the wonderful environment of the McKay Orthopaedic Labs. There are so many individuals that have made long-lasting impacts on my career and life. Dr. J Sarver was one of my first mentors in the lab and has been someone who has given me substantial guidance and sparked my creativity and passion in tendon biomechanics! I have also been fortunate to work with so many great graduate students and postdocs, and am so glad to have gotten to be friends and colleagues with Dr. Mark Buckley, Dr. Stephen Thomas, Dr. Katie Reuther, Dr. Sarah Rooney, Dr. Bri Connizzo, (almost Dr.) Cori Riggin, Dr. Julianne Potocek, Dr. Joshua Gordon, Dr. Snehal Shetye, Dr. Michael Hast, Jennica Tucker, Adam Pardes, and Zakary Beach. The group has been extremely fun to work with both in and out of lab. I am also appreciative for my friends and colleagues in the Mauck Lab who have supported me throughout this process, especially discussions with Brian Cosgrove and Dr. Spence Sczcesny. Finally, a big thank you (and hug) to Susan Dinella and Donna Seravello for everything that they have done for me and for making our McKay Lab a family.

I am also thankful for the opportunities I was afforded outside of lab. I'm thankful to the Graduate Association of Bioengineering (GABE) and our chapter of the BMES for allowing me to be part of their e-board for four years. I am grateful for the support of Dr. Jason Burdick and Dr. David Meaney to help develop many new activities for our Bioengineering Department, and the tremendous help of Jen Gillard along the way. I particularly enjoyed opportunities to collaborate with iPraxis and expand our outreach efforts with them. I am also thankful to Dr. Tomas Isakowitz for allowing me to participate in the Penn Center for Innovation Fellow's Program. Finally, I am thankful to the University of Puerto Rico Mayagüez for allowing me to be a visiting junior scientist.

I would like to thank so many of my past mentors that have taken their time to help and guide me. During my high school years at Longmeadow High, I was lucky to have an immensely dedicated pre-calculus teacher, Mrs. Susan Peters, who spent extra time tutoring me and shared so many creative teaching strategies that fostered my interests in teaching. During my undergraduate years at the University of Rochester, Dr. Amy Lerner played an instrumental role in my career development and start in the field of biomechanics. Dr. Frances Sheehan at the National Institutes of Health has been truly an amazing advocate and research mentor for me, an opportunity made possible by Dr. Bob Lutz through the BESIP program. My undergraduate advisor, Dr. Scott Seidman, played a large role in encouraging me to think big about what I wanted to do with my career, and I am thankful for his frequent attention to my questions.

My family has always been a central source of love and support. Growing up, my parents, Sheryl and Curt Freedman, were amazing role models and strived to nurture my interests in science and provide me many opportunities in engineering at a young age. I am also thankful for my brother, Alex, who has always been my there for me. I am grateful to have gotten so close with my grandparents, Ruth and Herb Freedman, and Ellie and Joel Glaser, and for their everlasting love and kindness in supporting me in my career paths. The past six years have not been easy ones, and I so appreciative to have had my amazing Aunt Brenda, Uncle Todd, and cousins nearby in Merion. They have continuously opened their doors for me—treating me like their own son. Finally, I am extremely thankful to my girlfriend, Jessica Liu, for all of her amazing support, enormous patience, and perseverance in pushing me to try and see new things.

ABSTRACT

MULTISCALE MECHANICAL, STRUCTURAL, AND COMPOSITIONAL RESPONSE OF TENDON TO STATIC AND DYNAMIC LOADING DURING HEALING

Benjamin Ross Freedman

Dr. Louis J. Soslowsky

The extracellular matrix (ECM) is a major component of the biomechanical environment with which tendon cells (tenocytes) interact. Alterations to matrix structural and mechanical properties due to mechanical loading may promote normal tendon homeostasis or create pathological conditions. For example, fatigue loading of tendon elevates collagen fiber waviness (crimp), which correlates linearly with tissue laxity. The tendon ECM may also be altered following tendon injury. Aberrant tissue phenotypes caused by tendon ruptures are exemplified not only at transcript and protein levels, but also can extend to include disorganized collagen structure, inferior mechanical properties, and reduced *in vivo* limb function in animals. This dissertation explores the interface between dynamic loading and tendon healing across multiple length scales using living tendon explants. This work begins to define the implications of macroscale mechanical loading on collagen structure and tenocyte response in uninjured and healing tendon, and provides a foundation for the development of new strategies to improve tendon healing. Ultimately, this work helps our understanding of tendon's multiscale response to loading, provides a framework for the micromechanical environment that tenocytes interact in

response to dynamic loading and healing, and lays important groundwork for benchmarks for tendon tissue engineering. The multiscale response to mechanical loading, which is a hallmark of clinical rehabilitation protocols, is necessary to determine the ramifications of various macroscale loading protocols. Additionally, these results provide benchmarks for the environments in which tendon cells may experience following cell delivery therapies. Several exciting future avenues of research are possible that would highly impact basic science research of tendon function and lead to potentially translatable approaches that could improve tendon injury onset and healing response. In conclusion, this dissertation provides a strong foundation on which future experimental and computational studies can build to fully elucidate the multiscale mechanisms that govern strain transfer in tendon.

TABLE OF CONTENTS

LIST OF TABLES

Chapter 2

Chapter 5

Chapter 6

LIST OF ILLUSTRATIONS

Chapter 1

Chapter 2

Chapter 3

Chapter 4

Chapter 5

CHAPTER I: INTRODUCTION

1.1 Introduction

Tendons function to transfer stresses and strains from muscle to bone during loading, resulting in multiscale changes to its extracellular matrix (ECM). The extracellular matrix (ECM) is a major component of the biomechanical environment with which tendon cells (tenocytes) interact. Alterations to matrix structural and mechanical properties due to mechanical loading may promote normal tendon homeostasis or create pathological conditions. For example, fatigue loading of tendon elevates collagen fiber waviness (crimp), which correlates linearly with tissue laxity (change in slack length). The tendon ECM may also be altered following tendon injury. Aberrant tissue phenotypes caused by tendon ruptures are exemplified not only at transcript and protein levels, but also can extend to include disorganized collagen structure, inferior mechanical properties, and reduced *in vivo* limb function in animals. This work explores the interface between dynamic loading and tendon healing across multiple length scales using living tendon explants. Overall, this work helps to define the implications of macroscale mechanical loading on collagen structure and tenocyte response in uninjured and healing tendon, and provides a foundation for the development of new strategies to improve tendon healing.

1.2 Background

1.2.1 Multiscale Tendon Mechanics and Structure

Multiscale strain transfer is the relationship of strain between structural hierarchies of materials. Tendons allow for multiscale strain transfer due to their fiber-reinforced structure.[1,2] For example, tendons strain stiffen during *quasi-static* mechanical

loading, as disorganized ECM at the fascicle, fiber, and fibril levels becomes more aligned and less wavy (i.e., crimped) (**Figure 1-1A**).[3-6] Multiscale strain transfer ultimately affects cell microenvironments and therefore proliferation, differentiation, and matrix production.[7] Alterations to cell microenvironments due to mechanical loading may provide a mechanism leading to normal tendon homeostasis[8-13] or pathology.[14-21] Previous studies have found that tissue and cellular level strains correlate in normal uninjured tissues during *quasi-static* tensile loading in a variety of fiber-reinforced tissues including tendons, menisci, and electrospun scaffolds.[22] However, such studies have not investigated the clinically important effects of dynamic loading and tendon healing, which likely alter tendon multiscale mechanical, structural, and spatial distributions of compositional proteins that affect how cells respond to their substrate, ECM loading, and transfer stress over long distances.

Multiscale relationships during dynamic loading at *high loads* are important for elucidating potential mechanical mechanisms governing *fatigue-induced* damage and injury. When tendons are subjected to high dynamic loading, fatigue damage accumulation occurs[23] in concert with alterations in crimp properties.[24] With fatigue loading, tendon stiffness increases initially, reaches a maximum, and then gradually decreases, and is coupled by a monotonic increase in peak cyclic strain (**Figure 1-1B**). This gradual decrease in stiffness is attributed to accumulated sub-rupture damage, which ultimately leads to the dramatic increase in peak deformation and decrease in stiffness prior to failure.[25-27] Repeated subrupture loading results in collagen fibril kinking,[28] which can affect cell morphology and matrix degradation.[29] As these studies were completed *ex vivo* with tissue tendon explants, they provides a controlled method for

evaluating the specific response of tendon to load, thus removing confounding variables present in whole tissue model systems. Many of the same mechanical and biological mechanisms also occur *in vivo*, demonstrating the validity of these *ex vivo* models.

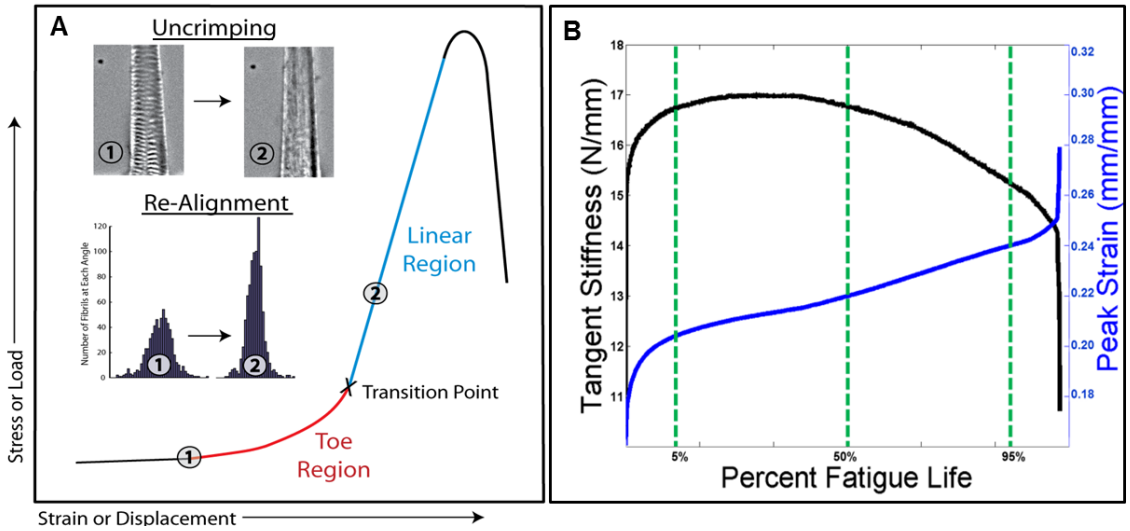

Figure 1-1: Structure-function relationships in tendon during quasi-static and dynamic fatigue loading. (**A**) During quasi-static tensile loading, a distinct nonlinearity or "toe" region exists that is attributed to collagen fiber uncrimping and re-alignment. (**B**) During fatigue testing, tendons follow a three-phase pattern of fatigue damage in both tangent stiffness and peak strain. Panels A and B were reproduced with permission from Connizzo, et al., 2013, and Freedman et al., 2013, respectively.

Multiscale tendon mechanics and structure can be evaluated using several methods. Whole tendon mechanical properties are commonly determined from force and displacement readings acquired with commercially available tensile testing systems. By placing fiduciary markers on tissues to serve as optical extensometers, images can be captured with external cameras to provide local assessment of tissue strain and stiffness. Structural assessment during mechanical loading can be achieved with the integration of a plane polariscope. Briefly, this device consists of two polarizing sheets on opposite sides of the tendon. Recently, crimp was visualized with polarized light imaging during dynamic loading.[30] This innovative approach allows whole tissue, region specific, and

load dependent crimp properties, to be inferred simultaneously during a mechanical test without destructively altering the tendon. If the polarizers are rotated, measures of collagen fiber orientation can be derived.[31] Whole tissue can also be mounted under a confocal microscope. Similar to fiduciary marker tracking of strain, microscale strains can be assessed through strain field mapping of cells embedded within the collagen matrix. If tendons are subject to sectioning, additional measures of multiscale mechanics and structure can be determined. First, micro/nanoscale mechanics is achieved through nanoindentation experiments using Atomic Force Microscopy (AFM).[32] In this method, a cantilever with a nano/micro-sized tip is placed on the surface of a tissue to derive local mechanical measurements. Structurally, AFM can be used to assess nanoscale collagen structural properties, such as fibril sliding.[33] Multiphoton imaging can also be used to study collagen structure through second harmonic generation. Additional nanometer resolution imaging techniques including scanning electron microscopy (SEM) and transmission electron microscopy (TEM), which are useful for looking at collagen fibrils in both the longitudinal and transverse axes to evaluate the presence of fibril ends and fibril diameters.[34,35]

1.2.2 Tendon Healing

Following injury, tendons are mechanically, structurally, and biologically altered.[36] Initially, the gross appearance of the tendon changes, becoming larger in cross section,[45, 46, 55] and translucent.[37] In addition, a high density of inflammatory cells within the repair site are present,[36,38] expression of scleraxis (a tenocyte marker) is substantially diminished, and apoptosis is evident.[39] Throughout early to moderate healing, collagen-3

and biglycan have been shown to be upregulated.[40] During this time, new fibrils are deposited with altered diameter distributions[39] and decreased longitudinal organization.[38,41] In addition, collagen-1,[40] versican,[40] decorin,[40] matrix metalloproteinases (MMPs),[42,43] tissue inhibitory metalloproteinases (TIMPs),[42] and ADAMs[42] become upregulated, indicating further tissue remodeling. With healing, cell number and density gradually return to baseline values,[36] but scarred portions may remain non-recoverably disorganized with associated inferior mechanical properties.[44] Examples of inferior quasi-static mechanical properties following injury include decreased ultimate stress, maximum load, stiffness, elongation to failure, modulus, and percent relaxation (a measure of tendon viscoelasticity).[36,45,46] Together, these findings suggest that healing results in altered tendon compositional properties that may likely reflect the structural and mechanical quality of the newly deposited tissue.

Tendon homeostasis and healing ultimately depends on the ability of tenocytes to remodel tissue. Due to the slow timescale of remodeling events in tendon,[47] it is likely that alterations in matrix properties (e.g., mechanics and structure) precede cell responses. Such structural and mechanical changes alter the fibrous architecture of the ECM, and may therefore influence the ability for resident tenocytes to recognize their native "tendon" environment. For example, changes in tendon phenotype are common with injury and healing. In particular, tendon stem cells are implicated to differentiate towards chondrocyte, osteoblast, or adipocyte lineages, as altered matrix properties and stresses on cells has been shown to affect cell fate.[48-50] Therefore, to model the cellular level implications, we propose that the matrix phenotype in diseased states is related to

the tenocyte response to load and distances that cells can exert matrix stresses during contraction.

1.2.3 Role of the Extracellular Matrix and Mechanical Loading on Cell Behavior

Tendons are fiber-reinforced musculoskeletal tissues that allow strain transfer from the whole tissue level to subcellular levels,[1,2] ultimately resulting in load-dependent biochemical responses (**Figure 1-2**). For example, although dynamic moderate loading increased tensile strength,[9] net collagen synthesis,[8-12] tenogenic differentiation,[13] and cross-sectional area,[9,51] excessive loading decreased tensile strength[52,53] and collagen organization,[54,55] and increased net collagen degradation,[56,57] aberrant differentiation,[13,58-62] cross-sectional area,[63] vascularization,[53,54,63] GAG production,[64] and inflammatory cytokines.[53,65,66] However, mechanistic interpretation for these findings remains limited—it is unknown what role mechanical loading played on the multiscale mechanical, structural, and compositional response. Fiber orientation in the matrix is also critical for various cell behaviors, including stem cell differentiation,[67] cell alignment,[68-70] and migration.[71] Quantifying these properties is necessary for understanding how mechanical signals are transduced into molecular responses. For example, since alterations in nuclear shape may affect cell phenotype,[72,73] understanding the multiscale mechanisms to elicit such changes is imperative. Knowledge of strain transfer is also important for defining tissue engineering benchmarks following construct implantation.

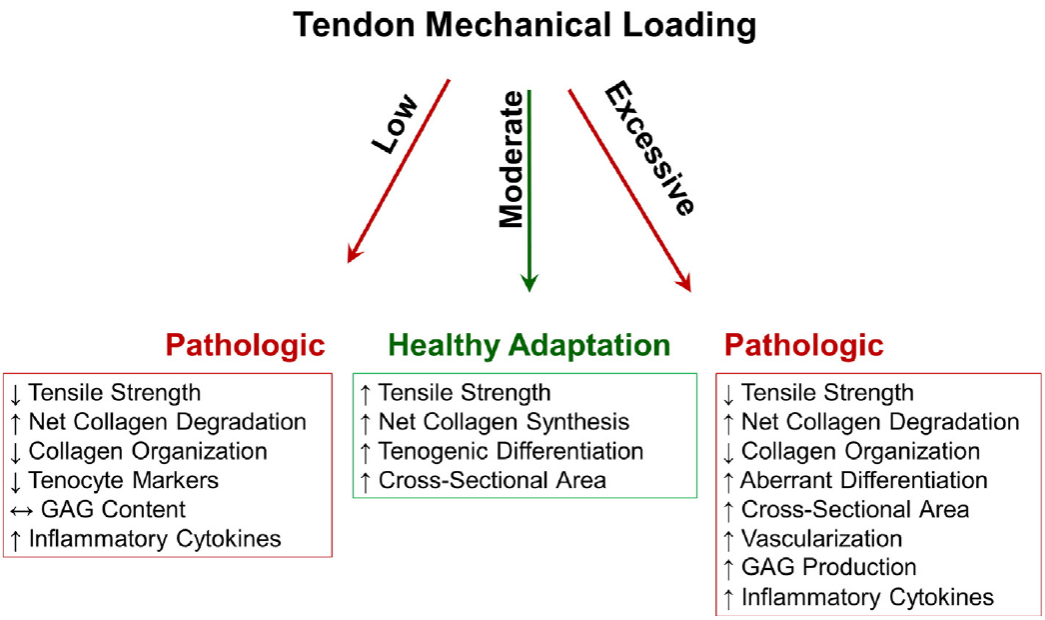

Figure 1-2: Response of tendon to mechanical loading. Low loading decreased tensile strength,[14-16] collagen organization,[14,15] and tenocyte markers;[74] net collagen degradation and inflammatory cytokines increased,[16,74] and GAG content was unchanged.[11] Moderate loading increased tensile strength,[9] net collagen synthesis,[8-12] tenogenic differentiation,[13] and cross-sectional area.[9,51] Knowledge regarding collagen organization, vascularization, GAG production, and inflammatory cytokines with moderate loading remains limited. Excessive loading decreased tensile strength[52,53] and collagen organization,[54,55] and increased net collagen degradation,[56,57] aberrant differentiation,[13,58-62] cross-sectional area,[63] vascularization,[53,54,63] GAG production,[64] and inflammatory cytokines.[53,65] Reproduced with permission from Freedman, et al., 2015.

1.3 Significance of Studies

1.3.1 Clinical Application

Musculoskeletal injuries affect 28.6 million Americans per year and account for $254 million in annual health care costs.[75] This includes over 450,000 tendon, ligament, or muscle related injuries each year.[75] With increased participation in recreational activities and sport, the incidence of acute and chronic tendon injuries is rising.[76,77] Unfortunately, many treatments for tendon injuries remain controversial, with “weak” or “inconclusive” evidence cited by a recent review from the American Academy of Orthopaedic Surgeons.[78] Basic scientific data describing tendon structure-function

relationships in an injured state have not been fully characterized, which may limit our ability to design new targeted therapies. Specifically, multiscale alterations to the ECM during macroscale mechanical loading may affect the local microenvironment of tenocytes, and therefore provide a mechanism leading to normal tendon homeostasis[8-13] or pathology.[14-21] Therefore, since mechanical loading is a hallmark of clinical rehabilitation protocols, fundamental, basic science studies are necessary to determine the ramifications of various macroscale dynamic tissue loading protocols (magnitude and duration) on the micro and nanoscale biomechanics in tendon during healing.

1.3.2 Structure-Function Relationships in Native Tendon

Tendon's composition and structure are related to its mechanical function. Non-linear mechanical properties of tendon are governed by changes in its architecture that occur as a function of the applied stress and strain. For example, during mechanical loading, a distinct nonlinearity or "toe" region is present that is often attributed to collagen fiber re-alignment and uncrimping[3-6] (**Figure 1-1**). Therefore, model systems which apply tensile loads to *ex vivo* tendon explants that preserve the native architecture of the ECM, while also providing more controlled experimental conditions than are possible *in vivo*, are important. Changes in tissue architecture may be critical for tissue homeostasis and injury, particularly in response to dynamic loading. In injured tissues, the formation of PG-rich inclusions has been implicated to attenuate strain transfer to cells that may contribute to their ability to maintain homeostasis.[22] Although tissue and cellular level strains correlate in normal uninjured tissues during *quasi-static* tensile loading,[22] such studies have not investigated the clinically important effects of dynamic

loading and tendon healing. Additionally, although much research has investigated structure-function relationships during quasi-static tensile loading (e.g., [54,79]), evaluation during dynamic loading has been limited.[34,80] This loading environment is likely generated in healing and injured tissues, and similar matrix disruption may be generated in response to high magnitude dynamic loading. High dynamic loading and healing likely alter tendon multiscale mechanical, structural, and spatial distributions of compositional proteins that affect how cells respond to their substrate, ECM loading, and transfer stress over long distances.

1.3.3 Assessment of Multiscale Properties on Living Tendons

Gross mechanical and biochemical changes may be due to aberrant strain transfer from the cell to their ECM and between cells. Since cells interact with their substrate, measures of fibril mechanics are also important. Substrate stiffness has been shown to guide stem cell lineage specification *in vitro* and affect proliferation, motility, contractility, and many other cell functions by changing both acute signaling and transcriptional programs.[48,81,82] Thus, specific measures of cell substrates (i.e., collagen fibrils) in native and healing tendon are necessary to fully describe the mechanisms of healing and response to dynamic loading. Altering tendon tensile forces can elicit changes in integrin receptors,[83] downstream ECM proteins,[74] as well as cell-cell contacts including N-cadherins and gap junctions[84,85] (**Figure 1-3**). However, much of these findings remain disjointed since studies identified them in isolation, and the complete multiscale mechanism remains unknown. Additionally, mechanisms of multiscale structure-function relationships during healing and dynamic loading are poorly

understood. This is of particular importance since accumulation of proteoglycan (PG)-rich inclusions or mucoid degeneration is common in injured tendon.[22,57] Recent studies showed that cells are more rounded within these regions and do not deform with applied strain as much as cells embedded in normal fibrous matrices.[22] This suggests that reduced transfer may contribute to altered mechanosensing and potentially altered cellular response.[22]

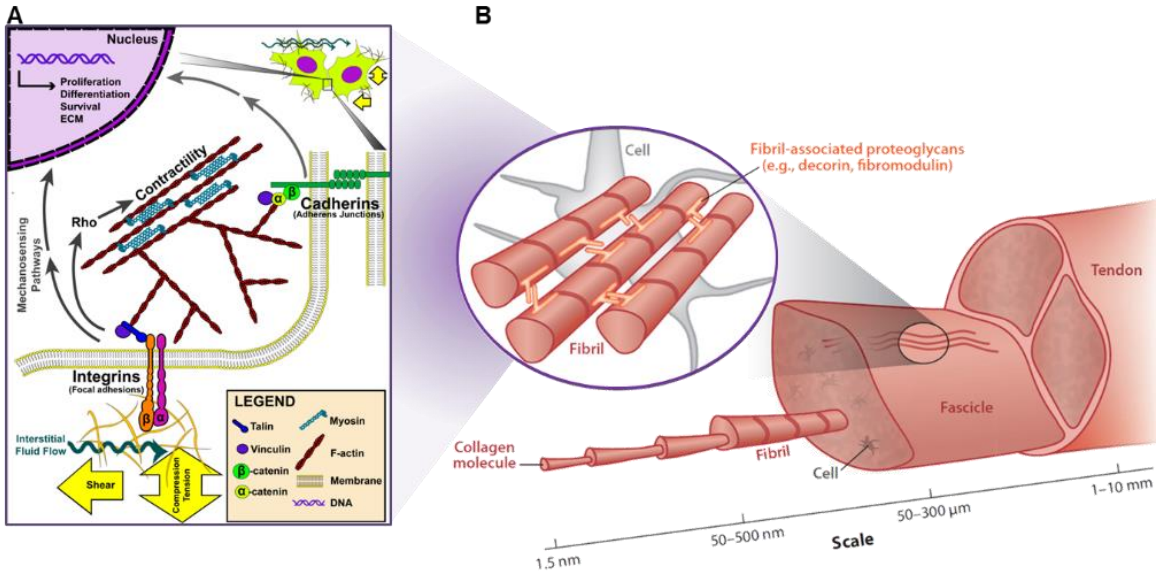

Figure 1-3: Multiscale tendon properties. Multiscale tendon response to load spanning from the subcellular (**A**) to whole tendon (**B**) levels. Macro-scale loading creates tension, compression, and shear loading on the ECM that is then transferred to the cell via transmembrane adhesion proteins termed integrins. Load is then transferred through the actin cytoskeleton via mechanosensitive pathways, such as RhoA, to the nucleus. It is noted that this illustration highlights only the basic subunits of these adhesion complexes, and that these components come together into higher order assemblies *in vivo*. Reproduced with permission from Freedman, et al., 2015.

This study will apply dynamic mechanical loading to uninjured and healing tendon explants. We will use a sophisticated mechanical testing system to apply a variety of dynamic mechanical loading protocols that vary both the magnitude and duration of loading, which we expect to reveal distinct ECM and cell changes, not present with the

commonly studied static loading. To maintain tendon health during loading, tissues will be immersed in a bath containing sterile DMEM supplemented with 5% fetal bovine serum (FBS) at 37ºC, 20% O_2, and 5% CO_2. This innovative approach allows the evaluation of multiscale mechanical and structural properties without any destructive dissection to the tissue. Since the structure of tendons relates to mechanical strains applied, following application of mechanical loading, tissues are flash frozen at set loads and strains to maintain their native tissue architecture for subsequent assays. This procedure provides advancement over traditional histological studies that do not control for tissue prestresses or strains applied prior to fixation.

1.3.4 Substrate Mechanics and Constitutive Models of Cell Mechanosensing

Cells can sense and respond to mechanical signals over distances nearly 20 times their cell radius (i.e., 250-1000μm).[86,87] Traction forces on the underlying substrate are generated during cell migration. These cell traction forces (CTF) are important for cell migration, phenotype, and homeostasis. For example, cell traction force microscopy can be shown to discriminate cell populations in tendon and are influenced by geometries that tenocytes adhere [88]. Recent modeling studies have suggested that the key mechanism driving this process is the fibrous nature of extracellular matrices.[1,89] Our collaborators have developed a constitutive law accounting for mechanically driven collagen fiber reorientation.[89] Results show that tension-driven collagen-fiber alignment plays a crucial role in force transmission.[1] Small critical stretch for fiber alignment, large fiber stiffness, and fiber strain-hardening behavior enable long-range interaction.[1] Furthermore, the range of collagen-fiber alignment for elliptical cells with polarized contraction is much

larger than that for spherical cells with diagonal contraction.[1] Building on this work, we propose to develop a 3D model to elucidate the role of dynamic mechanical loading and tendon healing on the ability for tenocytes to sense stress over long distances. In this model, mechanical and cell morphological properties are used as model inputs. Use of these properties at different strains following dynamic loading and healing provides initial conditions for the changes in matrix architecture in response to loading.

This modeling framework is adapted to include experimentally derived measures of tissue mechanics using AFM to evaluate the effects of dynamic loading and healing on tenocyte stress transmission. Tenocyte stress transmission provides knowledge that may have important ramifications for both cell-cell communication and load transfer within the ECM in tendon. One potential mechanism for continued maintenance or failure to heal following injury may be a lack of long range force transmission present in healing tissue that may lack fibrous architecture. Therefore, this modeling framework aims to build on previously existing models to develop a constitutive relationship that includes several key features that are critical for clarifying the ability for cells to sense mechanical perturbation and affect their surrounding matrix during contraction. These test conditions are essential to specifically address the fundamental mechanisms governing the response of tendon to dynamic loading and during healing.

To provide further insight into the relationships between multiscale mechanical, structural, and compositional properties following dynamic loading in uninjured and healing tendons, parameters from Aims 1 and 2 are used in single linear regressions to determine the variables that show significant coefficients of determination in predicting tenocyte stress transmission distances. Previous studies have provided insight into the

structure–function relationships in tendon.[90-92] Significant variables are used in multiple regression analyses to determine their predictability for tenocyte stress transmission distances. Together, these models reveal the structure-function pathways of mechanotransduction in normal and diseased tendons and elucidate the role of dynamic mechanical loading in this process.

1.4 Specific Aims

This study uses a comprehensive approach, including novel methods for: (1) application of mechanical loading on live tendons, (2) measurement of multiscale tendon mechanics and structure during dynamic mechanical loading and healing, (3) assessment of healing tissue composition using immunofluorescence (IF) and confocal imaging, and (4) application of a constitutive model for fibrous matrices based on experimentally derived parameters to predict tenocyte stress transmission and additional multiple regression analyses.

Specific Aim 1 evaluates the multiscale mechanical, structural, and compositional response of uninjured and healing tendon to quasi-static tensile loading. The first part of this aim examines how macroscale mechanical loading affects macroscale structural properties in nonliving uninjured control and healing tendons. Specifically, following quasi-static loading, tissues are snap-frozen, embedded in OCT, and sectioned for subsequent microscale assays.[4,33,93] For structural assessment, we measure fascicle/fiber alignment and crimp, and kinking using multiphoton confocal microscopy.

Specific Aim 2 evaluates the multiscale mechanical, structural, and compositional response of uninjured and healing tendon to dynamic tensile loading. Similar to Specific

Aim 1, the first part of this aim examines how macroscale mechanical loading affects macroscale structural properties in nonliving uninjured control and healing tendons. Subsequent parts of this aim will apply dynamic loading to living tendons to study how macroscale mechanical loading is transduced to changes in cell and nuclear shape, and the micro and nanoscale mechanical and structural properties that enable this mechanism. Specifically, following various bouts of dynamic protocols, tissues are snap-frozen, embedded in OCT, and sectioned for subsequent microscale assays.[4,33,93] For structural assessment, we will measure fascicle/fiber alignment and crimp, and kinking using multiphoton confocal microscopy.

Specific Aim 3 applies a novel fibrous constitutive law for tendon matrices to evaluate tenocyte stress transmission following low and high magnitude, long duration, dynamic loading. We also relate tenocyte stress transmission to multiscale mechanical, structural, and compositional properties determined from Aims 1 and 2 with multiple regression. Our previous experimental and modeling studies in tendon incorporating damage models have shown that empirical modeling techniques based on mechanical and image based measures can predict mechanical properties in healing,[94] aging,[94] and genetically altered[95] tendons. Proteoglycans may be implicated in reductions in tendons mechanical properties and collagen disorganization.[95] However, the underlying mechanisms for these processes have not been elucidated. As mentioned, mechanical perturbation likely causes alterations to multiscale ECM biomechanics, which ultimately affects cell behavior. Therefore, mechanical models that can directly measure the complex interactions between tenocytes and their ECM are necessary. Mechanical, structural, and compositional properties are used as model inputs for the fibrous

constitutive law or multiple regression analyses. Since this study aims to directly measure cell shape following various loading protocols, we apply realistic initial conditions for cell strains prior to contraction.

1.5 Approach

1.5.1 Overall Strategy

This study determines the ramifications of various macroscale dynamic tissue loading protocols on the micro and nanoscale biomechanics in tendon during healing. These properties will encompass multiscale mechanics (tensile, compression) and structure (alignment, kinking, crimp, composition), cell (shape, composition), and subcellular (shape, composition) components. This comprehensive approach has important implications for the fundamental mechanisms governing tendon homeostasis, healing, and phenotype. A mouse model is used with several innovative methodologies (mechanical testing with collagen fiber alignment, atomic force microscopy (AFM) to assess fibril mechanics, confocal imaging to assess ECM, cell, and nuclear morphology and composition, constitutive modeling to assess cell stress transmission, and multiple regression analysis) to provide rigorous mechanical, structural, and compositional data on the multiscale tendon response to dynamic loading during healing. Our overall hypothesis is that dynamic loading results in distinct ECM and cell changes, not present with static loading, which ultimately promote (e.g., via fiber recruitment) or reduce (e.g., via fiber damage) multiscale strain transfer during healing.

1.5.2 Study Design and Animal Model

This study employs a mouse patellar tendon injury model using female C57BL/6 mice at P150 (Figure 1-4). The patellar tendon model is advantageous since its tibia and patellar insertions allow for gripping during mechanical testing, without any fine dissection required of the patellar tendon. Additionally, the mouse patellar tendon allows light transmission making it capable of polarized light imaging during mechanical loading. Based on our previous rat Achilles mechanical data,[96] we estimated the normal variation in properties to determine our sample size. Given that rat Achilles stiffness after 8 weeks of exercise was 60.2±9.0 N/mm, we can detect differences of 10 N/mm, with 80% power using 10 animals per group.

An animal model is used to carefully control the injury and evaluate the multiscale the tissue

properties. Such properties are incorporated into a mathematical model to predict tenocyte stress transmission, for the first time, across a host of clinically relevant paradigms. The ability for cells to sense and respond to their ECM over long distances, we believe, is indicative of a return to a normal tissue phenotype.

1.5.3 Hypothesized Outcomes

Aim 1: We hypothesize that healing would reduce strain stiffening and fiber recruitment compared to uninjured tendons. We use a comprehensive approach, including application of mechanical loading on live tendons, measurement of multiscale tendon mechanics and structure during healing, assessment of healing tissue composition using confocal imaging, and assessment of tendon microstructure via multiphoton imaging.

Due to the slow timescale of remodeling events in tendon,[47] it is likely that alterations in matrix properties (e.g., mechanics and structure) precede cell responses. Such structural and mechanical changes alter the fibrous architecture of the ECM, and may therefore influence the ability for resident tenocytes to recognize their native "tendon" environment.

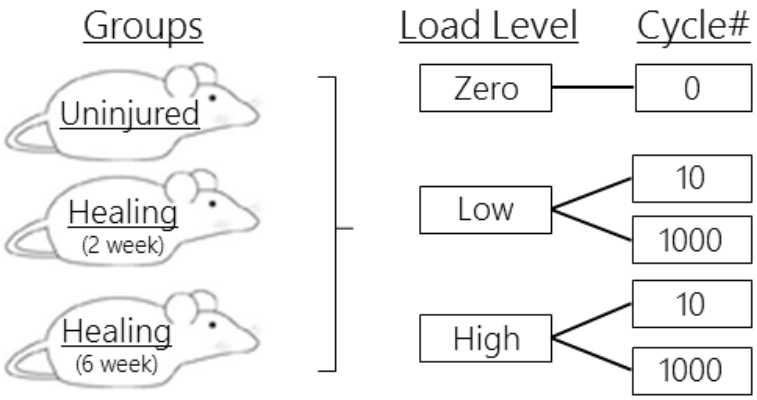

Figure 1-4: Study Design. (**A**) Mice are randomized into three groups before quasi-static and dynamic loading are completed. The dynamic loading protocols vary the magnitude (low or high load) and duration (0, 10, or 1000 cycles) of loading.

Aim 2: We hypothesize that high magnitude long duration dynamic loading and healing would reduce strain stiffening and fiber recruitment compared to uninjured tendons and low magnitude long duration dynamic loading. Additionally, we hypothesize that low magnitude dynamic loading will increase strain stiffening, stiffness, and alignment, which ultimately increases tendon cell nAR, unlike high dynamic loading.

Aim 3: We hypothesize that higher magnitude cyclic loading and healing decreases tenocyte stress transmission, as the ECM behaves more neo-Hookean than fibrous. Through multiple regression analysis, we expect that in *uninjured* tendon, modulus, and alignment contribute highest to cell strain and stress transmission.

However, *in healing* tendons, we hypothesize that modulus and crimp, contribute highest to cell strain and stress transmission. We first determine the material parameters in the model[1] that provide the best fit for tendon experimental data and implementation of the constitutive law in user material model in finite element software.

1.5.4 Ex-vivo Assays

Our mechanical loading approach allows for multiscale assessment of tendon mechanical and structural properties in uninjured and healing tendons. At the macroscale, we evaluate whole tissue dynamic mechanical properties and structural properties (matrix alignment and crimp) during mechanical loading. We have successfully measured collagen fiber alignment and crimp [97-100] using a custom apparatus with two precisely controlled offset polarizing sheets on either side of a specimen imaged during tensile testing, a linear backlight, and a digital camera. Briefly, as the tendon is loaded, a series of polarized images are captured and analyzed to produce an alignment map.

Following loading perturbation, tissues are flash frozen at low and high strains to provide load-dependent characterization of the effect of dynamic loading and healing. Frozen tendons are then sectioned for micro and nano-level mechanical and structural analysis, as well as confocal imaging of cell strains. Collagen fiber alignment is assessed using polarized light microscopy. Fibril mechanics are assessed using atomic force microscopy (AFM). Measurements using high resolution AFM provide nanometer resolution of fibril and interfibrillar matrix compression modulus.

Tenocytes and nuclear strains are imaged in their native ECM environment at different strain levels using a confocal microscope. Assessment of cell and nuclear strains

using confocal microscopy will provide a mechanistic foundation for observed alterations in multiscale mechanics and structure during healing and dynamic loading. Multiphoton imaging provides high resolution characterization of collagen structure and allows for simultaneous imaging of cell nuclei and the actin cytoskeleton. Together, these analyses will present the first-ever quantification of multiscale ECM environment following perturbation of dynamic loading in uninjured and healing tendons.

1.6 Chapter Overview

Chapter II will describe how macroscale mechanical and structural properties of tendon are altered **during fatigue loading** and tendon healing. Chapter III will describe the multiscale mechanical, structural, and compositional **response** of tendon to **quasi-static loading** during healing. Chapter IV will describe the multiscale mechanical, structural, and compositional **response** of tendon to **dynamic loading** during healing. Chapter V will describe **modeling** stress transmission in tendon during healing and dynamic loading. Chapter VI will summarize the **conclusions** of the previous chapters and provide future directions for this area of research.

1.7 References

1. Wang H, Abhilash AS, Chen CS, Wells RG, Shenoy VB. Long-range force transmission in fibrous matrices enabled by tension-driven alignment of fibers. *Biophys J.* Dec 2 2014;107(11):2592-2603.

2. Arnoczky SP, Lavagnino M, Whallon JH, Hoonjan A. In situ cell nucleus deformation in tendons under tensile load; a morphological analysis using confocal laser microscopy. *J Orthop Res.* Jan 2002;20(1):29-35.

3. Franchi M, Fini M, Quaranta M, et al. Crimp morphology in relaxed and stretched rat Achilles tendon. *J Anat.* Jan 2007;210(1):1-7.

4. Miller KS, Connizzo BK, Feeney E, Soslowsky LJ. Characterizing local collagen fiber re-alignment and crimp behavior throughout mechanical testing in a mature mouse supraspinatus tendon model. *J Biomech.* Aug 9 2012;45(12):2061-2065.

5. Diamant J, Keller A, Baer E, Litt M, Arridge RG. Collagen; ultrastructure and its relation to mechanical properties as a function of ageing. *Proc R Soc Lond B Biol Sci.* Mar 14 1972;180(1060):293-315.

6. Rigby BJ, Hirai N, Spikes JD, Eyring H. The Mechanical Properties of Rat Tail Tendon. *J Gen Physiol.* Nov 1 1959;43(2):265-283.

7. Mammoto A, Mammoto T, Ingber DE. Mechanosensitive mechanisms in transcriptional regulation. *J Cell Sci.* Jul 1 2012;125(Pt 13):3061-3073.

8. Mendias CL, Gumucio JP, Lynch EB. Mechanical loading and TGF-beta change the expression of multiple miRNAs in tendon fibroblasts. *J Appl Physiol (1985).* Jul 2012;113(1):56-62.

9. Heinemeier KM, Skovgaard D, Bayer ML, et al. Uphill running improves rat Achilles tendon tissue mechanical properties and alters gene expression without inducing pathological changes. *J Appl Physiol (1985).* Sep 1 2012;113(5):827-836.

10. Moerch L, Pingel J, Boesen M, Kjaer M, Langberg H. The effect of acute exercise on collagen turnover in human tendons: influence of prior immobilization period. *Eur J Appl Physiol.* Feb 2013;113(2):449-455.

11. Screen HR, Shelton JC, Bader DL, Lee DA. Cyclic tensile strain upregulates collagen synthesis in isolated tendon fascicles. *Biochem Biophys Res Commun.* Oct 21 2005;336(2):424-429.

12. Legerlotz K, Jones GC, Screen HR, Riley GP. Cyclic loading of tendon fascicles using a novel fatigue loading system increases interleukin-6 expression by tenocytes. *Scand J Med Sci Sports.* Feb 2013;23(1):31-37.

13. Zhang J, Wang JH. The effects of mechanical loading on tendons - an in vivo and in vitro model study. *PLoS One.* 2013;8(8):e71740.

14. Ikoma K, Kido M, Nagae M, et al. Effects of stress-shielding on the dynamic viscoelasticity and ordering of the collagen fibers in rabbit Achilles tendon. *J Orthop Res.* Jul 6 2013.

15. Hannafin JA, Arnoczky SP, Hoonjan A, Torzilli PA. Effect of stress deprivation and cyclic tensile loading on the material and morphologic properties of canine flexor digitorum profundus tendon: an in vitro study. *J Orthop Res.* Nov 1995;13(6):907-914.

16. Uchida H, Tohyama H, Nagashima K, et al. Stress deprivation simultaneously induces over-expression of interleukin-1beta, tumor necrosis factor-alpha, and transforming growth factor-beta in fibroblasts and mechanical deterioration of the tissue in the patellar tendon. *J Biomech.* Apr 2005;38(4):791-798.

17. Forde MS, Punnett L, Wegman DH. Prevalence of musculoskeletal disorders in union ironworkers. *J Occup Environ Hyg.* Apr 2005;2(4):203-212.

18. Jobe FW, Kvitne RS, Giangarra CE. Shoulder pain in the overhand or throwing athlete. The relationship of anterior instability and rotator cuff impingement. *Orthop Rev.* Sep 1989;18(9):963-975.

19. McMaster WC, Troup J. A survey of interfering shoulder pain in United States competitive swimmers. *Am J Sports Med.* Jan-Feb 1993;21(1):67-70.

20. Renstrom P, Johnson RJ. Overuse injuries in sports. A review. *Sports Med.* Sep-Oct 1985;2(5):316-333.

21. Sommerich CM, McGlothlin JD, Marras WS. Occupational risk factors associated with soft tissue disorders of the shoulder: a review of recent investigations in the literature. *Ergonomics.* Jun 1993;36(6):697-717.

22. Han WM, Heo SJ, Driscoll TP, Smith LJ, Mauck RL, Elliott DM. Macro- to microscale strain transfer in fibrous tissues is heterogeneous and tissue-specific. *Biophys J.* Aug 6 2013;105(3):807-817.

23. Wang XT, Ker RF, Alexander RM. Fatigue rupture of wallaby tail tendons. *J Exp Biol.* Mar 1995;198(Pt 3):847-852.

24. Freedman BR, Zuskov A, Sarver JJ, Buckley MR, Soslowsky LJ. Evaluating changes in tendon crimp with fatigue loading as an ex vivo structural assessment of tendon damage. *J Orthop Res.* Mar 13 2015.

25. Fung DT, Wang VM, Andarawis-Puri N, et al. Early response to tendon fatigue damage accumulation in a novel in vivo model. *J Biomech.* Jan 19 2010;43(2):274-279.

26. Fung DT, Wang VM, Laudier DM, et al. Subrupture tendon fatigue damage. *J Orthop Res.* Feb 2009;27(2):264-273.

27. Wren TA, Lindsey DP, Beaupre GS, Carter DR. Effects of creep and cyclic loading on the mechanical properties and failure of human Achilles tendons. *Ann Biomed Eng.* Jun 2003;31(6):710-717.

28. Veres SP, Harrison JM, Lee JM. Repeated subrupture overload causes progression of nanoscaled discrete plasticity damage in tendon collagen fibrils. *J Orthop Res.* May 2013;31(5):731-737.

29. Veres SP, Brennan-Pierce EP, Lee JM. Macrophage-like U937 cells recognize collagen fibrils with strain-induced discrete plasticity damage. *J Biomed Mater Res A.* Jan 2015;103(1):397-408.

30. Buckley MR, Sarver JJ, Freedman BR, Soslowsky LJ. The dynamics of collagen uncrimping and lateral contraction in tendon and the effect of ionic concentration. *J Biomech.* Sep 3 2013;46(13):2242-2249.

31. Lake SP, Miller KS, Elliott DM, Soslowsky LJ. Effect of fiber distribution and realignment on the nonlinear and inhomogeneous mechanical properties of human supraspinatus tendon under longitudinal tensile loading. *J Orthop Res.* Dec 2009;27(12):1596-1602.

32. Li Q, Doyran B, Gamer LW, et al. Biomechanical properties of murine meniscus surface via AFM-based nanoindentation. *J Biomech.* Mar 11 2015.

33. Connizzo BK, Sarver JJ, Han L, Soslowsky LJ. In situ fibril stretch and sliding is location-dependent in mouse supraspinatus tendons. *J Biomech.* Dec 18 2014;47(16):3794-3798.

34. Dunkman AA, Buckley MR, Mienaltowski MJ, et al. Decorin expression is important for age-related changes in tendon structure and mechanical properties. *Matrix Biol.* Jan 2013;32(1):3-13.

35. Provenzano PP, Vanderby R, Jr. Collagen fibril morphology and organization: implications for force transmission in ligament and tendon. *Matrix Biol.* Mar 2006;25(2):71-84.

36. Chamberlain CS, Duenwald-Kuehl SE, Okotie G, Brounts SH, Baer GS, Vanderby R. Temporal Healing in Rat Achilles Tendon: Ultrasound Correlations. *Ann Biomed Eng.* Nov 13 2012.

37. Eliasson P, Andersson T, Aspenberg P. Rat Achilles tendon healing: mechanical loading and gene expression. *J Appl Physiol (1985).* Aug 2009;107(2):399-407.

38. Ehrlich HP, Lambert PA, Saggers GC, Myers RL, Hauck RM. Dynamic changes appearing in collagen fibers during intrinsic tendon repair. *Ann Plast Surg.* Feb 2005;54(2):201-206.

39. Maeda T, Sakabe T, Sunaga A, et al. Conversion of mechanical force into TGF-beta-mediated biochemical signals. *Curr Biol.* Jun 7 2011;21(11):933-941.

40. Bring DK, Reno C, Renstrom P, Salo P, Hart DA, Ackermann PW. Joint immobilization reduces the expression of sensory neuropeptide receptors and impairs healing after tendon rupture in a rat model. *J Orthop Res.* Feb 2009;27(2):274-280.

41. Sasaki K, Yamamoto N, Kiyosawa T, Sekido M. The role of collagen arrangement change during tendon healing demonstrated by scanning electron microscopy. *J Electron Microsc (Tokyo).* 2012;61(5):327-334.

42. Jones GC, Corps AN, Pennington CJ, et al. Expression profiling of metalloproteinases and tissue inhibitors of metalloproteinases in normal and degenerate human achilles tendon. *Arthritis Rheum.* Mar 2006;54(3):832-842.

43. Karousou E, Ronga M, Vigetti D, Passi A, Maffulli N. Collagens, proteoglycans, MMP-2, MMP-9 and TIMPs in human achilles tendon rupture. *Clin Orthop Relat Res.* Jul 2008;466(7):1577-1582.

44. Freedman BR SJ, Buckley MR, Voleti PB, Soslowsky LJ. Biomechanical and structural response of healing Achilles tendon to

fatigue loading following acute injury. *(in review).* 2013.

45. Beason DP, Kuntz AF, Hsu JE, Miller KS, Soslowsky LJ. Development and evaluation of multiple tendon injury models in the mouse. *J Biomech.* Mar 7 2012.

46. Freedman BR, Sarver JJ, Buckley MR, Voleti PB, Soslowsky LJ. Biomechanical and structural response of healing Achilles tendon to fatigue loading following acute injury. *J Biomech.* Nov 11 2013.

47. Magnusson SP, Langberg H, Kjaer M. The pathogenesis of tendinopathy: balancing the response to loading. *Nat Rev Rheumatol.* May 2010;6(5):262-268.

48. Engler AJ, Sen S, Sweeney HL, Discher DE. Matrix elasticity directs stem cell lineage specification. *Cell.* Aug 25 2006;126(4):677-689.

49. Pelham RJ, Jr., Wang Y. Cell locomotion and focal adhesions are regulated by substrate flexibility. *Proc Natl Acad Sci U S A.* Dec 9 1997;94(25):13661-13665.

50. Chen CS, Mrksich M, Huang S, Whitesides GM, Ingber DE. Geometric control of cell life and death. *Science.* May 30 1997;276(5317):1425-1428.

51. Cho NS, Hwang JH, Lee YT, Chae SW. Tendinosis-like histologic and molecular changes of the Achilles tendon to repetitive stress: a pilot study in rats. *Clin Orthop Relat Res.* Nov 2011;469(11):3172-3180.

52. Lichtwark GA, Cresswell AG, Newsham-West RJ. Effects of running on human Achilles tendon length-tension properties in the free and gastrocnemius components. *J Exp Biol.* Sep 12 2013.

53. Flick J, Devkota A, Tsuzaki M, Almekinders L, Weinhold P. Cyclic loading alters biomechanical properties and secretion of PGE2 and NO from tendon explants. *Clin Biomech (Bristol, Avon).* Jan 2006;21(1):99-106.

54. Soslowsky LJ, Thomopoulos S, Tun S, et al. Neer Award 1999. Overuse activity injures the supraspinatus tendon in an animal model: a histologic and biomechanical study. *J Shoulder Elbow Surg.* Mar-Apr 2000;9(2):79-84.

55. Sun HB, Andarawis-Puri N, Li Y, et al. Cycle-dependent matrix remodeling gene expression response in fatigue-loaded rat patellar tendons. *J Orthop Res.* Oct 2010;28(10):1380-1386.

56. Hansen P, Kovanen V, Holmich P, et al. Micromechanical properties and collagen composition of ruptured human achilles tendon. *Am J Sports Med.* Feb 2013;41(2):437-443.

57. Kannus P, Jozsa L. Histopathological changes preceding spontaneous rupture of a tendon. A controlled study of 891 patients. *J Bone Joint Surg Am.* Dec 1991;73(10):1507-1525.

58. Perry SM, McIlhenny SE, Hoffman MC, Soslowsky LJ. Inflammatory and angiogenic mRNA levels are altered in a supraspinatus tendon overuse animal model. *J Shoulder Elbow Surg.* Jan-Feb 2005;14(1 Suppl S):79S-83S.

59. Archambault JM, Jelinsky SA, Lake SP, Hill AA, Glaser DL, Soslowsky LJ. Rat supraspinatus tendon expresses cartilage markers with overuse. *J Orthop Res.* May 2007;25(5):617-624.

60. Attia M, Scott A, Duchesnay A, et al. Alterations of overused supraspinatus tendon: a possible role of glycosaminoglycans and HARP/pleiotrophin in early tendon pathology. *J Orthop Res.* Jan 2012;30(1):61-71.

61. Rui YF, Lui PP, Ni M, Chan LS, Lee YW, Chan KM. Mechanical loading increased BMP-2 expression which promoted osteogenic differentiation of tendon-derived stem cells. *J Orthop Res.* Mar 2011;29(3):390-396.

62. Shi Y, Fu Y, Tong W, et al. Uniaxial mechanical tension promoted osteogenic differentiation of rat tendon-derived stem cells (rTDSCs) via the Wnt5a-RhoA pathway. *J Cell Biochem.* Oct 2012;113(10):3133-3142.

63. Malliaras P, Chan O, Simran G, Martinez de Albornoz P, Morrissey D, Maffulli N. Doppler ultrasound signal in Achilles tendinopathy reduces immediately after activity. *Int J Sports Med.* Jun 2012;33(6):480-484.

64. Devkota AC, Tsuzaki M, Almekinders LC, Banes AJ, Weinhold PS. Distributing a fixed amount of cyclic loading to tendon explants over longer periods induces greater cellular and mechanical responses. *J Orthop Res.* Aug 2007;25(8):1078-1086.

65. Barbe MF, Gallagher S, Popoff SN. Serum biomarkers as predictors of stage of work-related musculoskeletal disorders. *The Journal of the American Academy of Orthopaedic Surgeons.* Oct 2013;21(10):644-646.

66. Freedman B, Bade N, Riggin C, et al. The (dys)Functional Extracellular Matrix. *Biochimica et Biophysica Acta.* 2014;(in review).

67. Subramony SD, Dargis BR, Castillo M, et al. The guidance of stem cell differentiation by substrate alignment and mechanical stimulation. *Biomaterials.* Mar 2013;34(8):1942-1953.

68. Keller R, Shook D, Skoglund P. The forces that shape embryos: physical aspects of convergent extension by cell intercalation. *Phys Biol.* 2008;5(1):015007.

69. Horne-Badovinac S. The Drosophila egg chamber-a new spin on how tissues elongate. *Integr Comp Biol.* Oct 2014;54(4):667-676.

70. Barocas VH, Tranquillo RT. An anisotropic biphasic theory of tissue-equivalent mechanics: the interplay among cell traction, fibrillar network deformation, fibril alignment, and cell contact guidance. *J Biomech Eng.* May 1997;119(2):137-145.

71. Perris R, Perissinotto D. Role of the extracellular matrix during neural crest cell migration. *Mech Dev.* Jul 2000;95(1-2):3-21.

72. Lelievre SA, Weaver VM, Nickerson JA, et al. Tissue phenotype depends on reciprocal interactions between the extracellular matrix and the structural organization of the nucleus. *Proc Natl Acad Sci U S A.* Dec 8 1998;95(25):14711-14716.

73. Guilak F. Compression-induced changes in the shape and volume of the chondrocyte nucleus. *J Biomech.* Dec 1995;28(12):1529-1541.

74. Bayer ML, Schjerling P, Herchenhan A, et al. Release of tensile strain on engineered human tendon tissue disturbs cell adhesions, changes matrix architecture, and induces an inflammatory phenotype. *PLoS One.* 2014;9(1):e86078.

75. AAOS. *The Burden of Musculoskeletal Diseases in the United States*2008.

76. Suchak AA, Bostick G, Reid D, Blitz S, Jomha N. The incidence of Achilles tendon ruptures in Edmonton, Canada. *Foot Ankle Int.* Nov 2005;26(11):932-936.

77. Maffulli N, Wong J, Almekinders LC. Types and epidemiology of tendinopathy. *Clin Sports Med.* Oct 2003;22(4):675-692.

78. AAOS. Guideline on the Diagnosis and Treatment of Acute Achilles Tendon Rupture. 2009.

79. Fox AJ, Schar MO, Wanivenhaus F, et al. Fluoroquinolones Impair Tendon Healing in a Rat Rotator Cuff Repair Model: A Preliminary Study. *Am J Sports Med.* Aug 20 2014.

80. Lujan TJ, Underwood CJ, Jacobs NT, Weiss JA. Contribution of glycosaminoglycans to viscoelastic tensile behavior of human ligament. *J Appl Physiol (1985).* Feb 2009;106(2):423-431.

81. Wen JH, Vincent LG, Fuhrmann A, et al. Interplay of matrix stiffness and protein tethering in stem cell differentiation. *Nat Mater.* Oct 2014;13(10):979-987.

82. Wells RG. The role of matrix stiffness in regulating cell behavior. *Hepatology.* Apr 2008;47(4):1394-1400.

83. Ralphs JR, Waggett AD, Benjamin M. Actin stress fibres and cell-cell adhesion molecules in tendons: organisation in vivo and response to mechanical loading of tendon cells in vitro. *Matrix Biol.* Jan 2002;21(1):67-74.

84. Maeda E, Ye S, Wang W, Bader DL, Knight MM, Lee DA. Gap junction permeability between tenocytes within tendon fascicles is suppressed by tensile loading. *Biomech Model Mechanobiol.* Mar 2012;11(3-4):439-447.

85. Waggett AD, Benjamin M, Ralphs JR. Connexin 32 and 43 gap junctions differentially modulate tenocyte response to cyclic mechanical load. *Eur J Cell Biol.* Nov 2006;85(11):1145-1154.

86. Rudnicki MS, Cirka HA, Aghvami M, Sander EA, Wen Q, Billiar KL. Nonlinear strain stiffening is not sufficient to explain how far cells can feel on fibrous protein gels. *Biophys J.* Jul 2 2013;105(1):11-20.

87. Ma X, Schickel ME, Stevenson MD, et al. Fibers in the extracellular matrix enable long-range stress transmission between cells. *Biophys J.* Apr 2 2013;104(7):1410-1418.

88. Wang JH. Cell Traction Forces (CTFs) and CTF Microscopy Applications in Musculoskeletal Research. *Oper Tech Orthop.* Jun 01 2010;20(2):106-109.

89. Abhilash AS, Baker BM, Trappmann B, Chen CS, Shenoy VB. Remodeling of fibrous extracellular matrices by contractile cells: predictions from discrete fiber network simulations. *Biophys J.* Oct 21 2014;107(8):1829-1840.

90. Andarawis-Puri N, Kuntz AF, Jawad AF, Soslowsky LJ. Infraspinatus and supraspinatus tendon strain explained using multiple regression models. *Ann Biomed Eng.* Sep 2010;38(9):2979-2987.

91. Derwin KA, Soslowsky LJ. A quantitative investigation of structure-function relationships in a tendon fascicle model. *J Biomech Eng.* Dec 1999;121(6):598-604.

92. Robinson PS, Lin TW, Jawad AF, Iozzo RV, Soslowsky LJ. Investigating tendon fascicle structure-function relationships in a transgenic-age mouse model using multiple regression models. *Ann Biomed Eng.* Jul 2004;32(7):924-931.

93. Thornton GM, Shrive NG, Frank CB. Ligament creep recruits fibres at low stresses and can lead to modulus-reducing fibre damage at higher creep stresses: a study in rabbit medial collateral ligament model. *J Orthop Res.* Sep 2002;20(5):967-974.

94. Buckley MR DA, Reuther KE, Kumar AK, Pathmanathan L, Beason DP, Birk DE, Soslowsky LJ. Validation of an Empirical Damage Model for Aging and In Vivo Injury of the Murine Patellar Tendon. *Journal of Biomechanical Engineering.* 2013;135(April).

95. Gordon J, Freedman B, Zuskov A, Iozzo R, Birk D, Soslowsky L. Achilles tendons from decorin- and biglycan-null mouse models have inferior mechanical and structural properties predicted by an image-based empirical damage model. *Journal of Biomechanics.* 2014;In review.

96. Huang TF, Perry SM, Soslowsky LJ. The effect of overuse activity on Achilles tendon in an animal model: a biomechanical study. *Ann Biomed Eng.* Mar 2004;32(3):336-341.

97. Lake SP, Miller KS, Elliott DM, Soslowsky LJ. Effect of fiber distribution and realignment on the nonlinear and inhomogeneous mechanical properties of human

supraspinatus tendon under longitudinal tensile loading. *Journal of Orthopaedic Research.* 2009;27(12):1596-1602.

98. Lake SP, Miller KS, Elliott DM, Soslowsky LJ. Tensile properties and fiber alignment of human supraspinatus tendon in the transverse direction demonstrate inhomogeneity, nonlinearity, and regional isotropy. *J Biomech.* Mar 3 2010;43(4):727-732.

99. Miller K, Connizzo B, Soslowsky L. Collagen Fiber Re-Alignment in a Neonatal Developmental Mouse Supraspinatus Tendon Model. *Annals of Biomedical Engineering.* 2012;40(5):1102-1110.

100. Miller KS, Edelstein L, Connizzo BK, Soslowsky LJ. Effect of preconditioning and stress relaxation on local collagen fiber re-alignment: inhomogeneous properties of rat supraspinatus tendon. *J Biomech Eng.* Mar 2012;134(3):031007.

CHAPTER II: MACROSCALE MECHANICAL AND STRUCTURAL PROPERTIES OF TENDON ARE ALTERED DURING HIGH DYNAMIC LOADING AND TENDON HEALING

2.1 Introduction

Tendons have a complex hierarchical structure that relates to their mechanical properties. For example, during mechanical loading a distinct nonlinearity or "toe" region is present that is often attributed to collagen fiber straightening or "uncrimping."[1-4] Alterations in tendon crimp may portend changes in mechanical properties. Structure-function relationships are therefore important to both provide an understanding of healthy tendon properties and serve as a guideline for injury assessment and treatment.

Although much research has investigated structure-function relationships during quasi-static tensile loading,[5,6] evaluation during dynamic loading has been limited.[7,8] Recently, crimp was visualized with polarized light imaging during dynamic loading.[9] This technique, which consists of two polarizing sheets on either side of the tendon, depicts its birefringence, as a crimped waveform containing alternating patterns of bright and dark bands (**Figure 2-1**).[2-4,9] This innovative approach allows whole tissue, region specific, and load dependent crimp properties, to be inferred simultaneously during a mechanical test without destructively altering the tendon. Crimp is believed to be ubiquitous in all tendons,[10] and as a property, is strain dependent[2] and planar at this hierarchical level.[4,11] Understanding the process of uncrimping is significant as many tendons are believed to operate within the toe region of the stress-strain curve[12] and experience a wide range of *in vivo* strains and strain rates.

Studying structure-function relationships during dynamic loading at *high loads* is also important for elucidating potential mechanical mechanisms governing *fatigue-*

induced damage and injury. Cadaveric and animal studies have shown that the response of tendon to fatigue loading is marked by changes in stiffness and deformation (among other properties) that consists of three phases (**Figure 2-2**).[13,14] Specifically, tendon stiffness increases initially, reaches a maximum, and then gradually decreases. This gradual decrease in stiffness is attributed to accumulated sub-rupture damage, which ultimately leads to the dramatic increase in peak deformation and decrease in stiffness prior to failure.[13-15] This induction of subfailure damage accumulation with repetitive loading is suggested as the primary benefit of fatigue testing over conventional quasi-static methods. Initially, mechanical fatigue properties in tendon highlighted the three-phase pattern of fatigue damage accumulation,[16] but no structural evaluation was completed.[14,16,17] Questions regarding the structural alterations contributing to the monotonic increases in peak cyclic strain during fatigue loading led to work utilizing *in vivo* and *ex vivo* animal models with structural image-based measures.[13,18-21] Although these previous studies have used various imaging modalities to study the accumulation and progression of fatigue induced structural alterations, such studies were not designed to simultaneously evaluate the load and region dependence of tendon crimp in the entire tissue. In addition, the imaging techniques utilized may be costly, time consuming, or destructive to the tissue.[15,19,22]

Following injury, quasi-static test methods have shown decreased tissue stiffness, modulus, failure load, and increased tendon cross sectional area with healing. [23] However, it remains poorly understood whether these mechanical and structural property changes are also evident during fatigue loading and whether such assessment may be more indicative of *in vivo* tissue healing. Further, an often unstated assumption in

histological studies of tendon healing is that alterations in tendon structure are closely associated with changes in tendon mechanical properties and function. Understanding how mechanical properties in injured tissue relate to changes in structure during healing in response to fatigue loading is therefore an important step to elucidating the mechanical and structural mechanisms leading to specimen failure and to better define benchmarks for mechanically robust tissue engineering constructs.

The purpose of this study was to determine how tendon structural and mechanical properties vary during fatigue loading in uninjured and healing tendons. Specifically, we investigated if tendon crimp could serve as an *ex vivo* structural and region dependent metric of fatigue-induced structural alteration, as assessed by changes in crimp frequency and amplitude in the mouse patellar tendon using polarized light imaging. Additionally**,** we examined the mechanical and structural properties throughout the fatigue life of healing Achilles tendons, and investigated whether structural properties assessed during fatigue loading could predict fatigue properties throughout healing. A mouse model was used to carefully control the injury and quantify tendon fatigue and structural properties using state-of-the-art mechanical testing techniques to evaluate fatigue mechanics and structure simultaneously. We hypothesized that crimp properties would increase with fatigue loading, show regional differences, and correlate with mechanical properties assessed during fatigue loading. We also hypothesized that fatigue loading would decrease mechanical properties (dynamic modulus, stiffness, hysteresis, peak strain, damage) in conjunction with altered structure (fiber realignment and birefringence) that partially recover with healing. Our results demonstrate the importance for fatigue and

structural property assessment to evaluate tendon healing that may provide further benchmarks for image-based methods to assess tendon mechanical integrity.

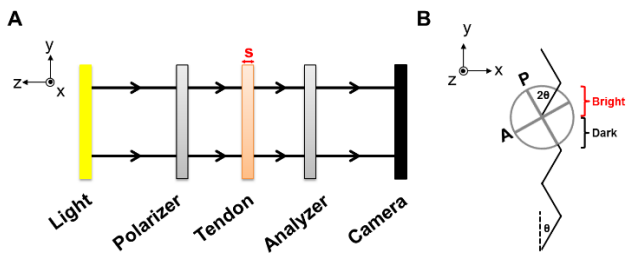

Figure 2-1. Experimental setup of a plane polariscope. The setup **(A)** consists of a backlight, two linear polarizers on either side of the tendon(s), and a camera. **(B)** The polarizer (P) and analyzer (A) are crossed at 90º and are oriented at the angle θ at which maximal extinction in the dark crimp bands occurred at preload.

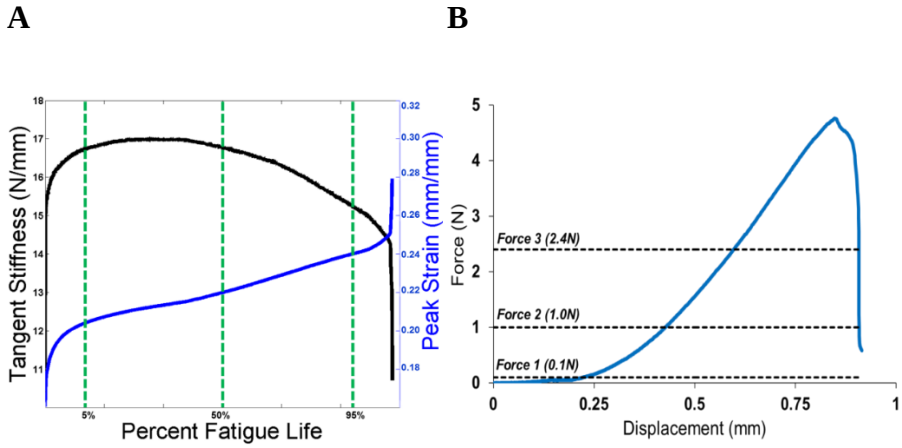

Figure 2-2: Effect of fatigue loading on tendon mechanics. (**A**) Typical mechanical response of a tendon undergoing fatigue loading. Briefly, changes in peak strain and stiffness undergo a three phase series of property changes leading to tendon rupture. 5%, 50%, and 95% indicate the time points of fatigue life from which mechanical parameters were evaluated. (**B**) Typical load displacement curve for an Achilles tendon during a ramp to failure. Dashed lines indicate the three loads that alignment maps were taken that approximate the toe, transition, and linear portions of the load displacement curve.

2.2 Methods

2.2.1 Study Design

To investigate changes in structural and mechanical properties during fatigue loading in uninjured tendons, patellar tendons from C57BL/6 mice at 150 days of age (IACUC approved) were used (N=10-11). To study similar changes during healing, a second cohort of 60 tendons from 30 C57BL/6 mice were used. Briefly, at 120 days of age, 24 mice received bilateral excisional injuries to the midsubstance of their Achilles tendons under aseptic conditions.[24] A single skin incision parallel to the tibia and lateral to the Achilles tendon was made. Next, a rubber-coated backing was placed deep to the Achilles tendon to provide support while a full thickness, partial width (~50%) region was excised using a 0.5 mm biopsy punch. Following the injury, the skin was closed with suture, and the animals returned to cage activity. Animals were euthanized after 0, 1, 3, and 6 weeks post-injury to evaluate the role of healing on tendon structural and mechanical properties during fatigue loading.

2.2.2 Sample Preparation

Following sacrifice, all tissues were frozen at -20ºC prior to gross and fine dissection. To prepare patellar tendons, the knee joint was exposed and patellar tendons were harvested while hydrated in phosphate buffered saline (PBS). The surrounding musculature was removed, and the patella-patellar tendon-tibia unit was prepared for mechanical testing.[8] To evaluate the effects of healing, Achilles tendons were thawed and the Achilles tendon and calcaneus were carefully harvested, removing all musculature and surrounding soft tissue, and were hydrated in phosphate buffered saline (PBS). A

laser device was used to measure tendon cross sectional area[25] and tendons were placed in custom fixtures to grip the calcaneus and tendon ends.

2.2.3 Fatigue Testing

To test the effect of fatigue loading on tendon crimp properties, patellar tendons were secured in a mechanical testing setup while submerged in a PBS bath. Tendons were preloaded, preconditioned, imaged at three loads (representing the toe (F=0.1N), transition (F=0.5N), and linear regions (F=2.0N) of the force-displacement curve), and fatigue tested at 1Hz between 2 and 4N corresponding to 25-75% of the ultimate failure load using an Instron Microtester (Instron 5848, Norwood, MA) (**Figure 2-2**). A preliminary study determined that the mean failure load of mouse patellar tendons was approximately 5.5N, from which the necessary target loads were computed for the load controlled fatigue test. During loading, force and displacement data were acquired at 100 Hz and analyzed using custom MATLAB code (Mathworks, Natick, MA). Several post processing parameters were computed:[18] 1) maximum/minimum cyclic displacement and strain; 2) tangent stiffness (calculated as the slope between the maximum and minimum force and displacements for each cycle); 3) stress (calculated as the force divided by the cross sectional area); 4) dynamic modulus (calculated as the slope between the maximum and minimum stress and strain for each cycle; 5) hysteresis (defined as the area enclosed by the stress-strain curve for a cycle); and 6) laxity (defined as the ratio of displacement and gauge length relative to the first cycle of fatigue loading, and assessed at constant load throughout fatigue testing).[26,27] Specifically, after each cycle of fatigue loading, the length (L_S) of the patellar tendon was measured at the load level of 2.5 N. The percent

change in nonrecoverable length (laxity) relative to the tendon's original length (L_o) is therefore defined as $L= 100*[(L_S - L_o)/L_o]$.[18,26-28]

Similarly, Achilles tendons were tensile tested according to the following protocol in a PBS bath. Zero strain was set as the strain at preload. First, specimens were preconditioned between 0.1 and 0.2N at 0.5Hz for 30 cycles using a sinusoidal waveform. To determine the necessary target loads for the load controlled fatigue test to simulate *in vivo* conditions, a preliminary study was conducted that determined the mean failure load of mouse Achilles tendons to be approximately 5N. Thus, during fatigue loading, specimens were cycled under load control between approximately 20 and 75% of their ultimate tensile strength (1-3.8N) at 1Hz until failure or 15,000 cycles. This upper cycle limit was determined from pilot tests to be an assumed theoretical endurance limit. In addition to the mechanical properties described, the number of cycles to failure (defined as the number of cycles until specimen failure) was also evaluated.

2.2.4 Collagen Fiber Uncrimping, Alignment, and Birefringence

Simultaneous evaluation of tendon structure via polarized light imaging was also conducted. This polarized light system[29] integrated with the mechanical testing system consisted of a backlight, 90º offset rotating polarizer sheets (Edmund Optics, Barrington, NJ) on both sides of the test sample (polarizer and analyzer), and a GigE aca2040gm camera (resolution: 2048x2048 pixels) (Basler, Exton, PA). This provided a pixel size of 3 microns, and the total average length at baseline was 820 pixels (~2.4 mm). The polarizer (P) and analyzer (A) were crossed at 90º and were oriented at the angle θ at which maximal extinction in the dark crimp bands occurred at preload. In this setup,

alternating light and dark bands appear in a crimped tendon. Images of the whole tendon were captured after 0, 10, 100, and 1000 fatigue loading cycles at loads described (**Figure 2-3**).

For evaluation of Achilles tendons during healing, sets of alignment maps (15-18 images) were taken prior to fatigue loading, after 10, 25, 50 cycles of fatigue loading, and at intervals of 100 cycles at three distinct loads (0.1N, 1.0N, 2.4N). These loads were chosen to be indicative of the toe, transition, and linear regions of the mouse Achilles load displacement curve (**Figure 2-2B**), and were investigated to evaluate the sensitivity of structural properties to load. This protocol was fully automated during the fatigue tests using analog outputs acquired by a data acquisition device (USB 6008, National Instruments, Austin, TX) at 100Hz that was monitored by a custom Labview program (Version 8.6, National Instruments, Austin, TX). Following each test, an alignment map was acquired using a quarter-wave retarder (Edmund Optics, Barrington, NJ) to normalize tissue intensities to account for slight variations in light source intensity.

2.2.5 Data Analysis

A custom program was created (MATLAB, Version: R2012a, Natick, MA) to quantify tendon crimp properties. Four regions of interest (ROIs) (200x30pixels) were chosen to represent the insertion and midsubstance, at the tendon center and lateral positions (**Figure 2-3C**). These same ROIs were used for the analysis of all images throughout the fatigue test across all loads evaluated. A Gaussian low-pass filter was applied to the image within the ROI to enhance the visibility of light and dark bands. Next, intensity values were averaged across the ROI width to give an intensity profile as

a function of the vertical axis of the region that was then high-pass filtered. The spectral power was determined using the Fast Fourier Transform (FFT), which was then integrated to determine the cumulative spectral power (CSP). Finally, the crimp frequency (F_{crimp}) was determined by taking the frequency at mean spectral power. Throughout specimen fatigue life, the CSP was evaluated at the F_{crimp} to provide an optical measure of average crimp amplitude (A_{crimp}). All post-processing procedures were completed for all images acquired throughout specimen testing.

For alignment and birefringence analysis, a custom MATLAB program (MATLAB, Natick, MA) was used to divide the image into a series of regions of length 10 pixels and spacing of 20 pixels that were individually averaged to filter noise. From these data, the signal phase and magnitude within each region from each alignment image series were used to determine the circular standard deviation (CSD), a measure of collagen fiber disorganization,[29] and the signal's peak-to-peak intensity. Briefly, circular standard deviation is calculated by fitting a $\sin^2$ function[30] to the pixel intensity-polarizer angle data to determine the angle corresponding to the minimum pixel intensity. This angle represents the average direction of fiber alignment. From photoelastic theory, the specimen's peak-to-peak intensity and thickness can be related to determine tissue birefringence.[30-32] Birefringence is a term used to describe the structural anisotropy of a tissue (i.e., the difference in index of refraction between its fast and slow axes).[33] As shown previously (Timoshenko, 1969), the intensity of light detected through the analyzer is given by the equation

$$I_c = I_p \sin^2(2\alpha)\sin^2\left(\frac{\Delta}{2}\right) \qquad (1)$$

where I_c is the intensity of light detected by the camera, I_p is the intensity of light passing through the polarizer, α is the angle between P and the tendon's slow axis (i.e., the aligned axis of the tendon), and Δ is the phase difference of light passing through the tendon. Since α varies from 0 to 360º as the polarizing sheets rotate during the test, Eq1 can be written as

$$I_{p2p\_t} = I_o \sin^2\left(\frac{\Delta}{2}\right) \tag{2}$$

where I_{p2p_t} is the tendon peak-to-peak intensity of light detected by the camera, I_o is the intensity of light passing through the polarizer, and Δ is the phase difference of light passing through the tendon. This phase difference Δ is related to the tissue birefringence (B), thickness (t), and wavelength (λ) of transmitted light as

$$\Delta = \frac{2\pi Bt}{\lambda} \tag{3}$$

Thus, a standardized peak-to-peak intensity, I_{p2p*} ($I_{p2p*} = I_{p2p\_t}/I_{p2p\_w}$), was computed for each specimen using the previously collected quarter wave plate peak-to-peak intensity (I_{p2p_w}) alignment maps. These equations assume that the initial thickness of the specimen determined from the optical-based method remains constant throughout the mechanical test. In addition, although π/λ is a scalar multiple for each specimen equivalent across all tests, we assumed λ to be 550nm as the mean wavelength of visible light. Given these assumptions, the apparent birefringence can be computed as

$$B_{app} = \frac{\lambda}{\pi t}\sin^{-1}\left(\sqrt{I_{p2p*}}\right) \tag{4}$$

2.2.6 Statistical Analysis

For statistical evaluation, one-way repeated measures ANVOAs followed by paired t-tests with Bonferroni corrections were used to evaluate the effect of fatigue loading on the change in crimp amplitude (ΔA_{crimp}) and frequency (ΔF_{crimp}) (SPSS, IBM SPSS Inc. Version 20, Armonk, New York). Two-way repeated measures ANOVAs were used to evaluate changes in region dependent crimp properties for each load and fatigue loading cycle evaluated. Significant relationships were assessed using post hoc paired T-tests (SPSS, IBM SPSS Inc. Version 20, Armonk, New York). One-way repeated measures ANOVAs were also used to determine if cycle number was a significant factor for the measured peak strain, tangent stiffness, hysteresis, and laxity. Pearson's correlation coefficients were used to determine if fatigue properties (i.e., peak strain, laxity, stiffness, hysteresis, and modulus) were correlated to the ΔA_{crimp} and ΔF_{crimp}. Significant relationships were defined as $\alpha \leq 0.05$ and trends $\alpha < 0.1$ after applying the appropriate Bonferroni correction factor.

One-way ANOVAs were used to determine whether mean mechanical and structural properties changed during healing. Properties that were significant were further analyzed with post hoc Student's T-tests. Significance was set at $\alpha = 0.05$, with Bonferroni corrections applied to account for multiple comparisons. Next, single and multiple linear regressions (Enter Method, IBM SPSS Inc. Version 20, Armonk, New York), were completed to determine if mechanical fatigue properties could be predicted from structural properties.

2.3 Results

2.3.1 Tissue-Level Mechanical Response During Fatigue Loading and Healing

After 1000 fatigue loading cycles, all tendons attained the secondary phase of fatigue loading[13] without rupture. Cycle number was a significant ($p<0.001$) factor for peak strain, tangent stiffness, hysteresis, and laxity (**Figure 2-4**). Specifically, as the number of cycles increased, the peak strain, tangent stiffness, and laxity also increased. In contrast, the hysteresis decreased through the secondary phase of fatigue loading.

All animals who underwent surgery recovered well. The whole tendon mechanical properties measured in this study were peak strain, hysteresis, damage, dynamic modulus, tangent stiffness, and cycles to failure. Injury resulted in a significant increase in tendon cross sectional area at weeks 0, 1, 3, and 6 compared to control tissue ($p<0.005$; CTRL: 0.256± 0.047mm², Week 0: 0.362 ± 0.040mm², Week 1: 0.595 ± 0.166mm², Week 3: 1.454 ± 0.829 mm², Week 6: 1.056 ± 0.219mm²). In all tests, peak cyclic strain followed the three phase pattern for fatigue testing (e.g., **Figure 2-2A**), with no statistical differences in peak strain between groups at 5%, 50%, and 95% of fatigue life (**Table 2-1**). As hypothesized, injury caused a decrease in mechanical properties that was evident throughout fatigue loading. Specifically, the number of cycles to failure decreased dramatically after week 0 (CTRL: 12075±1872 cycles, Week 0: 325±311 cycles) (37 fold), $p<0.001$), and was not significantly different after 6 weeks of healing (Week 6: 7666±977 cycles) **(Figure 2-5**). In addition, and contrary to our hypothesis, the tangent stiffness decreased from control tissue by approximately 20-30% in healing tendons (**Figure 2-5**) and did not improve with healing when compared throughout fatigue life. Furthermore, hysteresis increased following injury, but declined as the stages

of healing progressed (**Table 2-1**). As expected, damage increased with fatigue life (**Table 2-1**), but only differed statistically between healing time points at 5% of fatigue life.

The dynamic modulus decreased following injury and did not recover with healing (**Table 2-1**). Specifically, the dynamic modulus was approximately 50% of control tendon following injury and 19% of control tendon by week 6 (**Table 2-1**). Taken together in the context of changes in tendon cross sectional area, this suggests that the initial decrease in tendon tangent stiffness was the primary contributor to a loss in modulus, and increases in tissue area due to scar tissue accumulation further degrade the dynamic modulus with healing.

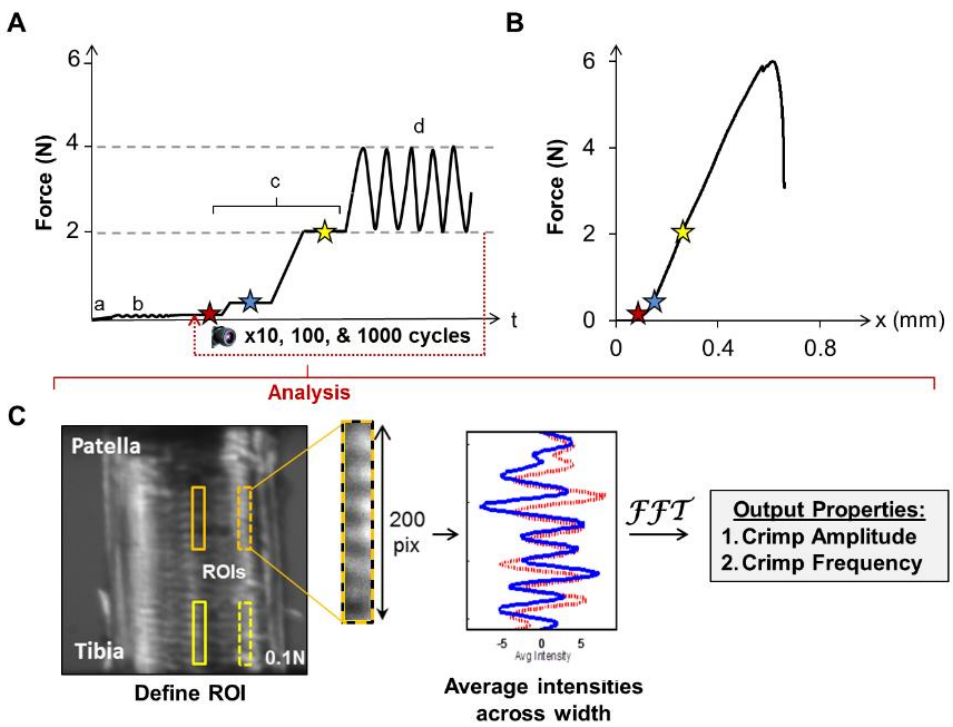

Figure 2-3. Mechanical testing and image capture protocol. (A) Tendons were preloaded (a), preconditioned (b), imaged at three loads (0.1N, 0.5N, and 2.0N) (c), and fatigue loaded (d). After 10, 100, and 1000 cycle intervals of fatigue loading, images were captured at these three loads to quantify tendon crimp properties in the toe, transition, and linear regions of a representative load-displacement curve (B). This process was repeated until tendons reached 1000 fatigue loading cycles. (C) Four ROIs were selected representing the midsubstance (orange), insertion (yellow), center (solid), and lateral (dashed) regions of

the tendon. ROIs were low pass filtered to enhance the visibility of light and dark bands and intensities were averaged across the ROI width (red dashed line) before being highpass filtered (blue line). From these spectra, the crimp amplitude and frequency were computed.

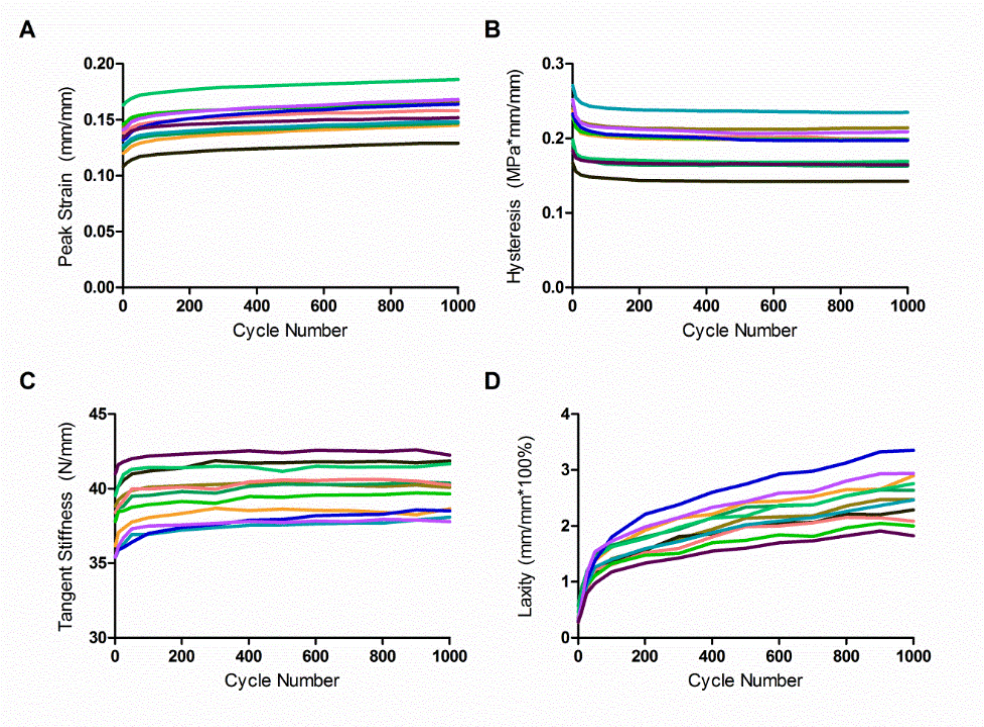

Figure 2-4. Effect of fatigue loading on tendon mechanical properties. Cycle number was a significant ($p<0.001$) factor for peak strain, tangent stiffness, hysteresis, and laxity. Individual lines indicate each specimen tested. With fatigue loading, peak strain, tangent stiffness, and laxity increased, whereas the hysteresis decreased.

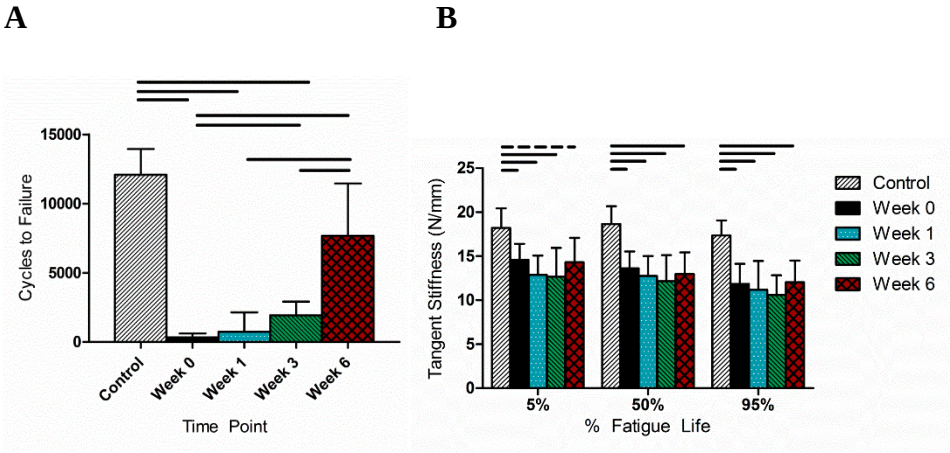

Figure 2-5: Effect of Healing on Fatigue Mechanics. (A) Following injury, the number of cycles to failure decreased dramatically (37-fold, $p<0.001$), and eventually recovered by 6 weeks of healing. Solid lines indicate significant relationships. Dashed lines indicate trends. Final specimen cohorts ranged from N=6-10 specimens, since some specimens in the earlier time points were not able to withstand the fatigue

testing protocol. Similarly, some control specimens reached a theoretical endurance limit. (**B**) Specimen tangent stiffness decreased following injury and this relationship remained consistent throughout fatigue life. On average, stiffness dropped by 25% and did not recover with healing. Final specimen cohorts ranged from N=6-10 specimens, since some specimens in the earlier time points were not able to withstand the fatigue testing protocol and some of the control specimens reached a theoretical endurance limit.

2.3.2 Collagen Fiber Structural Changes During Loading and Healing

At baseline, there were 14-18 crimps per mm, and the crimp amplitude ranged from 2.9-4.2 a.u. at 0.1N, 2.2-3.5 a.u. at 0.5N, and 1.8-2.4 a.u. at 2.0N depending on the ROI chosen. As hypothesized, fatigue loading resulted in crimp properties that were dependent on cycle number and the region of interest evaluated. The ΔA_{crimp} increased with fatigue loading (**Figure 2-6**), and demonstrated load and region dependence. At low loads (0.1N), the ΔA_{crimp} was greatest (**Figure 2-6A**). Additionally, the ΔA_{crimp} decreased at the higher loads evaluated (**Figure 2-6B,C**). In contrast, the ΔF_{crimp} decreased with fatigue loading, but this was region dependent (**Figure 2-7**). Regional variation was also evident in ΔA_{crimp} with fatigue loading (Fig. 4). The lateral region of the tendon demonstrated a larger increase in ΔA_{crimp} after 10, 100, and 1000 cycles of fatigue life at both lower loads (0.1 and 0.5N) when compared to the center region ($p<0.001$), but not at the higher load (2.0N) (**Figure 2-7**). Differences between the insertion and midsubstance regions were evident, but this response was load and cycle dependent.

Injured tendon had increased CSD (i.e., increased disorganization) by weeks 1, 3, and 6 ($p< 0.005$, **Figure 2-8),** and these changes in structure were observed throughout fatigue life at all loads tested (**Figure 2-9**). Following injury, B_{app} decreased dramatically (Figure 4B) and did not demonstrate a return to control values with healing, during fatigue life, or at the different loads measured (**Figure 2-10**). Such changes could be due

to the fact that tissue thickness alterations with healing were a dominant contributor to the birefringence calculations. The similar relationships in structural properties observed across loads and throughout tendon fatigue life primarily mirror alterations in mechanical properties with healing. However, because CSD and B_{app} do not return to baseline levels, such properties are best suited to provide insight to early and moderate stage healing, rather than end stage healing. Interestingly, if I_{p2p*} was considered (that does not account for tendon thickness changes), induction of fatigue loading increased differences observed between control and healing tendons. For example, in the low load case, no deficit in structural properties was observed by week 6, but by 50% and 95% of the fatigue life, differences in structure between groups were evident (**Figure 2-11**). This increase in measured group differences may not be detected using standard histological tests or quasi-static mechanical testing, though the present study did not test this.

2.3.3. Relationships Between Mechanics and Structure During Loading and Healing

Single linear regression analysis revealed that ΔA_{crimp} was strongly correlated to laxity at all loads and regions evaluated (r=0.72-0.89) (**Figure 2-12**). In addition, ΔA_{crimp} was correlated to tendon strain, but only at the higher load (r=0.53) at both the center midsubstance and lateral insertion regions. No other fatigue mechanical properties correlated with ΔA_{crimp} ($p>0.05$). ΔF_{crimp} was not related to any mechanical property measured ($p>0.05$).

Structural properties were able to partially predict the full mechanical response of Achilles tendons to fatigue loading. In particular, B_{app} strongly predicted dynamic modulus (R^2 = 0.88-0.92) and moderately predicted hysteresis (R^2 = 0.18-0.47) at all

loads and throughout fatigue life (**Table 2-2**). Although damage, tangent stiffness, and peak strain had significant regressions with B_{app}, these relationships were weak (**Table 2, Figure 2-10**). CSD was also able to predict dynamic modulus at all loads and throughout fatigue life (R^2 = 0.31-0.39, $p<0.001$, **Table 2-2**). At certain loads and stages of fatigue life, the tangent stiffness and hysteresis could be predicted by CSD (Table S1). Damage and peak strain showed similar relations to B_{app} and CSD. Cycles to failure could not be predicted by any structural measure. For B_{app}, all significant correlations between dependent and independent variables were positively correlated except damage and peak strain. For CSD, all significant correlations between dependent and independent variables were positively correlated except dynamic modulus, tangent stiffness, and hysteresis. As expected, these results indicate that a decrease in disorganization results in decreased damage and peak strain, and an increase in disorganization results in decreased dynamic modulus, tangent stiffness, and hysteresis. Interestingly, although B_{app} and CSD were strong predictors for certain mechanical properties, coefficients of determination generally did not improve when the two were used together in a multiple regression model (**Table 2-3**). These results demonstrate that certain tissue level structural properties determined by image-based measure directly relate to *ex vivo* tendon fatigue mechanics.

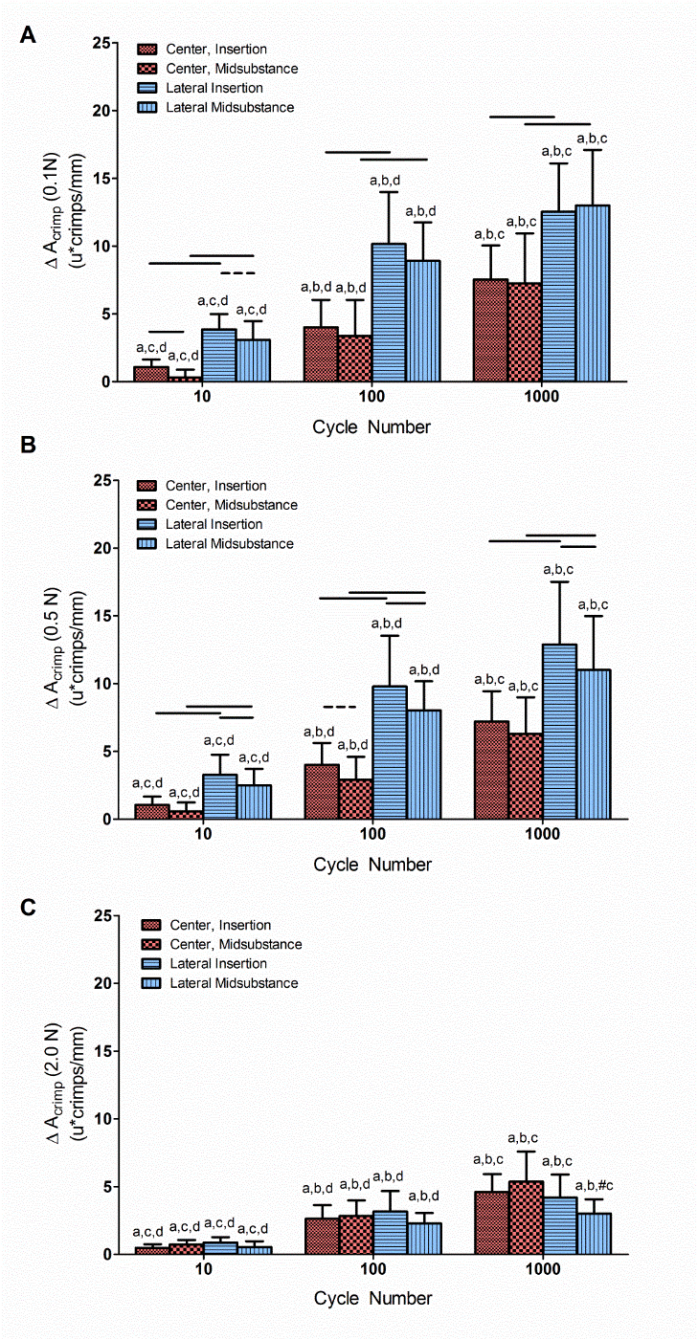

Figure 2-6. Effect of fatigue loading on crimp amplitude. Δ Crimp amplitude (ΔA_{crimp}) increased with fatigue loading when assessed at (**A**) 0.1N (representative of the toe region of the force-displacement curve), (**B**) 0.5 N (representative of the transition region of the force-displacement curve), and (**C**) 2.0 N (representative of the linear region of the force-displacement curve). The ΔA_{crimp} demonstrated a load-dependent response, with lower values at higher loads. Bars indicate significant paired differences ($p<0.0125$) between the center and lateral ROIs and their corresponding insertion and midsubstances for a tendon after 10, 100, or 1000 cycles of fatigue loading. "u" indicates an intensity unit ranging between 1 and 256. *a,b,c,d indicates significant differences ($p<0.0083$) in the ROI when compared to 0, 10, 100, and 1000 cycles, respectively. "#" indicates trends ($p<0.017$).

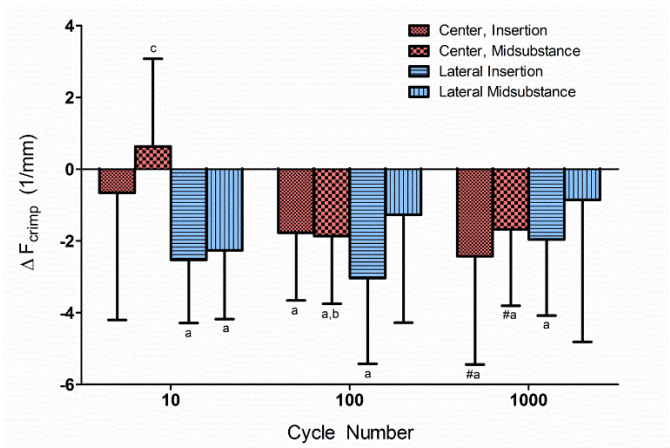

Figure 2-7. Effect of fatigue loading on crimp frequency. Δ Crimp frequency (ΔF_{crimp}) decreased with fatigue loading when assessed at 0.1N. Bars indicate significant paired differences ($p<0.0125$) between the center and lateral ROIs and their corresponding insertion and midsubstances for a tendon after 10, 100, or 1000 cycles of fatigue loading. *a,b,c,d indicates significant differences ($p<0.0083$) in the ROI when compared to 0, 10, 100, and 1000 cycles, respectively. "#" indicates trends ($p<0.017$). Data for ΔF_{crimp} at 0.5 and 2.0N are not shown since the power of crimp frequencies decreases to near the power of noise (high frequencies) at high loads. This is an unavoidable trade off with our high resolution images that does not exist in the evaluation of the ΔA_{crimp}.

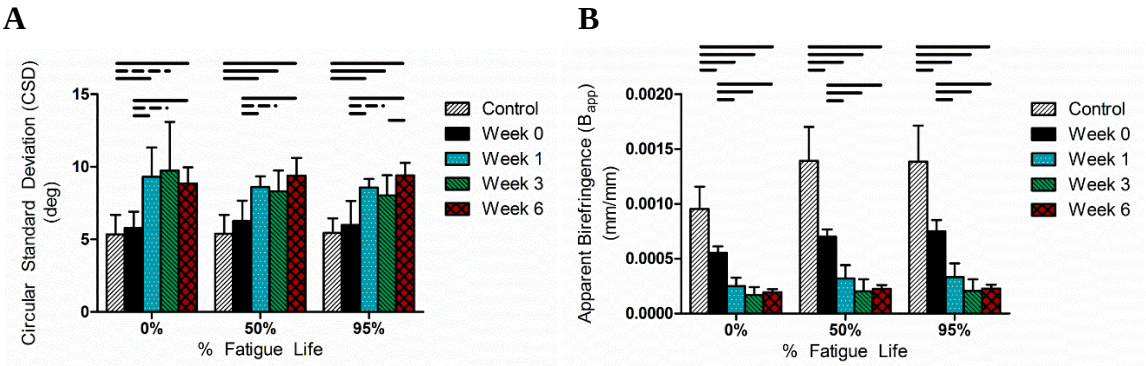

Figure 2-8: Effect of healing and fatigue on tendon structure. Assessment of (**A**) circular standard deviation (CSD) and (**B**) the apparent birefringence (B_{app}) throughout fatigue life and healing at 0.1 N. Together, these results demonstrate that the newly deposited matrix is highly disorganized throughout the specimen fatigue life. Final specimen cohorts ranged from N=4-10 specimens, since some specimens in the earlier time points were not able to withstand the fatigue testing protocol.

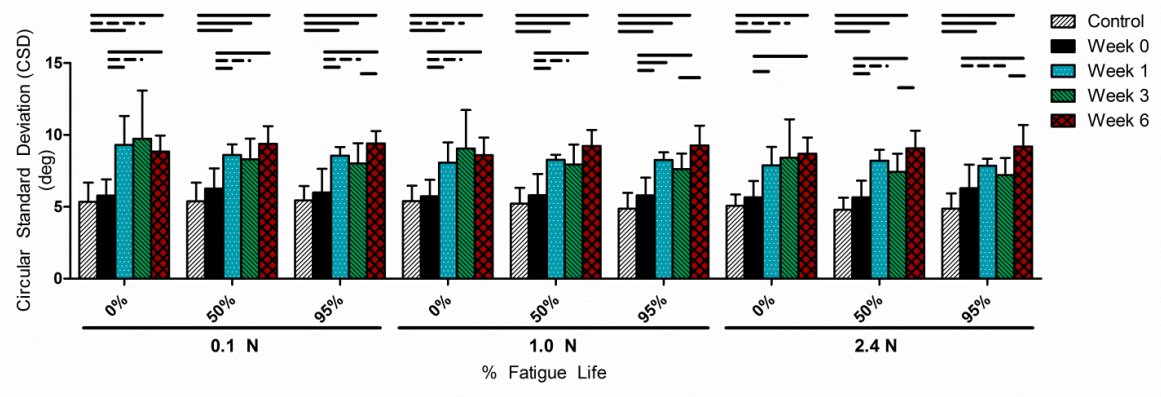

Figure 2-9: Circular standard deviation (CSD) throughout fatigue life, healing, and at all loads.

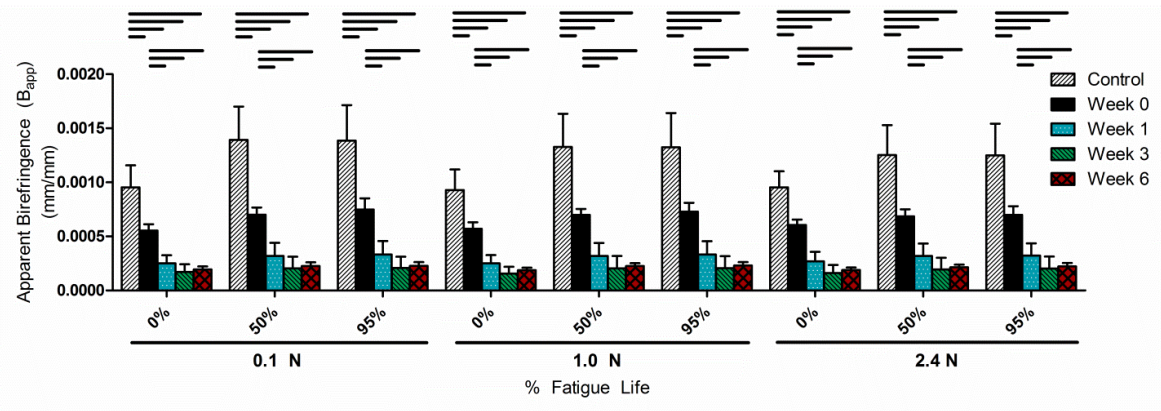

Figure 2-10: Apparent birefringence (B_{app}) throughout fatigue life, healing, and at all loads.

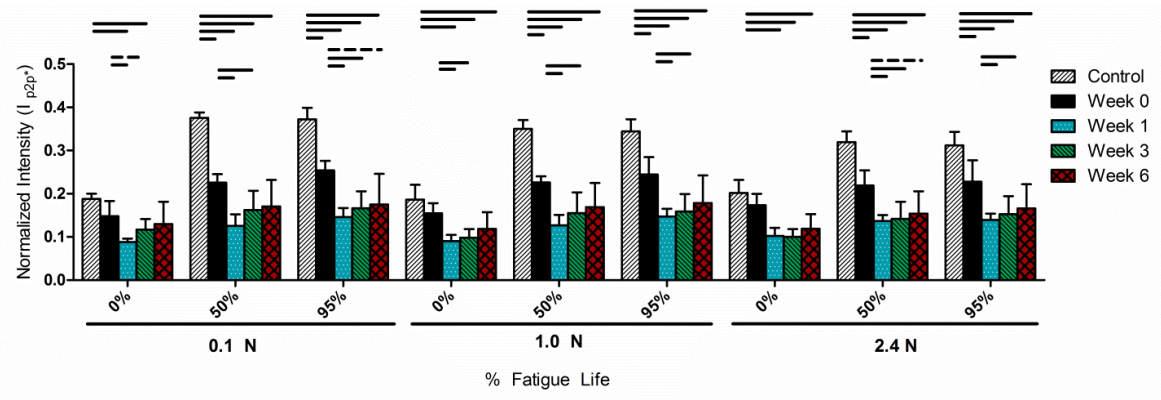

Figure 2-11: Normalized peak-to-peak intensity (I_{p2p*}) throughout fatigue life, healing, and at all loads.

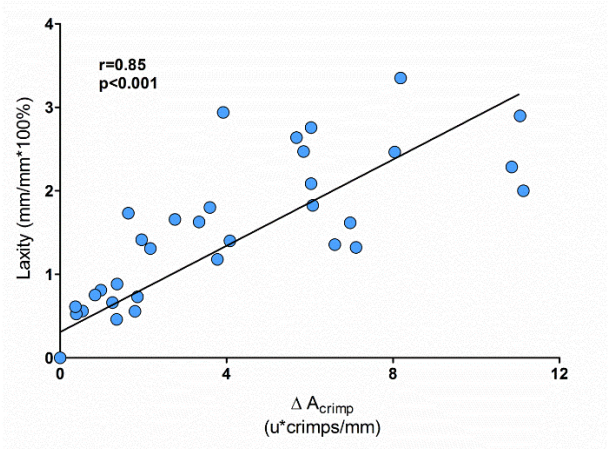

Figure 2-12. Relationship between tendon laxity and crimp amplitude. Tendon laxity (defined as the ratio of displacement from gauge length at a set threshold to the tissue displacement and displacement at a set threshold after the first cycle of fatigue loading) was strongly correlated to the change in crimp amplitude at 0.1N as assessed at 0, 10, 100, and 1000 cycles of fatigue life. This same relationship held at both higher loads (0.5N and 2.0N). "u" indicates an intensity unit ranging between 1 and 256.

Table 2-1: Mechanical parameter comparisons throughout healing and fatigue life.

		%Fatigue Life		
Parameter	**Group**	5%	50%	95%
Peak Strain (mm/mm)	CTRL	0.195 ± 0.059	0.211 ± 0.062	0.225 ± 0.074
	Week 0	0.190 ± 0.024	0.215 ± 0.029	0.248 ± 0.040
	Week 1	0.293 ± 0.104	0.325 ± 0.116	0.361 ± 0.129
	Week 3	0.324 ± 0.182	0.362 ± 0.197	0.406 ± 0.206
	Week 6	0.244 ± 0.048	0.289 ± 0.067	0.319 ± 0.079
Hysteresis (MPa*mm/mm)	CTRL	0.016 ± 0.004^{D,E}	0.014 ± 0.004^{D,E}	0.018 ± 0.003^{C,D,E}
	Week 0	0.026 ± 0.012^{D,e}	0.021 ± 0.007^{e}	0.035 ± 0.022^{d,e}
	Week 1	0.019 ± 0.011^{D}	0.017 ± 0.009	0.020 ± 0.010^{A}
	Week 3	0.006 ± 0.003^{A,B,C,E}	0.005 ± 0.003^{A}	0.007 ± 0.004^{A,b}
	Week 6	0.005 ± 0.001^{A,b,D}	0.005 ± 0.001^{A,b}	0.006 ± 0.002^{A,b}
Damage (mm/mm)	CTRL	1.68 ± 0.88^{B}	3.15 ± 0.82	4.67 ± 0.74
	Week 0	0.55 ± 0.34^{A,D,E}	2.56 ± 1.90	5.26 ± 3.14
	Week 1	1.54 ± 1.38	2.96 ± 0.65	6.88 ± 4.32
	Week 3	2.41 ± 1.15^{B}	5.26 ± 2.81	8.29 ± 3.58
	Week 6	2.43 ± 0.64^{B}	5.99 ± 3.64	8.47 ± 4.93
Dynamic Modulus (MPa)	CTRL	359.7 ± 98.0^{B,C,D,E}	368.9 ± 103.0 ^{B,C,D,E}	371.4 ± 109.9 ^{B,C,D,E}
	Week 0	179.7 ± 29.8^{A,C,D,E}	167.8 ± 28.8 ^{A,C,D,E}	146.8 ± 34.6 ^{A,D,E}
	Week 1	106.8 ± 31.2^{A,B,E}	106.1 ± 33.1^{A,B,E}	93.8 ± 39.0 ^{A,e}
	Week 3	64.0 ± 43.2^{A,B}	61.6 ± 41.9 ^{A,B}	53.7 ± 37.3 ^{A,B}
	Week 6	68.8 ± 18.4^{A,B,C}	62.4 ± 17.2 ^{A,B,C}	58.0 ± 17.0 ^{A,B,c}

$*^{A,B,C,D,E}$ denotes significant differences ($p<0.005$) from control, week 0, week 1, week 3, and week 6 specimens, respectively. ^{a,b,c,d,e} denotes a trend ($p<0.01$) from control, week 0, week 1, week 3, and week 6 specimens, respectively.

Table 2-2: Single linear regressions for structural and mechanical properties.

Parameter	B r	R^2	p	CSD r	R^2	p
Dynamic Modulus (MPa)	(0.94, 0.96)	(0.88, 0.92)	<0.001	(-0.56, -0.62)	(0.31, 0.39)	<0.001
Damage (mm/mm)	(-0.35, -0.49)	(0.12, 0.24)	(NS, 0.009)	(0.08, 0.29)	(0.00, 0.08)	NS
Tangent Stiffness (N/mm)	(0.46, 0.65)	(0.21, 0.42)	(0.004, <0.001)	(-0.24, -0.43)	(0.05, 0.18)	(NS, 0.007)
Peak Strain (mm/mm)	(-0.40, -0.49)	(0.16, 0.24)	(0.013, 0.003)	(0.05, 0.28)	(0.00, 0.08)	NS
Hysteresis (MPa*mm/mm)	(0.43, 0.69)	(0.18, 0.47)	(0.007, <0.001)	(-0.27, -0.52)	(0.07, 0.27)	(NS, <0.001)
Cycles to Failure	(0.21, 0.30)	(0.05, 0.09)	NS	(-0.08, 0.17)	(0.00, 0.03)	NS

*For each load, data are shown as ranges (min, max) between 5 and 95% of tendon fatigue life and all loads. Parameters with non-significant coefficients of determination are indicated as "NS."

Table 2-3: Single and multiple linear regressions for structural and mechanical properties.

		Single				Multiple	
		B		CSD		B and CSD	
Parameter	Load	R^2	p	R^2	p	R^2	p
Dynamic Modulus (MPa)	0.1N	(0.88, 0.92)	<0.001	(0.32, 0.37)	<0.001	(0.88, 0.92)	<0.001
	1.0N	(0.90, 0.92)	<0.001	(0.37, 0.38)	<0.001	(0.90, 0.92)	<0.001
	2.4N	(0.88, 0.91)	<0.001	(0.31, 0.39)	<0.001	(0.88, 0.91)	<0.001
Laxity (mm/mm* 100%)	0.1N	(0.12, 0.18)	(NS, 0.009)	(0.03, 0.08)	NS	(0.12, 0.18)	NS
	1.0N	(0.12, 0.21)	(NS, 0.004)	(0.05, 0.05)	NS	(0.12, 0.22)	NS
	2.4N	(0.13, 0.24)	(NS, 0.002)	(0.00, 0.05)	NS	(0.13, 0.29)	(NS, 0.010)
Tangent Stiffness (N/mm)	0.1N	(0.21, 0.42)	(0.004, <0.001)	(0.12, 0.18)	(NS, 0.007)	(0.22, 0.37)	(NS, <0.001)
	1.0N	(0.22, 0.40)	(0.004, <0.001)	(0.13, 0.14)	NS	(0.22, 0.41)	(NS, <0.001)
	2.4N	(0.23, 0.39)	(0.002, <0.001)	(0.05, 0.12)	NS	(0.24, 0.39)	(NS, <0.001)
Peak Strain (mm/mm)	0.1N	(0.16, 0.24)	(0.013, 0.003)	(0.01, 0.08)	NS NS	(0.16, 0.26)	NS
	1.0N	(0.19, 0.23)	(0.006, 0.003)	(0.02, 0.02)	NS	(0.23, 0.29)	NS
	2.4N	(0.20, 0.23)	(0.006, 0.003)	(0.00, 0.02)		(0.26, 0.32)	NS
Hysteresis (MPa* mm/mm)	0.1N	(0.18, 0.40)	(0.007, <0.001)	(0.11, 0.24)	(NS, 0.002)	(0.13, 0.43)	(NS, <0.001)
	1.0N	(0.23, 0.44)	(0.003, <0.001)	(0.10, 0.27)	(NS, <0.001)	(0.23, 0.45)	(NS, <0.001)
	2.4N	(0.24, 0.47)	(0.002, <0.001)	(0.07, 0.26)	(NS, 0.002)	(0.24, 0.47)	(NS, <0.001)

Cycles to Failure	0.1N	(0.07, 0.09)	NS	(0.00, 0.02)	NS	(0.08, 0.24)	NS
	1.0N	(0.06, 0.08)	NS	(0.00, 0.03)	NS	(0.10, 0.27)	NS
	2.4N	(0.05, 0.07)	NS	(0.00, 0.02)	NS	(0.09, 0.24)	NS

*For each load, data are shown as ranges (min, max) between 5 and 95% of tendon fatigue life. Parameters with non-significant coefficients of determination are indicated as "NS."

2.4 Discussion

Given that many tendons typically performs at high and repetitive loads at or near failure,[59,60] the clinical importance of utilizing methods to test this tendon at physiological levels via fatigue loading becomes increasingly evident.[13,14,16,17,52,61-64] This work evaluated real-time tendon crimp and mechanical properties nondestructively during tendon fatigue life using a plane polariscope. Additionally, we quantified tendon mechanical and structural properties during fatigue loading following acute injury to the Achilles tendon.

Results demonstrated that fatigue loading altered crimp properties and that this response was both region and load dependent. Such work is novel since it evaluated the effects of fatigue loading on tendon structure at several regions and loads simultaneously. This methodology provides further support for potential translation of other real-time structure-based assays, such as ultrasound,[34] into *in vivo* systems to assess tendon mechanics. Additionally, this study provides a significant advancement to the tendon literature since quasi-static mechanical testing to evaluate the effects of healing may not capture the same sub-rupture induction mechanism acquired during fatigue loading.[35] For tendons undergoing rigorous cyclic loading, such as the Achilles, it is of particular importance to accurately elucidate the fundamental mechanisms governing fatigue induced tendon failure. Knowledge of structural properties throughout fatigue loading and healing and their relationship to tendon mechanical properties further suggests

potential metrics for image-based measures to assess tissue mechanical integrity and serve as benchmarks for tissue engineering strategies.

The ΔA_{crimp} was region dependent, but region specific differences were muted at high loads. This supports the concept that crimp remains a primary factor at lower loads in the toe and transition regions of mechanical loading, but this response may be altered with fatigue loading. Furthermore, the regional difference in uncrimping across the tendon width and length, supports the observation that the structural response of collagen fibrils to loading is non-uniform.[2] Regional differences in crimp properties across the patellar tendon width may be expected as a result of physiologic *in vivo* function. Variation in fibril area fraction has been demonstrated across the patellar tendon thickness,[36] which may be due to the six degrees-of-freedom motion the patella[37] and adjacent patellar tendon experiences during knee flexion/extension. Changes in crimp properties across the tendon length may be explained by the transition in mechanical properties from the tendon midsubstance to its fibrocartilagenous insertion.[38] Similar changes in crimp properties with load have been observed in the supraspinatus.[2]

Several studies have measured structural changes in tendon following fatigue loading.[13,15,18,22,39-41] Structural assessment following fatigue loading has ranged from histology,[13] second harmonic generation,[19-21,39] polarized light imaging,[18] scanning electron microscopy,[40] and confocal imaging using photo bleaching.[42] However, few measures of tendon fatigue mechanics have been reported,[22,40,42] and only one study reported correlations between structure changes in tendon and fatigue loading.[18] Further, our observed changes in crimp properties throughout fatigue life were more dramatic than previous reports assessing disorganization with fatigue loading.[21,35,43] It is possible that

evaluation of tendon crimp alterations with fatigue loading provides a more sensitive and mechanistic description than other metrics, such as the damage area fraction.[21] In addition, recent studies have suggested that repeated subrupture loading results in fibril kinks that occur at distinct spacing intervals.[41] Such changes have been shown to primarily occur early during repeated loading at the nanostructural level,[40] which was also observed in this study for ΔA_{crimp} at the fascicle level. Thus, this provides support that fatigue loading alters collagen structure at several hierarchical levels of the tendon.

The strong relationship between ΔA_{crimp} and tendon laxity demonstrates both the use of laxity[27] as a parameter for modeling the response of patellar tendon to fatigue loading, and ΔA_{crimp} as an indicator of the progression of tendon laxity. The strong relationships between structural metrics and fatigue loading have not been reported previously, with only qualitative relationships presented.[13,15,19-21,39,42] Such changes may also be incorporated into structural fit fiber recruitment models[44] for the application of modeling tendon's response to fatigue loading. Although B_{app} and CSD were strong predictors of the dynamic modulus and moderate predictors of hysteresis, when they were used together in multiple regression analysis, their respective coefficients of determination did not advance, likely due to the fact that the two parameters are not independent. Additionally, since the regressions between structure and mechanics were similar across all loads and throughout fatigue life, this study demonstrates that such relationships are robust and should continue to be investigated. Although certain whole tissue structural properties correlated to mechanical parameters, the number of cycles to failure did not. This suggests that the structural mechanism governing this property originates from local damage accumulation rather than whole tissue level diffuse damage.

The primary limitation of the study was that relationships linking the induction of fatigue loading with concurrent cellular mechanisms were not investigated.[45] Such effects likely have profound implications on the extracellular matrix, as well as the intracellular milieu in the tendon that may promote matrix remodeling or degeneration. Another potential limitation is that tendon mechanical and structural recovery following fatigue loading was not investigated. However, all tendons followed the standard multiphase pattern of fatigue life.[13] Pilot tests evaluating the effect of a 45 minute recovery period following 1000 cycles of our fatigue loading protocol showed that whole tendon strain recovered less than 5%, and that this recovery was muted within 25 cycles of fatigue loading (data not shown). Therefore, we believe our fatigue protocol to be mechanically damaging, and suggest that our measure of nonrecoverable laxity in this study can be considered metrics of mechanical damage.[18,26-28] Additionally, given that fluid comprises 70% of the tendon wet weight,[31,46] it is possible that the alterations in ΔA_{crimp} observed were due to fluid exudation from the tendon.[9,47,48] Although tensile stress can cause induced lateral contraction independent of uncrimping,[9] this mechanism in the context of fatigue loading warrants future investigation. Another limitations is that no biological mechanisms were investigated that may further help elucidate the molecular events that govern changes in structural and mechanical properties during fatigue loading. For example, collagen type and other matrix components may be contributing factors to the overall tissue birefringence. Additionally, the injury made was acute and does not necessarily resemble the pattern seen in an acute Achilles rupture that may originate from preexisting damage. However, this injury method has previously been shown to be highly repeatable [24] and has been applied to study the dynamic properties of tendons.[52] Finally,

other factors may contribute to fatigue damage induction and progression, such as reductions in fibril continuity, and the role of glycosaminoglycans and other small matrix molecules.[49,50] Future studies will examine the effects of aging, additional tendon types,[51] pathology, and knockout models on fatigue mechanics and crimp properties.

Despite a modest improvement in the number of cycles to failure with healing, the initial decrease in tangent stiffness, dynamic modulus, hysteresis, and damage with injury did not recover through 6 weeks of healing. These changes were in agreement with previous work that found that the modulus decreased throughout healing in conjunction with increased tendon cross sectional area.[23,24] Thus, it is likely that a later healing time point may be necessary (e.g., 12 weeks)[65] to show full improved mechanical properties throughout fatigue life due to healing.

Several studies have used fatigue loading to induce damage in tissue,[13-15,39] investigate theoretical endurance limits in tendon,[16,17,64] quantify subsequent biological changes,[45,68,69] and identify potential causes of failure.[40,41] Although the specific structural mechanisms leading to failure were not investigated in the current study, Veres and colleagues have suggested that repeated subrupture loading results in fibril denaturation events that form progressive fibril kinks and the accumulation of damage in bovine tail tendons.[40,41] Such changes have been shown to primarily occur early during repeated loading,[40] which was also observed in the current study. In addition, our laboratory has recently developed a novel method to investigate crimp during mechanical testing,[31] which could be another imaged-based metric for subrupture damage accumulation. Still, other factors may contribute to the progression to failure in healing

tissues, such as reductions in fibril continuity, and the role of glycosaminoglycans and other small matrix molecules.[49,50]

In conclusion, this study revealed alterations in tendon crimp and mechanical properties nondestructively, and in real-time, during fatigue loading. This work may lead to improved diagnostic imaging methods based on tissue-level structural measures to assess injured and healing tendons, which may ultimately improve patient monitoring. Although periodic crimp in tendon has been studied using high-magnification optical microscopy,[2] electron microscopy,[70] optical coherence tomography,[71] and second harmonic generation,[72] its study using polarized light microscopy[4,9] has been limited. While decreases in tangent stiffness, dynamic modulus, and hysteresis are detected during healing, the most sensitive measure was cycles to failure. Knowledge that measured tendon stiffness drops by 25% whereas the number of cycles to failure decreases by nearly 37-fold was not expected and importantly, demonstrates that tissue properties only assessing stiffness metrics may provide an incomplete description of actual tissue healing. Thus, this information obtained at the early stages of healing is critical to fully characterize the healing response. The structural parameters B_{app} and CSD show promise as potentially translatable metrics to predict tendon dynamic modulus and hysteresis, yet the majority of mechanical parameters could only be predicted weakly, suggesting the need for additional experiments investigating structure-function relationships in tendon studying the response to fatigue loading. In light of our findings and the low cost of our system ($<1000), this methodology presents both a robust and economic opportunity for understanding structure function relationships of tendons.

2.5 References

1. Franchi M, Fini M, Quaranta M, et al. Crimp morphology in relaxed and stretched rat Achilles tendon. *J Anat.* Jan 2007;210(1):1-7.
2. Miller KS, Connizzo BK, Feeney E, Soslowsky LJ. Characterizing local collagen fiber re-alignment and crimp behavior throughout mechanical testing in a mature mouse supraspinatus tendon model. *J Biomech.* Aug 9 2012;45(12):2061-2065.
3. Diamant J, Keller A, Baer E, Litt M, Arridge RG. Collagen; ultrastructure and its relation to mechanical properties as a function of ageing. *Proc R Soc Lond B Biol Sci.* Mar 14 1972;180(1060):293-315.
4. Rigby BJ, Hirai N, Spikes JD, Eyring H. The Mechanical Properties of Rat Tail Tendon. *J Gen Physiol.* Nov 1 1959;43(2):265-283.
5. Soslowsky LJ, Thomopoulos S, Tun S, et al. Neer Award 1999. Overuse activity injures the supraspinatus tendon in an animal model: a histologic and biomechanical study. *J Shoulder Elbow Surg.* Mar-Apr 2000;9(2):79-84.
6. Fox AJ, Schar MO, Wanivenhaus F, et al. Fluoroquinolones Impair Tendon Healing in a Rat Rotator Cuff Repair Model: A Preliminary Study. *Am J Sports Med.* Aug 20 2014.
7. Lujan TJ, Underwood CJ, Jacobs NT, Weiss JA. Contribution of glycosaminoglycans to viscoelastic tensile behavior of human ligament. *J Appl Physiol (1985).* Feb 2009;106(2):423-431.
8. Dunkman AA, Buckley MR, Mienaltowski MJ, et al. Decorin expression is important for age-related changes in tendon structure and mechanical properties. *Matrix Biol.* Jan 2013;32(1):3-13.

9. Buckley MR, Sarver JJ, Freedman BR, Soslowsky LJ. The dynamics of collagen uncrimping and lateral contraction in tendon and the effect of ionic concentration. *J Biomech.* Sep 3 2013;46(13):2242-2249.

10. Dale WC, Baer E. Fiber-Buckling in Composite Systems - Model for Ultrastructure of Uncalcified Collagen Tissues. *J Mater Sci.* 1974;9(3):369-382.

11. Elliott DH. Structure and Function of Mammalian Tendon. *Biol Rev Camb Philos Soc.* Aug 1965;40:392-421.

12. Maganaris CN, Paul JP. In vivo human tendon mechanical properties. *J Physiol.* Nov 15 1999;521 Pt 1:307-313.

13. Fung DT, Wang VM, Laudier DM, et al. Subrupture tendon fatigue damage. *J Orthop Res.* Feb 2009;27(2):264-273.

14. Wren TA, Lindsey DP, Beaupre GS, Carter DR. Effects of creep and cyclic loading on the mechanical properties and failure of human Achilles tendons. *Ann Biomed Eng.* Jun 2003;31(6):710-717.

15. Fung DT, Wang VM, Andarawis-Puri N, et al. Early response to tendon fatigue damage accumulation in a novel in vivo model. *J Biomech.* Jan 19 2010;43(2):274-279.

16. Wang XT, Ker RF, Alexander RM. Fatigue rupture of wallaby tail tendons. *J Exp Biol.* Mar 1995;198(Pt 3):847-852.

17. Schechtman H, Bader DL. In vitro fatigue of human tendons. *J Biomech.* Aug 1997;30(8):829-835.

18. Freedman BR, Sarver JJ, Buckley MR, Voleti PB, Soslowsky LJ. Biomechanical and structural response of healing Achilles tendon to fatigue loading following acute injury. *J Biomech.* Nov 11 2013.

19. Fung DT, Sereysky JB, Basta-Pljakic J, et al. Second harmonic generation imaging and Fourier transform spectral analysis reveal damage in fatigue-loaded tendons. *Ann Biomed Eng.* May 2010;38(5):1741-1751.

20. Ros SJ, Andarawis-Puri N, Flatow EL. Tendon extracellular matrix damage detection and quantification using automated edge detection analysis. *J Biomech.* Nov 15 2013;46(16):2844-2847.

21. Sereysky JB, Andarawis-Puri N, Ros SJ, Jepsen KJ, Flatow EL. Automated image analysis method for quantifying damage accumulation in tendon. *J Biomech.* Sep 17 2010;43(13):2641-2644.

22. Thorpe CT, Riley GP, Birch HL, Clegg PD, Screen HR. Effect of fatigue loading on structure and functional behaviour of fascicles from energy-storing tendons. *Acta Biomater.* Jul 2014;10(7):3217-3224.

23. Gimbel JA, Van Kleunen JP, Williams GR, Thomopoulos S, Soslowsky LJ. Long durations of immobilization in the rat result in enhanced mechanical properties of the healing supraspinatus tendon insertion site. *J Biomech Eng.* Jun 2007;129(3):400-404.

24. Beason DP, Kuntz AF, Hsu JE, Miller KS, Soslowsky LJ. Development and evaluation of multiple tendon injury models in the mouse. *J Biomech.* Mar 7 2012.

25. Favata M. *Scarless Healing in the Fetus: Implications and Strategies for Postnatal Tendon Repair*: Bioengineering, University of Pennsylvania; 2006.

26. Duenwald-Kuehl S, Kondratko J, Lakes RS, Vanderby R, Jr. Damage mechanics of porcine flexor tendon: mechanical evaluation and modeling. *Ann Biomed Eng.* Aug 2012;40(8):1692-1707.

27. Provenzano PP, Heisey D, Hayashi K, Lakes R, Vanderby R, Jr. Subfailure damage in ligament: a structural and cellular evaluation. *J Appl Physiol.* Jan 2002;92(1):362-371.

28. Quinn KP, Lee KE, Ahaghotu CC, Winkelstein BA. Structural changes in the cervical facet capsular ligament: potential contributions to pain following subfailure loading. *Stapp Car Crash J.* Oct 2007;51:169-187.

29. Lake SP, Miller KS, Elliott DM, Soslowsky LJ. Effect of fiber distribution and realignment on the nonlinear and inhomogeneous mechanical properties of human supraspinatus tendon under longitudinal tensile loading. *J Orthop Res.* Dec 2009;27(12):1596-1602.

30. Glazer A, Lewis, JG., Kaminsky, W. An Automatic Optical Imaging System for Birefringent Media. *Proceedings: Mathematical, Physical and Engineering Sciences.* 1996;452(1955):2751-2765.

31. Buckley MR, Sarver JJ, Freedman BR, Soslowsky LJ. The dynamics of collagen uncrimping and lateral contraction in tendon and the effect of ionic concentration. *J Biomech.* Jul 19 2013.

32. Timoshenko S, Goodier, J.N. *Theory of Elasticity*. 3 ed. New York: McGraw-Hill; 1969.

33. Silva DF, Gomes AS, de Campos Vidal B, Ribeiro MS. Birefringence and second harmonic generation on tendon collagen following red linearly polarized laser irradiation. *Ann Biomed Eng.* Apr 2013;41(4):752-762.

34. Riggin CN, Sarver JJ, Freedman BR, Thomas SJ, Soslowsky LJ. Analysis of Collagen Organization in Mouse Achilles Tendon Using High-Frequency Ultrasound Imaging. *J Biomech Eng.* Dec 1 2013.

35. Shepherd JH, Screen HR. Fatigue loading of tendon. *Int J Exp Pathol.* Aug 2013;94(4):260-270.

36. Hansen P, Haraldsson BT, Aagaard P, et al. Lower strength of the human posterior patellar tendon seems unrelated to mature collagen cross-linking and fibril morphology. *J Appl Physiol (1985).* Jan 2010;108(1):47-52.

37. Freedman BR, Sheehan FT. Predicting three-dimensional patellofemoral kinematics from static imaging-based alignment measures. *J Orthop Res.* Mar 2013;31(3):441-447.

38. Thomopoulos S, Marquez JP, Weinberger B, Birman V, Genin GM. Collagen fiber orientation at the tendon to bone insertion and its influence on stress concentrations. *J Biomech.* 2006;39(10):1842-1851.

39. Sereysky JB, Andarawis-Puri N, Jepsen KJ, Flatow EL. Structural and mechanical effects of in vivo fatigue damage induction on murine tendon. *J Orthop Res.* Jun 2012;30(6):965-972.

40. Veres SP, Harrison JM, Lee JM. Repeated subrupture overload causes progression of nanoscaled discrete plasticity damage in tendon collagen fibrils. *J Orthop Res.* May 2013;31(5):731-737.

41. Veres SP, Lee JM. Designed to fail: a novel mode of collagen fibril disruption and its relevance to tissue toughness. *Biophys J.* Jun 20 2012;102(12):2876-2884.

42. Thorpe CT, Riley GP, Birch HL, Clegg PD, Screen HR. Fascicles from energy-storing tendons show an age-specific response to cyclic fatigue loading. *J R Soc Interface.* Mar 6 2014;11(92):20131058.

43. Parent G, Huppe N, Langelier E. Low stress tendon fatigue is a relatively rapid process in the context of overuse injuries. *Ann Biomed Eng.* May 2011;39(5):1535-1545.

44. Peltz CD, Sarver JJ, Dourte LM, Wurgler-Hauri CC, Williams GR, Soslowsky LJ. Exercise following a short immobilization period is detrimental to tendon properties and joint mechanics in a rat rotator cuff injury model. *J Orthop Res.* Jul 2010;28(7):841-845.

45. Andarawis-Puri N, Sereysky JB, Sun HB, Jepsen KJ, Flatow EL. Molecular response of the patellar tendon to fatigue loading explained in the context of the initial induced damage and number of fatigue loading cycles. *J Orthop Res.* Aug 2012;30(8):1327-1334.

46. Ethier C, Simmons C. *Introductory Biomechanics: From Cells to Organisms*: Cambridge Texts in Biomedical Engineering

2007.

47. Hannafin JA, Arnoczky SP. Effect of cyclic and static tensile loading on water content and solute diffusion in canine flexor tendons: an in vitro study. *J Orthop Res.* May 1994;12(3):350-356.

48. Ahmadzadeh H, Freedman B, Connizzo B, Soslowsky L, Shenoy V. A micromechanical poroelastic finite element model of tendon that predicts large Poisson's ratio and water expulsion under tensile loading *Acta Biomaterialia.* 2014;In review.

49. Provenzano PP, Vanderby R, Jr. Collagen fibril morphology and organization: implications for force transmission in ligament and tendon. *Matrix Biol.* Mar 2006;25(2):71-84.

50. Ahmadzadeh H CB, Freedman BR, Soslowsky LJ, Shenoy VB. Determining the Contribution of Glycosaminoglycans to Tendon Mechanical Properties with a Modified Shear-Lag Model. *Journal of Biomechanics.* 2013;in press.

51. Shepherd JH, Legerlotz K, Demirci T, Klemt C, Riley GP, Screen HR. Functionally distinct tendon fascicles exhibit different creep and stress relaxation behaviour. *Proc Inst Mech Eng H.* Jan 2014;228(1):49-59.

52. Dunkman B, Mienaltowski,Adams, Thomas, Satchell, Kumar, Pathmanathan, Beason; Iozzo, Birk, Soslowsky Decorin Expression Is Required for Age-Related Changes in Tendon Structure and Mechanical Properties *Matrix Biol.* 2012((in review)).

53. Quinn KP, Winkelstein BA. Altered collagen fiber kinematics define the onset of localized ligament damage during loading. *J Appl Physiol (1985).* Dec 2008;105(6):1881-1888.

54. Buckley MR DA, Reuther KE, Kumar AK, Pathmanathan L, Beason DP, Birk DE, Soslowsky LJ. Validation of an Empirical Damage Model for Aging and In

Vivo Injury of the Murine Patellar Tendon. *Journal of Biomechanical Engineering.* 2013;135(April).

55. Suchak AA, Bostick G, Reid D, Blitz S, Jomha N. The incidence of Achilles tendon ruptures in Edmonton, Canada. *Foot Ankle Int.* Nov 2005;26(11):932-936.

56. Maffulli N, Waterston SW, Squair J, Reaper J, Douglas AS. Changing incidence of Achilles tendon rupture in Scotland: a 15-year study. *Clin J Sport Med.* Jul 1999;9(3):157-160.

57. AAOS. Guideline on the Diagnosis and Treatment of Acute Achilles Tendon Rupture. 2009.

58. Chiodo CP, Glazebrook M, Bluman EM, et al. Diagnosis and treatment of acute Achilles tendon rupture. *The Journal of the American Academy of Orthopaedic Surgeons.* Aug 2010;18(8):503-510.

59. Fukashiro S, Komi PV, Jarvinen M, Miyashita M. In vivo Achilles tendon loading during jumping in humans. *Eur J Appl Physiol Occup Physiol.* 1995;71(5):453-458.

60. Komi PV, Fukashiro S, Jarvinen M. Biomechanical loading of Achilles tendon during normal locomotion. *Clin Sports Med.* Jul 1992;11(3):521-531.

61. Dourte LM, Pathmanathan L, Jawad AF, et al. Influence of decorin on the mechanical, compositional, and structural properties of the mouse patellar tendon. *J Biomech Eng.* Mar 2012;134(3):031005.

62. Fessel G, Snedeker JG. Evidence against proteoglycan mediated collagen fibril load transmission and dynamic viscoelasticity in tendon. *Matrix Biol.* Oct 2009;28(8):503-510.

63. Ikoma K, Kido M, Nagae M, et al. Effects of stress-shielding on the dynamic viscoelasticity and ordering of the collagen fibers in rabbit Achilles tendon. *J Orthop Res.* Jul 6 2013.

64. Schechtman H, Bader DL. Fatigue damage of human tendons. *J Biomech.* Mar 2002;35(3):347-353.

65. Carpenter JE, Thomopoulos S, Flanagan CL, DeBano CM, Soslowsky LJ. Rotator cuff defect healing: a biomechanical and histologic analysis in an animal model. *J Shoulder Elbow Surg.* Nov-Dec 1998;7(6):599-605.

66. Nagase S, Yamanari M, Tanaka R, et al. Anisotropic alteration of scleral birefringence to uniaxial mechanical strain. *PLoS One.* 2013;8(3):e58716.

67. Yamanari M, Ishii K, Fukuda S, et al. Optical rheology of porcine sclera by birefringence imaging. *PLoS One.* 2012;7(9):e44026.

68. Andarawis-Puri N, Sereysky JB, Jepsen KJ, Flatow EL. The relationships between cyclic fatigue loading, changes in initial mechanical properties, and the in vivo temporal mechanical response of the rat patellar tendon. *J Biomech.* Jan 3 2012;45(1):59-65.

69. Legerlotz K, Jones GC, Screen HR, Riley GP. Cyclic loading of tendon fascicles using a novel fatigue loading system increases interleukin-6 expression by tenocytes. *Scand J Med Sci Sports.* Nov 3 2011.

70. Dlugosz J, Gathercole LJ, Keller A. Transmission Electron-Microscope Studies and Their Relation to Polarizing Optical Microscopy in Rat Tail Tendon. *Micron.* 1978;9(2):71-82.

71. Hansen KA, Weiss JA, Barton JK. Recruitment of tendon crimp with applied tensile strain. *J Biomech Eng.* Feb 2002;124(1):72-77.

72. Goulam Houssen Y, Gusachenko I, Schanne-Klein MC, Allain JM. Monitoring micrometer-scale collagen organization in rat-tail tendon upon mechanical strain using second harmonic microscopy. *J Biomech.* Jul 28 2011;44(11):2047-2052.

CHAPTER III: MULTISCALE MECHANICAL, STRUCTURAL, AND COMPOSITIONAL RESPONSE OF TENDON TO *QUASI-STATIC* LOADING DURING HEALING

3.1 Introduction

The extracellular matrix (ECM) is a major component of the biomechanical environment with which tendon cells (tenocytes) interact. Alterations to tendon due to injury may create pathological conditions across several length scales. Aberrant tissue phenotypes caused by acute and chronic tendon ruptures are exemplified not only at transcript and protein levels, but also include disorganized collagen structure, inferior mechanical properties, and reduced *in vivo* limb function in animals.[1-5] Following injury, tendons are mechanically, structurally, and biologically altered.[6] With healing, cell number and density gradually return to baseline values,[6] but scarred portions may remain disorganized with associated inferior mechanical properties.[7] Examples of inferior quasi-static mechanical properties following injury include decreased ultimate stress, maximum load, stiffness, elongation to failure, modulus, and stress relaxation.[5,6,8] Together, these findings suggest that healing results in altered tendon compositional properties that likely reflect the structural and mechanical quality of the newly deposited tissue.

Restoration of multiscale mechanical, structural, and compositional properties following injury may indicate a return to normal tendon phenotype. As tendon is a load-bearing tissue that undergoes highly nonlinear behavior during loading, quantification of properties at several stresses and strains is particularly important. Tendons allow for multiscale strain transfer, the relationship of strains between structural hierarchies of materials, due to their fiber-reinforced structure as stresses and strains are transferred from muscle to bone during loading.[9,10] For example, tendon stiffness increases with

strain, as disorganized ECM at the fascicle, fiber, and fibril levels becomes more aligned and less crimped.[11-13] However, defining the relationships of these properties with applied strain has been limited. Previous work has shown that tissue level strains correlate with cellular and nuclear strains in uninjured tendons (as well as other fiber-reinforced tissues such as meniscus and electrospun scaffolds) during *quasi-static* tensile loading.[14,15] Han and colleagues found that mean strain was heterogeneous and attenuated at the local matrix level in native tissues, unlike scaffolds. Additionally, proteoglycan (PG)-rich microdomains were identified containing cells that experienced increased strain attenuation compared to cells in neighboring fibrous regions. In injured tissues, the formation of PG-rich inclusions has been implicated to attenuate strain transfer to cells that may contribute to their ability to maintain homeostasis.[15] Although tissue and cellular level strains correlate in normal uninjured tissues during *quasi-static* tensile loading,[15] such studies have not investigated the clinically important effects of tendon healing. It remains unknown how ECM stresses are altered in tendon *healing*, which may propagate to alter strain transfer to cellular components.

The objective of this study was to evaluate the multiscale mechanical, structural, and compositional response of uninjured and healing tendon to quasi-static tensile loading and how macroscale mechanical loading is transduced to changes in cell and nuclear shape, and the micro and nanoscale mechanical and structural properties that enable this mechanism. We hypothesized that healing would reduce strain stiffening and fiber recruitment compared to uninjured tendons. We use a comprehensive approach, including application of mechanical loading on live tendons, measurement of multiscale tendon mechanics and structure during healing, assessment of healing tissue composition

using confocal imaging, and assessment of tendon microstructure via multiphoton imaging. Due to the slow timescale of remodeling events in tendon,[16] it is likely that alterations in matrix properties (e.g., mechanics and structure) precede cell responses. Such structural and mechanical changes alter the fibrous architecture of the ECM, and may therefore influence the ability for resident tenocytes to recognize their native "tendon" environment.

3.2 Methods

3.2.1 Study Design

Female C57BL/6 mice at 150 days of age (N=75) were randomized into an uninjured control group and groups that received bilateral injury to their patellar tendons (IACUC approved) (**Figure 3-1**).[8,17,18] Mice in injury groups were first anesthetized (isoflurane) and both hindlimbs were shaven and sterilized. Using aseptic procedures, a single incision was made through the skin near the knee, and longitudinal incisions were made adjacent to and on either side of the patellar tendon. A rubber-coated backing was placed under the tendon, and a full thickness, partial width (~60% width) excisional injury was created using a 0.75mm biopsy punch. Skin was closed with 5-0 prolene suture, and the animals were returned to cage activity. Doses of buprenorphine (0.1mg/kg; Penn Investigational Drug Service) were given pre-surgery, and sustained-release buprenorphine (1.0mg/kg; ZooPharm; Windsor, CO) was given post-surgery. Injured animals were randomized into groups euthanized at 2 or 6 weeks post-injury to evaluate the role of healing on multiscale tendon properties. At these timepoints, mice were sacrificed and tendons were mechanically tested *ex vivo* with tissue tendon explants.

This model provides a controlled method for evaluating the specific response of tendon to load, thus removing confounding variables present in whole tissue model systems. Many of the same mechanical and biological mechanisms also occur *in vivo*, demonstrating the validity of these *ex vivo* models.

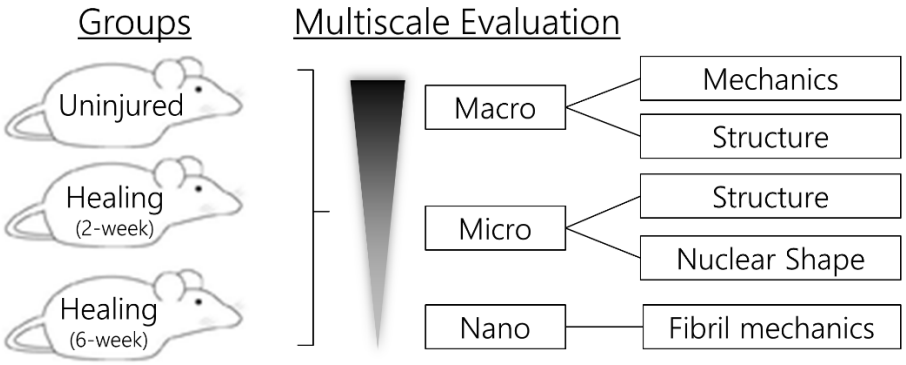

Figure 3-1: Study Design. Animals are divided into three groups (uninjured, 2-weeks post-injury, and 6-weeks post-injury)

3.2.2 Sample Preparation and Mechanical Testing

For evaluation of macroscale tendon structure, tendons (N=10/group) were frozen at -20ºC, thawed, and fine dissected, as done previously.[17,19,20] Briefly, tissues were harvested immediately after euthanizing the mice, hind limbs were removed, and a randomly selected limb was wrapped in phosphate buffered saline (PBS) soaked gauze, then frozen for later biomechanical testing. Patella–patellar tendon–tibia complexes were carefully dissected and tendons were stamped into a “dog-bone shape” of width 0.75mm. Before and after stamping, tendon cross-sectional area was measured with a custom, laser-based device.[21] The distal half of the tibia was then secured in a custom fixture and loaded into a material’s testing system (Model 5848, Instron; Norwood, MA) with a 10N load cell. Tendons were preconditioned and ramped at a constant strain rate (0.1% strain/s) until failure while collagen structure was evaluated using an integrated polarized

light imaging system. During loading, force and displacement data were acquired and analyzed using MATLAB (Mathworks, Natick, MA). The change in equilibrium stress (force divided by the cross sectional area) between 1 and 10% strain was used to indicate the amount of strain stiffening, and the dynamic modulus assessed during dynamic loading were computed.

For multiscale evaluation relating applied macroscale mechanical loading to microscale properties (cell, nuclear, and collagen morphology), tendons (N=10/group) were harvested immediately after sacrifice and kept in standard media conditions to maintain cell viability. Maintenance of cell viability was important to preserve *in vivo* cell migration and contraction during loading, which are ATP driven processes.[22] The patellar tendon was stamped into a "dog-bone" shape to isolate the injury site, and measured for cross sectional area at the injury site.[21] To maintain tenocyte viability during loading, tissues were immersed in a bath containing sterile DMEM supplemented with 5% fetal bovine serum (FBS), maintained at 37ºC integrated with a tensile testing device (Instron 5848; Norwood, MA). To evaluate the effect of healing on strain stiffening, tendons (n=10-13/group) were preconditioned and ramped at constant strain rate (0.1% strain/s) until 1% or 10% strain prior to a frequency sweep (0.125% strain amplitude at 0.1, 1, 5, and 10Hz) (**Figure 3-2**) and snap freezing (**Figure 3-3**).

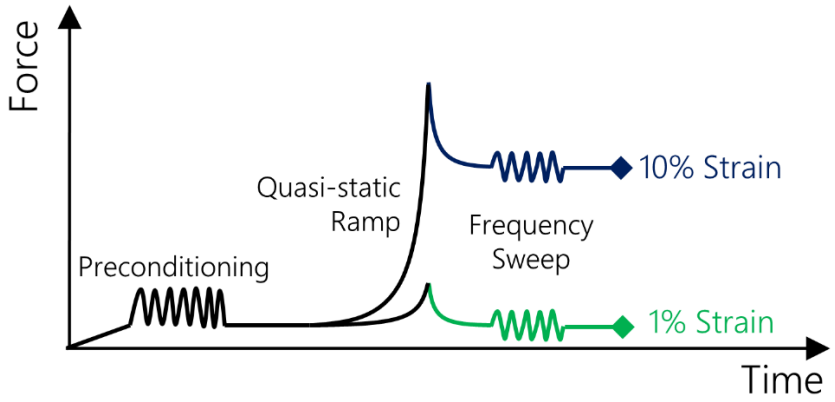

Figure 3-2: Quasi-static Mechanical Testing Protocol. Tendons were preconditioned and then ramped at 0.1% strain/s to either 1% or 10% strain followed by a frequency sweep. After the frequency sweep, tendons were snap frozen for microscale assessment.

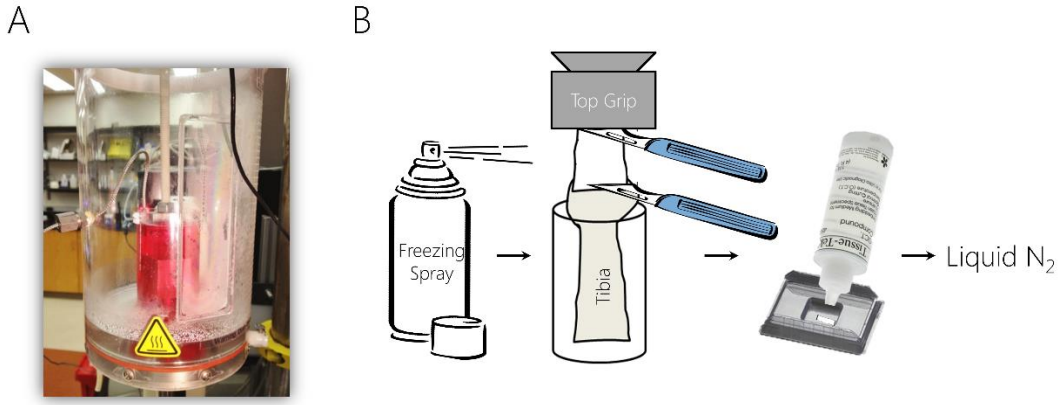

Figure 3-3: Experimental setup for live tendon testing. Following mechanical loading, tendons were snap frozen, embedded in OCT, and frozen in liquid N_2 prior to microscale assessment.

3.2.3 Cell Viability

Cell viability was evaluated with an MTT assay, which exploits the redox potential of active respiring cells. In live cells, water-soluble MTT is converted to an insoluble purple formazan, which is solubilized and determined for concentration by optical density. A 12mM MTT stock solution was prepared by adding 1mL of sterile PBS to 5mg of MTT under sterile conditions. For labeling viable cells in tissue, 100uL of stock solution was added to 1000uL of DMEM, keeping the mixture at 37C at 5%CO2 prior. Following tissue harvest, tissue was placed immediately in Eppendorf tubes left

open in an incubator for 1-hour. The tissue was then transferred to PBS for 30 min at room temp and fixed with 4% PFA at 4ºC overnight prior to cryosectioning. Tissue sections were counter stained with DAPI to qualitatively compare viable cells with all cells.

3.2.4 Polarized Light Imaging

A polarized light system[5] was integrated with the mechanical testing, consisting of a backlight, 90º offset rotating polarizer sheets (Edmund Optics, Barrington, NJ) on both sides of the test sample (polarizer and analyzer), and a GigE aca2040gm camera (resolution: 2048x2048 pixels) (Basler, Exton, PA). Sets of alignment maps (30 images) were taken during the quasi-static ramp. This protocol was fully automated during the fatigue tests using analog outputs acquired by a data acquisition device (USB 6008, National Instruments, Austin, TX) at 100Hz that was monitored by a custom Labview program (Version 8.6, National Instruments, Austin, TX).

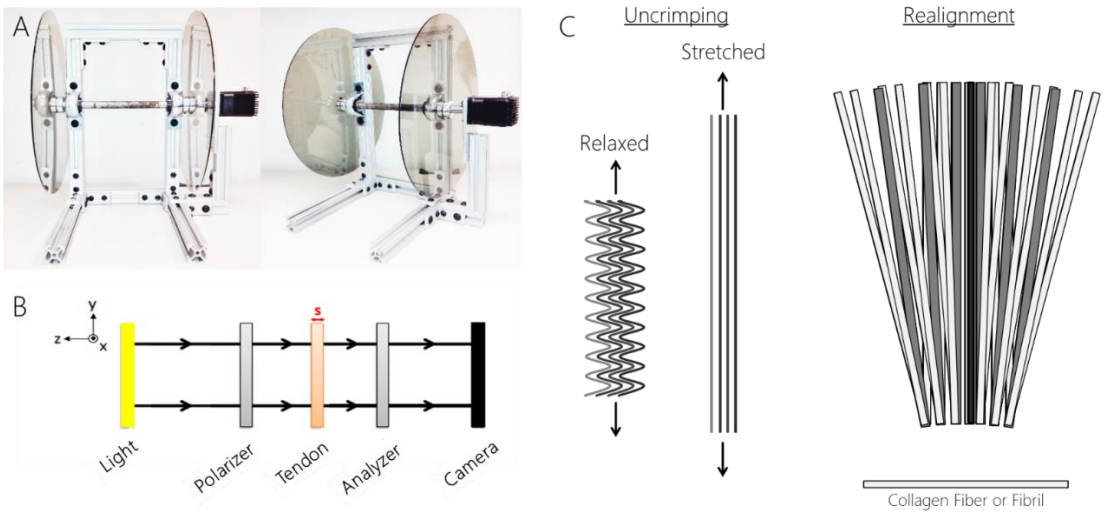

Figure 3-4: Polarized Light Imaging. (**A**) Polarized light setup containing (**B**) two polarizers crossed at 90º on either side of the tendon. During loading, collagen fibers (**C**) uncrimp and (**D**) realign in the direction of loading.

A custom MATLAB program (MATLAB, Natick, MA) was used to divide the image into a series of regions of area 100 pixels² and spacing of 20 pixels that were individually averaged to filter noise. From these data, the signal phase and magnitude, within each region from each alignment image series, was used to determine the circular standard deviation (CSD), a measure of collagen fiber disorganization,[23] and the signal's peak-to-peak intensity. Briefly, the CSD was calculated by fitting a $\sin^2 2\theta$ function[24] to the pixel intensity-polarizer angle data to determine the angle corresponding to the minimum pixel intensity. This angle represents the average direction of fiber alignment.

3.2.5 Fiber Recruitment Model

Using quasi-static ramp data, we applied a structurally based elastic model[25-27] to quantify the non-linear force-displacement behavior as fibers uncrimp to their slack length. This model assumes that tendon contains linearly elastic fibers that uncrimp during loading. After fiber uncrimping, at the fiber's slack length, fibers contribute to force linearly. The combination of these factors gives rise to tendon's non-linear force-displacement behavior, and was modeled using a cumulative probability distribution function (Eq. 3-2). Briefly, p is the cumulative probability of a fiber being uncrimped (range: 0-100%), σ is the standard deviation of fiber slack-lengths (mm), L_0 is the fiber slack length (mm), and μ is the average fiber slack length (mm). Fibers were considered uncrimped once the tendon length has exceeded the fiber's slack-length (Eq. 3-3). Here, K_{avg} is the average fiber stiffness (N/mm), x is the tendon length (mm), L_0^i is the slack length of fiber i, and H is the heavy side step function (H = 0 for $x < L_0^i$ and 1 for $x > L_0^i$). Generally, disorganized tissues such as skin have an elongated toe-region, which results

in slack lengths with high means and standard deviations. Force and displacement data from the ramp to 10% strain portion of the mechanical tests were fit to this model using the nonlinear least squares function (MATLAB) to quantify fiber slack length distribution parameters (mean and standard deviation) throughout healing.

$$p(L_0) = \frac{1}{\sigma\sqrt{2\pi}} \int_{-\infty}^{L_0} e^{\frac{-(t-\mu)^2}{\sigma}} \qquad \text{(Eq. 3-2)}$$

$$F(x) = K_{avg} \sum_{i=1}^{N} (x - L_0^i) \cdot H(x - L_0^i) \qquad \text{(Eq. 3-3)}$$

3.2.6 Immunofluorescence Staining

At each healing time point, tissues were snap frozen, and immediately embedded in Optimum Cutting Temperature (OCT) compound (Tissue-Tek, Sakura Finetek USA, Torrance, CA, USA), prior to sectioning at 15µm (Leica CM1950; Wetzlar Germany) using Kawamoto's Film.[28] Following cryosectioning, sections were placed in 4% paraformaldehyde (Fisher) for 3 minutes and attached to slides with a chitosan film adhesive solution. Briefly, the solution was prepared by dissolving 0.25ml acetic acid (Sigma Aldrich) in 100mL DI water to create a 0.25% v/v. A chitosan (C 3646, Sigma Aldrich) solution in 0.25%, v/v acetic acid solution was prepared by adding 1-1.6g of chitosan in 100ml acetic acid solution, stirred overnight. Tissue sections were rehydrated in 1xPBS, blocked for non-specific binding in 5% BSA and 0.1% triton for 1-hour at 4°C, and then stained with primary conjugated antibodies for cell and nuclear shape analysis.

Sections were stained for F-actin with Alexa Fluor® phalloidin (1:20; 555/565; Fisher Scientific), nuclei with DRAQ5 Fluorescent Probe Solution (1:1000; 647/681; Fisher Scientific), and denatured collagen with collagen hybridizing peptide (CHP) (1:10; 490/525; Echelon Biosciences) for 12 hours at 4°C. CHP was prepared by diluting the stock solution in 1xPBS and heating at 80°C for 5 minutes prior to quenching on ice. Nuclei long and short axes are measured using a custom MATLAB program and ImageJ (v1.48, NIH, Bethesda, MD) to derive aspect ratios.

3.2.7 Confocal and Multiphoton Imaging

Sequential scans on an upright laser-scanning multiphoton confocal microscope (Leica TCS SP8; Wetzlar Germany; 1024x1024 pixel resolution, fov: 277µm x 277µm, scan speed: 400Hz) were completed to evaluate stains for denatured collagen, collagen, F-actin, and nuclei in tendon sections. Nuclei fluorescence were captured simultaneously with excitation using 488nm and 638nm wavelength lasers, followed by F-actin with a 552nm wavelength laser (all with PMT detectors). Second harmonic generation (SHG) imaging was achieved a Coherent Chameleon Vision II Ti:Sapphire laser tuned to 880nm. For all imaging, a 40x oil immersion objective (HC PL APO 40x/1.30 oil CS2) was used for focusing the excitation beam on slides mounted on the stage with the longitudinal axis of the tendon aligned with the horizontal axis of the visual field. Transmitted and reflected SHG signals were collected using 440/20 emission filters on PMT NDD and PMT-RLD detectors. Z-stacks were taken at 1.5µm intervals to capture the tendon midsubstance or injury site. Images from 2-3 tendon sections were taken per specimen.

We determined the average collagen fiber organization by computing the angular orientation of fibers in the SHG images with custom code (MATLAB; v2015a; Natick, MA).[29] Images were selected from the middle of each Z-stack with fibers aligned along the horizontal direction. These images were then first converted to 8-bit format, contrasted, and enhanced. The region of interest (ROI) was selected from the composite image and applied for all images in the Z-stack. Uninjured samples used individual slices from the Z-stack for analysis, while healing samples used the maximum projection of selected images in the Z-stack for analysis due to the lack of SHG signal in each individual slice. Each image was then divided into smaller bundles (4µm x 4µm); and any residual bundles at the edges of the image smaller than the bundle size were excluded from the analysis. The fast Fourier transform power spectrum (FFT-ps) was taken for each bundle, and an ellipse was fit around the processed FFT-ps. As the major axis of the FFT-ps ellipse will point in the direction of increasing intensity, the direction of the collagen fibers were determined by computing the angle of the semi-minor axis of the ellipse from the positive *x*-axis.[29,30] To prevent redundancy in determined angles (i.e., fiber orientation at 0° is the same orientation as 180°), angles were corrected to fit within the range -90° to 90°, with 0° being horizontal and aligned in the direction of loading. A quiver plot was superimposed on the original image to ensure that collagen fiber orientation was computed correctly. Angles were plotted in a histogram to determine angular distribution. For average organization, the circular standard deviation was calculated at 1% or 10% strain to evaluate changes in fiber orientation during tendon loading. The average circular statistics was taken across all selected images in the Z-stack for uninjured samples.

3.2.8 Atomic Force Microscopy (AFM)

For each tendon section, AFM-based nanoindentation was performed on the surface of the central midsubstance using a microspherical probe tip and a Dimension Icon AFM (BrukerNano, Santa Barbara, CA) (Figure 3-5). The spherical tip was prepared by attaching a polystyrene colloid ($R_{tip} \approx 5\mu m$) (Polyscience; Warrington, PA) onto the tipless cantilever (nominal spring constant k ≈ 0.3N/m, TipB; HQ:CSC37/tipless/Cr-Au , NanoAndMore, MikroMasch; Watsonville, CA) using the M-Bond 610 epoxy (SPI supplies; Westchester, PA) under the Dimension Icon AFM. For each tendon, 12 different locations were tested to an indentation depth of ~1μm at 5μm/s rates at each location. Furthermore, to compare the mechanical properties of tendon groups, nanoindentation was also performed on the healing tendons. During all indentation experiments, tendon tissues (15μm sections) were immersed in 1x PBS (pH = 7.4) to maintain the physiological-like fluid environment.

Each indentation force versus depth, F-D, curve was analyzed to calculate the effective indentation modulus, E_{ind}, at each location by fitting the entire portion of each loading *F-D* curve with the Hertz model (Eq. 3-4) using least square linear regression.

$$F = \frac{4}{3}\frac{E_{ind}}{(1-\nu^2)} R_{tip}^{1/2} D^{3/2} \qquad \text{(Eq. 3-4)}$$

In this model, R_{tip} is the tip radius (≈5μm), ν is the Poisson's ratio (~0.3 for tendon). The choice of the Poisson's ratio was based on the estimate from tissue-level studies on other tendons indented perpendicular to the longitudinal direction.[31-36]

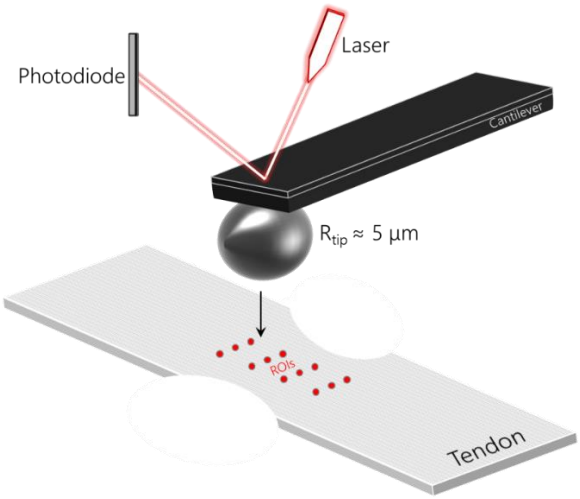

Figure 3-5: AFM Experimental Setup and Testing.

3.2.9 F-Actin and Nuclear Shape Analysis

F-actin was quantified by determining the percent positive staining per ROI. Images were imported into FIJI, cropped, max projected, converted to 8-bit greyscale, contrast enhanced, and thresholded to isolate F-actin filaments. The number of F-actin positive pixels was determined and normalized to the total cropped ROI. The same ROIs for nuclei were similarly selected in FIJI, and segmented and analyzed using CellProfiler[37] to evaluate nuclear shape (major/minor axis, nuclear aspect ratio (nAR)) and orientation (nOrientation).

3.2.10 Statistical Analysis

Data normality was assessed and confirmed with Shapiro Wilk tests. To determine the role of healing on multiscale tendon properties, data were evaluated with one-way ANOVAs with post hoc Student's or paired t-tests with Bonferroni corrections. To determine the role of strain on tendon multiscale properties, data were similarly

evaluated with one-way ANOVAs with post hoc Student's or paired t-tests with Bonferroni corrections. Linear and power regression were used to determine relationships between microscale structure, composition, and nuclear shape.

3.3 Results

3.3.1 Macroscale Mechanics and Structure Are Inferior in Healing Tendon Across Applied Strain

Cell viability was maintained throughout mechanical testing (**Figure 3-6**). Tendon healing affected tissue strain stiffening, as the change in equilibrium stress was reduced at both 2- and 6-weeks post-injury compared to uninjured control tendons (**Figure 3-7A**). This decrease in strain stiffening was coupled with decreased dynamic modulus in healing tendons regardless of applied strain (**Figure 3-7B**). Force and displacement data was also used to fit a fiber recruitment model to predict average fiber slack lengths.[38] In agreement with predictions of increased slack lengths in healing tendons (indicating decreased fiber recruitment) (**Figure 3-7C**), we found that fibers became more organized under loading in uninjured tendons compared to healing tendons (**Figure 3-8A**). Although uninjured tendons exhibited a dose-dependent reduction in macroscale fiber disorganization with applied strain, this response was generally absent in healing tendons (**Figure 3-8B**). Taken together, these results suggest that tendon strain stiffening is reduced in healing tendon and occurs in concert with decrease matrix reorganization during mechanical loading.

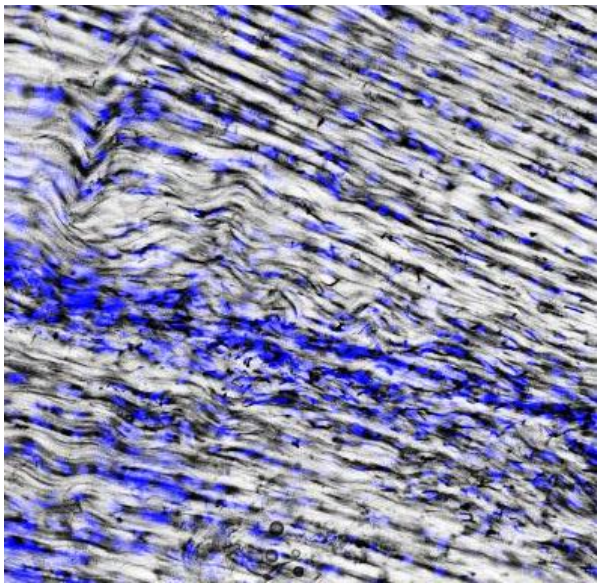

Figure 3-6: Cell viability. An MTT assay was used to confirm cells remained viable after mechanical loading. Black indicates metabolically active cells counterstained with DAPI (nuclei).

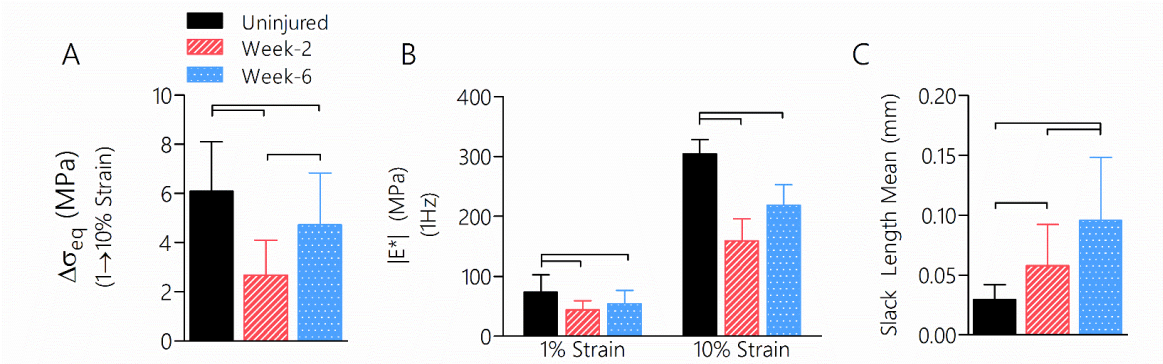

Figure 3-7: Macroscale Mechanical Properties and Fiber Recruitment Model. (**A**) The change in equilibrium stress was decreased in healing tendons compared to uninjured tendons. (**B**) Dynamic modulus was inferior in healing tendons compared to uninjured tendons regardless of applied strain (**C**) Tendon fiber slack lengths, as predicted by a fiber recruitment model, increased in tendons 2 and 6-weeks post-injury compared to uninjured tendons. Solid lines indicate significant differences ($p<0.017$) and dashed lines indicate trends ($p<0.033$).

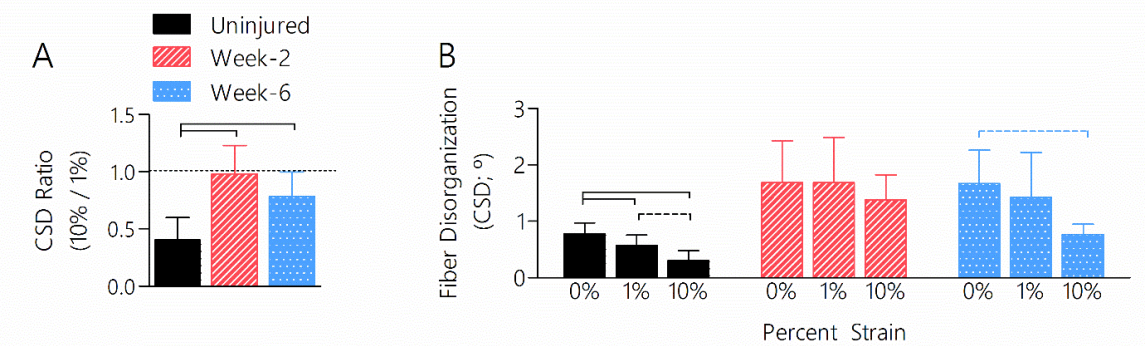

Figure 3-8: Macroscale Collagen Fiber Alignment. (**A**) Uninjured tendons decreased in disorganization more than tendons 2 and 6-weeks post-injury. (**B**) Uninjured tendons were significantly more disorganized

at low strains compared to high strains, unlike tendons 2- and 6-weeks post-injury. Solid lines indicate significant differences ($p<0.017$) and dashed lines indicate trends ($p<0.033$).

3.3.2 Microscale Structural And Compositional Properties Are Inferior In Healing Tendon

To investigate whether the macroscale changes in mechanics and structure propagate to the microscale, we evaluated tendon structure using MP imaging and simultaneously evaluated tendon cell shape and F-actin (**Figure 3-9,10,11,12**). Confocal and MP imaging revealed that changes in collagen organization, actin staining, and nuclear shape that were dependent on tendon healing and applied strain (**Figure 3-13**). Similar to macroscale structural properties, microstructural collagen alignment was more disorganized in healing tendon than uninjured control tendon, and this response regardless of applied strain (**Figure 3-14A**). Interestingly, microscale alignment was much more disorganized compared to macroscale alignment. Additionally, uninjured and 2-week post-injury healing tendons exhibited strain dependent response in matrix organization unlike tendons 6-weeks post-injury (**Figure 3-14B**).

Healing tendons had increased cell counts and F-actin staining compared to uninjured tendon (**Figure 3-15**). However, the amount of F-actin staining was reduced in tendons 6-weeks post-injury compared to 2-weeks post-injury (**Figure 3-15B**). Nuclei had decreased aspect ratios and increased disorganization in healing tendons compared to uninjured tendons (**Figure 3-16A; Figure 3-17,18**). Although nAR increased from 2 to 6-weeks post-injury, it remained inferior to uninjured tendons and lost their ability to reorganize with applied strain (**Figure 3-19**). This ability for nuclei to deform under applied stain was greatly reduced in tendons 2- and 6-weeks post-injury (**Figure 3-16B**).

Nuclear disorganization correlated linearly with collagen disorganization (R^2 = 0.83; **Figure 3-21A**). In addition, the nAR decreased with increased actin staining (R^2 = 0.63; **Figure 3-21B**) and collagen disorganization (R^2 = 0.80; **Figure 3-21C**) according to a power law.

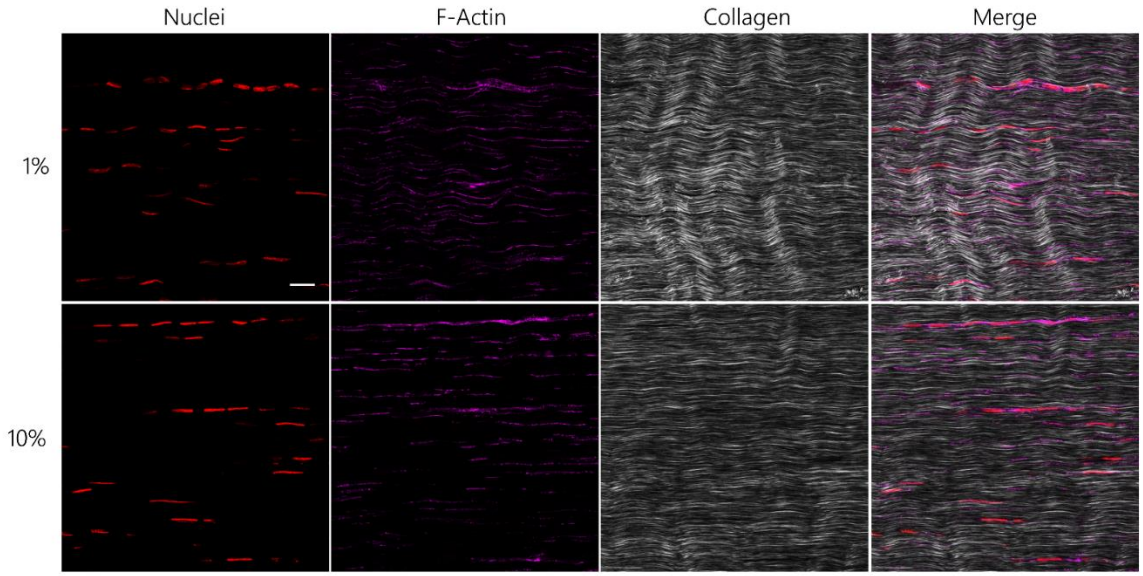

Figure 3-9: Confocal and MP imaging. Overlay confocal and multiphoton images for uninjured control groups comparing 1% and 10% strain. Scale bar = 20µm.

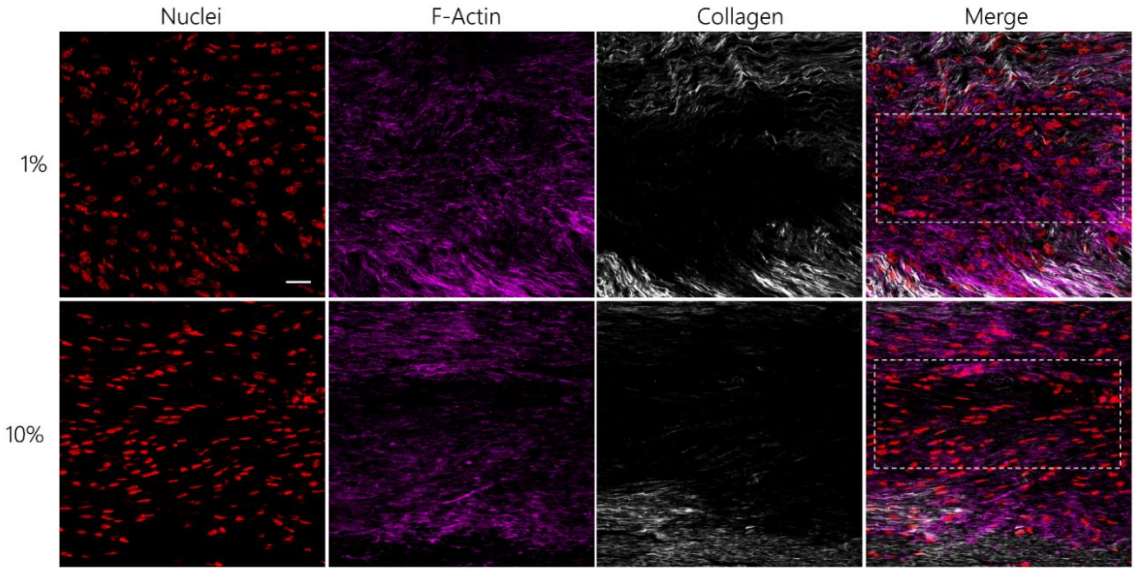

Figure 3-10: Confocal and MP imaging. Overlay confocal and multiphoton images 2-weeks post-injury comparing 1% and 10% strain. The white dotted box in merged panel depicts the ROI selected for analysis. Scale bar = 20µm.

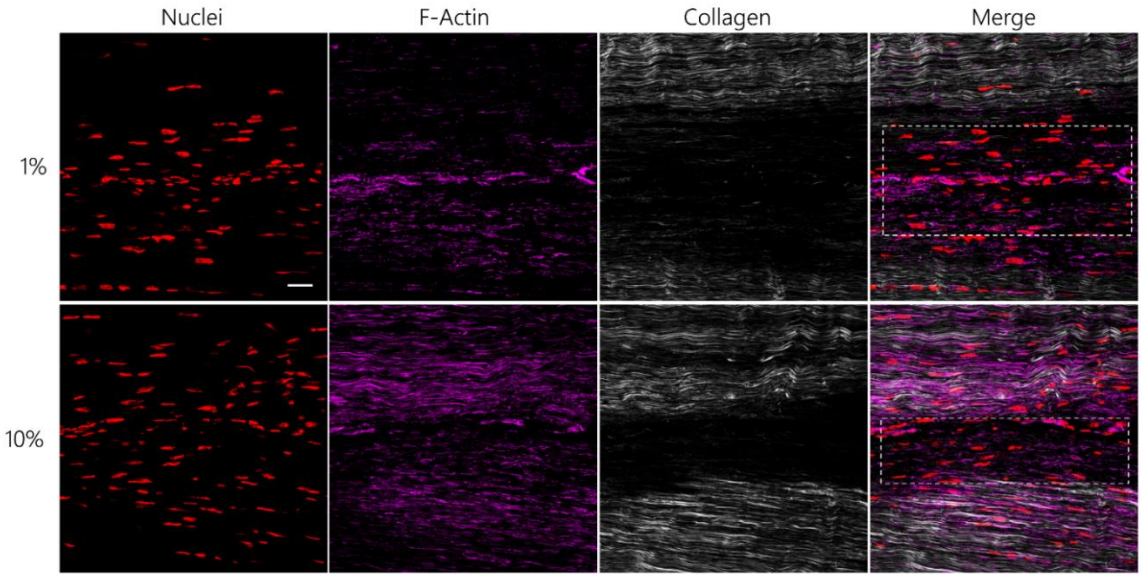

Figure 3-11: Confocal and MP imaging. Overlay confocal and multiphoton images 6-weeks post-injury comparing 1% and 10% strain. The white dotted box in merged panel depicts the ROI selected for analysis. Scale bar = 20µm.

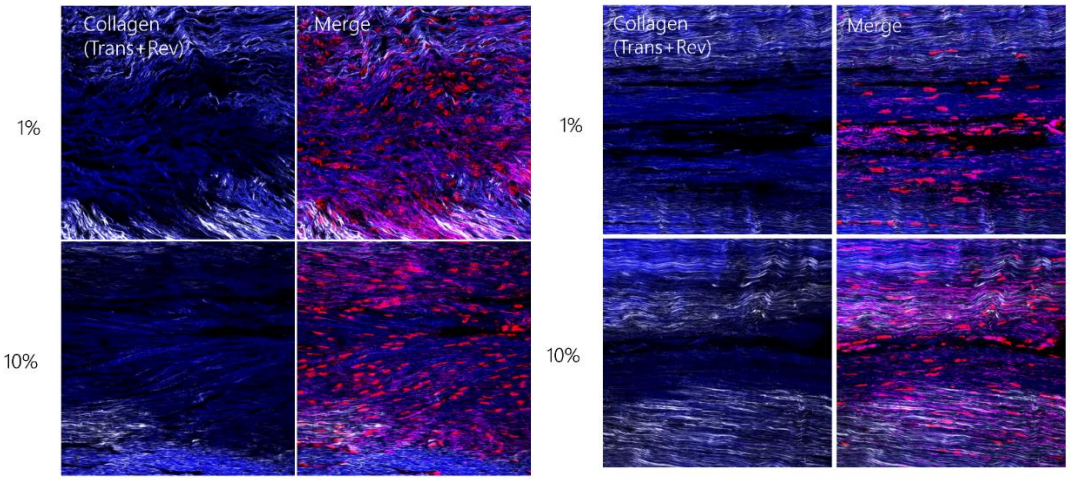

Figure 3-12: Confocal and MP imaging. Forward and backward scatter present in the injury site in both tendon (left) 2-weeks post-injury and (right) 6-weeks post-injury. Scale bar = 20µm.

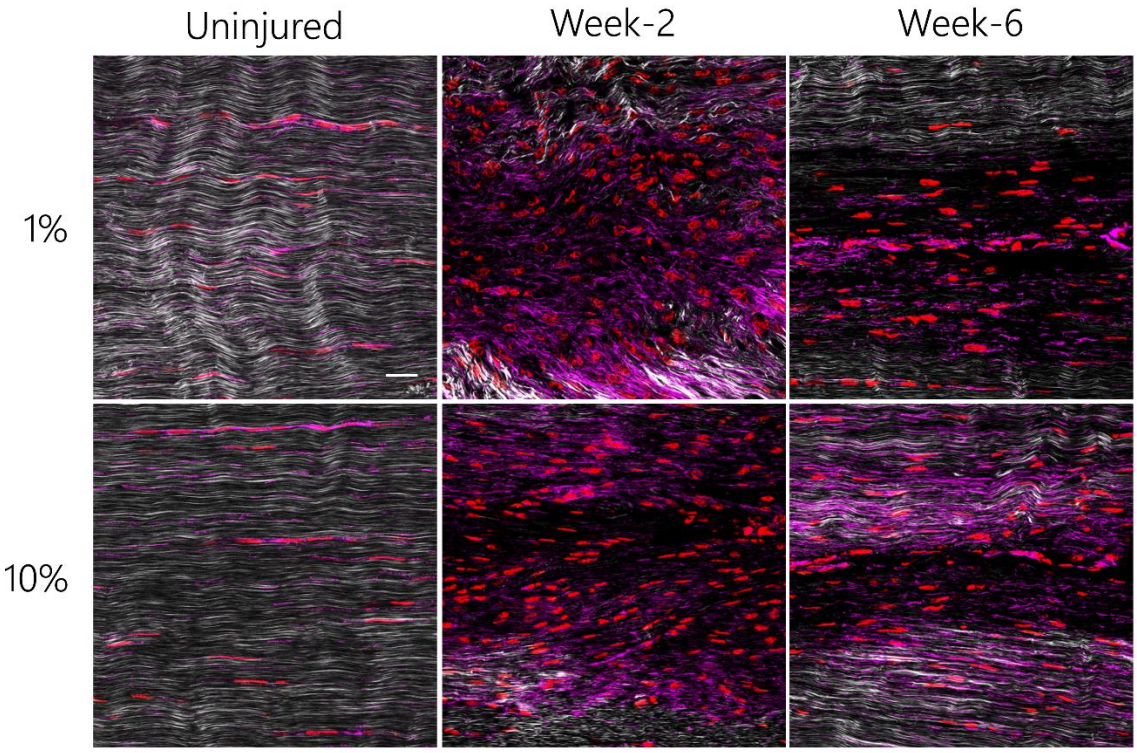

Figure 3-13: Confocal and MP Imaging. Tendon sections were stained to identify the nucleus and F-actin, and MP imaging captured collagen structure throughout healing (uninjured, 2-weeks post-injury, and 6-weeks post-injury) and applied strain (1 and 10% strain). Scale bar = 20µm.

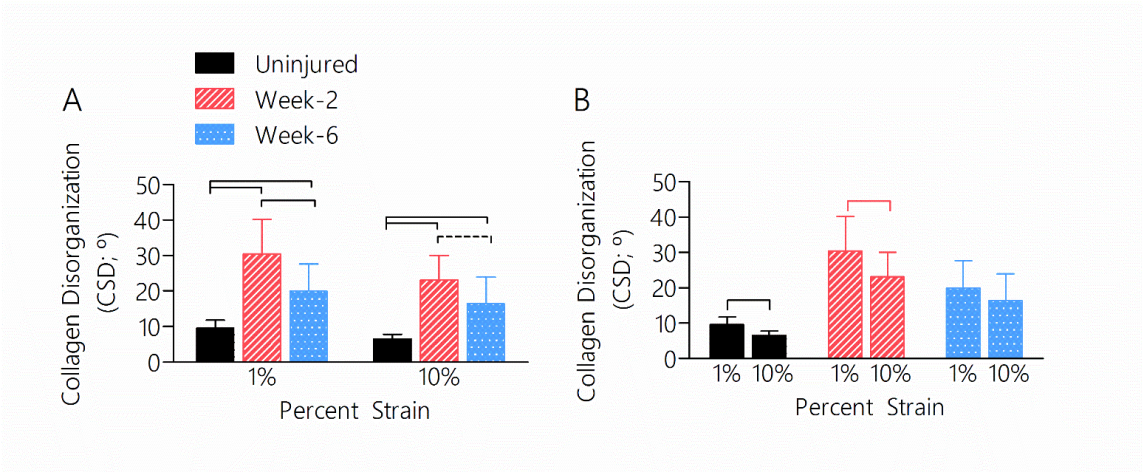

Figure 3-14: Local Matrix Alignment. (**A**) Local matrix alignment was more disorganized in tendons 2-weeks post-injury compared uninjured and 6-week post-injury tendons, regardless of applied strain. (**B**) Although uninjured tendons and 2-week post-injury tendons become less disorganized with applied strain, tendons 6-weeks post-injury do not demonstrate changes in local matrix orientation with loading. Data shown as mean ± SD.
*Panel A: Solid lines indicate significant differences ($p<0.017$) and dashed lines indicate trends ($p<0.033$).
**Panel B: Solid lines indicate significant differences ($p<0.05$)

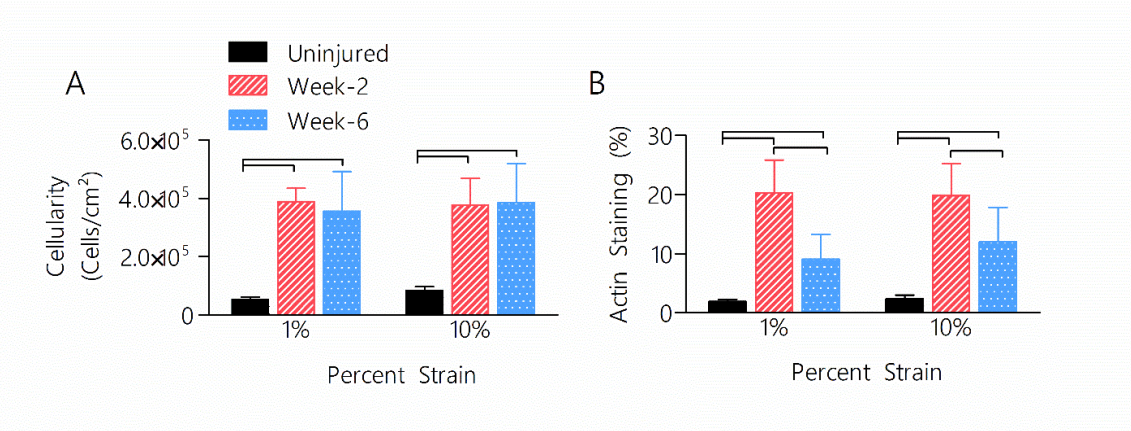

Figure 3-15: Cellularity and Actin Staining.

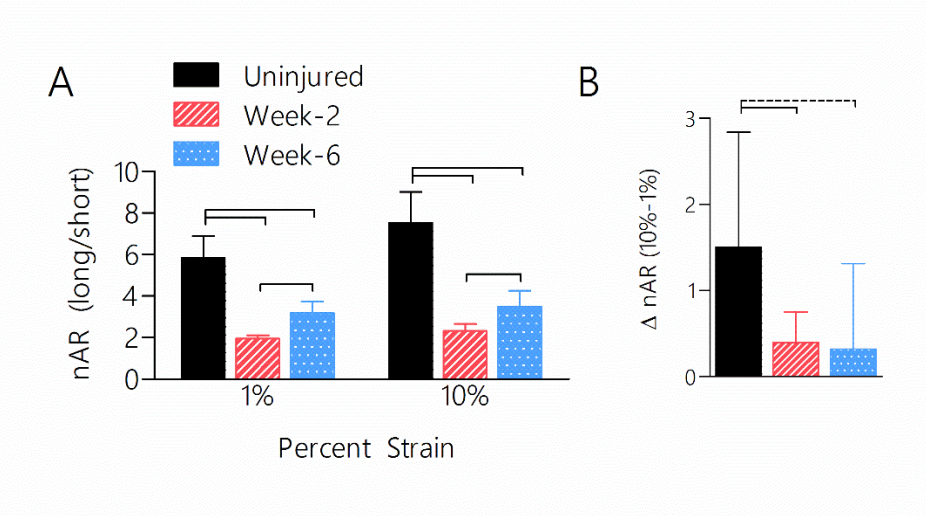

Figure 3-16: Nuclear Aspect Ratio. (**A**) Nuclear aspect ratios were decreased in healing specimens compared to uninjured tendons regardless of applied strain. (**B**) The change in nAR from 1 to 10% strain was greatest in uninjured tendons, and was significantly reduced in healing tendons. Data shown as mean ± SD. Solid lines indicate significant differences ($p<0.017$) and dashed lines indicate trends ($p<0.033$).

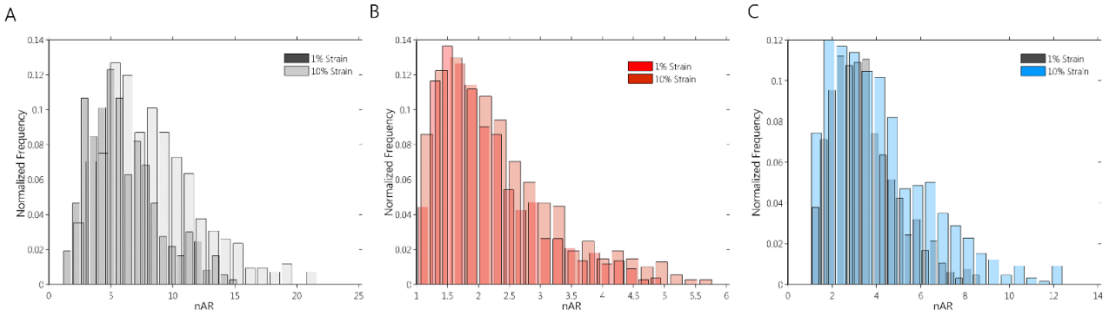

Figure 3-17: Nuclear Aspect Ratio Histograms. Histograms depicting differences across strains for (**A**) uninjured, (**B**) 2-weeks post-injury, and (**C**) 6-weeks post-injury groups. N = 366-1105 cells/group.

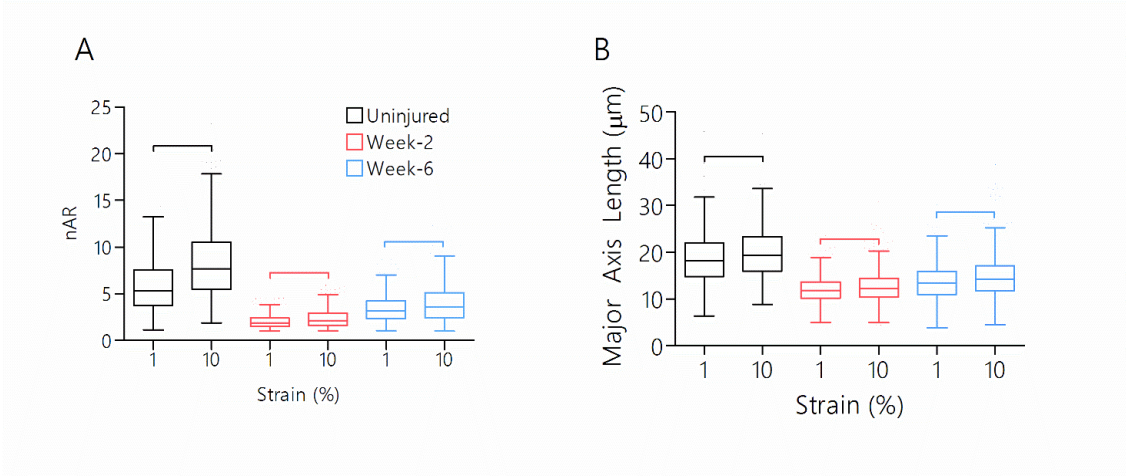

Figure 3-18: Nuclear Aspect Ratio Population Statistics. N~=300-1500 cells/group.

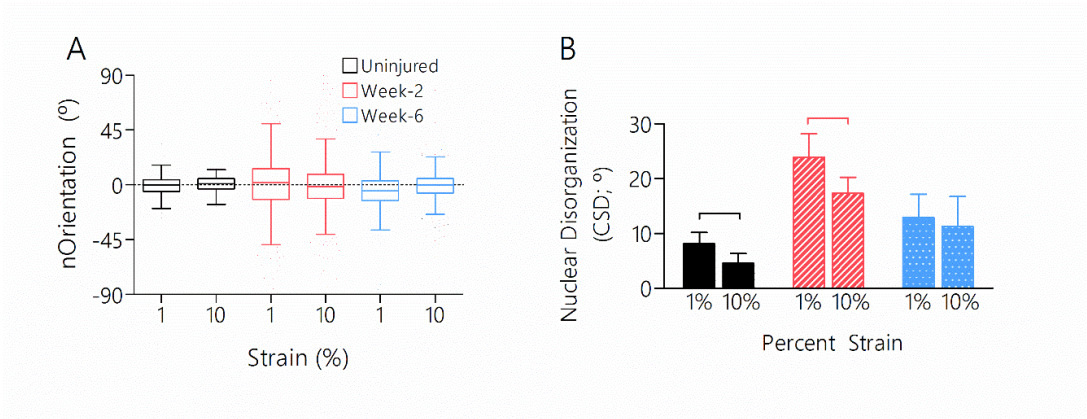

Figure 3-19: Nuclear organization. N~=300-1500 cells/group.

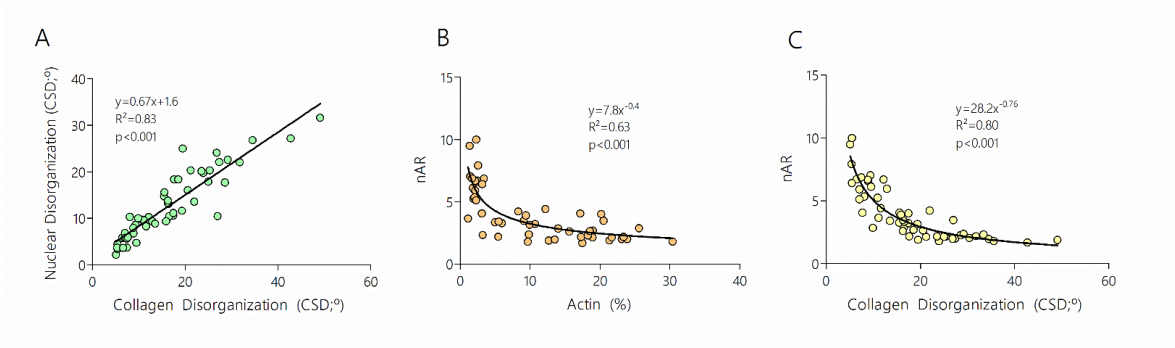

Figure 3-20: Correlations. (**A**) Nuclear disorganization correlated linearly with collagen disorganization. (**B**) The nAR decreased with increased actin staining and (**C**) collagen disorganization according to a power law.

3.3.3 Nanoscale Mechanical Properties are Inferior in Healing Tendon

To investigate whether the microscale changes in structure and nuclear properties propagated to the nanoscale, we evaluated tendon nanomechanical properties using AFM. In agreement with our hypothesis, tendon nanoscale indentation modulus was decreased in healing tendon (**Figure 3-21**).

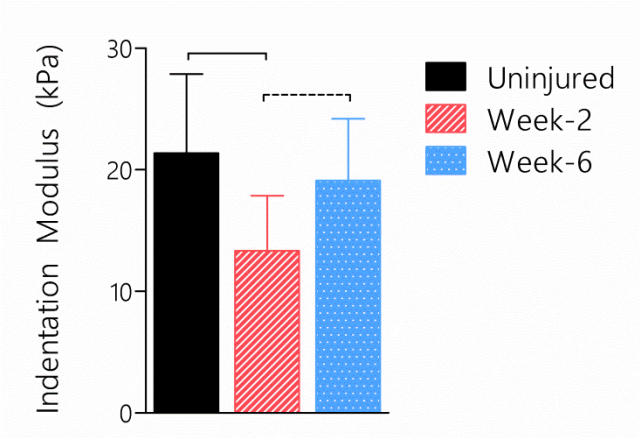

Figure 3-21: Nanomechanical Properties. The indentation modulus was decreased in tendon 2-weeks post-injury compared to uninjured tendon, and gradually recovered with time. N=5-9/group. Data shown as mean ± SD. Solid lines indicate significant differences ($p<0.017$) and dashed lines indicate trends ($p<0.033$).

3.4 Discussion

This study evaluated multiscale structure-function mechanisms in response to quasi-static tensile loading in uninjured and healing tendons. Using an established mouse patellar tendon injury model,[17,18,39] we harvested living tendon explants, that preserve the native architecture of the tendon ECM. Together, our approach allows for the evaluation of multiscale mechanical and structural properties without destructive dissection to the tissue. This procedure provides advancement over traditional histological studies that do not control for tissue pre-stresses or strains applied prior to fixation.

We first showed that tendon healing affects the macroscale mechanical and structural response to mechanical loading. As hypothesized, we found that healing tendons exhibited decreased strain stiffening, which occurred in concert with decreased dynamic moduli and elevated predicted fiber slack lengths. Increases in fiber slack lengths indicate an extension in the toe region of the stress-strain curve, which suggests that the structural response to strain during healing may be compromised. Indeed, macroscale structural properties were inferior in healing tendons and the matrix showed a reduced capacity to realign under loading. To determine how these macroscale properties were related to microscale properties, we used MP imaging to evaluate the collagen structure. Similarly, healing tendons also demonstrated increased collagen fiber disorganization compared to uninjured tendons, however, MP imaging was able to detect substantially more disorganization in all groups indicating that the tendon microstructure and macrostructure may be correlated, but are not identical.

Historically, tendon's composition and structure are often related to its mechanical function as disorganized collagen becomes more aligned and less crimped during loading.[11,40-42] However, extension of these mechanisms to the response of tendon cells during loading has been limited.[14,15] Therefore, we next evaluated how macroscale loading was transduced to changes in microscale structure, nuclear shape, and nuclear orientation. We identified that healing tendons experience reductions in nAR and nuclear re-organization in response to loading compared to uninjured tendons, and that these responses are ultimately related to organization of the microscale collagen structure and amount of F-actin. This work adds to previous literature by evaluating multiscale tendon properties during healing. Although tissue and cellular level strains correlated in normal

uninjured tendons during *quasi-static* tensile loading,[15] the multiscale response to loading during tendon healing had not been investigated. This is particularly important as tendons heal through scar formation, do not regain pre-injury material properties, and often display aberrant phenotypes, and contribute to poor functional outcomes.[4,39,43-45] Tendon stem/progenitor cells (TSPCs) are implicated to differentiate towards chondrocyte, osteoblast, or adipocyte lineages, as altered matrix properties and stresses on cells has been shown to affect cell fate.[46-48] As TSPCs reside in a niche environment that combines mechanical and biochemical cues,[49-52] alterations to this microenvironment may drive tendons toward an aberrant differentiation (chondrogenic, osteogenic, or adipogenic), but this description had remained limited.[53] Our results not only add to the understanding for how tendon healing affects the local microenvironment of residing tendon cells in native tissue, but identify the capacity for these cells to respond to external mechanical cues.

Interestingly, although actin staining and collagen disorganization decreased at 6-weeks post-injury compared to 2-weeks post-injury, cellularity remained elevated and nuclei showed a reduced ability to respond to loading. This response is in stark contrast to the uninjured condition whereby low cellularity is coupled with low actin staining, high collagen organization, and high capacity for changes in nAR and nOrientation with applied strain. It is possible that cells within the injured region become stress shielded overtime, leading to an inferior response and potential presence of PG-rich inclusions.[15] Although our regression analysis revealed that actin staining and collagen organization were related to nAR, there is a distinct threshold in which these factors contribute to large changes in nAR.

This study is not without limitations. First, we only investigated tensile loading, and adding in additional loading paradigms that apply shear, compression, and biaxial forces may provide further insight into behavior *in vivo*. Next, we investigated the multiscale response at two distinct strains (1% and 10%). These strains were chosen to represent the toe and linear portion of the force-displacement curve. However, it is well established that tendon's response to loading is inherently nonlinear; therefore, evaluation at additional strains is necessary to fully describe the responses presented. Future studies will examine how dynamic loading affects the multiscale mechanical, structural, and compositional properties in healing tendon. Although we employed many tools to assess multiscale tendon properties, other measurements may provide additional support of findings. Mechanically, we focused on quantifying macroscale tensile properties in the direction of loading and nano/microscale indentation of tendon fibrils/fibers, perpendicular to their orientation. Although indentation mechanics may be important for the underlying fibrous substrate that tendon cells sense and respond to, its relationship to fibril mechanical properties in the direction of loading remains unknown. In addition, previous studies have used AFM to assess fibril sliding,[54] which may provide another metric for tendon's response to loading following the various dynamic loading protocols and healing time points evaluated in this work. Compositionally, previous studies have established that cell- and environment-generated mechanical loads on the ECM can induce a variety of cell responses. The healing process may create PG-rich domains, which create distinct tissue and cell biomechanics that are believed to be prevalent in injured tissues.[22] Further, the amount of lamin-A in the nucleus has been directly correlated to tissue stiffness.[103] Therefore, future studies should specifically evaluate the

spatial distributions of ECM, cell-ECM, and cell proteins that may regulate cell mechanics (collagen-1,3,5; PGs; integrin-α11; F-actin; lamin-A; N-cadherin; and connexin43).

Taken together, our work supports a new understanding for how macroscale loading affects multiscale tendon properties in the clinically relevant case of tendon healing. Unfortunately, many clinical treatments for tendon injuries remain controversial, [55] and basic scientific data describing tendon structure-function relationships in an injured state have not been fully characterized, which may limit our ability to design new targeted therapies. The multiscale response to mechanical loading, which is a hallmark of clinical rehabilitation protocols, is therefore necessary to determine the ramifications of various macroscale loading protocols. Additionally, these results provide benchmarks for the environments in which tendon cells may experience following cell delivery therapies.

References

1. Freedman BR, Bade ND, Riggin CN, et al. The (dys)functional extracellular matrix. *Biochim Biophys Acta.* Nov 2015;1853(11 Pt B):3153-3164.
2. Freedman BR, Fryhofer GW, Salka NS, et al. Mechanical, histological, and functional properties remain inferior in conservatively treated Achilles tendons in rodents: Long term evaluation. *In Review.* 2016.
3. Freedman BR, Gordon JA, Bhatt PB, et al. Nonsurgical treatment and early return to activity leads to improved Achilles tendon fatigue mechanics and functional outcomes during early healing in an animal model. *J Orthop Res.* Apr 2 2016.

4. Freedman BR, Gordon JA, Soslowsky LJ. The Achilles tendon: fundamental properties and mechanisms governing healing. *Muscles Ligaments Tendons J.* Apr 2014;4(2):245-255.

5. Freedman BR, Sarver JJ, Buckley MR, Voleti PB, Soslowsky LJ. Biomechanical and structural response of healing Achilles tendon to fatigue loading following acute injury. *J Biomech.* Nov 11 2013.

6. Chamberlain CS, Duenwald-Kuehl SE, Okotie G, Brounts SH, Baer GS, Vanderby R. Temporal Healing in Rat Achilles Tendon: Ultrasound Correlations. *Ann Biomed Eng.* Nov 13 2012.

7. Freedman BR SJ, Buckley MR, Voleti PB, Soslowsky LJ. Biomechanical and structural response of healing Achilles tendon to fatigue loading following acute injury. *(in review).* 2013.

8. Beason DP, Kuntz AF, Hsu JE, Miller KS, Soslowsky LJ. Development and evaluation of multiple tendon injury models in the mouse. *J Biomech.* Mar 7 2012.

9. Wang H, Abhilash AS, Chen CS, Wells RG, Shenoy VB. Long-range force transmission in fibrous matrices enabled by tension-driven alignment of fibers. *Biophys J.* Dec 2 2014;107(11):2592-2603.

10. Arnoczky SP, Lavagnino M, Whallon JH, Hoonjan A. In situ cell nucleus deformation in tendons under tensile load; a morphological analysis using confocal laser microscopy. *J Orthop Res.* Jan 2002;20(1):29-35.

11. Miller KS, Connizzo BK, Feeney E, Soslowsky LJ. Characterizing local collagen fiber re-alignment and crimp behavior throughout mechanical testing in a mature mouse supraspinatus tendon model. *J Biomech.* Aug 9 2012;45(12):2061-2065.

12. Diamant J, Keller A, Baer E, Litt M, Arridge RG. Collagen; ultrastructure and its relation to mechanical properties as a function of ageing. *Proc R Soc Lond B Biol Sci.* Mar 14 1972;180(60):293-315.

13. Buckley MR, Sarver JJ, Freedman BR, Soslowsky LJ. The dynamics of collagen uncrimping and lateral contraction in tendon and the effect of ionic concentration. *J Biomech.* Jul 19 2013.

14. Han WM, Heo SJ, Driscoll TP, et al. Microstructural heterogeneity directs micromechanics and mechanobiology in native and engineered fibrocartilage. *Nat Mater.* Apr 2016;15(4):477-484.

15. Han WM, Heo SJ, Driscoll TP, Smith LJ, Mauck RL, Elliott DM. Macro- to microscale strain transfer in fibrous tissues is heterogeneous and tissue-specific. *Biophys J.* Aug 6 2013;105(3):807-817.

16. Magnusson SP, Langberg H, Kjaer M. The pathogenesis of tendinopathy: balancing the response to loading. *Nat Rev Rheumatol.* May 2010;6(5):262-268.

17. Dunkman AA, Buckley MR, Mienaltowski MJ, et al. The tendon injury response is influenced by decorin and biglycan. *Ann Biomed Eng.* Mar 2014;42(3):619-630.

18. Lin TW, Cardenas L, Glaser DL, Soslowsky LJ. Tendon healing in interleukin-4 and interleukin-6 knockout mice. *J Biomech.* 2006;39(1):61-69.

19. Dunkman B, Mienaltowski,Adams, Thomas, Satchell, Kumar, Pathmanathan, Beason; Iozzo, Birk, Soslowsky Decorin Expression Is Required for Age-Related Changes in Tendon Structure and Mechanical Properties *Matrix Biol.* 2012((in review)).

20. Freedman BR, Zuskov A, Sarver JJ, Buckley MR, Soslowsky LJ. Evaluating changes in tendon crimp with fatigue loading as an ex vivo structural assessment of tendon damage. *J Orthop Res.* Mar 13 2015.

21. Favata M. *Scarless Healing in the Fetus: Implications and Strategies for Postnatal Tendon Repair*: Bioengineering, University of Pennsylvania; 2006.

22. Cooper G. *The Cell: A Molecular Approach*. 2 ed: Sinauer Associates; 2000.

23. Lake SP, Miller KS, Elliott DM, Soslowsky LJ. Effect of fiber distribution and realignment on the nonlinear and inhomogeneous mechanical properties of human supraspinatus tendon under longitudinal tensile loading. *J Orthop Res.* Dec 2009;27(12):1596-1602.

24. Glazer A, Lewis, JG., Kaminsky, W. An Automatic Optical Imaging System for Birefringent Media. *Proceedings: Mathematical, Physical and Engineering Sciences.* 1996;452(1955):2751-2765.

25. Hurschler C, Loitz-Ramage B, Vanderby R, Jr. A structurally based stress-stretch relationship for tendon and ligament. *J Biomech Eng.* Nov 1997;119(4):392-399.

26. Belkoff SM, Haut RC. A structural model used to evaluate the changing microstructure of maturing rat skin. *J Biomech.* 1991;24(8):711-720.

27. Lanir Y. A structural theory for the homogeneous biaxial stress-strain relationships in flat collagenous tissues. *J Biomech.* 1979;12(6):423-436.

28. Kawamoto T, Kawamoto K. Preparation of thin frozen sections from nonfixed and undecalcified hard tissues using Kawamot's film method (2012). *Methods Mol Biol.* 2014;1130:149-164.

29. Sereysky JB, Andarawis-Puri N, Ros SJ, Jepsen KJ, Flatow EL. Automated image analysis method for quantifying damage accumulation in tendon. *J Biomech.* Sep 17 2010;43(13):2641-2644.

30. Lee KL, Chen LH. A New Method for Coarse Classification of Textures and Class Weight Estimation for Texture Retrieval. *Pattern Recognition and Image Analysis.* 2002;12(4):400-410.

31. Marturano JE, Arena JD, Schiller ZA, Georgakoudi I, Kuo CK. Characterization of mechanical and biochemical properties of developing embryonic tendon. *Proc Natl Acad Sci U S A.* Apr 16 2013;110(16):6370-6375.

32. Marturano JE, Schiele NR, Schiller ZA, Galassi TV, Stoppato M, Kuo CK. Embryonically inspired scaffolds regulate tenogenically differentiating cells. *J Biomech.* Oct 3 2016;49(14):3281-3288.

33. Andriotis OG, Manuyakorn W, Zekonyte J, et al. Nanomechanical assessment of human and murine collagen fibrils via atomic force microscopy cantilever-based nanoindentation. *J Mech Behav Biomed Mater.* Nov 2014;39:9-26.

34. Kemp AD, Harding CC, Cabral WA, Marini JC, Wallace JM. Effects of tissue hydration on nanoscale structural morphology and mechanics of individual Type I collagen fibrils in the Brtl mouse model of Osteogenesis Imperfecta. *J Struct Biol.* Dec 2012;180(3):428-438.

35. Kahn CJ, Dumas D, Arab-Tehrany E, et al. Structural and mechanical multi-scale characterization of white New-Zealand rabbit Achilles tendon. *J Mech Behav Biomed Mater*. Oct 2013;26:81-89.

36. Yoo SD, Choi S, Lee GJ, et al. Effects of extracorporeal shockwave therapy on nanostructural and biomechanical responses in the collagenase-induced Achilles tendinitis animal model. *Lasers Med Sci.* Nov 2012;27(6):1195-1204.

37. Carpenter AE, Jones TR, Lamprecht MR, et al. CellProfiler: image analysis software for identifying and quantifying cell phenotypes. *Genome Biol.* 2006;7(10):R100.

38. Peltz CD, Sarver JJ, Dourte LM, Wurgler-Hauri CC, Williams GR, Soslowsky LJ. Exercise following a short immobilization period is detrimental to tendon properties and joint mechanics in a rat rotator cuff injury model. *J Orthop Res.* Jul 2010;28(7):841-845.

39. Mienaltowski MJ, Dunkman AA, Buckley MR, et al. Injury response of geriatric mouse patellar tendons. *J Orthop Res.* Jul 2016;34(7):1256-1263.

40. Franchi M, Fini M, Quaranta M, et al. Crimp morphology in relaxed and stretched rat Achilles tendon. *J Anat.* Jan 2007;210(1):1-7.

41. Diamant J, Keller A, Baer E, Litt M, Arridge RG. Collagen; ultrastructure and its relation to mechanical properties as a function of ageing. *Proc R Soc Lond B Biol Sci*. Mar 14 1972;180(1060):293-315.

42. Rigby BJ, Hirai N, Spikes JD, Eyring H. The Mechanical Properties of Rat Tail Tendon. *J Gen Physiol.* Nov 1 1959;43(2):265-283.

43. Zhang K, Asai S, Hast MW, et al. Tendon mineralization is progressive and associated with deterioration of tendon biomechanical properties, and requires BMP-Smad signaling in the mouse Achilles tendon injury model. *Matrix Biol.* May-Jul 2016;52-54:315-324.

44. Olsson N, Nilsson-Helander K, Karlsson J, et al. Major functional deficits persist 2 years after acute Achilles tendon rupture. *Knee Surg Sports Traumatol Arthrosc.* Aug 2011;19(8):1385-1393.

45. Olsson N, Petzold M, Brorsson A, Karlsson J, Eriksson BI, Silbernagel KG. Predictors of Clinical Outcome After Acute Achilles Tendon Ruptures. *Am J Sports Med.* Jun 2014;42(6):1448-1455.

46. Engler AJ, Sen S, Sweeney HL, Discher DE. Matrix elasticity directs stem cell lineage specification. *Cell.* Aug 25 2006;126(4):677-689.

47. Pelham RJ, Jr., Wang Y. Cell locomotion and focal adhesions are regulated by substrate flexibility. *Proc Natl Acad Sci U S A.* Dec 9 1997;94(25):13661-13665.

48. Chen CS, Mrksich M, Huang S, Whitesides GM, Ingber DE. Geometric control of cell life and death. *Science.* May 30 1997;276(5317):1425-1428.

49. Bi Y, Ehirchiou D, Kilts TM, et al. Identification of tendon stem/progenitor cells and the role of the extracellular matrix in their niche. *Nat Med.* Oct 2007;13(10):1219-1227.

50. Jones DL, Wagers AJ. No place like home: anatomy and function of the stem cell niche. *Nat Rev Mol Cell Biol.* Jan 2008;9(1):11-21.

51. Mienaltowski MJ, Adams SM, Birk DE. Regional differences in stem cell/progenitor cell populations from the mouse achilles tendon. *Tissue Eng Part A.* Jan 2013;19(1-2):199-210.

52. Khan KM, Cook JL, Bonar F, Harcourt P, Astrom M. Histopathology of common tendinopathies. Update and implications for clinical management. *Sports Med.* Jun 1999;27(6):393-408.

53. Patel S, Gualtieri AP, Lu HH, Levine WN. Advances in biologic augmentation for rotator cuff repair. *Ann N Y Acad Sci.* Oct 17 2016.

54. Connizzo BK, Sarver JJ, Han L, Soslowsky LJ. In situ fibril stretch and sliding is location-dependent in mouse supraspinatus tendons. *J Biomech.* Dec 18 2014;47(16):3794-3798.

55. AAOS. Guideline on the Diagnosis and Treatment of Acute Achilles Tendon Rupture. 2009.

CHAPTER IV: MULTISCALE MECHANICAL, STRUCTURAL, AND COMPOSITIONAL RESPONSE OF TENDON TO *DYNAMIC* LOADING DURING HEALING

4.1 Introduction

Tendons transfer stresses and strains from muscle to bone during loading, which cause multiscale matrix changes. Tendon composition and structure are related to mechanical function as disorganized collagen becomes more aligned and less crimped during loading, which creates nonlinearity in load-displacement relations.[1-4] However, extension of these strain-dependent mechanisms in the context of tendon healing and response to dynamic loading has been limited.[5,6] Recently, crimp was visualized with polarized light imaging during dynamic loading.[7] Our work demonstrated that tendon crimp amplitude is altered with fatigue loading. Fatigue loading increased the crimp amplitude, and was both region and load dependent. Although the process of uncrimping is significant as many tendons are believed to operate within the toe region of the stress-strain curve[8] and experience a wide range of *in vivo* strains and strain rates, its role on the tendon cell biomechanical microenvironment remains unknown. Relationships between applied loading and nuclear shape are important because mechanical forces to the nucleus can regulate transcriptional activity.[9,10] Additionally, the role of less injurious magnitude loading on multiscale alterations remains unknown.

Previous work has shown that tissue level strains correlate with cellular and nuclear strains in uninjured tendons during *quasi-static* tensile loading [2]. However, it remains unknown how ECM stresses are altered in clinically relevant situations, such as high *dynamic* loading and *healing*, which may propagate to alter strain transfer to cellular components. We recently evaluated multiscale structure-function mechanisms in

response to quasi-static tensile loading in uninjured and healing tendons. Using an established mouse patellar tendon injury model,[11-13] we harvested living tendon explants that preserve the native architecture of the tendon ECM. Together, our approach allows for the evaluation of multiscale mechanical and structural properties without destructive dissection to the tissue. This procedure provides advancement over traditional histological studies that do not control for tissue pre-stresses or strains applied prior to fixation. We identified that healing tendons experience reductions in nuclear aspect ratio (nAR) and nuclear re-organization in response to loading compared to uninjured tendons, and that these responses are ultimately related to organization of the microscale collagen structure and amount of F-actin. However, it remained unknown what role dynamic loading may play in contributing to or impeding multiscale strain transfer in healing tendon.

The objective of this study was to investigate the role of tendon healing and dynamic loading on mechanical strain stiffening, fiber recruitment, and strain transfer to tendon cell nuclei. The importance of using native matrices that preserve *in vivo* architecture are important as validation measures as tissue engineered constructs can over estimate strain transfer compared to native tissue.[6] We hypothesized that high magnitude long duration dynamic loading and healing would reduce strain stiffening and fiber recruitment compared to uninjured tendons and low magnitude long duration dynamic loading. Additionally, we hypothesized that low magnitude dynamic loading will increase strain stiffening, stiffness, and alignment, which ultimately increases tendon cell nAR, unlike high dynamic loading.

4.2 Methods

4.2.1 Study Design

Female C57BL/6 mice (N=188) at 150 days of age were randomized into an uninjured control group and groups that received bilateral injury to their patellar tendons (N=375 total tendons) (IACUC approved) (**Figure 4-1**).[11,12,14] Mice in injury groups were first anesthetized (isoflurane) and both hindlimbs were shaven and sterilized. Using aseptic procedures, a single incision was made through the skin near the knee, and longitudinal incisions were made adjacent to and on either side of the patellar tendon. A rubber-coated backing was placed under the tendon, and a full thickness, partial width (~60% width) excisional injury was created using a 0.75mm biopsy punch. Skin was closed with 5-0 prolene suture, and the animals were returned to cage activity. Doses of buprenorphine (0.1mg/kg; Penn Investigational Drug Service) were given pre-surgery, and sustained-release buprenorphine (1.0mg/kg; ZooPharm; Windsor, CO) was given post-surgery. Injured animals were randomized into groups euthanized at 2 or 6 weeks post-injury to evaluate the role of healing on multiscale tendon properties. At these timepoints, mice were sacrificed and tendons were mechanically tested *ex vivo* with tissue tendon explants.

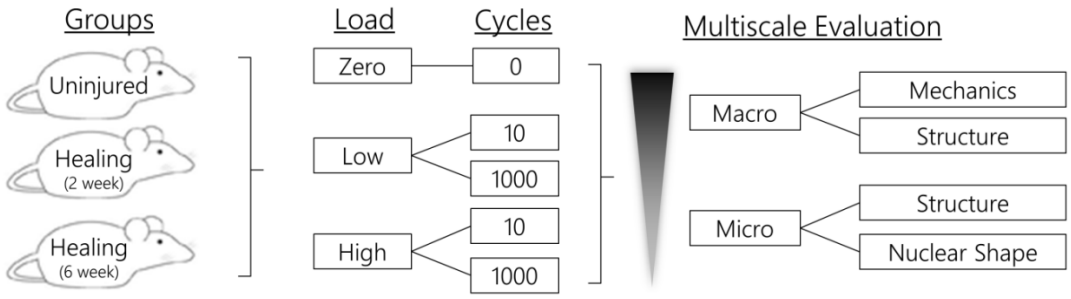

Figure 4-1: Study Design. Animals are divided into three groups (uninjured, 2-weeks post-injury, and 6-weeks post-injury)

4.2.2 Sample Preparation and Mechanical Testing

For multiscale evaluation relating applied macroscale mechanical loading to microscale properties (cell, nuclear, and collagen morphology), tendons were harvested immediately after sacrifice and kept in standard media conditions to maintain cell viability. Maintenance of cell viability was important to preserve *in vivo* cell migration and contraction during loading, which are ATP driven processes.[15] The patellar tendon was stamped into a "dog-bone" shape to isolate the injury site, and measured for cross sectional area at the injury site.[16] To maintain tenocyte viability during loading, tissues were immersed in a bath containing sterile DMEM supplemented with 5% fetal bovine serum (FBS), maintained at 37ºC integrated with a tensile testing device (Instron 5848; Norwood, MA). To evaluate the effect of dynamic loading and healing on strain stiffening, tendons were randomized into a zero, low, or high magnitude loading protocol (corresponding to the toe or linear regions of the force-displacement curve) for either 10 or 1000 cycles at 1Hz (Groups: Low/10, Low/1000, High/10, High/1000). Loading levels were determined from ramp-to-failure data derived from uninjured and healing patellar tendons, with loading regimes representing the transition (low) and linear (high) portions of the load-displacement curve. Tendons (n=10-13/group) were preconditioned and ramped at constant strain rate (0.1% strain/s) until 1% or 10% strain prior to a frequency sweep (0.125% strain amplitude at 0.1, 1, 5, and 10Hz) (**Figure 4-2**) and snap freezing (**Figure 4-3**).

During loading, force and displacement data were acquired from 100-1000 Hz and analyzed using custom MATLAB code (Mathworks, Natick, MA). Several post processing parameters are computed both during the mechanical and diagnostic tests: 1)

maximum/minimum cyclic displacement and strain; 2) tangent stiffness (calculated as the slope between the maximum and minimum force and displacements for each cycle); 3) stress (calculated as the force divided by the cross sectional area); 4) dynamic modulus (calculated as the slope between the maximum and minimum stress and strain for each cycle; 5) hysteresis (defined as the area enclosed by the stress-strain curve for a cycle); and 6) laxity (defined as the ratio of displacement and gauge length relative to the first cycle of fatigue loading, and assessed at constant load throughout fatigue testing). In addition to properties quantified during dynamic loading, we evaluated dynamic properties at 1% and 10% strain. The change in equilibrium stress (force divided by the cross sectional area) between 1 and 10% strain was used to indicate the amount of strain stiffening, and the dynamic modulus and phase shift assessed during frequency sweeps were computed.

For evaluation of macroscale tendon structure, a separate cohort of tendons (N=10/group) were frozen at -20°C, thawed, and fine dissected, as done previously.[12,17,18] Patella–patellar tendon–tibia complexes were carefully isolated by dissection under magnification and tendons were carefully stamped into a “dog-bone” shape of width 0.75mm. Before and after stamping, tendon cross-sectional area was measured with a custom, laser-based device.[16] The distal half of the tibia was then secured in a custom fixture and loaded into a material testing system (Model 5848, Instron; Norwood, MA) with a 10N load cell. During loading, force and displacement data were acquired and analyzed using MATLAB (Mathworks, Natick, MA). In addition, these experiments were used to evaluate the role of recovery. Following cyclic loading, tendons were maintained at 0% strain for 1000s.[19] This recovery period is commonly used in tendon, and ranges

from 1-45 minutes.[19-23] Following recovery periods, tendons were subjected to the same quasi-static loading protocol to both 1 and 10% strain during which polarized light images were taken.

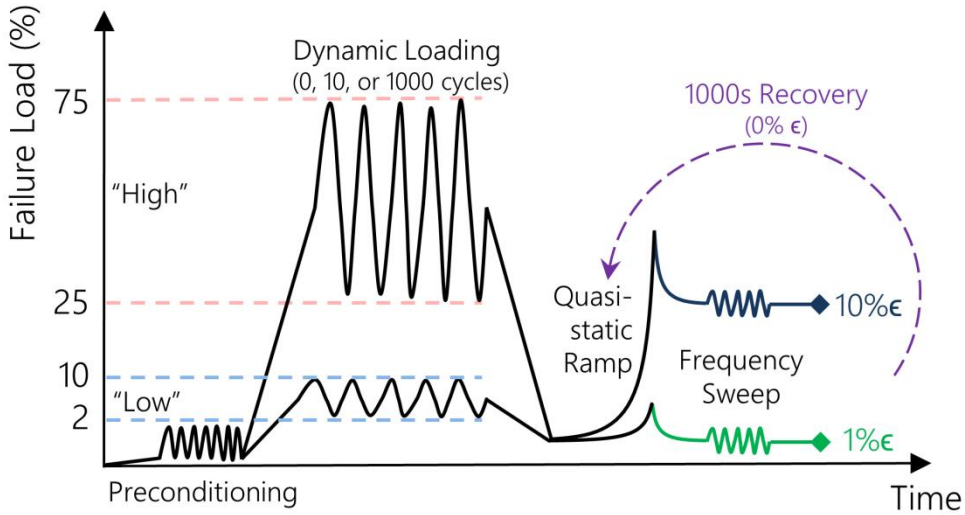

Figure 4-2: Mechanical Testing Protocol. Tendons were preconditioned and then dynamic loaded for 0, 10, or 1000 cycles at either high (25-75% UTS) or low (2-10% UTS) loads. Following loading, tendons underwent a quasi-static ramp to 1% or 10% strain followed by a frequency sweep. For recovery experiments, tendons were allowed 1000s of rest at 0% strain prior to a second quasi-static ramp. For non-recovery experiments, tendons were snap frozen at either 1% or 10% strain for microscale assessment.

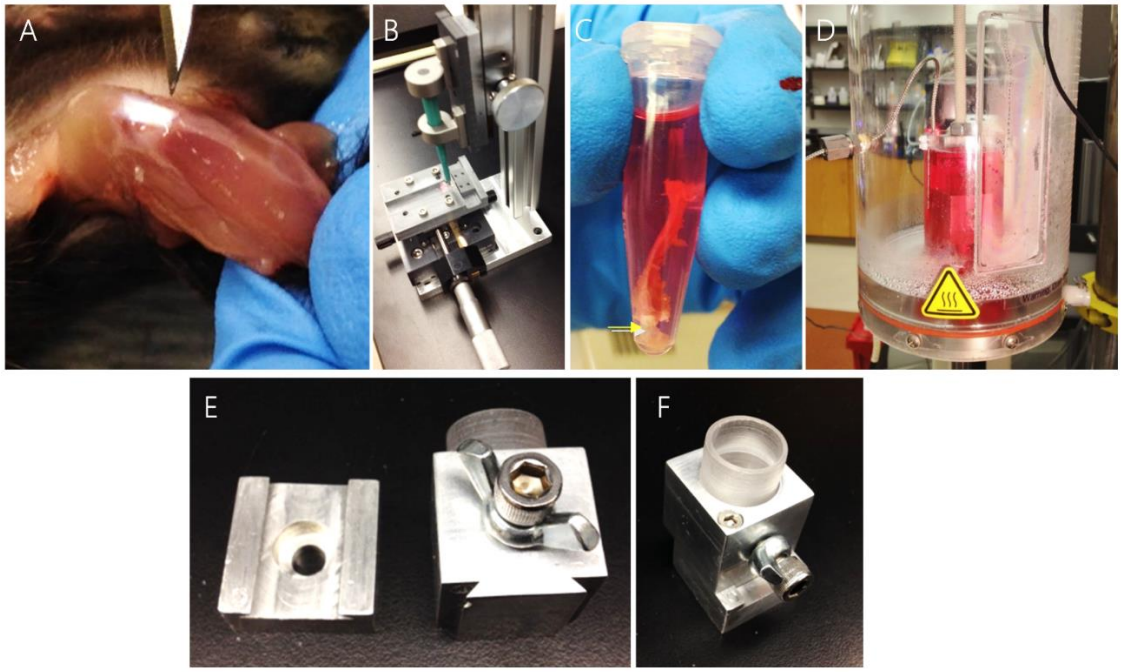

Figure 4-3: Experimental setup for live tendon testing. (**A**) Patellar tendons were immediately harvested, (**B**) stamped into a dog bone shape, and (**C**) maintained hydrated in basal media prior to (**D**) mechanical loading.

4.2.3 Cell Viability

Cell viability was evaluated with an MTT assay, which exploits the redox potential of actively respiring cells. In live cells, water-soluble MTT is converted to an insoluble purple formazan, which is solubilized and determined for concentration by optical density. A 12mM MTT stock solution was prepared by adding 1mL of sterile PBS to 5mg of MTT under sterile conditions. For labeling viable cells in tissue, 100uL of stock solution is added to 1000uL of DMEM, keeping the mixture at 37C at 5%CO_2 prior. Following tissue harvest, tissue was placed immediately in Eppendorf tubes left open in an incubator for 1-hour. Tissues were transferred to PBS for 30 min at room temperature and fixed with 4% PFA at 4°C overnight prior to cryosectioning. Tissue sections were counter stained with DAPI to qualitatively compare viable cells with all cells.

4.2.4 Polarized Light Imaging

A polarized light system[24] was integrated with the mechanical testing, consisting of a backlight, 90° offset rotating polarizer sheets (Edmund Optics, Barrington, NJ) on both sides of the test sample (polarizer and analyzer), and a GigE aca2040gm camera (resolution: 2048x2048 pixels) (Basler, Exton, PA). Sets of alignment maps (30 images) were taken during the quasi-static ramp and following frequency sweeps at 1% or 10% strain.

A custom MATLAB program (MATLAB, Natick, MA) divided images into a series of regions of 100 pixels^2 spaced at 20 pixels and individually averaged to filter

noise. From these data, the signal phase and magnitude, within each region from each alignment image series, was used to determine the circular standard deviation (CSD), a measure of collagen fiber disorganization.[25] Briefly, the CSD was calculated by fitting a $\sin 2\theta^2$ function[26] to the pixel intensity-polarizer angle data to determine the angle corresponding to the minimum pixel intensity. This angle represents the average direction of fiber alignment.

4.2.5 Fiber Recruitment Model

We applied a structurally based elastic model[27-29] to our mechanical data to quantify the non-linear force-displacement behavior as fibers uncrimp to their slack length. This model assumes that fiber uncrimping gives rise to tendon's non-linear force-displacement behavior, and is modeled using a cumulative probability distribution function (Eq. 3-2). Briefly, p is the cumulative probability of a fiber being uncrimped (range: 0-100%), σ is the standard deviation of fiber slack-lengths (mm), L_0 is the fiber slack length (mm), and μ is the average fiber slack length (mm). Fibers are considered uncrimped once the tendon length has exceeded the fiber's slack-length (Eq. 3-3). Here, K_{avg} is the average fiber stiffness (N/mm), x is the tendon length (mm), L_0^i is the slack length of fiber i, and H is the heavy side step function (H = 0 for $x < L_0^i$ and 1 for $x > L_0^i$). Disorganized tissues, such as skin, have an elongated toe-region, which results in slack lengths with high means and standard deviations.

$$p(L_0) = \frac{1}{\sigma\sqrt{2\pi}} \int_{-\infty}^{L_0} e^{\frac{-(t-\mu)^2}{\sigma}} \qquad \text{(Eq. 3-2)}$$

$$F(x) = K_{avg} \sum_{i=1}^{N} (x - L_0^i) \cdot H(x - L_0^i) \qquad \text{(Eq. 3-3)}$$

4.2.6 Immunofluorescence Staining

After each loading protocol, tissues were snap frozen, and immediately embedded in Optimum Cutting Temperature (OCT) compound (Tissue-Tek, Sakura Finetek USA, Torrance, CA, USA), prior to sectioning at 15µm (Leica CM1950; Wetzlar Germany) using Kawamoto's Film.[30] Following cryosectioning, sections were placed in 4% paraformaldehyde (Fisher) for 3 minutes and attached to slides with a chitosan film adhesive solution. Tissue sections were rehydrated in 1xPBS, blocked for non-specific binding in 5% BSA and 0.1% triton for 1-hour at 4°C, and then stained with primary conjugated antibodies for cell and nuclear shape analysis. Sections were stained for F-actin with Alexa Fluor® phalloidin (1:20; 555/565; Fisher Scientific), nuclei with DRAQ5 Fluorescent Probe Solution (1:1000; 647/681; Fisher Scientific), and denatured collagen with collagen hybridizing peptide (CHP) (1:10; 490/525; Echelon Biosciences) for 12 hours at 4°C. Cell and nucleus long and short axes were measured using a custom MATLAB program and ImageJ (v1.48, NIH, Bethesda, MD) to derive aspect ratios.

4.2.7 Confocal and Multiphoton Imaging

Sequential scans on an upright laser-scanning multiphoton confocal microscope (Leica TCS SP8; Wetzlar Germany; 1024x1024 pixel resolution, fov: 277µm x 277µm, scan speed: 400Hz) were completed to evaluate stains for denatured collagen, collagen, F-actin, and nuclei in tendon sections, as done previously (Chapter 3). Z-stacks were

taken at 1.5μm intervals to capture the tendon midsubstance or injury site. Images from 2-3 tendon sections were taken per specimen.

We determined the average collagen fiber organization by computing the angular orientation of fibers in the SHG images with custom code (MATLAB; v2015a; Natick, MA), as done previously (Chapter 3).[31] Briefly, images were selected from the middle of each Z-stack with fibers aligned along the horizontal direction, images were contrast enhanced, and determined for fiber alignment using Fourier analysis. A quiver plot was superimposed on the original image to ensure that collagen fiber orientation was computed correctly. Angles were plotted in a histogram to determine angular distribution. For average organization, the circular standard deviation was calculated at 1% or 10% strain to evaluate changes in fiber orientation during tendon loading. The average circular statistics was taken across all selected images in the Z-stack for uninjured samples.

4.2.8 F-Actin and Nuclear Shape Analysis

F-actin was quantified by determining the percent positive staining per ROI. Images were imported into FIJI, cropped, max projected, converted to 8-bit greyscale, contrast enhanced, and thresholded to isolate F-actin filaments. The number of F-actin positive pixels was determined and normalized to the total cropped ROI. The same ROIs for nuclei were similarly selected in FIJI, and segmented and analyzed using CellProfiler[32] to evaluate nuclear shape (major/minor axis, nuclear aspect ratio (nAR)) and orientation (nOrientation).

4.2.9 Statistical Analysis

Data normality was assessed and confirmed with Shapiro Wilk tests. To determine the role of loading magnitude and duration on multiscale tendon properties, data were evaluated with two-way ANOVAs with post hoc Student's t-tests with Bonferroni corrections (SPSS). To determine the role of strain on tendon multiscale properties, data were evaluated with Student's t-tests with Bonferroni corrections. Linear regression was used to determine relationships between microscale structure, composition, and nuclear shape.

4.3 Results

4.3.1 Macroscale Mechanics and Structure are Inferior Following High Magnitude Dynamic Loading

Cell viability was maintained throughout mechanical testing. Cycle number and loading magnitude affected tissue strain stiffening, as the change in equilibrium stress was reduced due in the high/1000 group compared to the low/10 group (**Figure 4-4A**). This decrease in strain stiffening was coupled with decreased dynamic modulus in longer duration and high magnitude loading groups at 1% strain (**Figure 4-4B**), with reduced effects present at 10% strain (**Figure 4-4C**). Cycle number was a significant factor, regardless of applied load, on increasing tendon laxity (**Figure 4-5A**). As tendons were loaded dynamically in different regimes of the stress-strain curve, the secant modulus detected showed a significant increase in the high magnitude cases, as expected (**Figure 4-5B**). Force and displacement data was also used to fit a fiber recruitment model to

predict average fiber slack lengths.[33] In agreement with decreased strain stiffening and increased laxity, elevated fiber slack lengths were predicted in the high/1000 group (**Figure 4-5C**). As these predictions of increased slack lengths indicate decreased fiber recruitment, we assessed collagen fiber re-alignment to verify this finding. Indeed, the low/10 loading group resulted in collagen fiber re-alignment at lower strains compared to the high/1000 loading group (**Figure 4-6**). Taken together, these results suggest that tendon strain stiffening is reduced due to high magnitude long duration loading and occurs in concert with increased laxity and delayed fiber re-alignment with applied strain. Notably, these macroscale mechanical property changes with high dynamic loading were found to be non-recoverable after 1000s of rest at 0% strain, indicating that sustained macroscale mechanical alteration is present in these groups (**Figure 4-7**).

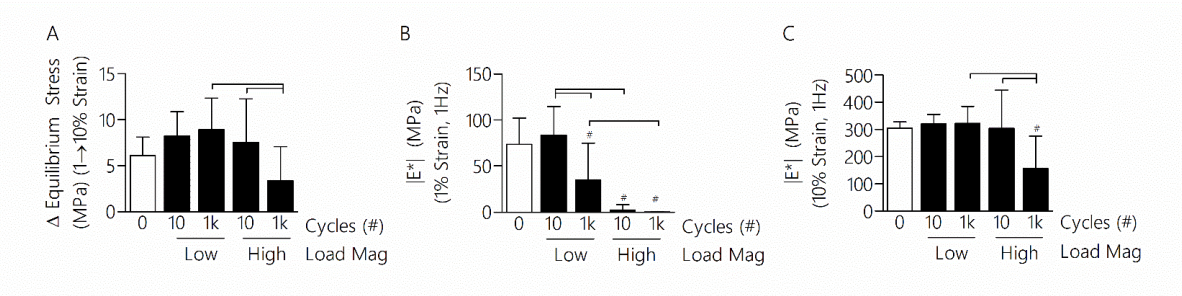

Figure 4-4: Macroscale Strain Stiffening. The effects of cycle duration and loading magnitude on (**A**) the change in equilibrium stress, (**B**) |E*| at 1% strain, and (**C**) |E*| at 10% strain were evaluated. Data shown as mean±SD. Lines indicate significant differences ($p<0.0125$). "#" indicates differences relative to quasi-static controls (unshaded) ($p<0.0125$). N=7-12/group.

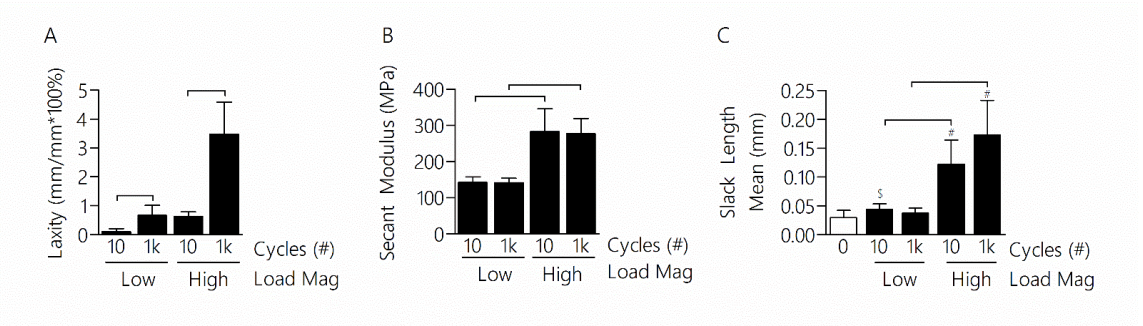

Figure 4-5: Macroscale Dynamic Mechanical Properties. The effects of cycle duration and loading magnitude on (**A**) tendon laxity, (**B**) the secant modulus, and (**C**) tendon slack length were evaluated. Data

shown as mean±SD. Lines indicate significant indicates differences (p<0.0125). "#"and "$" indicates statistical trends relative to quasi-static controls (unshaded). N=7-12/group.

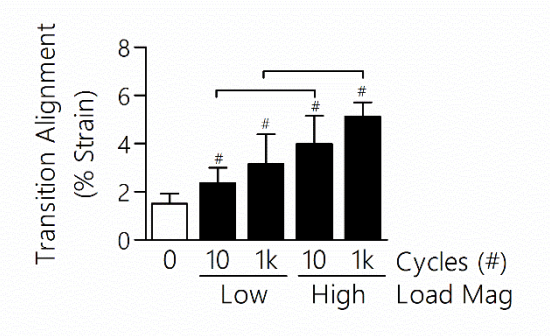

Figure 4-6: Macroscale Collagen Alignment. The effects of cycle duration and loading magnitude on collagen fiber transition alignment was evaluated. Data shown as mean±SD. Lines indicate significant differences (p<0.0125). "#" indicates differences relative to quasi-static controls (unshaded) (p<0.0125). N=5-8/group.

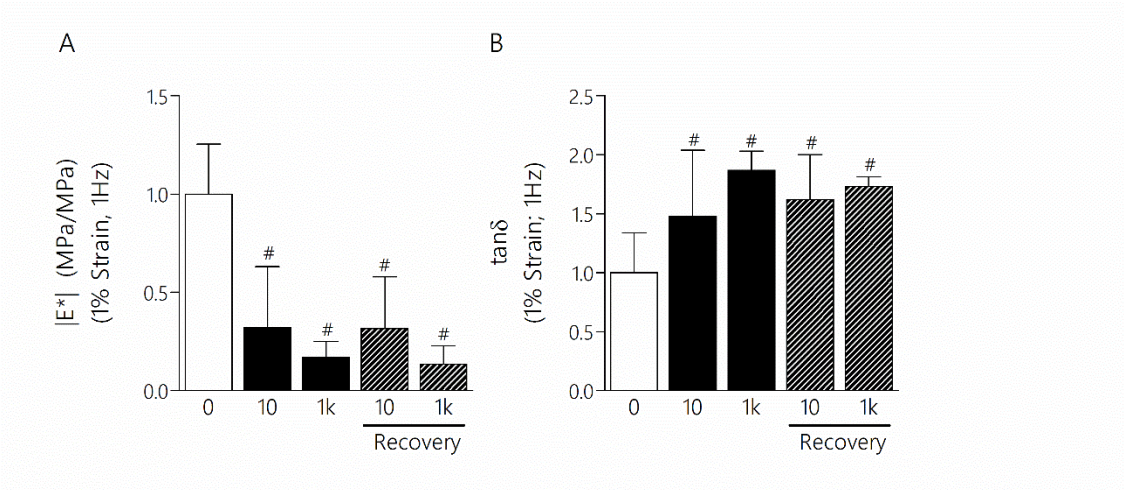

Figure 4-7: Macroscale Mechanical Recovery. The effects of recovery following high magnitude loading were evaluated. Data shown as mean±SD. "#" indicates differences relative to quasi-static controls (unshaded) (p<0.0125). N=7-10/group.

4.3.2 Microscale Structural and Compositional Properties are Inferior Following High Magnitude Dynamic Loading

To investigate whether macroscale changes in mechanics and structure propagate to the microscale, we evaluated tendon structure using MP imaging and simultaneously evaluated tendon nuclei shape and F-actin following both low (high) magnitude and short (long) duration loading (**Figures 4-8,9,10,11**). Confocal and MP imaging revealed that

changes in collagen organization, nuclei shape, and nuclei organization were dependent on the loading protocol and applied strain (**Figure 4-12**). Although group showed similar collagen organization regardless of loading protocol at 1% strain, fatigue loaded samples had elevated fiber disorganization at 10% strain (**Figure 4-13A**), and thus was strain insensitive (**Figure 4-13B**). Similar negative effects of fatigue loading also reduced strain transfer to nuclei, as the change in nAR from 1% to 10% strain was diminished in fatigue loaded samples compared to low-magnitude loading and quasi-static controls (**Figure 4-14**). This decreased change in nAR was coupled with increased nuclei disorganization in the high/10 and high/1000 loaded tendons (**Figure 4-15A**), that remained strain insensitive following fatigue loading (**Figure 4-15B**). This nuclear disorganization correlated linearly with collagen disorganization (R^2 = 0.90; **Figure 4-16**). Actin staining and collagen alignment were not significant predictors of nAR.

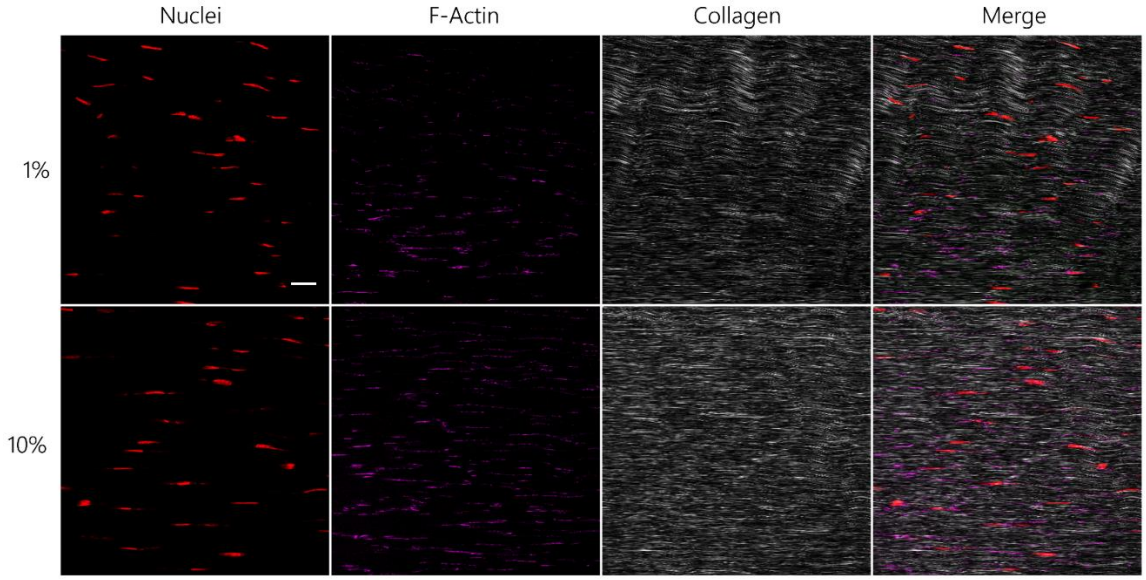

Figure 4-8: Multiphoton Imaging Comparing Effects of Strain Following Low Magnitude Short Duration Loading. Scale bar = 20μm.

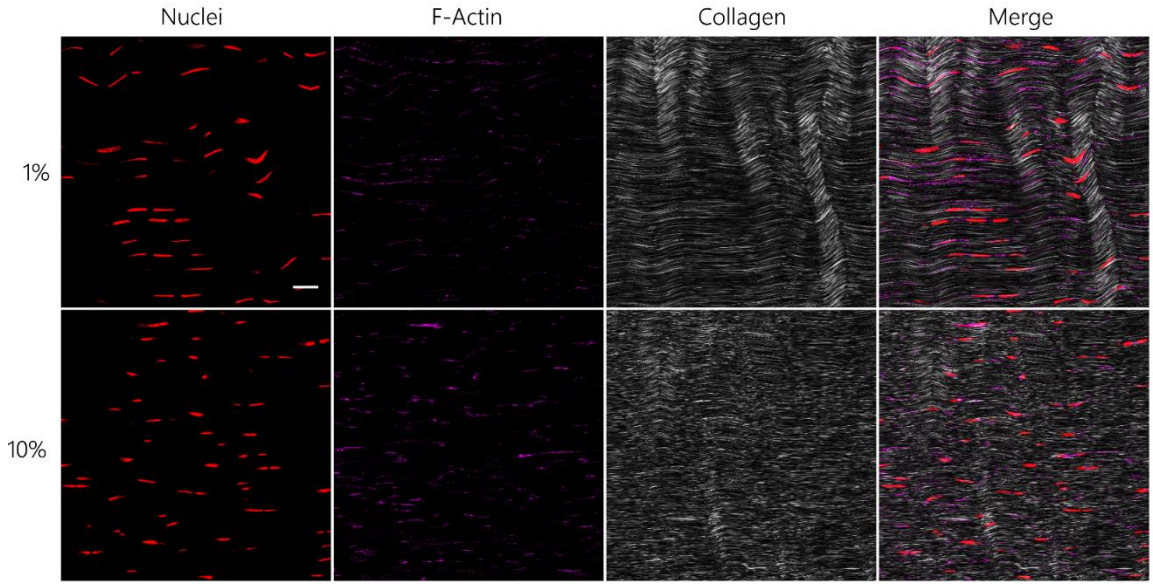

Figure 4-9: Multiphoton Imaging Comparing Effects of Strain Following Low Magnitude Long Duration Loading. Scale bar = 20μm.

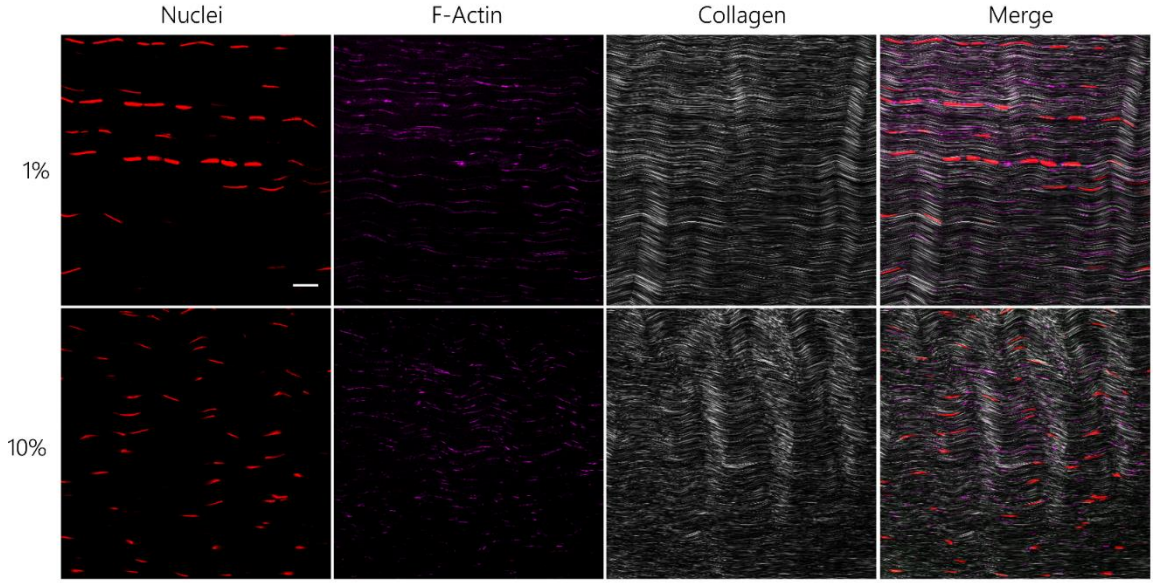

Figure 4-10: Multiphoton Imaging Comparing Effects of Strain Following High Magnitude Short Duration Loading. Scale bar = 20μm.

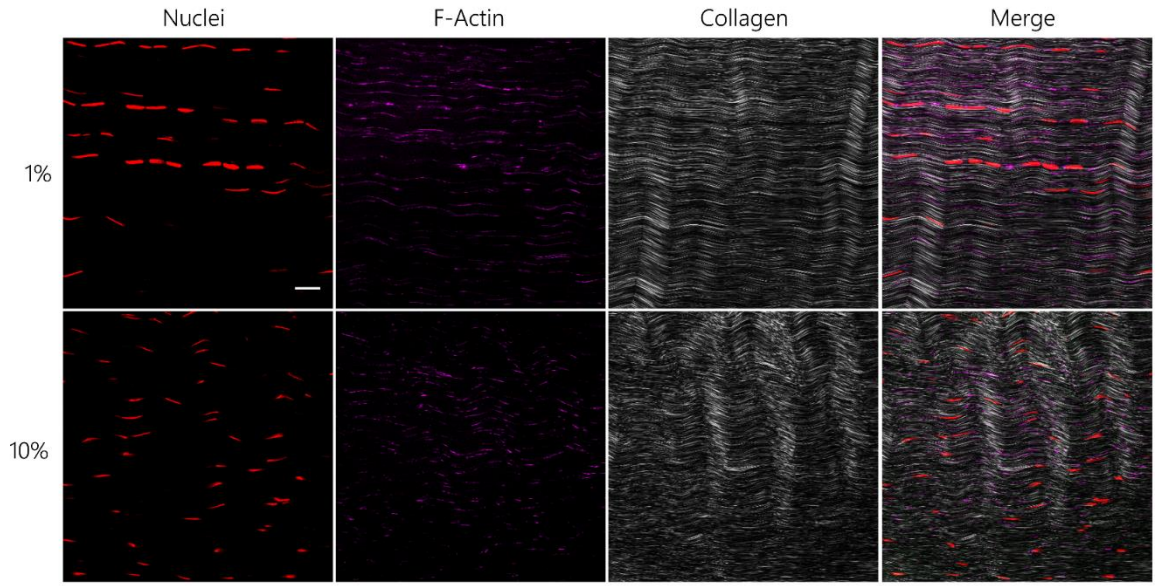

Figure 4-11: Multiphoton Imaging Comparing Effects of Strain Following High Magnitude Long Duration Loading. Scale bar = 20μm.

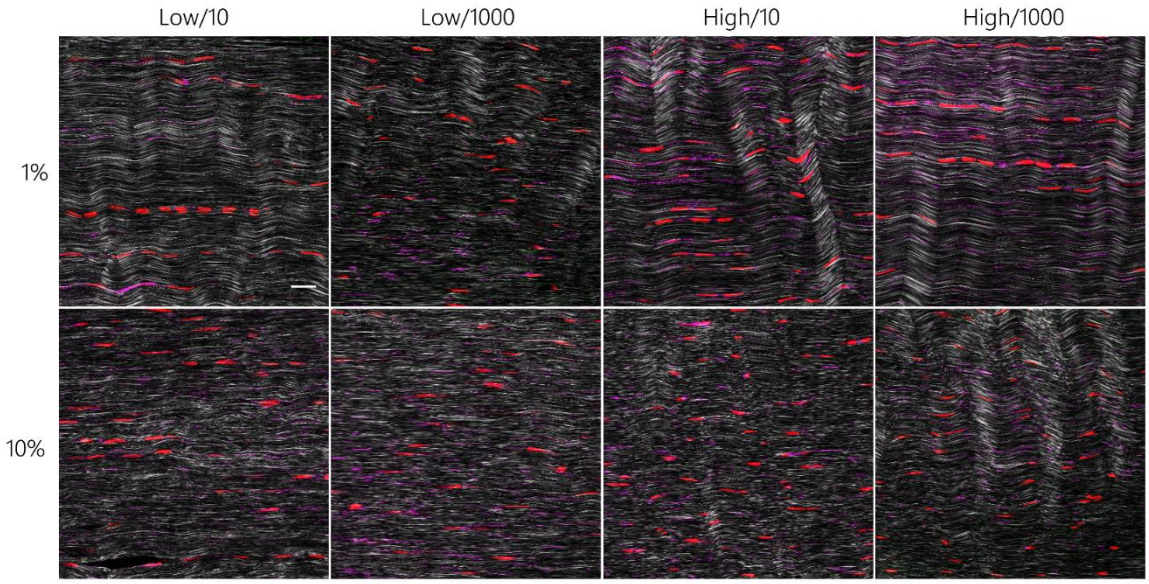

Figure 4-12: Multiphoton Imaging: Group Comparisons. Red: Nuclei; Magenta: F-Actin; White: Collagen. Scale bar = 20μm.

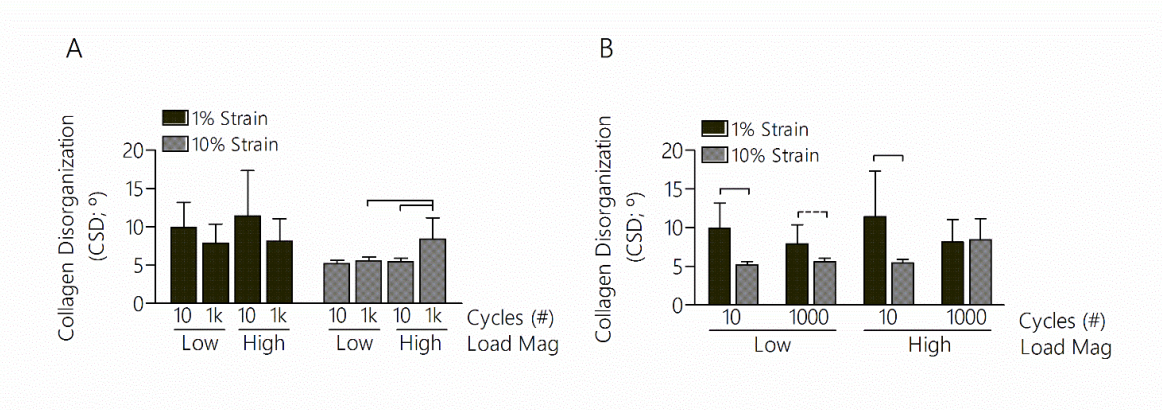

Figure 4-13: Microscale Collagen Organization. The effects of (**A**) cycle duration and loading magnitude and (**B**) applied strain on collagen disorganization were evaluated. Data shown as mean±SD. Lines indicate significant differences (p<0.0125) and dashed lines indicate trends (p<0.025). N=7-12/group.

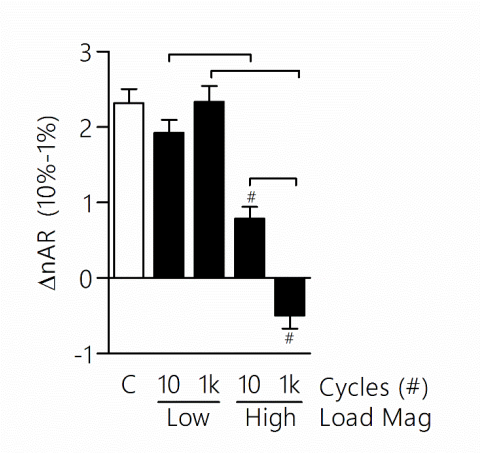

Figure 4-14: Nuclear Aspect Ratio. The effects of cycle duration and loading magnitude on the change in nAR were evaluated. Data shown as mean±SEM. Lines indicate significant differences (p<0.0125) and dashed lines indicate trends (p<0.025). "#" indicates differences relative to quasi-static controls (unshaded) (p<0.0125). N=363-511/group.

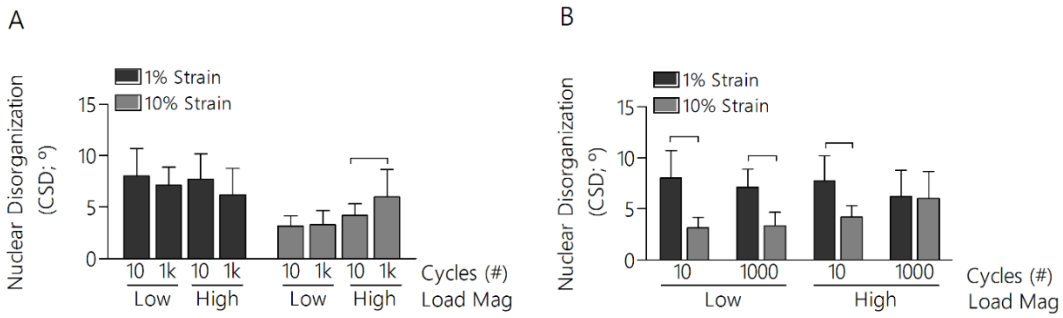

Figure 4-15: Nuclear Organization. The effects of (**A**) cycle duration and loading magnitude and (**B**) applied strain on nuclear disorganization were evaluated. Data shown as mean±SD. Lines indicate significant differences (p<0.0125) and dashed lines indicate trends (p<0.025). N=7-12/group.

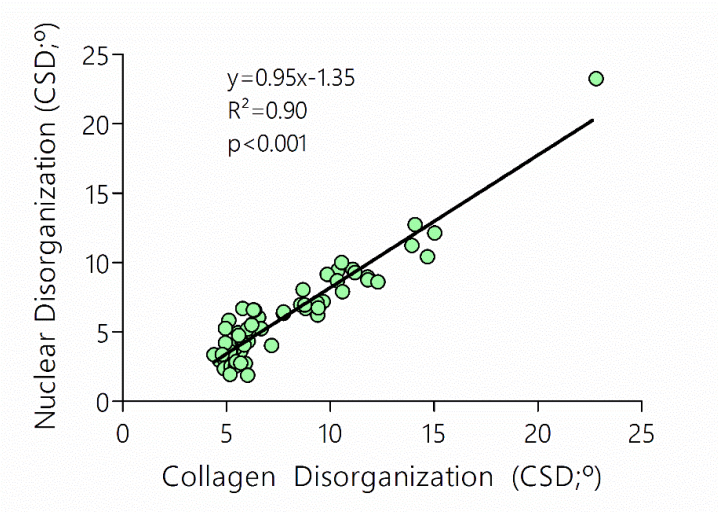

Figure 4-16: Correlations. Nuclear disorganization was significantly correlated with collagen disorganization (R^2=0.90).

4.3.3 Effect of Dynamic Loading on Macroscale Tendon Properties in Healing Tendon

We next investigated whether healing the multiscale mechanisms in response to dynamic loading observed in uninjured controlled tendon extended to healing tendon. Loading magnitude affected tissue strain stiffening in healing tendon, as the change in equilibrium stress was reduced due to high magnitude, long duration loading compared to low magnitude loading (**Figure 4-17**). This decrease in strain stiffening was coupled with decreased dynamic modulus at 1% strain (**Figure 4-18A,B**) and elevated viscous dissipation (**Figure 4-18C**). Cycle number was a significant factor, regardless of applied load, on increasing tendon laxity (**Figure 4-19A**). Unlike uninjured tendons, healing tendon modulus was affected by cycle number in high/1000 groups (**Figure 4-19B**). As seen previously with uninjured tendon, the response of healing tendon to dynamic loading showed elevated laxity during high/1000 loading, which correlated with predicted fiber slack lengths (**Figure 4-19C**). Interestingly, low/1000 loading, but not

high/1000 loading, resulted in gradual reductions in lengthening replaced by matrix shortening in living tendons (compared to fresh frozen) (**Figure 4-20**).

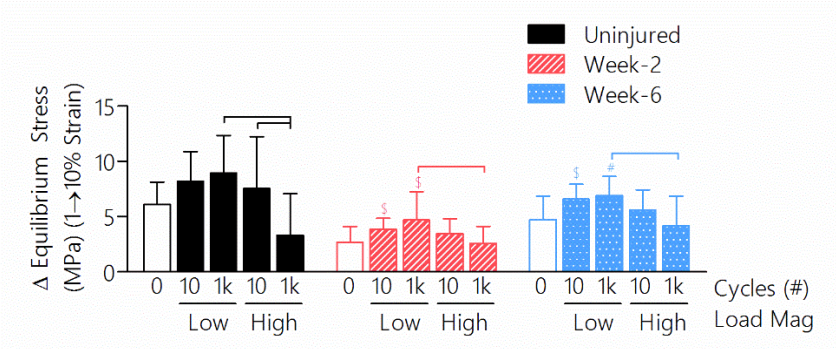

Figure 4-17: Effect of Healing on Equilibrium Stress. The effects of cycle duration and loading magnitude on the change in equilibrium stress throughout healing were evaluated. Data shown as mean±SD. Lines indicate significant differences (p<0.0125). "#" indicates differences (p<0.0125) and "$" indicate trends (p<0.025) relative to quasi-static controls (unshaded). N=7-12/group.

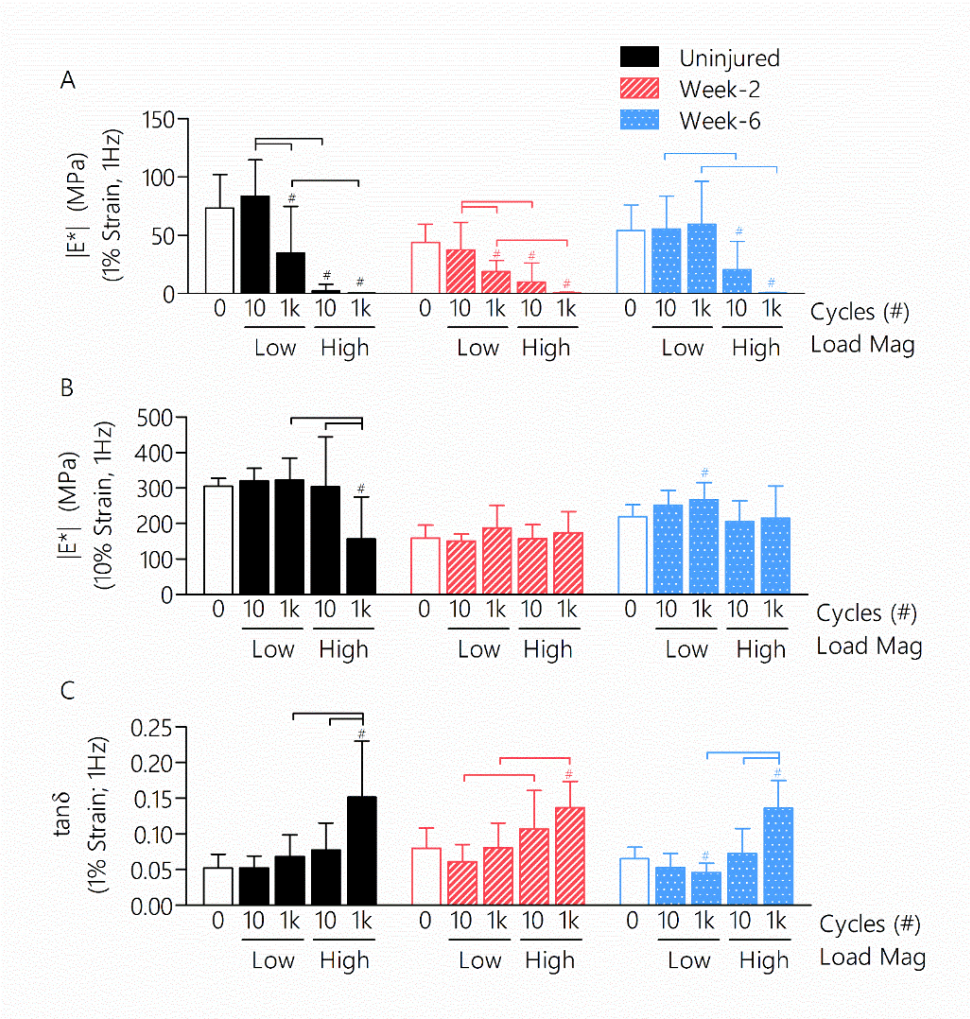

Figure 4-18: Effect of Healing on Dynamic Mechanical Properties. The effects of cycle duration and loading magnitude on (**A**) |E*| at 1% strain, (**B**) |E*| at 10% strain, and (**C**) tanδ at 1% strain were evaluated. Data shown as mean±SD. Lines indicate significant differences (p<0.0125). "#" indicates significant differences (p<0.0125) relative to quasi-static controls (unshaded). N=7-12/group.

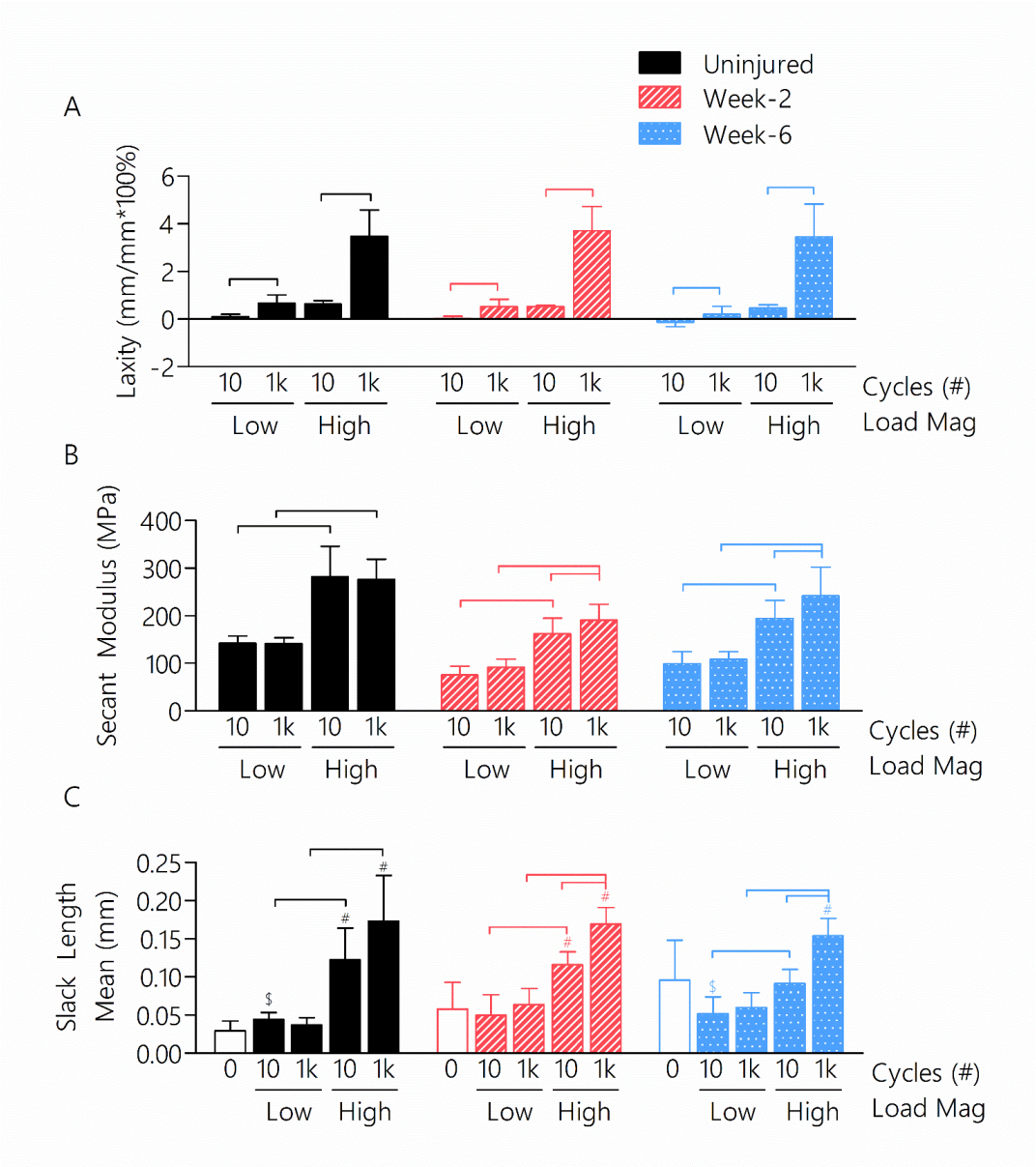

Figure 4-19: Effect of Healing on Fatigue Properties. Data shown as mean±SD. Lines indicate significant differences (p<0.0125). "$" and "#" indicate trends (p<0.025) and significant differences (p<0.0125) relative to quasi-static controls (unshaded). N=7-12/group.

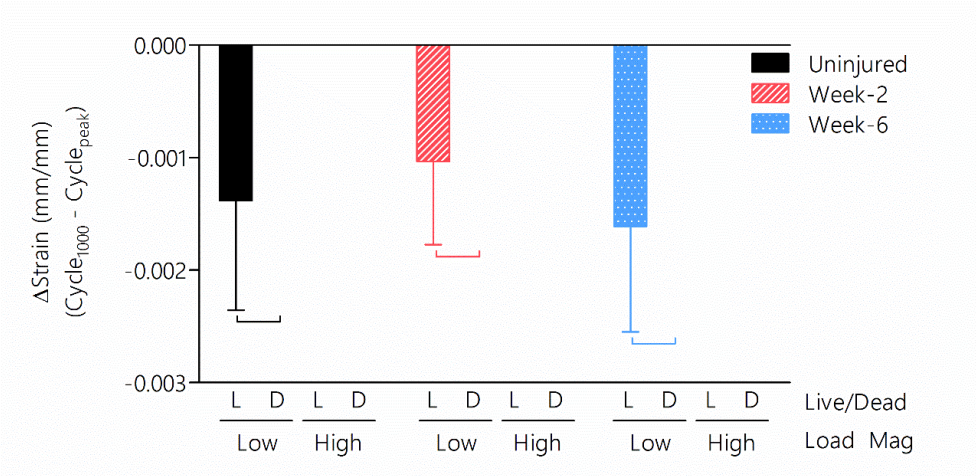

Figure 4-20: Effect of Low Magnitude Long Duration Loading on Strain. Data shown as mean±SD. Lines indicate significant differences ($p<0.025$). N=7-12/group.

4.3.4 Effect of Dynamic Loading on Microscale Tendon Properties in Healing Tendon

To determine whether macroscale mechanical changes observed during dynamic loading in healing tendon propagated to the microscale, microstructural and nuclear evaluation was completed. Although healing had an effect on actin staining, dynamic loading did not (**Figure 4-21**). Overall, unlike uninjured tendons, dynamic loading did not affect collagen disorganization during healing (**Figure 4-22**). However, dynamic loading led to decreased nuclei disorganization at 2-weeks post-injury, but not at 6-weeks post-injury (**Figure 4-23**). Interestingly, although high magnitude loading decreased the change in aspect ratio in uninjured tendons, the opposite was observed in healing tendons, although the changes observed were small (**Figure 4-24**).

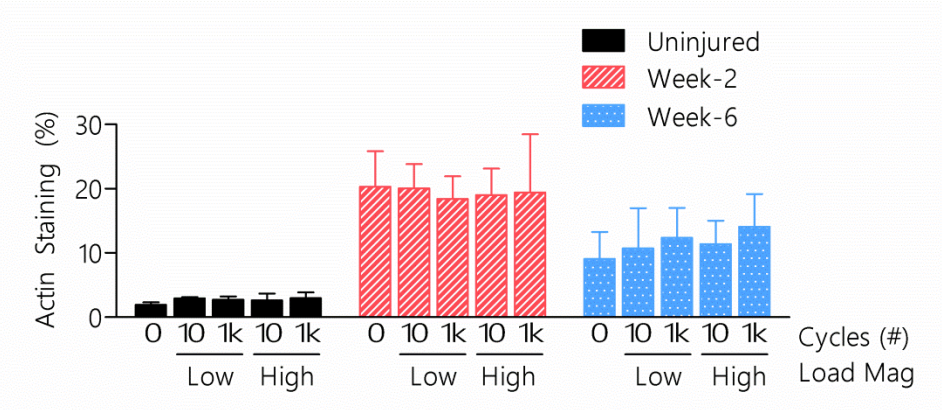

Figure 4-21: Effect of dynamic loading and healing on actin staining. Data shown as mean±SD. N=7-10/group.

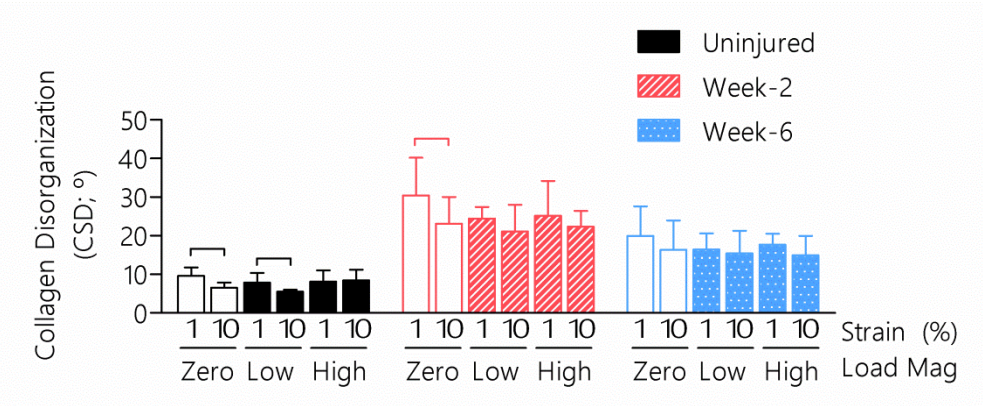

Figure 4-22: Effect of dynamic loading and healing on microscale collagen disorganization. Dynamic loading did not affect collagen disorganization during healing. Data shown as mean±SD. N=7-10/group. Lines indicate significant differences (p<0.05).

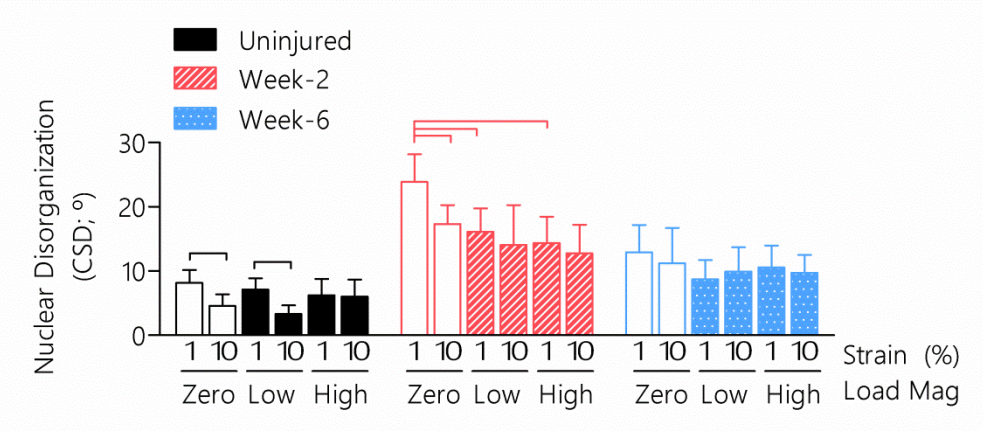

Figure 4-23: Effect of dynamic loading and healing on nuclear disorganization. Dynamic loading decreased nuclear disorganization at 2-weeks post injury, but did not affect uninjured or 6-week post-injury tendon. Data shown as mean±SD. N=7-11/group. Lines indicate significant differences (p<0.05).

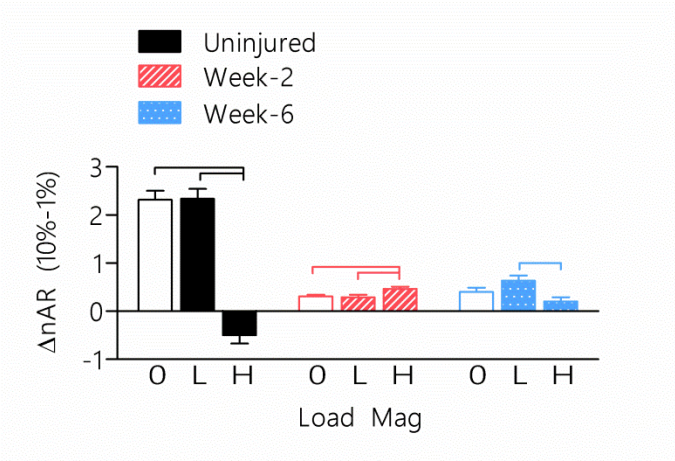

Figure 4-24: Effect of dynamic loading and healing on ΔnAR. Although high magnitude loading decreased the change in aspect ratio in uninjured tendons, the opposite was observed in healing tendons. Data shown as mean±SEM. N=363-1105 cells/group. Lines indicate significant differences ($p<0.017$).

4.4 Discussion

This study evaluated multiscale structure-function mechanisms in response to dynamic tensile loading (varying magnitude and duration). We used an established patellar tendon model,[12,17,18] modified to evaluate properties in living tendon explants. After establishing multiscale relationships in uninjured tendon, we evaluated whether similar effects would exist in healing tendon. These procedures allow for a comprehensive evaluation of tendon properties and are highly repeatable.

We first showed that tendon strain stiffening is reduced, and non-recoverable, due to high magnitude long duration loading and occurs in concert with increased laxity and delayed fiber re-alignment with applied strain. These macroscale properties correlated to microscale properties; high magnitude long duration loading resulted in collagen and nuclear disorganization at high strains, and decreased change in nAR with applied loading. Results in uninjured tendons were largely extendable to healing tendons, however, the reduced modulus and increased laxity observed during high/1000 loading

may indicate inferior fiber recruitment in healing tendons compared to uninjured tendons.[34]

Several *in vitro* bioreactor systems have been utilized to apply tensile loads to tendon explants.[35-47] Such studies have evaluated the effects of cyclic loading on tendon macromechanics,[35,39,41,42,44,45] inflammatory cytokines,[36,41] ECM components,[36,39,40,43] and gene expression.[35,37,38,47] Model systems typically utilize fascicles derived from tail,[37,38,40,43] flexor,[45] extensor,[35] and patellar tendons[42,44] cultured in standard media conditions under various amounts of applied load, duration, and frequency. However, none of these studies examined potential acute changes to the tendon cell microenvironment and resulting morphological properties of the nucleus or surrounding matrix that may play important roles in mechanotransduction. The methods used are necessary for validation in tissue engineered constructs that may over estimate strain transfer compared to native tissue.[6] This remains critical for accurate comparisons to model *in vivo* microenvironments.

Although chondrocyte nuclei have been shown to be shape and volume sensitive to compression induced changes since 1995,[48] tenocyte nuclei were first observed to be strain responsive in rat tail in 2002.[49] Since then, our understanding for the implications of nuclear strain transfer has increased dramatically. Nuclear shape and organization are important because mechanical forces to the nucleus can regulate transcriptional activity[9,10] and protein synthesis.[10] Relations between the ECM and structural organization of the nucleus can further modulate tissue phenotype.[50] During loading, strain transfer to the nucleus can direct access of chromatin to transcriptional regulators, as nascent RNA synthesis is detected in interchromatin regions.[51] Another mediator of

nuclear deformation are A-type lamins, which affect nucleus structure, shape and stability.[52,53] Nuclear strain transfer may also affect Yes-Associated-Protein (YAP) signaling (a MSC mechanosensing pathway that relays mechanical input through Rho-GTPase-dependent translocation to the nucleus) in MSCs.[54]

Tendon homeostasis and healing ultimately depends on the ability of tenocytes to remodel tissue. Due to the slow timescale of remodeling events in tendon,[55] it is likely that alterations in matrix properties (e.g., mechanics and structure) precede cell responses. Such structural and mechanical changes alter the fibrous architecture of the ECM, and may therefore influence the ability for resident tenocytes to recognize their native "tendon" environment. For example low and moderate loading have been shown to have no effect on water content [45] or GAG production,[43] whereas longer periods of loading affect GAG content,[36] and overloading may cause lower strength and release of proinflammatory cytokines such as PGE_2 and NO.[41] An optimal loading regime has been proposed to promote mechanics,[44] potentially through collagen synthesis[35,43] as the molecular mechanisms switch from a catabolic to anabolic response.[37] Such mechanisms may be frequency and duration dependent.[42] Additionally, changes in tendon phenotype are common with injury and healing. In particular, tendon stem cells are implicated to differentiate towards chondrocyte, osteoblast, or adipocyte lineages, as altered matrix properties and stresses on cells has been shown to affect cell fate.[56-58]

This work is not without limitations. First, we only investigated tensile loading, and adding in additional loading paradigms that apply shear, compression, and biaxial forces may provide further insight into behavior *in vivo*. Next, we investigated the multiscale response at two distinct strains (1% and 10%). These strains were chosen to

represent the toe and linear portion of the force-displacement curve. However, it is well established that tendon's response to loading is inherently nonlinear; therefore, evaluation at additional strains is necessary to fully describe the responses presented. Although we employed many tools to assess multiscale tendon properties, other measurements may provide additional support of findings. Compositionally, previous studies have established that cell- and environment-generated mechanical loads on the ECM can induce a variety of cell responses. The healing process may create PG-rich domains, which create distinct tissue and cell biomechanics that are believed to be prevalent in injured tissues.[22] Further, the amount of lamin-A in the nucleus has been directly correlated to tissue stiffness.[103] Therefore, future studies should specifically evaluate the spatial distributions of ECM, cell-ECM, and cell proteins that may regulate cell mechanics (collagen-1,3,5; PGs; integrin-α11; F-actin; lamin-A; N-cadherin; and connexin43)), as well as pericellular matrix proteins (e.g, collagen-6) that may contribute to strain transfer. Future studies will also apply a constitutive model for fibrous matrices based on experimentally derived parameters to predict tenocyte stress transmission and additional multiple regression analyses.

Taken together, our work supports a new understanding for how macroscale dynamic loading affects multiscale tendon properties. Unfortunately, many clinical treatments for tendon injuries remain controversial, [59] and our understanding on the role of mechanical loading on cell microenvironments is limited. The multiscale response to dynamic mechanical loading (of varying magnitude and duration), which is a hallmark of clinical rehabilitation protocols, is therefore necessary to determine the ramifications of such rehabilitation procedures. Additionally, these results provide insight into the

micromechanical environments tendon cells may experience during dynamic loading and healing.

4.5 References

1. Franchi M, Fini M, Quaranta M, et al. Crimp morphology in relaxed and stretched rat Achilles tendon. *J Anat.* Jan 2007;210(1):1-7.
2. Miller KS, Connizzo BK, Feeney E, Soslowsky LJ. Characterizing local collagen fiber re-alignment and crimp behavior throughout mechanical testing in a mature mouse supraspinatus tendon model. *J Biomech.* Aug 9 2012;45(12):2061-2065.
3. Diamant J, Keller A, Baer E, Litt M, Arridge RG. Collagen; ultrastructure and its relation to mechanical properties as a function of ageing. *Proc R Soc Lond B Biol Sci.* Mar 14 1972;180(1060):293-315.
4. Rigby BJ, Hirai N, Spikes JD, Eyring H. The Mechanical Properties of Rat Tail Tendon. *J Gen Physiol.* Nov 1 1959;43(2):265-283.
5. Han WM, Heo SJ, Driscoll TP, et al. Microstructural heterogeneity directs micromechanics and mechanobiology in native and engineered fibrocartilage. *Nat Mater.* Apr 2016;15(4):477-484.
6. Han WM, Heo SJ, Driscoll TP, Smith LJ, Mauck RL, Elliott DM. Macro- to microscale strain transfer in fibrous tissues is heterogeneous and tissue-specific. *Biophys J.* Aug 6 2013;105(3):807-817.
7. Buckley MR, Sarver JJ, Freedman BR, Soslowsky LJ. The dynamics of collagen uncrimping and lateral contraction in tendon and the effect of ionic concentration. *J Biomech.* Sep 3 2013;46(13):2242-2249.

8. Maganaris CN, Paul JP. In vivo human tendon mechanical properties. *J Physiol.* Nov 15 1999;521 Pt 1:307-313.

9. Mammoto A, Mammoto T, Ingber DE. Mechanosensitive mechanisms in transcriptional regulation. *J Cell Sci.* Jul 1 2012;125(Pt 13):3061-3073.

10. Thomas CH, Collier JH, Sfeir CS, Healy KE. Engineering gene expression and protein synthesis by modulation of nuclear shape. *Proc Natl Acad Sci U S A.* Feb 19 2002;99(4):1972-1977.

11. Lin TW, Cardenas L, Glaser DL, Soslowsky LJ. Tendon healing in interleukin-4 and interleukin-6 knockout mice. *J Biomech.* 2006;39(1):61-69.

12. Dunkman AA, Buckley MR, Mienaltowski MJ, et al. The tendon injury response is influenced by decorin and biglycan. *Ann Biomed Eng.* Mar 2014;42(3):619-630.

13. Mienaltowski MJ, Dunkman AA, Buckley MR, et al. Injury response of geriatric mouse patellar tendons. *J Orthop Res.* Jul 2016;34(7):1256-1263.

14. Beason DP, Kuntz AF, Hsu JE, Miller KS, Soslowsky LJ. Development and evaluation of multiple tendon injury models in the mouse. *J Biomech.* Mar 7 2012.

15. Cooper G. *The Cell: A Molecular Approach*. 2 ed: Sinauer Associates; 2000.

16. Favata M. *Scarless Healing in the Fetus: Implications and Strategies for Postnatal Tendon Repair*: Bioengineering, University of Pennsylvania; 2006.

17. Dunkman B, Mienaltowski,Adams, Thomas, Satchell, Kumar, Pathmanathan, Beason; Iozzo, Birk, Soslowsky Decorin Expression Is Required for Age-

Related Changes in Tendon Structure and Mechanical Properties *Matrix Biol.* 2012((in review)).

18. Freedman BR, Zuskov A, Sarver JJ, Buckley MR, Soslowsky LJ. Evaluating changes in tendon crimp with fatigue loading as an ex vivo structural assessment of tendon damage. *J Orthop Res.* Mar 13 2015.

19. Duenwald SE, Vanderby R, Jr., Lakes RS. Viscoelastic relaxation and recovery of tendon. *Ann Biomed Eng.* Jun 2009;37(6):1131-1140.

20. Duenwald SE, Vanderby R, Jr., Lakes RS. Stress relaxation and recovery in tendon and ligament: experiment and modeling. *Biorheology.* 2010;47(1):1-14.

21. Graf BK, Vanderby R, Jr., Ulm MJ, Rogalski RP, Thielke RJ. Effect of preconditioning on the viscoelastic response of primate patellar tendon. *Arthroscopy.* Feb 1994;10(1):90-96.

22. Fung DT, Wang VM, Laudier DM, et al. Subrupture tendon fatigue damage. *J Orthop Res.* Feb 2009;27(2):264-273.

23. Andarawis-Puri N, Sereysky JB, Jepsen KJ, Flatow EL. The relationships between cyclic fatigue loading, changes in initial mechanical properties, and the in vivo temporal mechanical response of the rat patellar tendon. *J Biomech.* Jan 3 2012;45(1):59-65.

24. Freedman BR, Sarver JJ, Buckley MR, Voleti PB, Soslowsky LJ. Biomechanical and structural response of healing Achilles tendon to fatigue loading following acute injury. *J Biomech.* Nov 11 2013.

25. Lake SP, Miller KS, Elliott DM, Soslowsky LJ. Effect of fiber distribution and realignment on the nonlinear and inhomogeneous mechanical properties of human

supraspinatus tendon under longitudinal tensile loading. *J Orthop Res.* Dec 2009;27(12):1596-1602.

26. Glazer A, Lewis, JG., Kaminsky, W. An Automatic Optical Imaging System for Birefringent Media. *Proceedings: Mathematical, Physical and Engineering Sciences.* 1996;452(1955):2751-2765.

27. Hurschler C, Loitz-Ramage B, Vanderby R, Jr. A structurally based stress-stretch relationship for tendon and ligament. *J Biomech Eng.* Nov 1997;119(4):392-399.

28. Belkoff SM, Haut RC. A structural model used to evaluate the changing microstructure of maturing rat skin. *J Biomech.* 1991;24(8):711-720.

29. Lanir Y. A structural theory for the homogeneous biaxial stress-strain relationships in flat collagenous tissues. *J Biomech.* 1979;12(6):423-436.

30. Kawamoto T, Kawamoto K. Preparation of thin frozen sections from nonfixed and undecalcified hard tissues using Kawamot's film method (2012). *Methods Mol Biol.* 2014;1130:149-164.

31. Sereysky JB, Andarawis-Puri N, Ros SJ, Jepsen KJ, Flatow EL. Automated image analysis method for quantifying damage accumulation in tendon. *J Biomech.* Sep 17 2010;43(13):2641-2644.

32. Carpenter AE, Jones TR, Lamprecht MR, et al. CellProfiler: image analysis software for identifying and quantifying cell phenotypes. *Genome Biol.* 2006;7(10):R100.

33. Peltz CD, Sarver JJ, Dourte LM, Wurgler-Hauri CC, Williams GR, Soslowsky LJ. Exercise following a short immobilization period is detrimental to tendon

properties and joint mechanics in a rat rotator cuff injury model. *J Orthop Res.* Jul 2010;28(7):841-845.

34. Thornton GM, Shrive NG, Frank CB. Ligament creep recruits fibres at low stresses and can lead to modulus-reducing fibre damage at higher creep stresses: a study in rabbit medial collateral ligament model. *J Orthop Res.* Sep 2002;20(5):967-974.

35. Legerlotz K, Jones GC, Screen HR, Riley GP. Cyclic loading of tendon fascicles using a novel fatigue loading system increases interleukin-6 expression by tenocytes. *Scand J Med Sci Sports.* Feb 2013;23(1):31-37.

36. Devkota AC, Weinhold PS. Prostaglandin E(2), collagenase, and cell death responses depend on cyclical load magnitude in an explant model of tendinopathy. *Connect Tissue Res.* Aug 2010;51(4):306-313.

37. Maeda E, Fleischmann C, Mein CA, Shelton JC, Bader DL, Lee DA. Functional analysis of tenocytes gene expression in tendon fascicles subjected to cyclic tensile strain. *Connect Tissue Res.* Dec 2010;51(6):434-444.

38. Maeda E, Shelton JC, Bader DL, Lee DA. Differential regulation of gene expression in isolated tendon fascicles exposed to cyclic tensile strain in vitro. *J Appl Physiol (1985).* Feb 2009;106(2):506-512.

39. Devkota AC, Tsuzaki M, Almekinders LC, Banes AJ, Weinhold PS. Distributing a fixed amount of cyclic loading to tendon explants over longer periods induces greater cellular and mechanical responses. *J Orthop Res.* Aug 2007;25(8):1078-1086.

40. Maeda E, Shelton JC, Bader DL, Lee DA. Time dependence of cyclic tensile strain on collagen production in tendon fascicles. *Biochem Biophys Res Commun.* Oct 19 2007;362(2):399-404.

41. Flick J, Devkota A, Tsuzaki M, Almekinders L, Weinhold P. Cyclic loading alters biomechanical properties and secretion of PGE2 and NO from tendon explants. *Clin Biomech (Bristol, Avon).* Jan 2006;21(1):99-106.

42. Yamamoto E, Kogawa D, Tokura S, Hayashi K. Effects of the frequency and duration of cyclic stress on the mechanical properties of cultured collagen fascicles from the rabbit patellar tendon. *J Biomech Eng.* Dec 2005;127(7):1168-1175.

43. Screen HR, Shelton JC, Bader DL, Lee DA. Cyclic tensile strain upregulates collagen synthesis in isolated tendon fascicles. *Biochem Biophys Res Commun.* Oct 21 2005;336(2):424-429.

44. Yamamoto E, Tokura S, Hayashi K. Effects of cyclic stress on the mechanical properties of cultured collagen fascicles from the rabbit patellar tendon. *J Biomech Eng.* Dec 2003;125(6):893-901.

45. Hannafin JA, Arnoczky SP, Hoonjan A, Torzilli PA. Effect of stress deprivation and cyclic tensile loading on the material and morphologic properties of canine flexor digitorum profundus tendon: an in vitro study. *J Orthop Res.* Nov 1995;13(6):907-914.

46. Slack C, Flint MH, Thompson BM. The effect of tensional load on isolated embryonic chick tendons in organ culture. *Connect Tissue Res.* 1984;12(3-4):229-247.

47. Asundi KR, Rempel DM. Cyclic loading inhibits expression of MMP-3 but not MMP-1 in an in vitro rabbit flexor tendon model. *Clin Biomech (Bristol, Avon).* Jan 2008;23(1):117-121.

48. Guilak F. Compression-induced changes in the shape and volume of the chondrocyte nucleus. *J Biomech.* Dec 1995;28(12):1529-1541.

49. Arnoczky SP, Lavagnino M, Whallon JH, Hoonjan A. In situ cell nucleus deformation in tendons under tensile load; a morphological analysis using confocal laser microscopy. *J Orthop Res.* Jan 2002;20(1):29-35.

50. Lelievre SA, Weaver VM, Nickerson JA, et al. Tissue phenotype depends on reciprocal interactions between the extracellular matrix and the structural organization of the nucleus. *Proc Natl Acad Sci U S A.* Dec 8 1998;95(25):14711-14716.

51. Henderson JT, Shannon G, Veress AI, Neu CP. Direct measurement of intranuclear strain distributions and RNA synthesis in single cells embedded within native tissue. *Biophys J.* Nov 19 2013;105(10):2252-2261.

52. Broers JL, Kuijpers HJ, Ostlund C, Worman HJ, Endert J, Ramaekers FC. Both lamin A and lamin C mutations cause lamina instability as well as loss of internal nuclear lamin organization. *Exp Cell Res.* Apr 01 2005;304(2):582-592.

53. Lammerding J, Fong LG, Ji JY, et al. Lamins A and C but not lamin B1 regulate nuclear mechanics. *J Biol Chem.* Sep 01 2006;281(35):25768-25780.

54. Driscoll TP, Cosgrove BD, Heo SJ, Shurden ZE, Mauck RL. Cytoskeletal to Nuclear Strain Transfer Regulates YAP Signaling in Mesenchymal Stem Cells. *Biophys J.* Jun 16 2015;108(12):2783-2793.

55. Magnusson SP, Langberg H, Kjaer M. The pathogenesis of tendinopathy: balancing the response to loading. *Nat Rev Rheumatol.* May 2010;6(5):262-268.

56. Engler AJ, Sen S, Sweeney HL, Discher DE. Matrix elasticity directs stem cell lineage specification. *Cell.* Aug 25 2006;126(4):677-689.

57. Pelham RJ, Jr., Wang Y. Cell locomotion and focal adhesions are regulated by substrate flexibility. *Proc Natl Acad Sci U S A.* Dec 9 1997;94(25):13661-13665.

58. Chen CS, Mrksich M, Huang S, Whitesides GM, Ingber DE. Geometric control of cell life and death. *Science.* May 30 1997;276(5317):1425-1428.

59. AAOS. Guideline on the Diagnosis and Treatment of Acute Achilles Tendon Rupture. 2009.

CHAPTER V: MODELING STRESS TRANSMISSION IN TENDON DURING HEALING AND DYNAMIC LOADING

5.1 Introduction

The extracellular matrix (ECM) is a major component of the biomechanical environment with which tendon cells (tenocytes) interact. Alterations to matrix structural and mechanical properties due to mechanical loading may promote normal tendon homeostasis[1-6] or create pathological conditions.[7-14] For example, fatigue loading of tendon elevates collagen crimping, which correlates linearly with tissue laxity (change in slack length).[15] The tendon ECM may also be altered following tendon injury. Aberrant tissue phenotypes caused by tendon ruptures are exemplified not only at transcript and protein levels, but also can extend to include disorganized collagen structure, inferior mechanical properties, and reduced *in vivo* limb function in animals. Changes in multiscale strain transfer, made possible through tendon's fiber-reinforced structure,[16,17] may affect cell microenvironments and therefore feedback to affect proliferation, differentiation, and matrix production.[18]

Cells can sense and respond to mechanical signals over distances nearly 20 times their cell radius (i.e., 250-1000μm).[19,20] Traction forces on the underlying substrate are generated during cell migration. These cell traction forces (CTF) are important for cell migration, phenotype, and homeostasis. For example, cell traction force microscopy can be shown to discriminate cell populations in tendon and are influenced by geometries that tenocytes adhere.[21,22] Recent modeling studies have suggested that the key mechanism driving this process is the fibrous nature of extracellular matrices[16,23] using a constitutive law accounting for mechanically driven collagen fiber reorientation.[23] Specifically,

tension-driven collagen-fiber alignment plays a crucial role in force transmission,[16] and that by employing a small critical stretch for fiber alignment, large fiber stiffness, and fiber strain-hardening behavior enable long-range interaction.[16] Furthermore, the range of collagen-fiber alignment for elliptical cells with polarized contraction is much larger than that for spherical cells with diagonal contraction.[16]

Tendon cell stress transmission may have important ramifications for both cell-cell communication and load transfer within the tendon ECM. One potential mechanism for continued maintenance or failure to heal following injury may be a lack of long range force transmission present in healing tissue that may lack fibrous architecture and compensation for cell-cell communication with increased cellularity. Therefore, the objective of this study is to apply this constitutive model to elucidate the role of dynamic mechanical loading and tendon healing on the ability for tenocytes to sense stress over long distances. In this model, mechanical and cell morphological properties are used as model inputs. Use of these properties at different strains following dynamic loading and healing provides initial conditions for the changes in matrix architecture in response to loading. A secondary objective of this study is to predict nuclear strain transfer using multiscale mechanical, structural, and compositional data from previous studies examining tendon during healing and after perturbations of dynamic loading in multiple regression models.

We hypothesized that higher magnitude cyclic loading and healing would decrease tenocyte stress transmission, as the ECM behaves more neo-Hookean than fibrous. Through multiple regression analysis, we hypothesize that in *uninjured* and dynamically loaded tendon, modulus and collagen alignment contribute highest to

nuclear strain transfer. However, *in healing* tendons, we hypothesized that modulus, cellularity, nuclear disorganization, and F-actin contribute highest to nuclear strain transfer.

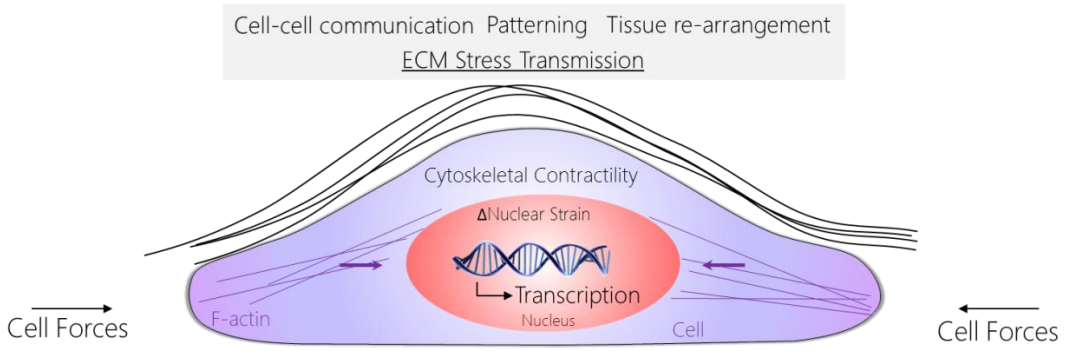

Figure 5-1: ECM Stress Transmission. Cell-generated forces via contraction of the actin cytoskeleton can result in ECM stress transmission, which can affect cell-cell communication, and can drive tissue patterning and re-arrangement.

5.2 Methods

5.2.1 Background on the Constitutive Law

We applied a constitutive law for fibrous matrices[16] to model stress transmission in tendon using experimental inputs. Finite-element simulations of this constitutive law were used to study the effect of material properties of the isotropic (E_b) and fibrous (E_f) components of the matrix, the shape of cells, and the polarization of cell contractile forces on force transmission in fibrous matrices in response to dynamic loading and healing. In this constitutive law, two distinct groups of aligned and isotropic fibers were incorporated. Isotropic fibers were modeled as neo-Hookean hyperelastic,[16] and energy functions describing aligned fibers were chosen so that the tendon matrix increases in stiffness under tensile loading.[16] Briefly, the Cauchy stress was decomposed into isotropic (σ^b) and fibrous (σ^f) contributions (Eqs. 1-4).[16] The amount of interaction between the two families of fibers is given by the ratio, of E_f/E_b.[16] Previous work showed

that this model captured the essential features of discrete fiber simulations during mechanical loading, such as the toe in the stress strain curve.[16,23]

$$\boldsymbol{\sigma} = \boldsymbol{\sigma}^{\mathbf{b}} + \boldsymbol{\sigma}^{\mathbf{f}} \qquad (1)$$

$$\boldsymbol{\sigma}^{\mathbf{b}} = \kappa(J-1)\boldsymbol{I} + \mu \mathrm{dev}(\overline{\boldsymbol{B}})/J \qquad (2)$$

$$\boldsymbol{\sigma}^{\mathbf{f}} = \frac{1}{J}\sum_{a=1}^{3}\frac{\partial f(\lambda_a)}{\partial \lambda_a}\lambda_a(\boldsymbol{n_a} \otimes \boldsymbol{n_a}) \qquad (3)$$

$$\frac{\partial f(\lambda_a)}{\partial \lambda_a} = \begin{cases} 0 & \lambda_a < \lambda_1 \\ \dfrac{E_f\left(\dfrac{\lambda_a - \lambda_1}{\lambda_2 - \lambda_1}\right)^n (\lambda_a - \lambda_1)}{n+1}, & \lambda_1 \le \lambda_a < \lambda_2 \\ E_f\left[\dfrac{\lambda_2 - \lambda_1}{n+1} + \dfrac{(1+\lambda_a - \lambda_2)^{m+1} - 1}{m+1}\right], & \lambda_a \ge \lambda_2 \end{cases} \qquad (4)$$

For finite element implementation of the constitutive law derived (Eqns. 1-4), several parameters were included: λ_a are the principle stretches, F_{ij} is the deformation gradient tensor, κ is the initial bulk modulus, and μ is the initial shear modulus, n_a are the unit vectors in the principle stretch orientations, **C** (**C=F^{T}F**) and **B** (**B=FF^T**) are the right and left Cauchy-Green deformation tensors, and J is the Jacobian (J=det(**F**)).[16] Specific tendon cell aspect ratios and strain polarizations, were input from experimental data. Simulations were completed using Abaqus/CAE (Dassault Systemes, 2016) in a finite deformation setting, with matrices modeled using 3-node bilinear axisymmetric tri elements.[16] The material form of the tangent modulus tensor $\boldsymbol{C^{SC}}$, the tangent modulus tensor for the convected rate of the Kirchhoff stress $\boldsymbol{C^{\tau C}}$, the tangent modulus tensor for the Jaumann rate of the Kirchhoff stress $\boldsymbol{C^{\tau J}}$, and the material Jacobian $\boldsymbol{C^{MJ}}$ for the material model were implemented.[16]

As an illustration of this model, for the special case of spherically symmetry, the analytical solution reduces to:

$$\varepsilon_\theta = \varepsilon_\varphi(r) = \frac{u_o}{r_o}\left(\frac{r_o}{r}\right)^{n+1} \tag{5}$$

$$\sigma_r = -\left\{\frac{E_b}{(1+\nu)(1-2\nu)}[(1-\nu)n-2\nu]+nE_f\right\}\frac{u_o}{r_o}\left(\frac{r_o}{r}\right)^{n+1} \tag{6}$$

$$n = \frac{1}{2}\left(\sqrt{\frac{9+\chi}{1+\chi}}+1\right) \text{ and } \chi = \frac{(1+\nu)(1-2\nu)}{(1-\nu)}\frac{E_f}{E_b} \tag{7}$$

This simple solution (Eqs. 5-7) shows that distances that stress act in the ECM following cell contraction is dependent on the modulus of the fibrous and bulk matrix (E_f and E_b), the displacement of cell contraction (u_o), the initial cell radius (r_o), and the matrix Poisson's ratio, (ν). As seen above, for a strongly fibrous response, the ratio, E_f/E_b >>1 and the exponent n→1, however, for an isotropic material, this ratio <<1 and n→2. By this logic, highly fibrous matrices exhibit long range force transmission (as we expect in normal uninjured tendon), whereas non-fibrous matrices exhibit short range force transmission (as we hypothesize in injured/healing/ fatigue damaged tendon).

5.2.2 Model Inputs, Optimization, and Simulations

This modeling framework was adapted to include experimentally derived tendon mechanical properties during healing and following dynamic loading. We first determined the model parameters by optimizing simulated model predictions to experimentally derived stress-stretch data. Briefly, a 3D 1-element model was

constructed with tendon-specific geometries in Abaqus/CAE. Uniaxial displacements to 10% strain were applied to match experimental procedures. Boundary conditions on the bottom surface restricted displacements in the vertical direction, and a bottom node was applied to restrict displacements in the horizontal and vertical directions. After an iterative procedure, the best fits were determined (**Table 5-1**).

Using the experimentally determined cell geometries (**Table 5-1**), a 3D axi-symmetric model was created (Mesh size: 1-6μm). The ECM boundary was located at least 10x the radius of the input cell geometry. Boundary conditions restricting displacements and rotations in all directions were applied on the periphery of the matrix and displacement in the horizontal direction was restricted along the centerline. Cells were allowed to contract up to 5% of their volume along their principal axis. During cell contraction, the maximum principal stresses, nodal displacements, and nodal coordinates were output and analyzed in MATLAB (v2012a; Mathworks; Natick, MA). Ratios of the ECM displacement to the displacement adjacent to the contracting cell were computed as a function of the distance from the cell surface. These distance transmission profiles were compared between groups. A convergence study was completed to determine appropriate mesh size.

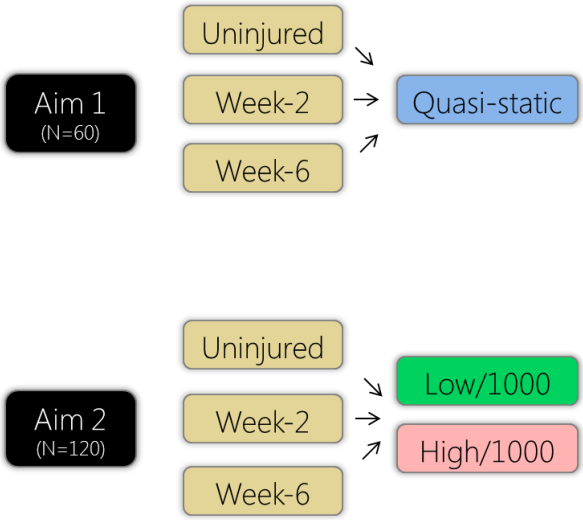

Figure 5-2: Data sets included in models. Data from Chapters 3 and 4 were included to generate the models in this Chapter.

5.2.3 Multiple Regression Analysis

Prior to model incorporation, data were examined for outliers, defined as being at least 2.2*IQR above (below) the third (first) quartile.[24]. The R^2 was chosen assuming the current study would predict mechanical parameters better than our previous studies.[25,26] Multiple regression analysis assumed that each dependent and independent parameter is obtained from a single specimen (a mouse).

Summary statistics of all variables were examined to ensure that assumptions for linear analysis were satisfied. Pearson's correlations were calculated between independent variables. A general linear model (GLM) was evaluated to determine if dependent variables (nAR and ΔnAR) were significantly related to the independent parameters: equilibrium stress (σ_{eq}), the change in σ_{eq} from 1-10% strain, |E*|, tanδ, collagen disorganization (CSD), the change CSD from 1-10% strain (ΔCSD), cell number, F-actin, fiber mean slack length (SL_mn), nuclear disorganization (nCSD), and the change in nCSD from 1-10% strain (ΔnCSD). These properties were measured after

two cyclic loading protocols (low magnitude and high magnitude) at two strains (1 and 10%) for three treatment groups (Uninjured, healing 2-weeks post-injury, healing 6-weeks post-injury). Data from both strain levels were pooled together for subsequent analysis to identify key variables and create model fits used to predict responses in a subset of the data. This same process was repeated for each treatment and mechanical loading group.

Backward linear regression was performed (Probability of F to enter is set at 0.05 and to be removed is set at 0.10).[27,28] The criteria for choosing the appropriate range of F to enter and F to remove were based on the degrees of freedom in the model. This range for F corresponds to a significance level of 0.1 for a single test. The tolerance level, defined as $1-R_k^2$, was set to 0.01 to prevent entry of variables that are highly correlated to other x-variables. In other words, a variable was excluded if its coefficient of multiple determinations, when regressed over the other x-variables, exceeds 0.99. Significance was again set at $p<0.05$, per regression model and variances within the data. The Durbin Watson (DW) statistic was calculated to identify the existence of correlations between independent variables. For each equation, based on established guidelines for interpretation of DW statistic, a DW value lower than 1.08 indicates correlation between the independent variables.[27,28]

5.2.4 Statistical Analysis

Tendon stress transmission was compared between test groups by determining the power rate of decay from matrix displacement profiles. Coefficients of determination, p-values, DW statistic and correlation coefficients were determined from the single linear and multiple linear regression models.

5.3 Results

5.3.1 Model Optimization

Model input parameters were determined by fitting stress-stretch relationships to experimental data (**Table 5-1; Figure 5-3**). Using these inputs, we applied varying cell contraction in an axi-symmetric model. For the uninjured quasi-static loading case, model mesh converged and remaining simulations proceeded with mesh densities of 1µm local to the cell that increased to 6µm at 100µm from the cell.

Table 5-1. Model Inputs. Model inputs were determined by optimizing the input coefficients E_b, E_f, λ_c, and m to experimentally derived quasi-static mechanical data collected in Chapters 3 and 4.

Study	Group	Loading	Eb	Ef	λc	m	Cell (µm²)	Area	nAR
Healing	Uninjured	Quasi-static	300	$202*E_b$	1.005	17	38		7.5
	Week-2	Quasi-static	300	$182*E_b$	1.005	12	55		2.3
	Week-6	Quasi-static	300	$162*E_b$	1.009	22	46		3.9
Dynamic	Uninjured	Low/1000	250	$377*E_b$	1.006	16	51		6.5
	Uninjured	High/1000	300	$323*E_b$	1.049	26	48		7.1
	Week-2	Low/1000	300	$123* E_b$	1.012	14	70		2.0
	Week-2	High/1000	300	$70*E_b$	1.035	48	67		1.9
	Week-6	Low/1000	250	$280*E_b$	1.010	14	49		3.1
	Week-6	High/1000	300	$100*E_b$	1.035	47	47		2.9

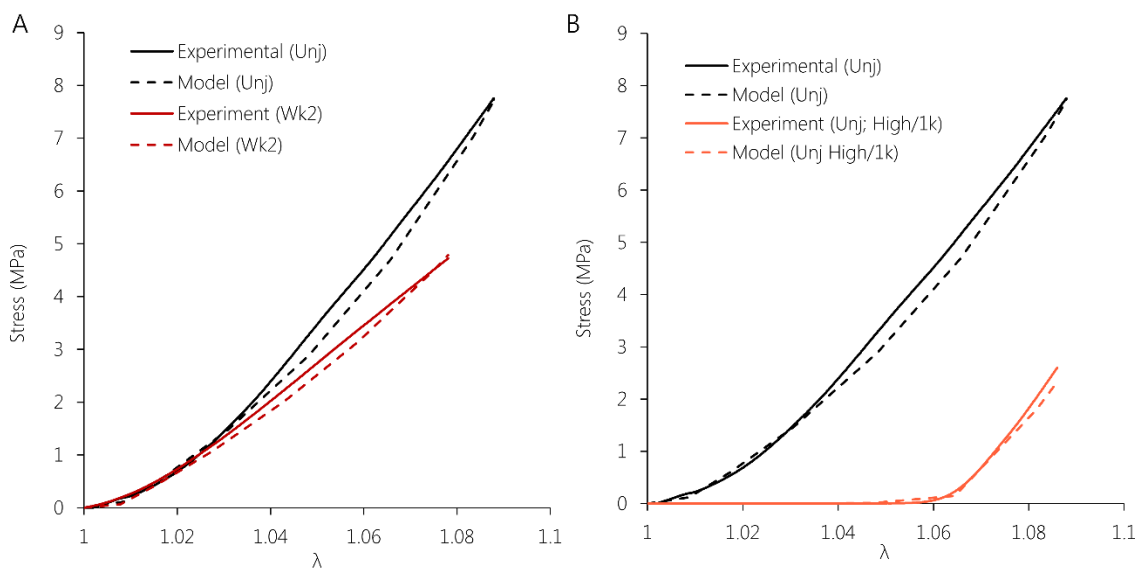

Figure 5-3: Model fits for tendon healing. Experimental curves and model fits for (**A**) quasi-static uninjured and 2-weeks post-injury, and (**B**) quasi-static uninjured and High/1000 dynamic loading.

5.3.2 Tendon Cells in Uninjured Tissues Sense Further than in Healing and Fatigue Loaded Tissues

We first investigated how displacements are transmitted in healing tendon compared to uninjured intact tendon. Model parameters (**Table 1**) were input for the test conditions and two independent models were generated encompassing the appropriate tendon cell geometry and material properties. In both cases, the cell was allowed to contract 5% (95% of original volume). We found that healing tendon demonstrated decreased displacement transmission profiles compared to uninjured intact tendon (**Figure 5-4**). As the tendon cell contracts, displacements were transmitted almost 10x the cell radius (**Figure 5-5**). However, in healing tendon, these profiles decayed much more quickly.

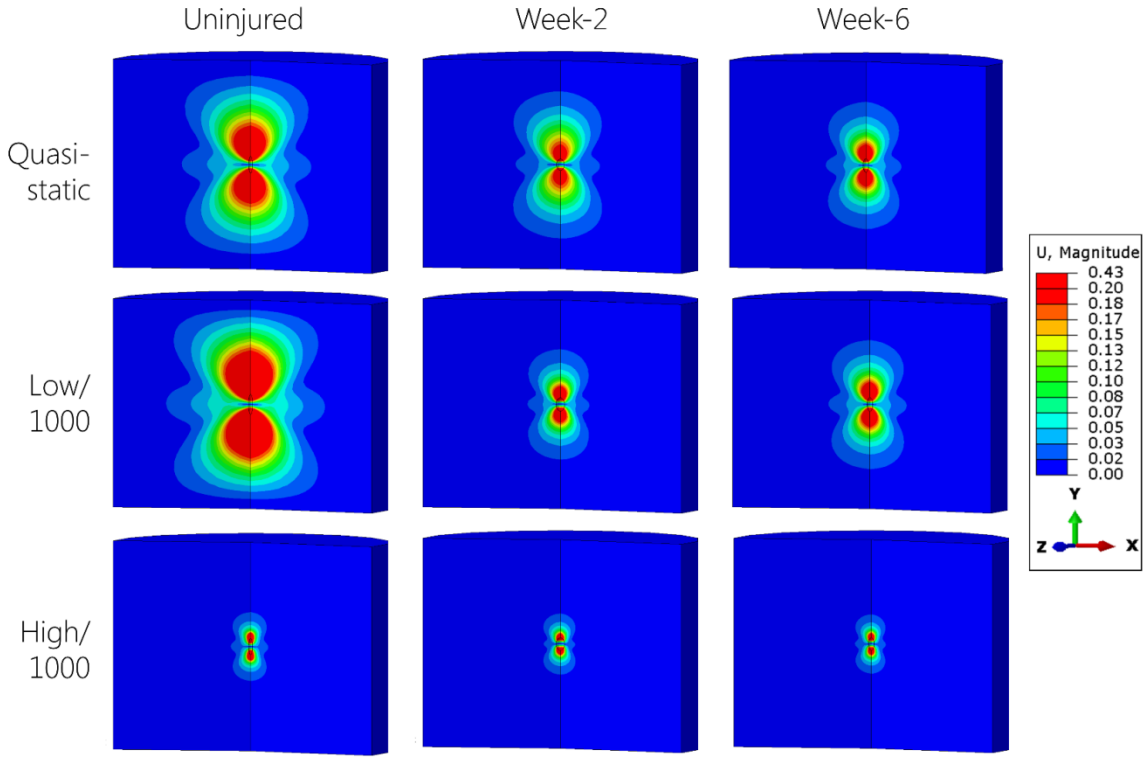

Figure 5-4: Displacement profiles comparing the effect of healing and cyclic loading ECM stress transmission. Data are separated by healing timepoint (columns: uninjured, 2-week post-injury, 6-week post-injury) and loading paradigm (rows: quasi-static, low/1000, high/1000). In all cases, tendon cells contract to 5% of its volume. Units: microns.

We next investigated how displacements are transmitted in fatigue loaded tendon compared to uninjured intact tendon. As done previously, model parameters were input and tendon contraction (5%) was simulated. We found that fatigue loaded tendon had decreased displacement transmission profiles compared to uninjured intact tendon (**Figure 5-4**). Regardless of the applied contraction, fatigue loaded tendon displacement profiles decayed rapidly within short distances from the cell surface (**Figure 5-6**). Taken together, both tendon healing and fatigue loading attenuate stress transmission through the ECM compared to uninjured tendon (**Figure 5-7**).

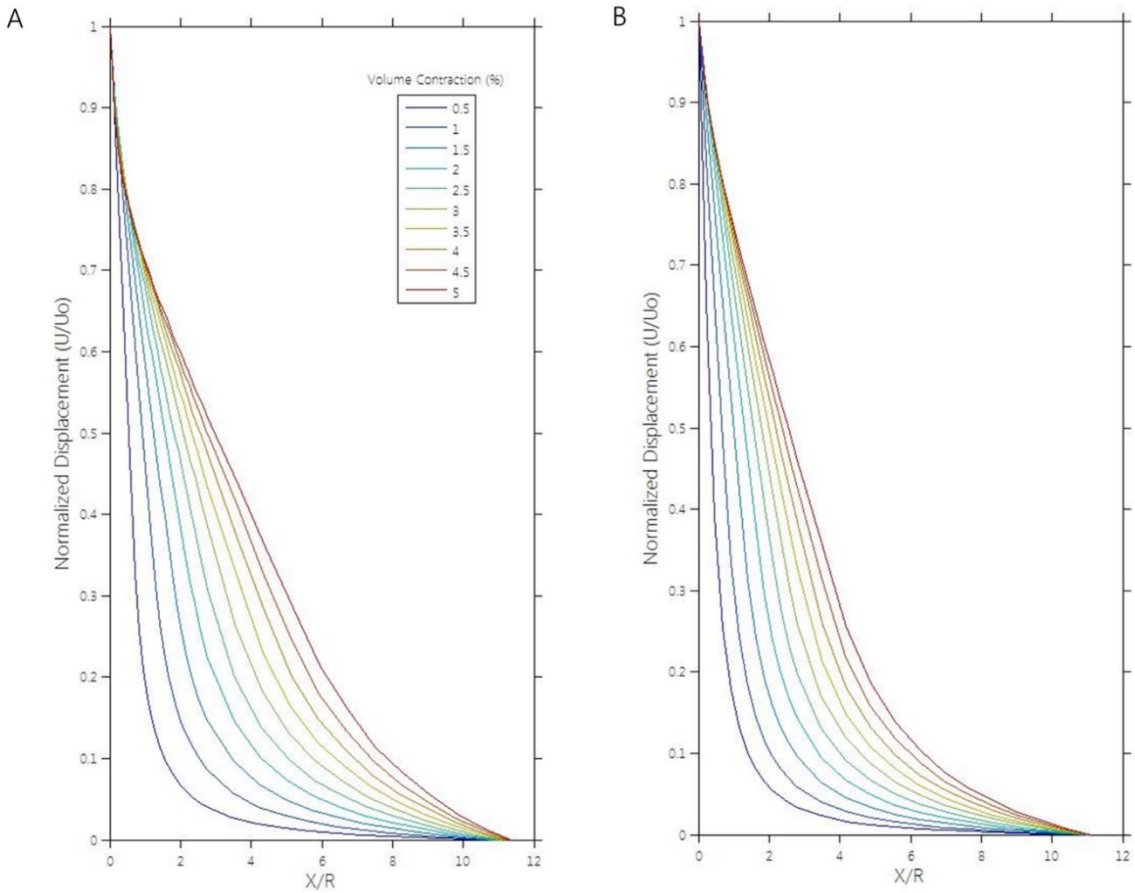

Figure 5-5: Normalized displacement transmission in uninjured and healing tendon. ECM displacement profiles from the top pole of the cell normalized to the initial displacement at the cell surface as a function of cell radius. Colors indicate the progression of a 5% contraction. Displacement profiles decayed faster in (**A**) uninjured intact tendon compared to (**B**) healing tendon (high/1000).

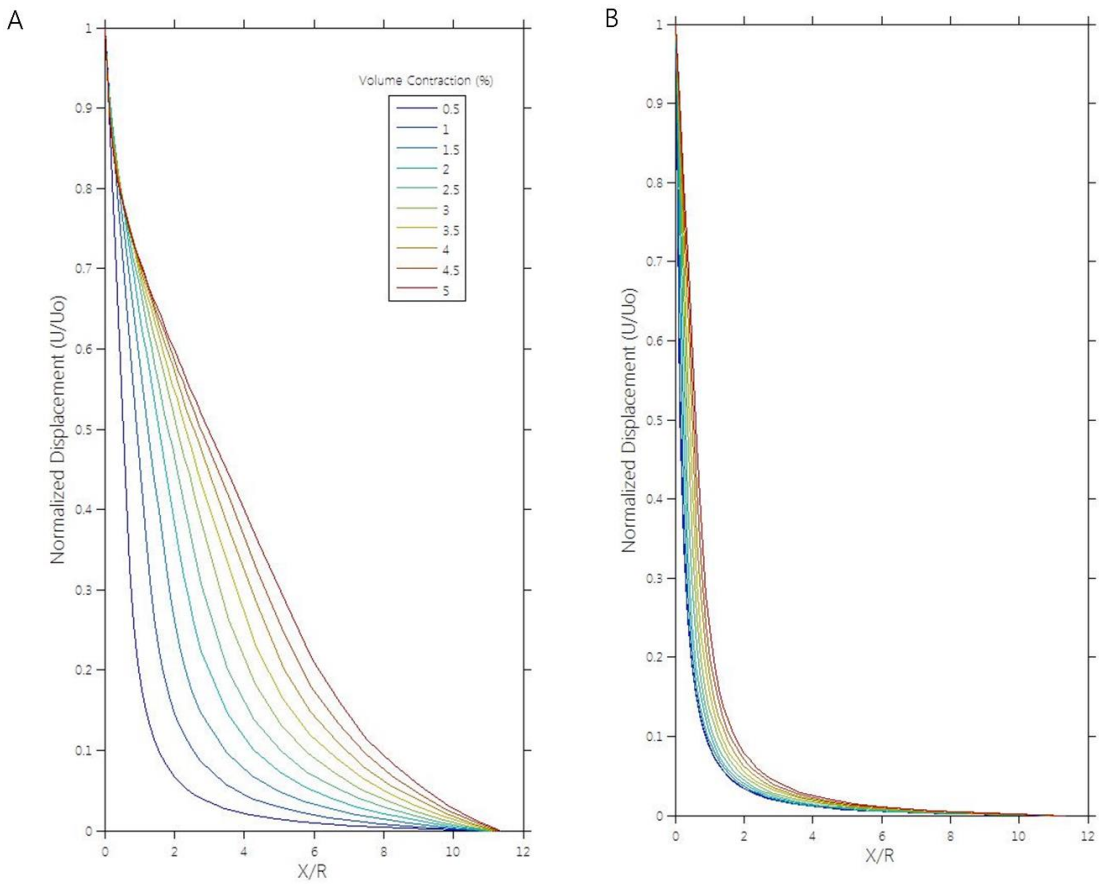

Figure 5-6: Normalized displacement transmission in uninjured and fatigue loaded tendon. ECM displacement profiles from the top pole of the cell normalized to the initial displacement at the cell surface as a function of cell radius. Colors indicate the progression of a 5% contraction. Displacement profiles decayed faster in (**A**) uninjured intact tendon compared to (**B**) fatigue loaded tendon (high/1000).

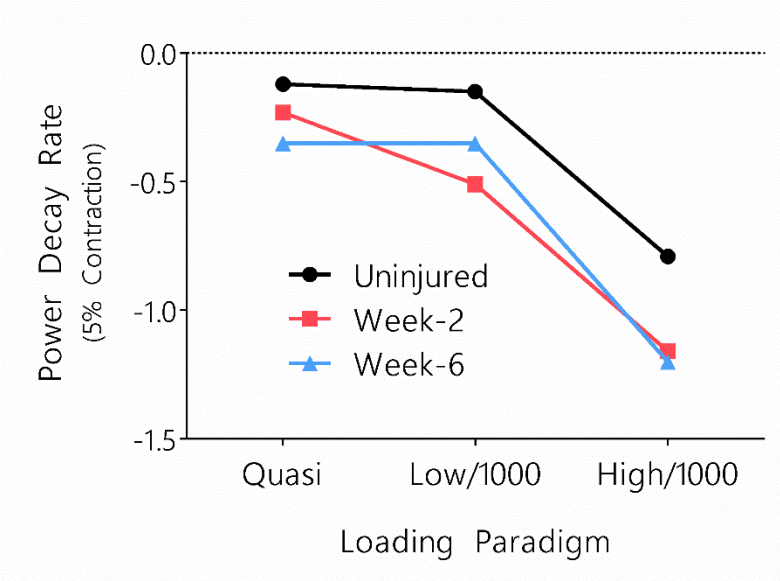

Figure 5-7: Power Decay Fitting. Power decay constant is shown for each simulation. Tendon healing reduced ECM stress transmission, with fatigue loading having the greatest effects.

5.3.3 Matrix Alignment, Nuclear Organization, Cellularity, and F-Actin Predict Nuclear Deformation under Load

Using experimental data derived from previous studies (Chapters 3 and 4), we first investigated whether nuclear aspect ratio (nAR) could be predicted from macroscale and microscale properties. Initial screening using bivariate correlation revealed that the change in equilibrium stress, dynamic modulus, cellularity, F-actin staining, matrix disorganization, nuclear disorganization, and healing correlated with the nAR, with correlation coefficient magnitudes ranging from r=0.33 to r=0.85 (**Table 5-2**). Using these parameters, we conducted backward linear multiple regression. Results of the regression model found that cellularity, nuclear disorganization, and healing were significant predictors of nAR ($R^2 = 0.85$, $p<0.001$; DW = 2.074) (**Table 5-3**).

Table 5-2: Correlation to nAR from full dataset.

		$\Delta\sigma_{eq}$	|E*|	Cellularity	F-Actin	CSD	nCSD	Heal
nAR	**Pearson Correlation**	0.40	0.33	-0.74	-0.83	-0.85	-0.81	-0.89

	Sig. (2-tailed)	<0.0001	<0.0001	<0.0001	<0.0001	<0.0001	<0.0001	<0.0001
	N	91	172	176	170	178	175	181

Table 5-3: Multiple regression modeling to predict nAR. R^2 = 0.85.

Parameter	β	t	sig
Constant	**-0.40**	**-0.12**	**0.903**
Cellularity	**1.81**	**2.61**	**0.011**
nCSD	**-2.44**	**-4.40**	**<0.000**
Healing	**-4.22**	**-8.60**	**<0.000**

Given this relationship to nAR, we wanted to determine if the change in nAR, ΔnAR, could be predicted using multiple regression models. ΔnAR is indicated of the capacity for nuclei to deform under applied loading. Initial screening using bivariate correlation determined that $\Delta\sigma_{eq}$, tanδ, cellularity, F-actin, Δ nCSD, healing, and high magnitude loading were significantly correlated to ΔnAR (**Table 5-4**). Surprisingly, predictions of ΔnAR were not increased greatly through structural properties in multiple regression analysis, as the categorical variables healing and fatigue loading were the strongest predictors (R^2=0.39, p<0.001; DW=1.61) (**Table 5-5**).

Table 5-4: Correlation coefficients for ΔnAR from full dataset.

		$\Delta\sigma_{eq}$	tanδ	Cellularity	F-Actin	Δ nCSD	Heal	High Mag
nAR	**Pearson Correlation**	0.34	-0.33	-0.43	-0.30	-0.32	-0.39	-0.36
	Sig. (2-tailed)	<0.001	<0.001	<0.001	0.003	<0.001	<0.001	<0.001
	N	89	96	98	94	98	100	100

Table 5-5: Multiple regression modeling coefficients to predict ΔnAR. R^2 = 0.39.

Parameter	β	t	sig
Constant	1.50	9.94	<0.000
Healing	-1.05	-5.86	<0.000
Fatigue	-0.63	-3.36	0.001

5.4 Discussion

This study investigated the effects of healing and dynamic loading on tendon cell stress transmission. Additionally, we determined whether multiscale mechanical, structural, and compositional properties could predict the change in nAR with applied strain using multiple regression analysis. Application of either model has not been completed previously to study changes in stress transmission and nAR in tendon. Knowledge gained from these models may advance our understanding for cell-ECM and cell-cell communication within tendon throughout healing and in response to dynamic loading.

Both tendon healing and fatigue loading affected ECM stress transmission. Strikingly, fatigue loaded tendons demonstrated drastic decreases in simulated stress transmission compared to uninjured control tendons. These large differences are likely attributed to an elongated toe-region created from the repeated high magnitude loading (**Table 1**). Differences in healing tendon were also apparent, but not as dramatic, likely because tendon healing reduced matrix stiffening parameters in the model and not the initial toe region.

nAR was strongly correlated with many macroscale and microscale properties, highlighting its relationship to multiscale tendon properties. nAR was most correlated to nCSD and F-actin staining. From previous studies (Chapter 3), more disorganized nuclei were found in healing tendon along with increased F-actin staining. Thus, it is likely that the elevated nCSD and F-actin staining with healing tendon occur in concert with reduced nAR. Although many parameters had strong correlations to nAR, much of the variance could not be explained when predicting ΔnAR in dynamically loaded tendon.

This discrepancy may be explained as the right and left limbs from the animal were pooled together to derive the ΔnAR. Additionally, it is possible that there are competing effects due to dynamic loading. Fatigue loading reduces ΔnAR, along with ΔCSD and ΔnCSD (Chapter 4). As this is not the case with low magnitude dynamic loading, it may be necessary to add a categorical variable to future models to capture this potential group variation.

Previous experimental and modeling studies in tendon incorporating damage models have shown that empirical modeling techniques based on mechanical and image based measures can predict mechanical properties in healing,[29] aging,[29] and genetically altered[30] tendons. Proteoglycans have been implicated in reductions in tendons mechanical properties and collagen disorganization.[30] However, the underlying mechanisms for these processes have not been elucidated. As mentioned, mechanical perturbation likely causes alterations to multiscale ECM biomechanics, which ultimately affects cell behavior. Therefore, mechanical models presented here, that can directly measure the complex interactions between tenocytes and their ECM is necessary. Mechanical, structural, and compositional properties were used as model inputs for the fibrous constitutive law or multiple regression analyses. Since this study directly measured cell shape following various loading protocols, we applied in vivo initial conditions for cell strains prior to contraction. This study therefore adds to our understanding of cell-matrix interactions in tendon and provides insight into how multiscale properties relate in the context of clinically-relevant situations of healing and response to dynamic loading.

This work is not without limitations. First, in vivo cell contractions were not assessed, and therefore were assumed to range from 0-5% volume contraction. Second, we did not investigate the role and interactions of several cells embedded in matrix as is present *in vivo*. Third, additional model validation simulating the loading of discrete fiber networks with strong initial unloaded alignment may be investigated. Several improvements can be made to our modeling framework to better represent the *in vivo* condition. First, the model assumes that there are only two sets of fibers present: those that align in the direction of loading and those that do not. This may not be the case *in vivo*, where this distribution of fiber types may vary as a function of tissue health. Additionally, the modeling framework could incorporate initial anisotropy instead of assuming a random fiber network at low strains. Second, the model assumes that contractile strains occur primarily along the long axis of the cell and that the volume of the cell is the same before and after contraction. However, this may also vary *in* vivo as a function of tissue health, changes in calcium ion concentration, and initial strain applied. Incorporating this detail from experiments designed to evaluate cell traction forces would provide for more detailed loading conditions to be applied to the model. Additionally, fiber viscoelasticity, poroelasticity, and uncrimping that change with tissue health, and are key features in describing tendon's response to loading, could be incorporated in future studies. Finally, recent, unpublished work has suggested that larger stress transmission is achieved through the incorporation of large Poisson's ratios to the model. As tendon typically experiences large Poisson's ratios, this addition to the modeling framework would enhance application of the model to represent *in vivo* conditions.

In conclusion, our model showed that tendon healing and dynamic loading affect stress transmission in tendon. Additionally, knowledge gained from the multiple regression model highlights mechanical, structural, and compositional properties that contribute to the dynamic capacity of tendon nuclei to respond to loading. Continued work in this space will investigate the interactions between tendon healing and dynamic loading, which will provide further insight into the role rehabilitation may have on tendon following injury.

5.5 References

1. Mendias CL, Gumucio JP, Lynch EB. Mechanical loading and TGF-beta change the expression of multiple miRNAs in tendon fibroblasts. *J Appl Physiol (1985).* Jul 2012;113(1):56-62.
2. Heinemeier KM, Skovgaard D, Bayer ML, et al. Uphill running improves rat Achilles tendon tissue mechanical properties and alters gene expression without inducing pathological changes. *J Appl Physiol (1985).* Sep 1 2012;113(5):827-836.
3. Moerch L, Pingel J, Boesen M, Kjaer M, Langberg H. The effect of acute exercise on collagen turnover in human tendons: influence of prior immobilization period. *Eur J Appl Physiol.* Feb 2013;113(2):449-455.
4. Screen HR, Shelton JC, Bader DL, Lee DA. Cyclic tensile strain upregulates collagen synthesis in isolated tendon fascicles. *Biochem Biophys Res Commun.* Oct 21 2005;336(2):424-429.

5. Legerlotz K, Jones GC, Screen HR, Riley GP. Cyclic loading of tendon fascicles using a novel fatigue loading system increases interleukin-6 expression by tenocytes. *Scand J Med Sci Sports.* Feb 2013;23(1):31-37.

6. Zhang J, Wang JH. The effects of mechanical loading on tendons - an in vivo and in vitro model study. *PLoS One.* 2013;8(8):e71740.

7. Ikoma K, Kido M, Nagae M, et al. Effects of stress-shielding on the dynamic viscoelasticity and ordering of the collagen fibers in rabbit Achilles tendon. *J Orthop Res.* Jul 6 2013.

8. Hannafin JA, Arnoczky SP, Hoonjan A, Torzilli PA. Effect of stress deprivation and cyclic tensile loading on the material and morphologic properties of canine flexor digitorum profundus tendon: an in vitro study. *J Orthop Res.* Nov 1995;13(6):907-914.

9. Uchida H, Tohyama H, Nagashima K, et al. Stress deprivation simultaneously induces over-expression of interleukin-1beta, tumor necrosis factor-alpha, and transforming growth factor-beta in fibroblasts and mechanical deterioration of the tissue in the patellar tendon. *J Biomech.* Apr 2005;38(4):791-798.

10. Forde MS, Punnett L, Wegman DH. Prevalence of musculoskeletal disorders in union ironworkers. *J Occup Environ Hyg.* Apr 2005;2(4):203-212.

11. Jobe FW, Kvitne RS, Giangarra CE. Shoulder pain in the overhand or throwing athlete. The relationship of anterior instability and rotator cuff impingement. *Orthop Rev.* Sep 1989;18(9):963-975.

12. McMaster WC, Troup J. A survey of interfering shoulder pain in United States competitive swimmers. *Am J Sports Med.* Jan-Feb 1993;21(1):67-70.

13. Renstrom P, Johnson RJ. Overuse injuries in sports. A review. *Sports Med.* Sep-Oct 1985;2(5):316-333.

14. Sommerich CM, McGlothlin JD, Marras WS. Occupational risk factors associated with soft tissue disorders of the shoulder: a review of recent investigations in the literature. *Ergonomics.* Jun 1993;36(6):697-717.

15. Freedman BR, Zuskov A, Sarver JJ, Buckley MR, Soslowsky LJ. Evaluating changes in tendon crimp with fatigue loading as an ex vivo structural assessment of tendon damage. *J Orthop Res.* Jun 2015;33(6):904-910.

16. Wang H, Abhilash AS, Chen CS, Wells RG, Shenoy VB. Long-range force transmission in fibrous matrices enabled by tension-driven alignment of fibers. *Biophys J.* Dec 2 2014;107(11):2592-2603.

17. Arnoczky SP, Lavagnino M, Whallon JH, Hoonjan A. In situ cell nucleus deformation in tendons under tensile load; a morphological analysis using confocal laser microscopy. *J Orthop Res.* Jan 2002;20(1):29-35.

18. Mammoto A, Mammoto T, Ingber DE. Mechanosensitive mechanisms in transcriptional regulation. *J Cell Sci.* Jul 01 2012;125(Pt 13):3061-3073.

19. Rudnicki MS, Cirka HA, Aghvami M, Sander EA, Wen Q, Billiar KL. Nonlinear strain stiffening is not sufficient to explain how far cells can feel on fibrous protein gels. *Biophys J.* Jul 2 2013;105(1):11-20.

20. Ma X, Schickel ME, Stevenson MD, et al. Fibers in the extracellular matrix enable long-range stress transmission between cells. *Biophys J.* Apr 2 2013;104(7):1410-1418.

21. Wang JH. Cell Traction Forces (CTFs) and CTF Microscopy Applications in Musculoskeletal Research. *Oper Tech Orthop.* Jun 1 2010;20(2):106-109.

22. Wang JH, Zhao G, Li B. The Study of Cell Motility by Cell Traction Force Microscopy (CTFM). *Methods Mol Biol.* 2016;1365:301-313.

23. Abhilash AS, Baker BM, Trappmann B, Chen CS, Shenoy VB. Remodeling of fibrous extracellular matrices by contractile cells: predictions from discrete fiber network simulations. *Biophys J.* Oct 21 2014;107(8):1829-1840.

24. Hoaglin DC, Iglewicz B, Tukey JW. Performance of some resistant rules for outlier labeling. *J American Statistical Association.* 1986;81(396):991-999.

25. Ansorge HL, Adams S, Jawad AF, Birk DE, Soslowsky LJ. Mechanical property changes during neonatal development and healing using a multiple regression model. *J Biomech.* Apr 30 2012;45(7):1288-1292.

26. Robinson PS, Lin TW, Jawad AF, Iozzo RV, Soslowsky LJ. Investigating tendon fascicle structure-function relationships in a transgenic-age mouse model using multiple regression models. *Ann Biomed Eng.* Jul 2004;32(7):924-931.

27. Neter J. *Building the Regression Model i: Selection of Predictor Variables, Applied linear Regression Models.* . Chicago, IL: Irwin; 1996a.

28. Neter J. *Table B.7 Durbin-Watson Test Bounds. Applied Linear Regression Models*. Chicago, IL: Irwin; 1996b.

29. Buckley MR DA, Reuther KE, Kumar AK, Pathmanathan L, Beason DP, Birk DE, Soslowsky LJ. Validation of an Empirical Damage Model for Aging and In Vivo Injury of the Murine Patellar Tendon. *Journal of Biomechanical Engineering.* 2013;135(April).

30. Gordon J, Freedman B, Zuskov A, Iozzo R, Birk D, Soslowsky L. Achilles tendons from decorin- and biglycan-null mouse models have inferior mechanical and structural properties predicted by an image-based empirical damage model. *Journal of Biomechanics.* 2014;In review.

CHAPTER VI: CONCLUSIONS AND FUTURE DIRECTIONS

6.1 Chapter Conclusions

6.1.1 Chapter II Conclusions

Since many tendons perform at high and repetitive loads at or near failure,[1,2] it has become increasingly important to utilize mechanical testing methods at physiological levels.[3-11] This work evaluated real-time tendon crimp and mechanical properties nondestructively during tendon fatigue life using a plane polariscope. Additionally, we quantified tendon mechanical and structural properties during fatigue loading following acute injury to the Achilles tendon. This study revealed alterations in tendon crimp and mechanical properties nondestructively, and in real-time, during fatigue loading. This work may lead to improved diagnostic imaging methods based on tissue-level structural measures to assess injured and healing tendons, which may ultimately improve patient monitoring. Although periodic crimp in tendon has been studied using high-magnification optical microscopy,[12] electron microscopy,[13] optical coherence tomography,[14] and second harmonic generation,[15] its study using polarized light microscopy[16,17] has been limited. While decreases in tangent stiffness, dynamic modulus, and hysteresis are detected during healing, the most sensitive measure was cycles to failure. Knowledge that measured tendon stiffness drops by 25% whereas the number of cycles to failure decreases by nearly 37-fold was not expected and importantly, demonstrates that tissue properties only assessing stiffness metrics may provide an incomplete description of actual tissue healing. Thus, this information obtained at the early stages of healing is critical to fully characterize the healing response. The structural parameters B_{app} and CSD show promise as potentially translatable metrics to predict

tendon dynamic modulus and hysteresis, yet the majority of mechanical parameters could only be predicted weakly, suggesting the need for additional experiments investigating structure-function relationships in tendon studying the response to fatigue loading. In light of our findings and the low cost of our system, this methodology presents both a robust and economic opportunity for understanding structure function relationships of tendons.

6.1.2 Chapter III Conclusions

This study evaluated multiscale structure-function mechanisms in response to quasi-static tensile loading in uninjured and healing tendons. Using an established mouse patellar tendon injury model,[18-20] we harvested living tendon explants that preserve the native architecture of the tendon ECM. Together, our approach allows for the evaluation of multiscale mechanical and structural properties without destructive dissection to the tissue. This procedure provides advancement over traditional histological studies that do not control for tissue pre-stresses or strains applied prior to fixation. We first showed that tendon healing affects the macroscale mechanical and structural response to mechanical loading. As hypothesized, we found that healing tendons exhibited decreased strain stiffening, which occurred in concert with decreased dynamic moduli and elevated predicted fiber slack lengths. Increases in fiber slack lengths indicate an extension in the toe region of the stress-strain curve, which suggests that the structural response to strain during healing may be compromised. Indeed, macroscale structural properties were inferior in healing tendons and the matrix showed a reduced capacity to realign under loading. To determine how these macroscale properties were related to microscale

properties, we used MP imaging to evaluate the collagen structure. Similarly, healing tendons also demonstrated increased collagen fiber disorganization compared to uninjured tendons, however, MP imaging was able to detect substantially more disorganization in all groups indicating that the tendon microstructure and macrostructure may be correlated, but are not identical. Taken together, this work investigated how macroscale quasi-static loading affects multiscale tendon properties during tendon healing. We have identified numerous structural and compositional differences between uninjured and healing tendon that may contribute to deficits in nuclear strain transfer.

6.1.3 Chapter IV Conclusions

This study evaluated multiscale structure-function mechanisms in response to dynamic tensile loading (varying magnitude and duration). We used our established patellar tendon model,[4,19,21] modified to evaluate properties in living tendon explants. After establishing multiscale relationships in uninjured tendon, we evaluated whether similar effects would exist in healing tendon. These procedures allow for a comprehensive evaluation of tendon properties and are highly repeatable. We first showed that tendon strain stiffening is reduced, and non-recoverable, due to high magnitude long duration loading and occurs in concert with increased laxity and delayed fiber re-alignment with applied strain. These macroscale properties correlated to microscale properties; high magnitude long duration loading resulted in collagen and nuclear disorganization at high strains, and decreased change in nAR with applied loading. Results in uninjured tendons were largely extendable to healing tendons, however, the reduced modulus and increased laxity observed during fatigue loading may

indicate inferior fiber recruitment in healing tendons compared to uninjured tendons.[22] Notably, high magnitude loading does not produce the same effects as tendon healing, likely due differences in matrix structure and response to loading between healing states. Additionally, it is possible that other cell microenvironmental changes may be present during healing and cyclic loading that alter the multiscale response to loading including pH, redox, hypoxia, ATP, glucose, enzymes, and temperature.[23]

Taken together, this work supports a new understanding for how macroscale dynamic loading affects multiscale tendon properties and highlights differential strain transfer mechanisms in healing tendon versus dynamically loaded tendon. Unfortunately, many clinical treatments for tendon injuries remain controversial,[24] and our understanding on the role of mechanical loading on cell microenvironments is limited. The multiscale response to dynamic mechanical loading (of varying magnitude and duration), which is a hallmark of clinical rehabilitation protocols, is therefore necessary to determine the ramifications of such rehabilitation procedures. Additionally, these results provide benchmarks for the microenvironments in which tendon cells may experience following cell delivery therapies.

6.1.4 Chapter V Conclusions

This study investigated the effects of healing and dynamic loading on tendon cell stress transmission through the ECM. We also determined whether multiscale mechanical, structural, and compositional properties could predict the change in nAR with applied strain using multiple regression analysis. Application of either model has not been completed previously to study changes in stress transmission and nAR in tendon.

Knowledge gained from these models may advance our understanding for cell-ECM and cell-cell communication within tendon throughout healing and in response to dynamic loading. Both tendon healing and fatigue loading affected ECM stress transmission. As hypothesized, fatigue loaded tendons demonstrated drastic decreases in simulated stress transmission compared to uninjured control tendons. These large differences are likely attributed to an elongated toe-region created from the repeated high magnitude loading. Additionally, the failed capacity for matrix realignment in fatigue loaded tendons may reduce ECM stress transmission. Differences in healing tendon were also apparent, but not as dramatic, likely because tendon healing reduced matrix stiffening parameters in the model and not the initial toe region. nAR was strongly correlated with many macroscale and microscale properties, highlighting its relationship to multiscale tendon properties. nAR was most correlated to F-actin staining, CSD, nCSD, and tendon healing. Interestingly, the ΔnAR, was primarily correlated to cellularity, the change in equilibrium stress, and tendon healing. Therefore, it is likely that the mechanisms of initial nuclear shape and strain transfer are inherently very different. Future work is needed to fully establish which property is the key determinant for ΔnAR during tendon healing and in response to dynamic loading.

6.1.5 Overall Study Conclusions

This dissertation explored the interface between dynamic loading and tendon healing across multiple length scales using living tendon explants (**Figure 6-1**). Overall, this work helps to define the implications of macroscale mechanical loading on collagen structure and tenocyte response in uninjured and healing tendon, and provides a

foundation for the development of new strategies to improve tendon healing. Specifically, we determined the ramifications of various macroscale quasi-static and dynamic loading protocols on macro and microscale biomechanics in tendon during healing. These properties included multiscale mechanics (|E*|, σ_{eq}, tanδ, transition strain) and structure (alignment, transition alignment composition), and subcellular (shape, organization) components. This comprehensive approach has important implications for the fundamental mechanisms governing tendon homeostasis, healing, and phenotype. A mouse model was used with several innovative methodologies (mechanical testing with collagen fiber alignment, AFM to assess fibril mechanics, confocal imaging to assess ECM, cell, and nuclear morphology and composition, constitutive modeling to assess cell stress transmission, and multiple regression analysis) to provide rigorous mechanical, structural, and compositional data on the multiscale tendon response to dynamic loading during healing. Importantly, tendon cells remained viable during testing leading to potential cell-mediated contraction and differential mechanical properties when compared to fresh frozen tendon.

We began, in Chapter II, by determining how macroscale mechanical and structural properties of tendon are altered during fatigue loading and tendon healing. Next, in Chapter III, we evaluated the multiscale mechanical, structural, and compositional response of tendon to quasi-static loading during healing. In Chapter IV, we quantified the multiscale mechanical, structural, and compositional response of tendon to dynamic loading during healing. Finally, in Chapter V, we described modeling stress transmission and changes in nAR in tendon during healing and dynamic loading.

Taken together, we found that macroscale mechanical and structural properties were altered during fatigue loading in uninjured and healing tendon. Tendon healing created inferior multiscale mechanical and structural changes, including decreased equilibrium stress, modulus, and fiber realignment with applied strain. Microstructural analysis revealed that healing tendons had more rounded nuclei and greater collagen fiber disorganization compared to uninjured tendons. Further, nuclei in healing tendons had a smaller change in aspect ratio with applied strain compared to uninjured tendons. In response to dynamic loading, we found that high magnitude cyclic loading decreased the change in equilibrium stress through increases in tendon laxity and delayed fiber recruitment and realignment in uninjured tendons. These mechanical changes were found to be non-recoverable following 1000s of recovery. High magnitude long duration loading increased collagen disorganization at high strains and eliminated the capacity for tendon fibers to realign with loading. In turn, the ΔnAR was decreased dramatically in high/1000 tendons compared to low magnitude and quasi-static loaded tendons. Macroscale mechanical results showed similar effects of dynamic loading in healing tendons as in uninjured tendons. When used in models of stress transmission, we found that both tendon healing and dynamic loading attenuated ECM displacement following tendon cell contraction. The ΔnAR, in healing tendon was primarily correlated to matrix mechanical properties (|E*|, CSD) and cellular properties (cellularity, F-actin, and nCSD), whereas the ΔnAR in dynamically loaded tendon was primarily correlated to mechanical properties (σ_{eq}, tanδ, |E*|, SL_mn, and ΔCSD) and nuclear organization (nCSD, ΔnCSD). Therefore, it is likely that the mechanisms of nuclear strain transfer are inherently very different between these groups.

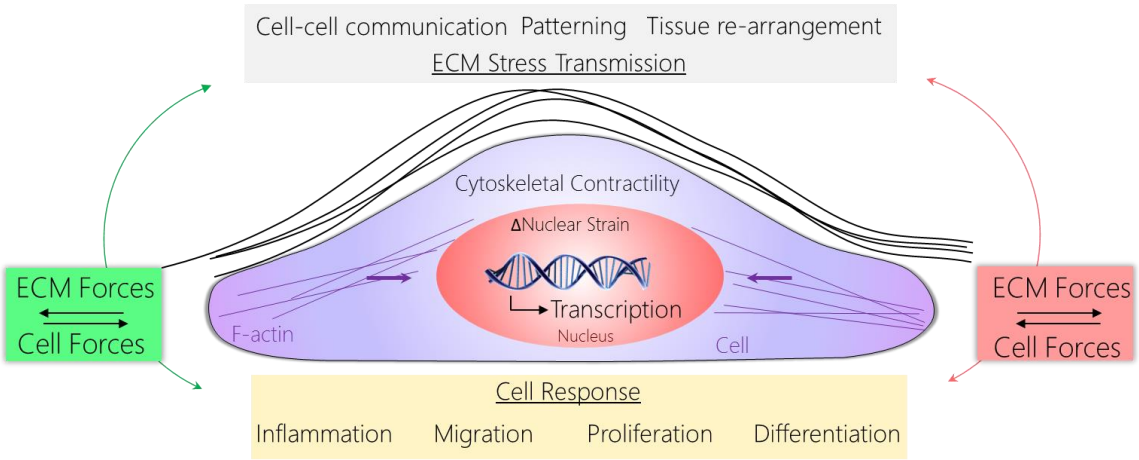

Figure 6-1: ECM and cell forces can have important physiological consequences. In this simplified illustration, as forces from the extracellular matrix are applied, cell deformation through the actin cytoskeleton to the nucleus can result in changes in nuclear strain, that, in turn, can affect transcription and a host of cell responses, such as inflammation, migration, proliferation, and differentiation. Although changes in gene and protein expression have been studied, our appreciation for how applied strains result in initial nuclear shape changes that may drive these downstream responses remains limited. The ability or hindrance of cells to deform under applied strain, may have important physiological consequences and may be a potential therapeutic target in the future. Additionally, cells have the ability to contract their cytoskeleton, which can give rise to force transmission through the ECM. Stress transmission has important implications including cell-cell communication, and can drive tissue patterning and re-arrangement. This may then feedback to promote a healthy or pathologic matrix phenotype.

6.2 Future Directions

6.2.1 Additional Models and Perturbations of Tendon Loading

Although this study provided a thorough and comprehensive evaluation of tendon's response to quasi-static and dynamic loading during healing, many additional models and perturbations of the loading environment could be completed in the future. First, this study only investigated tensile loading, and adding in additional loading paradigms that apply shear, compression, and biaxial forces may provide further insight into behavior *in vivo*. Next, we only investigated the multiscale response at two distinct strains (1% and 10%). These strains were chosen to represent the toe and linear portion of the force-displacement curve. However, it is well established that tendon's response to

loading is inherently nonlinear; therefore, evaluation at additional strains is necessary to fully describe the responses presented in this dissertation. This may be best achieved by utilizing additional systems that provide real-time evaluation of cell imaging during loading. Horizontally mounted loading systems, such as the BioTense Perfusion Bioreactor (ADMET, Inc), can be placed directly on an inverted microscope. This tool could therefore reduce required sample sizes and eliminate the need for cryosectioning currently required to produce thin sections for imaging. Further, addition of transgenic mice with fluorescently expressed genes would allow for evaluation of specific cell types, thus removing the ambiguity of evaluating all cells detected with generic cell stains. Microscopes capable of multiphoton imaging of collagen, as well as calcium signaling,[25] may provide novel characterization of living tendons during loading.

Although four dynamic loading protocols were used to evaluate long (short) duration and high (low) magnitude loading, additional moderate duration and magnitude loading levels would be beneficial for further evaluating this dose response. This is important since the responses to loading evaluated should represent loading conditions that may occur *in vivo*. Next, the effects observed in these studies were strictly acute; however, the effects of a 1000s recovery period were evaluated in non-living tendons. There exists a capacity for *in vivo* cellular response to dynamic loading, as tendons may restore their crimp length with time due to tensional homeostasis.[26] Examining the role of longer periods of recovery with living tendon experiments on multiscale mechanical and structural properties would greatly improve our understanding of tissue remodeling following loading. If cell mediated, further application of agents to inhibit or enhance cell contractility (**Table 6-1**) could enable a deeper understanding of these mechanisms.

Additionally, validation in other tendon types and in different species is necessary. Application of other injuries (e.g., complete rupture or incisional) are ultimately necessary to fully understand stress transmission in healing tendons. Indeed, previous work from our group has investigated the role of different injury models on macroscale healing of mouse tendons.[27]

Comparing the multiscale response to loading in other force bearing soft tissues, such as lung and heart, may provide further understanding of the way that cells interact with their microenvironment and respond to mechanical loading.[28] For example, although tendon and heart are both soft tissues, they demonstrate distinct composition, structure, and function in both normal and diseased states. Tenocytes are present in lower cell densities in tendon than cardiomyocytes in heart.[28] In heart failure (HF), the stiffening of the heart tissue is a result of the production of fibrotic ECM by myofibroblasts as well as the stiffening of cardiomyocytes themselves in response to an altered microenvironment.[28] Although the ECM in tendon also adapts, changes in tenocyte biomechanics during disease progression remains unknown.[28] Excessive loading from repetitive overuse activity causes TSCs to differentiate into non-tenocyte lineages which produce aberrant ECM components, further altering the mechanical environment and perpetuating the degeneration of native tendon properties. In the case of cardiac tissue, increased ECM stiffness causes fibroblasts to differentiate into myofibroblasts, which produce more ECM components and stiffen the local environment.[28] Although the ECMs in diseased tendon and heart are reorganized in dramatically different ways in response to their respective sources of disease onset, cells in these two tissues respond to changes in the same ECM mechanical properties using similar mechanotransduction machinery.[28]

Despite this wealth of knowledge that highlights the central interaction between the ECM and cell mechanotransduction, current treatments ameliorating dysfunctional ECM and cell mechanosensing are limited. In addition to continued work using human and animal model systems, additional knowledge may be gained from newt and zebrafish models that undergo unique ECM remodeling to regenerate heart and limb tissues without scarring.[29-33] Understanding how this remodeling supports regeneration biochemically and mechanically may lead to novel therapeutic strategies for targeting the dysfunctional ECM.[28]

6.2.2 Additional Assessment of Multiscale Tendon Properties

This dissertation employed many tools to assess multiscale tendon properties, but other measurements may provide additional support of findings. Mechanically, we focused on quantifying macroscale tensile properties in the direction of loading and nano/microscale indentation of tendon fibrils/fibers, perpendicular to their orientation. Although indentation mechanics may be important for the underlying fibrous substrate that tendon cells sense and respond to, its relationship to fibril mechanical properties in the direction of loading remains unknown. Longitudinal fibril mechanical properties may also be determined using AFM, but would require tissue sectioning in the transverse plane (as opposed to coronal sectioning in the present study). Transverse sections would also supply knowledge of fibril diameter distributions using TEM, which has been widely reported in our past studies.[34,35] In addition, previous studies have used AFM to assess fibril sliding,[36] which may provide another metric for tendon's response to loading following the various dynamic loading protocols and healing time points evaluated in this work. Another useful structural metric is SEM, which could be applied to further

understand structural properties local to tendon cells following dynamic loading and during healing. This method can be extended with histomorphometric and ultrastructural analysis to provide nanometer resolution of cell-matrix morphology.[37]

Within our modeling framework in Aim 3, we approximate stress transmission due to contracting tenocytes through the tendon ECM. This model could be validated experimentally, in part, by conducting lateral force microscopy using AFM on the tendon surface to simulate cell contraction. By applying a small and controlled perturbation, the resulting tissue strain fields could be computed. Additionally, our model assumes the *in vivo* traction forces in fibroblasts and tenocytes. These cell traction forces could be evaluated experimentally with traction force microscopy[38-40] following the various loading and healing paradigms in this study.

Compositionally, previous studies have established that cell- and environment-generated mechanical loads on the ECM can induce a variety of cell responses. Transformation of internal and external mechanical cues into cellular responses occurs via collagen fiber kinematics,[93] focal adhesions (macromolecular assemblies of integrins and proteoglycans),[94] and cell-cell contacts.[95-97] Cell adhesion to the ECM is primarily, but not exclusively, mediated by integrins.[98-100] Integrins interact with the force-producing actin cytoskeleton, where changes in force alter the assembly of adhesion complexes and activate adhesion-mediated cell signaling.[101,102] Integrin-dependent actomyosin contraction allows cells to sense substrate stiffness. Additionally, the healing process may create PG-rich domains, which create distinct tissue and cell biomechanics that are believed to be prevalent in injured tissues.[22] Several pericellular matrix proteins are present in the developing mouse tendon including collagens, fibronectin, integrins,

and membrane-bound receptors, and may also play a role in multiscale strain transfer.[41] Collagen type V is a component of the tendon pericellular matrix during collagen fibrillogenesis.[42] Additionally, collagen type VI is evenly distributed in tensional areas of tendons[43] and its binding to the cell surface may be affected by NG2 proteoglycan.[44] Further, the amount of lamin-A in the nucleus has been directly correlated to tissue stiffness.[103] Therefore, future studies should specifically evaluate the spatial distributions of ECM, cell-ECM, and cell proteins that may regulate multiscale strain transfer to cells (collagen-1,3,5; PGs; integrin-α11; F-actin; lamin-A; N-cadherin; and connexin-43).

6.2.3 Biological Adaptation and Remodeling Following Loading and Identification of Cell Types

This study specifically examined the acute response to loading and did not evaluate biological adaptation and tissue remodeling following dynamic loading during healing. As this question is important for ultimate translation of findings, many future studies are possible. Using the tools of molecular profiling and proteomics arrays would provide a complete description of the healing pathways active in these conditions and would then allow for well-motivated questions to be asked on specific pathways shown to be active in these models. Numerous signaling motifs have been demonstrated to participate in the orchestration of tendon healing. It is no surprise that several such pathways shown to have a significant impact on healing are also key regulators of development (e.g., BMP, TGF-β) and early growth response (EGR).[45] In the rat, overexpression of BMP-14 at the Achilles tendon during healing resulted in increased tendon tensile strength as compared to control tendons.[46] As BMP signaling has been

demonstrated to interfere with Scx expression, this highlights the intricate and not always straight forward nature of healing. In contrast, EGR1, a transcription factor that unlike BMP has been demonstrated to participate in tendon differentiation, also promoted healing of the Achilles tendon in a rat model. Further, and similar to development, there are numerous other molecular signaling pathways involved in healing (e.g., CTGF, VEGF, TGF-β, IGF-1, and FGF).[47] As each of these pathways appears to play a specific role in development, exploration of their function in healing as well as tissue engineering remains critical.

Mechanical and structural remodeling of the ECM following loading likely occurs, and reductions in strain transfer may happen over several lengths scales. Therefore, future studies should be aimed to compare the spatial and temporal distributions of ECM, cell-ECM, cell-cell, and sub-cellular proteins in normal and healing tendons initially, and after periods of remodeling for low and high magnitude, long duration, dynamic loading. Cytochalasin-D (cyto-D) may be added to evaluate the effects of F-actin disruption on cell-ECM recovery after long duration dynamic loading. Despite our results, much remains unknown regarding how multiscale components transfer strain under load; such information could explain how varying levels of mechanical loading can result in both normal homeostasis[8-13] and pathology.[14-21] Adding in other antagonists or agonists of cell contractility, such as blebbistatin, ML7, lysophosphatadic acid, and vascular endothelial growth factor may be investigated in future studies.

Future work could incorporate a Scx-GFP transgenic mouse model[48] to better define cell types evaluated; however, this approach also has limitations.[49] Another

approach is to utilize methods such as flow cytometry[50] to quantify markers of tenocytes or tendon stem/progenitor cells, or perform stains for these cell types. For example, several immunohistochemistry stains relevant for TSPCs can be used including: CD146, CD105, CD90.2, CD73, CD44, Sca-1, Nestin, Nanog, Scx, and Tnmd.[50,51]

6.2.4 Drug Delivery, Therapeutics, and Tissue Engineering

Several studies have used therapeutics and tissue engineering approaches in attempts to reduce signs of tendinopathy and to enhance tendon healing following rupture. Studies have suggested the prospect of stem cell therapies in the treatment of tendinopathy.[52] When seeded on decellularized tendon matrices[53,54] these cells produced a surrounding environment very similar to native tissue. In addition, compared to traditional culture, MSCs maintained under hypoxic conditions[55] were found to demonstrate a more physiologic phenotype. Other therapeutics such as amnion derived multipotent progenitor cells demonstrated improved mechanical properties after application in injured rat Achilles tendons.[56] Finally, although whole blood injection,[57] platelet rich plasma (PRP),[58,59] and other adjuvant therapies have demonstrated potential clinical use,[60] some even supported by small trials, none has a sufficiently consistent track record to merit a consensus recommendation. Tissue engineering strategies utilizing 3D scaffolds have been engineered to integrate between ruptured ends of Achilles tendons in rats[61] and rabbits.[62] For example, *in vivo* and *ex vivo* experiments demonstrating that collagen-PDF implants recapitulate the structural, compositional, and mechanical properties of control tendons, and show capacity for good integration *in vivo.*[63] Incorporation of biodegradable synthetic scaffolds may present an additional

strategy for future research.[64,65] However, the capacity for these treatments to restore multiscale strain transfer has not been investigated, and may be critical for ultimate success *in vivo*.

Tendons harbor tendon stem/progenitor cells (TSPCs) that exhibit the classic stem cell properties of clonogenicity, multipotency, and self-renewal.[50] Unlike bone marrow-derived mesenchymal stem cells, TSPCs express higher levels of the tendon markers Scleraxis (Scx) and tenomodulin (Tnmd), and can regenerate tendon-like tissue.[50] TSPCs contribute to growth, tissue homeostasis, and repair,[66,67] and their ability to self-renew and differentiate is niche-dependent. However, the limited capacity of native tendon stem/progenitor cells (TSPCs) to aid in the repair process may contribute to deficiencies in homeostasis and healing. Unlike normal tendon,[50] degenerate and aged tendon contains TSPCs that exhibit deficits in clonogenicity, multipotency, and self-renewal capacity, as well as early maturation into senescence.[68-74] When implanted as an allogeneic fibrin glue construct, TSPCs may promote earlier and more complete repair.[67,75] Therefore, TSPC replacement therapies have the potential to improve tendon healing following injury.[67,76,77]

Another consideration for therapeutic intervention is using agents to affect multiscale strain transfer. Additional studies are still required to identify the key structural proteins that affect strain transfer. Once this is determined, many agents may be used (**Table 6-1**). For example, F-actin may be increased with jasplakinolide or decreased with cytochalasin-D or latrunculinA. Combinations of these agents with TSPCs may be necessary to fully control cell fate and tissue health upon implantation *in vivo*.

Table 6-1: Potential therapeutic targets to increase or decrease multiscale strain transfer.

Target	Increase	Decrease	Reference
Collagen Type I	PEMF, ESWT, PDGF-BB, Scx, TGF-β	Collagenase	78-80
Collagen Type III	TGF-β	PEMF, ESWT	78,81,82
Collagen Type V	-	PEMF, ESWT	81,82
Biglycan	cAMP, Forskolin	Chondroitinase ABC	83
Decorin	-	Chondroitinase ABC	84
Integrin-α11	GFOGER	-	85,86
N-cadherin	IL-6, β-catenin	MMP-7	87-89
Connexins	↓ intracellular redox, ↑kinases, retinoids and carotenoids, PGN	S. Aureus	90-92
F-actin	Jasplakinolide	Cytochalasin-D, latrunculinA	93,94
Lamin-A	Collagen	Farnesyl transferase inhibitor	95,96
Contractility	LPA, VEGF, calyculinA	Blebbistatin, ML-7, Y27	97
Collagen Crosslinking	Genipin	Collagenase	98

6.2.5 Improved Models of Stress Transmission

Several improvements can be made to our modeling framework to better represent the *in vivo* condition. First, the model assumes that there are only two sets of fibers present: those that align in the direction of loading and those that do not. This may not be the case *in vivo*, where this distribution of fiber types may vary as a function of tissue health. Additionally, the modeling framework could incorporate initial anisotropy instead of assuming a random fiber network at low strains. Second, the model assumes that contractile strains occur primarily along the long axis of the cell and that the volume of the cell is the same before and after contraction. However, this may also vary *in* vivo as a function of tissue health, changes in calcium ion concentration, and initial strain applied. Incorporating this detail from experiments designed to evaluate cell traction forces would provide for more detailed loading conditions to be applied to the model. Additionally, fiber viscoelasticity, poroelasticity, and uncrimping that change with tissue health, and are key features in describing tendon's response to loading, could be incorporated in future studies. Improved evaluation of tendon damage and plasticity due to dynamic

loading may also be investigated in the future.[99] Finally, recent, unpublished work has suggested that larger stress transmission is achieved through the incorporation of large Poisson's ratios to the model. As tendon typically experiences large Poisson's ratios, this addition to the modeling framework would enhance application of the model to represent *in vivo* conditions.

6.2.6 Development and Aging

Tendon development and healing is a well-orchestrated process requiring highly ordered molecular signaling events influenced by mechanical stimulation and surrounding environmental factors.[100] To best augment tendon healing through targeted therapeutics and tissue engineering strategies requires sufficient understanding of the *in-vivo* milieu that dictates tendon development. Importantly, tendons injured during early phases of development heal without scar at an accelerated rate.[101,102] As mentioned, following injury, tendons heal through scar formation, do not regain pre-injury material properties, often display aberrant phenotypes, and contribute to poor functional outcomes that worsen with aging.[20,103-106] Aged tendons have an increased risk for injury due to changes in tendon properties (mechanics, structural integrity, and composition),[20,107-109] lipid deposition, decreased vascularization, altered cell response to cellular stimuli, reduced cell activity, and inferior ability to repair.[72,110]

To combat age-induced deficits in healing, recent studies suggest that the micromechanical environment may contribute to development,[111,112] which may in turn regulate tissue development. It has become increasingly evident that mechanical properties, in addition to soluble factors and matrix ligands, affect stem cell behavior via

mechanotransduction through the actin cytoskeleton.[112] Additionally, high cell-cell contacts promote adipogenesis while inhibiting osteogenesis, which, in part is mediated through N-cadherin interactions and its adhesive domains. However, our understanding of these mechanisms in tendon remains limited. Age-related deficits may be due to inferior cell mechanosensing. These deficits may arise in many places given the potential multiscale areas affected. Identification of (1) changes in multiscale properties and (2) location of changes may result in specific therapeutics to combat age-induced deficits in tendon healing. Therefore, the overall objective of this work is to determine the effect of development and aging on multiscale mechanical, structural, and compositional properties in tendon, and their relationship to changes in nuclear shape. The global hypothesis of this proposed study is that multiscale strain transfer in tendon differs drastically from development to aging. In development, multiscale strain transfer is promoted through cell contacts and matrix re-organization, whereas in aging tendon, strain transfer is promoted through collagen interactions.

Series of experiments that vary animal age may provide insight into how macroscale forces are transferred to changes in matrix organization and nuclear deformations. Responses observed during development may be compared to adult tissues as well as in aged tissues, which can also play a role in tendon mechanics in multiple tendon types.[4,113] Together, this future work provides both fundamental understanding of the tendon microenvironment during development and aging, and would provide insight in potential strategies for neonatal-inspired tissue engineering.

6.2.7 Sex Differences

Sex differences are becoming increasing cited as contributing factors towards tendon injury risk and differential healing outcomes. For example, Achilles tendon ruptures are common injuries that affect 15 (female) to 55 (male) per 100,000 people each year.[114] The majority of Achilles tendon injuries are sports-related, which may explain why Achilles tendon rupture is associated with younger age at time of injury compared to other tendons.[115-118] Biochemical components of the tendon microenvironment that may contribute have identified estrogen receptors in lower limb tendons,[119,120] which may provide a mechanism for some of the estrogen-related changes in tendon material properties observed in humans.[121] In male, female, and ovariectomized (OVX) female rat Achilles tendons, the linear modulus was inferior in males compared to females.[122] Following injury in these animals, loss of ovarian hormones was clearly associated with inferior limb function, inferior tendon mechanics, and inferior tendon composition, all of which further highlight the biological importance of sex hormones in musculoskeletal connective tissue function. High GAG deposits were observed in OVX groups.[123] These changes highlight potential microenvironmental (both hormonal and biomechanical) differences that likely exist between these groups. Therefore, the objective of this proposed study is to determine the role of sex on multiscale properties in uninjured and healing tendons. Knowledge of strain transfer may explain potential sex-related differences that could be caused from inferior cell mechanosensing and may lead to sex-specific therapeutics to aid in tendon healing. In this proposed study, we hypothesize that female sex increases strain transfer in both uninjured and healing

tendons unlike in male tendons. Multiscale mechanical, structural, and compositional properties are evaluated in uninjured and healing male, female, and OVX tendons and evaluated for their healing response over time.

Sex may also play a role in other tendon types where microenvironments differ considerably, such as in the rotator cuff and the knee that experience compressive loading and a synovial environment. A recent study from our group (Robinson+2017, in review), has detailed specific sex differences in the rotator cuff, including changes in maximum load, area, and modulus. Given the identified changes in macroscale ECM modulus between these groups, changes in multiscale mechanical, structural, and compositional properties may also occur and be contributing factors towards macroscale properties. Sex differences may also contribute to the severity of genetic disease. Classic Ehlers–Danlos syndrome (EDS) is a heritable connective tissue disorder and is defined by collagen V mutations with haploinsufficiency for COL5A1 present in ~67% of affected individuals.[124,125] The classic form of EDS is characterized by hyperextensible skin, joint laxity and instability, as well as abnormal wound healing.[126] Although the prevalence of EDS is 1 in 20,000, this may be skewed towards the female population. Coupled with increased joint laxity in females, effects of EDS may be increasingly detrimental, and likely has large multiscale implications given the potential range of large tissue deformations possible. Understanding multiscale properties that couple hormonal differences with alterations in tissue mechanics may provide insight into the feedback mechanisms at play in this disease state.

6.2.8 Genetic Knockout Studies

Previous studies in our group have used many *in vivo* knockout mouse models to examine the role of non-collagenous and collagenous matrix components in tendons. Although many of these studies[3,4,35,113,127] have long established that macroscale tendon mechanics may be altered in both native and injured tissues, the role of multiscale mechanisms incorporating dynamic tenocyte or tendon stem/progenitor cells remains limited. Understanding the multiscale mechanical, structural, and compositional effects of genetic knockout models that specifically target proteins potentially involved in nuclear strain transfer would provide both an understanding of the regulatory roles of strain-transferring proteins and their role of promoting or impeding strain transfer. Therefore, the objective of this proposed study is to determine the multiscale mechanical, structural, and compositional response of tendon to tensile loading and their relationship to nuclear strain transfer. This proposed work will specifically determine the role of the following genetic knockout models (ECM→Nucleus): (1) colV, (2) biglycan, (3) integrin-α11,[128] (4) N-cadherin, (5) connexin-43,[129] (6) nesprin, and (7) laminA.[130] We hypothesize that knockdown of proteins will affect strain transfer to the subsequent hierarchical scale. This work would provide both understanding for the regulatory role of strain-transferring proteins and their role in promoting or impeding strain transfer. The next paragraphs describe these knockout models in more detail and their potential clinical impact, if uncovered.

Several of our previous knockout models could be used in future studies to examine changes in nuclear strain transfer. First, our haploinsufficient collagen V EDS model results in tendons with reduced fibril number, abnormal fibril structure, decreased

cross sectional area, and a reduction in the stiffness of the flexor digitorum longus (FDL). Further modification of this model by using inducible gene deletion prior to injury can allow for the analyses of the injury response with differing collagen V expression (i.e., $Col5a1^{+/+}$, $Col5a1^{flox/+}$, $Col5a1^{flox/flox}$). Multiscale evaluation in both of these models is possible, which would specifically identify the role of collagen V on nuclear strain transfer and stress transmission.

Second, similar experiments are ongoing to determine the effects of inducible deletion of SLRP-related genes (decorin and biglycan). As these molecules ultimately affect fibril mechanics and structure, the microenvironment and response of tenocytes to loading is likely also altered in these models. We found that Achilles tendons lacking decorin and biglycan had inferior mechanical and structural properties that were age dependent; and that simple empirical models, based on previously described damage models, were predictive of Achilles tendon dynamic modulus in both decorin- and biglycan-null mice. The mechanism for the effects on mechanics may be due to both regulatory and mechanical factors. Using a shear-lag model, we showed that the non-linear mechanical response of the GAGs leads to a distinct toe region in the stress-strain response of the tendon.[131] When the fibril lengths are significantly larger than this length scale (related to microstructural parameters (GAG spacing, stiffness, and geometry) over which load is transferred), the mechanical properties of the tendon are relatively insensitive to deletion of GAGs. Understanding the role of proteoglycans on strain transfer in these model systems is important to establish how applied macroscale loading may result in aberrant gene and protein changes present in these knockout models.

Several other knockout models, not currently used in our group, should be investigated that specifically affect proteins involved in mechanotransduction. Mouse models of superior healing may present additional models to study multiscale tendon properties in response to loading and injury. For example, the Murphy Roths Large (MRL/MpJ) mouse model, an autoimmune-prone mouse strain, has been shown to have superior adult healing capacity evidenced early through the closing of ear punches.[132] This phenomenon has been extended to also enhance regeneration in myocardial tissue,[133] articular cartilage,[134] and the central nervous system.[135] Recent work in tendon,[136] has shown that MMP-2 and TGF-β1 protein levels were significantly altered in MRL/MpJ mice compared to C57BL/6J tendons, with elevated TGF-β1 protein levels in MRL/MpJ mice.[136] MRL/MpJ mice also exhibited decreased proteoglycan staining, increased vascularization, and improved collagen structure compared to C56BL/6 mice.[136] Thus, significant research opportunities exist in this domain.

6.2.9 Clinical Translation: Combining In Vitro and In Vivo Animal Models to Design Studies in Humans

There is much information regarding the anatomy, diagnosis, treatment, and biomechanics of normal and healing tendons, however there remains many research areas requiring further investigation. Although well controlled basic science studies are not a direct substitute for large scale clinical trials, they are important in resolving outstanding fundamental questions regarding means of treatment in a consistent and well established model. Future studies should provide a comprehensive approach to study tendon healing, through careful evaluation of mechanical, structural, compositional, and functional tissue

properties. There is a need for greater characterization of the dose-dependent response of mechanical load on tendon. Results from such studies would further allow for much needed research into development of effective adjuvant therapies that could be translated into improved outcomes. In addition to healing models, investigation of other diseased states known to adversely affect tendon are warranted (e.g., high cholesterol, diabetes, and obesity).

One solution to streamline animal studies may be the development of a tendon-on-a-chip system that can serve as a native tendon surrogate. To accomplish this, one could: (1) develop a mechanically loaded collagenous network with gradient in material properties as a model of tendon insertion/myotendinous unit, (2) develop muscle module by assembling smooth muscle tissues in hydrogel around fibers, (3) develop vascular network around tendinous tissues, (4) conduct studies of response to therapeutics with mechanical loading, injury, and healing, for individual components, and multi-tissue platform, and (5) investigate human physiology in multi-tissue platforms. This approach would be validated in mouse models as well as human tissues and may have many broad applications across several fields. These applications include injury (e.g., tendinopathy, acute and chronic injury), hormones, mechanical loading, metabolic diseases (e.g., diabetes, high cholesterol), aging, partial and complete rupture, inflammation and vascularity, development and aging, and circadian rhythms. Additionally, this model would be useful to screen potential therapeutics, scaffold and drug delivery methods, and evaluate specific questions regarding tendon structure and tissue mechanics.

Continued investigation into promising direct biologic interventions that may regulate strain transfer and stress transmission may be capable of generating useful

therapies. Lessons from development may continue to expand this list of putative treatments, as well as our fundamental understanding of the healing process. Cell based therapies and tissue engineering also represent a related avenue well suited to facilitate tendon healing. While none of these promising therapies has had a marked impact on patient outcomes thus far, recent and ongoing work offers reasons to be optimistic regarding facilitation of tendon healing and coming improvements in patient centered outcomes.

6.3 Final Conclusions

This dissertation explored the interface between dynamic loading and tendon healing across multiple length scales using living tendon explants. This work begins to define the implications of macroscale mechanical loading on collagen structure and tenocyte response in uninjured and healing tendon, and provides a foundation for the development of new strategies to improve tendon healing. Ultimately, this work helps our understanding of tendon's multiscale response to loading, provides a framework for the micromechanical environment that tenocytes interact in response to dynamic loading and healing, and lays important groundwork for benchmarks for tendon tissue engineering. The multiscale response to mechanical loading, which is a hallmark of clinical rehabilitation protocols, is necessary to determine the ramifications of various macroscale loading protocols. Additionally, these results provide benchmarks for the environments in which tendon cells may experience following cell delivery therapies. Several exciting future avenues of research are possible that would highly impact basic science research of tendon function and lead to potentially translatable approaches that could improve tendon

injury onset and healing response. In conclusion, this dissertation provides a strong foundation on which future experimental and computational studies can build to fully elucidate the multiscale mechanisms that govern strain transfer in tendon.

6.4 References

1. Fukashiro S, Komi PV, Jarvinen M, Miyashita M. In vivo Achilles tendon loading during jumping in humans. *Eur J Appl Physiol Occup Physiol.* 1995;71(5):453-458.

2. Komi PV, Fukashiro S, Jarvinen M. Biomechanical loading of Achilles tendon during normal locomotion. *Clin Sports Med.* Jul 1992;11(3):521-531.

3. Dourte LM, Pathmanathan L, Jawad AF, et al. Influence of decorin on the mechanical, compositional, and structural properties of the mouse patellar tendon. *J Biomech Eng.* Mar 2012;134(3):031005.

4. Dunkman B, Mienaltowski,Adams, Thomas, Satchell, Kumar, Pathmanathan, Beason; Iozzo, Birk, Soslowsky Decorin Expression Is Required for Age-Related Changes in Tendon Structure and Mechanical Properties *Matrix Biol.* 2012((in review)).

5. Fessel G, Snedeker JG. Evidence against proteoglycan mediated collagen fibril load transmission and dynamic viscoelasticity in tendon. *Matrix Biol.* Oct 2009;28(8):503-510.

6. Ikoma K, Kido M, Nagae M, et al. Effects of stress-shielding on the dynamic viscoelasticity and ordering of the collagen fibers in rabbit Achilles tendon. *J Orthop Res.* Jul 6 2013.

7. Schechtman H, Bader DL. In vitro fatigue of human tendons. *J Biomech.* Aug 1997;30(8):829-835.

8. Schechtman H, Bader DL. Fatigue damage of human tendons. *J Biomech.* Mar 2002;35(3):347-353.

9. Wren TA, Lindsey DP, Beaupre GS, Carter DR. Effects of creep and cyclic loading on the mechanical properties and failure of human Achilles tendons. *Ann Biomed Eng.* Jun 2003;31(6):710-717.

10. Fung DT, Wang VM, Laudier DM, et al. Subrupture tendon fatigue damage. *J Orthop Res.* Feb 2009;27(2):264-273.

11. Wang XT, Ker RF, Alexander RM. Fatigue rupture of wallaby tail tendons. *J Exp Biol.* Mar 1995;198(Pt 3):847-852.

12. Miller KS, Connizzo BK, Feeney E, Soslowsky LJ. Characterizing local collagen fiber re-alignment and crimp behavior throughout mechanical testing in a mature mouse supraspinatus tendon model. *J Biomech.* Aug 9 2012;45(12):2061-2065.

13. Dlugosz J, Gathercole LJ, Keller A. Transmission Electron-Microscope Studies and Their Relation to Polarizing Optical Microscopy in Rat Tail Tendon. *Micron.* 1978;9(2):71-82.

14. Hansen KA, Weiss JA, Barton JK. Recruitment of tendon crimp with applied tensile strain. *J Biomech Eng.* Feb 2002;124(1):72-77.

15. Goulam Houssen Y, Gusachenko I, Schanne-Klein MC, Allain JM. Monitoring micrometer-scale collagen organization in rat-tail tendon upon mechanical strain using second harmonic microscopy. *J Biomech.* Jul 28 2011;44(11):2047-2052.

16. Rigby BJ, Hirai N, Spikes JD, Eyring H. The Mechanical Properties of Rat Tail Tendon. *J Gen Physiol.* Nov 1 1959;43(2):265-283.

17. Buckley MR, Sarver JJ, Freedman BR, Soslowsky LJ. The dynamics of collagen uncrimping and lateral contraction in tendon and the effect of ionic concentration. *J Biomech.* Sep 3 2013;46(13):2242-2249.

18. Lin TW, Cardenas L, Glaser DL, Soslowsky LJ. Tendon healing in interleukin-4 and interleukin-6 knockout mice. *J Biomech.* 2006;39(1):61-69.

19. Dunkman AA, Buckley MR, Mienaltowski MJ, et al. The tendon injury response is influenced by decorin and biglycan. *Ann Biomed Eng.* Mar 2014;42(3):619-630.

20. Mienaltowski MJ, Dunkman AA, Buckley MR, et al. Injury response of geriatric mouse patellar tendons. *J Orthop Res.* Jul 2016;34(7):1256-1263.

21. Freedman BR, Zuskov A, Sarver JJ, Buckley MR, Soslowsky LJ. Evaluating changes in tendon crimp with fatigue loading as an ex vivo structural assessment of tendon damage. *J Orthop Res.* Mar 13 2015.

22. Thornton GM, Shrive NG, Frank CB. Ligament creep recruits fibres at low stresses and can lead to modulus-reducing fibre damage at higher creep stresses: a study in rabbit medial collateral ligament model. *J Orthop Res.* Sep 2002;20(5):967-974.

23. Zhang Y, Yu J, Bomba HN, Zhu Y, Gu Z. Mechanical Force-Triggered Drug Delivery. *Chem Rev.* Oct 12 2016;116(19):12536-12563.

24. AAOS. Guideline on the Diagnosis and Treatment of Acute Achilles Tendon Rupture. 2009.

25. Han WM, Heo SJ, Driscoll TP, et al. Microstructural heterogeneity directs micromechanics and mechanobiology in native and engineered fibrocartilage. *Nat Mater.* Apr 2016;15(4):477-484.

26. Lavagnino M, Brooks AE, Oslapas AN, Gardner KL, Arnoczky SP. Crimp length decreases in lax tendons due to cytoskeletal tension, but is restored with tensional homeostasis. *J Orthop Res.* Nov 23 2016.

27. Beason DP, Kuntz AF, Hsu JE, Miller KS, Soslowsky LJ. Development and evaluation of multiple tendon injury models in the mouse. *J Biomech.* Mar 7 2012.

28. Freedman BR, Bade ND, Riggin CN, et al. The (dys)functional extracellular matrix. *Biochim Biophys Acta.* Nov 2015;1853(11 Pt B):3153-3164.

29. Mercer SE, Odelberg SJ, Simon HG. A dynamic spatiotemporal extracellular matrix facilitates epicardial-mediated vertebrate heart regeneration. *Dev Biol.* Oct 15 2013;382(2):457-469.

30. Wang J, Karra R, Dickson AL, Poss KD. Fibronectin is deposited by injury-activated epicardial cells and is necessary for zebrafish heart regeneration. *Dev Biol.* Oct 15 2013;382(2):427-435.

31. Calve S, Odelberg SJ, Simon HG. A transitional extracellular matrix instructs cell behavior during muscle regeneration. *Dev Biol.* Aug 1 2010;344(1):259-271.

32. Brockes JP, Kumar A. Plasticity and reprogramming of differentiated cells in amphibian regeneration. *Nat Rev Mol Cell Biol.* Aug 2002;3(8):566-574.

33. Gemberling M, Bailey TJ, Hyde DR, Poss KD. The zebrafish as a model for complex tissue regeneration. *Trends Genet.* Nov 2013;29(11):611-620.

34. Dunkman AA, Buckley MR, Mienaltowski MJ, et al. Decorin expression is important for age-related changes in tendon structure and mechanical properties. *Matrix Biol.* Jan 2013;32(1):3-13.

35. Sun M, Connizzo BK, Adams SM, et al. Targeted deletion of collagen V in tendons and ligaments results in a classic Ehlers-Danlos syndrome joint phenotype. *Am J Pathol.* May 2015;185(5):1436-1447.

36. Connizzo BK, Sarver JJ, Han L, Soslowsky LJ. In situ fibril stretch and sliding is location-dependent in mouse supraspinatus tendons. *J Biomech.* Dec 18 2014;47(16):3794-3798.

37. Kanazawa T, Gotoh M, Ohta K, et al. Histomorphometric and ultrastructural analysis of the tendon-bone interface after rotator cuff repair in a rat model. *Sci Rep.* Sep 20 2016;6:33800.

38. Oakes PW, Banerjee S, Marchetti MC, Gardel ML. Geometry regulates traction stresses in adherent cells. *Biophys J.* Aug 19 2014;107(4):825-833.

39. Maeda E, Sugimoto M, Ohashi T. Cytoskeletal tension modulates MMP-1 gene expression from tenocytes on micropillar substrates. *J Biomech.* Mar 15 2013;46(5):991-997.

40. Wang JH. Cell Traction Forces (CTFs) and CTF Microscopy Applications in Musculoskeletal Research. *Oper Tech Orthop.* Jun 01 2010;20(2):106-109.

41. Arnoczky SP, Lavagnino M, Egerbacher M, Caballero O, Gardner K. Matrix metalloproteinase inhibitors prevent a decrease in the mechanical properties of stress-deprived tendons: an in vitro experimental study. *Am J Sports Med.* May 2007;35(5):763-769.

42. Smith SM, Zhang G, Birk DE. Collagen V localizes to pericellular sites during tendon collagen fibrillogenesis. *Matrix Biol.* Jan 2014;33:47-53.

43. Carvalho HF, Felisbino SL, Keene DR, Vogel KG. Identification, content, and distribution of type VI collagen in bovine tendons. *Cell Tissue Res.* Aug 2006;325(2):315-324.

44. Sardone F, Santi S, Tagliavini F, et al. Collagen VI-NG2 axis in human tendon fibroblasts under conditions mimicking injury response. *Matrix Biol.* Sep 2016;55:90-105.

45. Guerquin MJ, Charvet B, Nourissat G, et al. Transcription factor EGR1 directs tendon differentiation and promotes tendon repair. *J Clin Invest.* Aug 1 2013;123(8):3564-3576.

46. Majewski M, Betz O, Ochsner PE, Liu F, Porter RM, Evans CH. Ex vivo adenoviral transfer of bone morphogenetic protein 12 (BMP-12) cDNA improves Achilles tendon healing in a rat model. *Gene Ther.* Aug 2008;15(16):1139-1146.

47. Chen CH, Cao Y, Wu YF, Bais AJ, Gao JS, Tang JB. Tendon healing in vivo: gene expression and production of multiple growth factors in early tendon healing period. *J Hand Surg Am.* Dec 2008;33(10):1834-1842.

48. Pryce BA, Brent AE, Murchison ND, Tabin CJ, Schweitzer R. Generation of transgenic tendon reporters, ScxGFP and ScxAP, using regulatory elements of the scleraxis gene. *Dev Dyn.* Jun 2007;236(6):1677-1682.

49. Huang AH, Lu HH, Schweitzer R. Molecular regulation of tendon cell fate during development. *J Orthop Res.* Feb 9 2015.

50. Bi Y, Ehirchiou D, Kilts TM, et al. Identification of tendon stem/progenitor cells and the role of the extracellular matrix in their niche. *Nat Med.* Oct 2007;13(10):1219-1227.

51. Alberton P, Dex S, Popov C, Shukunami C, Schieker M, Docheva D. Loss of tenomodulin results in reduced self-renewal and augmented senescence of tendon stem/progenitor cells. *Stem Cells Dev.* Mar 1 2015;24(5):597-609.

52. Muttini A, Salini V, Valbonetti L, Abate M. Stem cell therapy of tendinopathies: suggestions from veterinary medicine. *Muscles Ligaments Tendons J.* Jul 2012;2(3):187-192.

53. Yin Z, Chen X, Zhu T, et al. The effect of decellularized matrices on human tendon stem/progenitor cell differentiation and tendon repair. *Acta Biomater.* Jul 26 2013.

54. Ning LJ, Zhang Y, Chen XH, et al. Preparation and characterization of decellularized tendon slices for tendon tissue engineering. *J Biomed Mater Res A.* Jun 2012;100(6):1448-1456.

55. Huang TF, Yew TL, Chiang ER, et al. Mesenchymal stem cells from a hypoxic culture improve and engraft Achilles tendon repair. *Am J Sports Med.* May 2013;41(5):1117-1125.

56. Philip J, Hackl F, Canseco JA, et al. Amnion-derived multipotent progenitor cells improve achilles tendon repair in rats. *Eplasty.* 2013;13:e31.

57. Bell KJ, Fulcher ML, Rowlands DS, Kerse N. Impact of autologous blood injections in treatment of mid-portion Achilles tendinopathy: double blind randomised controlled trial. *BMJ.* 2013;346:f2310.

58. de Vos RJ, Weir A, van Schie HT, et al. Platelet-rich plasma injection for chronic Achilles tendinopathy: a randomized controlled trial. *JAMA.* Jan 13 2010;303(2):144-149.

59. Parafioriti A, Armiraglio E, Del Bianco S, Tibalt E, Oliva F, Berardi AC. Single injection of platelet-rich plasma in a rat Achilles tendon tear model. *Muscles Ligaments Tendons J.* Apr 2011;1(2):41-47.

60. Al-Abbad H, Simon JV. The effectiveness of extracorporeal shock wave therapy on chronic achilles tendinopathy: a systematic review. *Foot Ankle Int.* Jan 2013;34(1):33-41.

61. Webb WR, Dale TP, Lomas AJ, et al. The application of poly(3-hydroxybutyrate-co-3-hydroxyhexanoate) scaffolds for tendon repair in the rat model. *Biomaterials.* Sep 2013;34(28):6683-6694.

62. Meimandi-Parizi A, Oryan A, Moshiri A. Tendon tissue engineering and its role on healing of the experimentally induced large tendon defect model in rabbits: a comprehensive in vivo study. *PLoS One.* 2013;8(9):e73016.

63. Oryan A, Moshiri A, Parizi Meimandi A, Silver IA. A long-term in vivo investigation on the effects of xenogenous based, electrospun, collagen implants on the healing of experimentally-induced large tendon defects. *J Musculoskelet Neuronal Interact.* Sep 2013;13(3):315-329.

64. Reverchon E, Baldino L, Cardea S, De Marco I. Biodegradable synthetic scaffolds for tendon regeneration. *Muscles Ligaments Tendons J.* Jul 2012;2(3):181-186.

65. Padulo J, Oliva F, Frizziero A, Maffulli N. Muscle, Ligaments and Tendons Journal. Basic principles and recommendations in clinical and field science research. *Muscles Ligaments Tendons J.* Oct 2013;3(4):250-252.

66. Jones DL, Wagers AJ. No place like home: anatomy and function of the stem cell niche. *Nat Rev Mol Cell Biol.* Jan 2008;9(1):11-21.

67. Mienaltowski MJ, Adams SM, Birk DE. Regional differences in stem cell/progenitor cell populations from the mouse achilles tendon. *Tissue Eng Part A.* Jan 2013;19(1-2):199-210.

68. Rui YF, Lui PP, Wong YM, Tan Q, Chan KM. Altered fate of tendon-derived stem cells isolated from a failed tendon-healing animal model of tendinopathy. *Stem Cells Dev.* Apr 1 2013;22(7):1076-1085.

69. Kohler J, Popov C, Klotz B, et al. Uncovering the cellular and molecular changes in tendon stem/progenitor cells attributed to tendon aging and degeneration. *Aging Cell.* Dec 2013;12(6):988-999.

70. Zhou Z, Akinbiyi T, Xu L, et al. Tendon-derived stem/progenitor cell aging: defective self-renewal and altered fate. *Aging Cell.* Oct 2010;9(5):911-915.

71. Zhang J, Yuan T, Wang JH. Moderate treadmill running exercise prior to tendon injury enhances wound healing in aging rats. *Oncotarget.* Feb 23 2016;7(8):8498-8512.

72. Zhang J, Wang JH. Moderate Exercise Mitigates the Detrimental Effects of Aging on Tendon Stem Cells. *PLoS One.* 2015;10(6):e0130454.

73. Jiang D, Jiang Z, Zhang Y, et al. Effect of young extrinsic environment stimulated by hypoxia on the function of aged tendon stem cell. *Cell Biochem Biophys.* Nov 2014;70(2):967-973.

74. Chen L, Wang GD, Liu JP, et al. miR-135a modulates tendon stem/progenitor cell senescence via suppressing ROCK1. *Bone.* Feb 2015;71:210-216.

75. Ni M, Lui PP, Rui YF, et al. Tendon-derived stem cells (TDSCs) promote tendon repair in a rat patellar tendon window defect model. *J Orthop Res.* Apr 2012;30(4):613-619.

76. Patel S, Gualtieri AP, Lu HH, Levine WN. Advances in biologic augmentation for rotator cuff repair. *Ann N Y Acad Sci.* Oct 17 2016.

77. Lui PP. Identity of tendon stem cells--how much do we know? *J Cell Mol Med.* Jan 2013;17(1):55-64.

78. Kenyon NJ, Ward RW, McGrew G, Last JA. TGF-beta1 causes airway fibrosis and increased collagen I and III mRNA in mice. *Thorax.* Sep 2003;58(9):772-777.

79. Espira L, Lamoureux L, Jones SC, Gerard RD, Dixon IM, Czubryt MP. The basic helix-loop-helix transcription factor scleraxis regulates fibroblast collagen synthesis. *J Mol Cell Cardiol.* Aug 2009;47(2):188-195.

80. Thomopoulos S, Zaegel M, Das R, et al. PDGF-BB released in tendon repair using a novel delivery system promotes cell proliferation and collagen remodeling. *J Orthop Res.* Oct 2007;25(10):1358-1368.

81. Mani-Babu S, Morrissey D, Waugh C, Screen H, Barton C. The effectiveness of extracorporeal shock wave therapy in lower limb tendinopathy: a systematic review. *Am J Sports Med.* Mar 2015;43(3):752-761.

82. Tucker JJ, Cirone JM, Morris TR, et al. Pulsed electromagnetic field therapy improves tendon-to-bone healing in a rat rotator cuff repair model. *J Orthop Res.* Jun 10 2016.

83. Ungefroren H, Cikos T, Krull NB, Kalthoff H. Biglycan gene promoter activity in osteosarcoma cells is regulated by cyclic AMP. *Biochem Biophys Res Commun.* Jun 18 1997;235(2):413-417.

84. Yan W, Wang P, Zhao CX, Tang J, Xiao X, Wang DW. Decorin gene delivery inhibits cardiac fibrosis in spontaneously hypertensive rats by modulation of transforming growth factor-beta/Smad and p38 mitogen-activated protein kinase signaling pathways. *Hum Gene Ther.* Oct 2009;20(10):1190-1200.

85. Zhang WM, Kapyla J, Puranen JS, et al. alpha 11beta 1 integrin recognizes the GFOGER sequence in interstitial collagens. *J Biol Chem.* Feb 28 2003;278(9):7270-7277.

86. Goodman SL, Picard M. Integrins as therapeutic targets. *Trends Pharmacol Sci.* Jul 2012;33(7):405-412.

87. Williams H, Johnson JL, Jackson CL, White SJ, George SJ. MMP-7 mediates cleavage of N-cadherin and promotes smooth muscle cell apoptosis. *Cardiovasc Res.* Jul 01 2010;87(1):137-146.

88. Liu Q, Wang W, Zhang L, et al. Involvement of N-cadherin/beta-catenin interaction in the micro/nanotopography induced indirect mechanotransduction. *Biomaterials.* Aug 2014;35(24):6206-6218.

89. Na YR, Lee JS, Lee SJ, Seok SH. Interleukin-6-induced Twist and N-cadherin enhance melanoma cell metastasis. *Melanoma Res.* Dec 2013;23(6):434-443.

90. King TJ, Bertram JS. Connexins as targets for cancer chemoprevention and chemotherapy. *Biochim Biophys Acta.* Dec 20 2005;1719(1-2):146-160.

91. Solan JL, Lampe PD. Connexin phosphorylation as a regulatory event linked to gap junction channel assembly. *Biochim Biophys Acta.* Jun 10 2005;1711(2):154-163.

92. Retamal MA, Schalper KA, Shoji KF, Bennett MV, Saez JC. Opening of connexin 43 hemichannels is increased by lowering intracellular redox potential. *Proc Natl Acad Sci U S A.* May 15 2007;104(20):8322-8327.

93. Holzinger A. Jasplakinolide: an actin-specific reagent that promotes actin polymerization. *Methods Mol Biol.* 2009;586:71-87.

94. Lee E, Shelden EA, Knecht DA. Formation of F-actin aggregates in cells treated with actin stabilizing drugs. *Cell Motil Cytoskeleton.* 1998;39(2):122-133.

95. Swift J, Ivanovska IL, Buxboim A, et al. Nuclear lamin-A scales with tissue stiffness and enhances matrix-directed differentiation. *Science.* Aug 30 2013;341(6149):1240104.

96. Dechat T, Pfleghaar K, Sengupta K, et al. Nuclear lamins: major factors in the structural organization and function of the nucleus and chromatin. *Genes Dev.* Apr 01 2008;22(7):832-853.

97. Cho YE, Ahn DS, Morgan KG, Lee YH. Enhanced contractility and myosin phosphorylation induced by Ca(2+)-independent MLCK activity in hypertensive rats. *Cardiovasc Res.* Jul 01 2011;91(1):162-170.

98. Alfredo Uquillas J, Kishore V, Akkus O. Genipin crosslinking elevates the strength of electrochemically aligned collagen to the level of tendons. *J Mech Behav Biomed Mater*. Nov 2012;15:176-189.

99. Ciarletta P, Ben Amar M. A finite dissipative theory of temporary interfibrillar bridges in the extracellular matrix of ligaments and tendons. *J R Soc Interface.* Oct 06 2009;6(39):909-924.

100. Killian ML, Cavinatto L, Galatz LM, Thomopoulos S. The role of mechanobiology in tendon healing. *J Shoulder Elbow Surg.* Feb 2012;21(2):228-237.

101. Ansorge HL, Hsu JE, Edelstein L, Adams S, Birk DE, Soslowsky LJ. Recapitulation of the Achilles tendon mechanical properties during neonatal development: a study of differential healing during two stages of development in a mouse model. *J Orthop Res.* Mar 2012;30(3):448-456.

102. Beredjiklian PK, Favata M, Cartmell JS, Flanagan CL, Crombleholme TM, Soslowsky LJ. Regenerative versus reparative healing in tendon: a study of biomechanical and histological properties in fetal sheep. *Ann Biomed Eng.* Nov 2003;31(10):1143-1152.

103. Freedman BR, Gordon JA, Soslowsky LJ. The Achilles tendon: fundamental properties and mechanisms governing healing. *Muscles Ligaments Tendons J.* Apr 2014;4(2):245-255.

104. Zhang K, Asai S, Hast MW, et al. Tendon mineralization is progressive and associated with deterioration of tendon biomechanical properties, and requires BMP-Smad signaling in the mouse Achilles tendon injury model. *Matrix Biol.* May-Jul 2016;52-54:315-324.

105. Olsson N, Nilsson-Helander K, Karlsson J, et al. Major functional deficits persist 2 years after acute Achilles tendon rupture. *Knee Surg Sports Traumatol Arthrosc.* Aug 2011;19(8):1385-1393.

106. Olsson N, Petzold M, Brorsson A, Karlsson J, Eriksson BI, Silbernagel KG. Predictors of Clinical Outcome After Acute Achilles Tendon Ruptures. *Am J Sports Med.* Jun 2014;42(6):1448-1455.

107. Pardes AM, Beach ZM, Raja H, Rodriguez AB, Freedman BR, Soslowsky LJ. Aging leads to inferior Achilles tendon mechanics and altered ankle function in rodents. *In Review.* 2016.

108. Peffers MJ, Thorpe CT, Collins JA, et al. Proteomic analysis reveals age-related changes in tendon matrix composition, with age- and injury-specific matrix fragmentation. *J Biol Chem.* Sep 12 2014;289(37):25867-25878.

109. Gillis C, Sharkey N, Stover SM, Pool RR, Meagher DM, Willits N. Effect of maturation and aging on material and ultrasonographic properties of equine superficial digital flexor tendon. *Am J Vet Res.* Oct 1995;56(10):1345-1350.

110. Kannus P, Jozsa L. Histopathological changes preceding spontaneous rupture of a tendon. A controlled study of 891 patients. *J Bone Joint Surg Am.* Dec 1991;73(10):1507-1525.

111. Nelson CM, Gleghorn JP. Sculpting organs: mechanical regulation of tissue development. *Annu Rev Biomed Eng.* 2012;14:129-154.

112. Cosgrove BD, Mui KL, Driscoll TP, et al. N-cadherin adhesive interactions modulate matrix mechanosensing and fate commitment of mesenchymal stem cells. *Nat Mater.* Dec 2016;15(12):1297-1306.

113. Gordon J, Freedman B, Zuskov A, Iozzo R, Birk D, Soslowsky L. Achilles tendons from decorin- and biglycan-null mouse models have inferior mechanical and structural properties predicted by an image-based empirical damage model. *Journal of Biomechanics.* 2014;In review.

114. Huttunen TT, Kannus P, Rolf C, Fellander-Tsai L, Mattila VM. Acute Achilles Tendon Ruptures: Incidence of Injury and Surgery in Sweden Between 2001 and 2012. *The American journal of sports medicine.* Jul 23 2014.

115. Houshian S, Tscherning T, Riegels-Nielsen P. The epidemiology of Achilles tendon rupture in a Danish county. *Injury.* Nov 1998;29(9):651-654.

116. Jozsa L, Kvist M, Balint BJ, et al. The role of recreational sport activity in Achilles tendon rupture. A clinical, pathoanatomical, and sociological study of 292 cases. *The American journal of sports medicine.* May-Jun 1989;17(3):338-343.

117. Leppilahti J, Puranen J, Orava S. Incidence of Achilles tendon rupture. *Acta orthopaedica Scandinavica.* Jun 1996;67(3):277-279.

118. Moller A, Astron M, Westlin N. Increasing incidence of Achilles tendon rupture. *Acta orthopaedica Scandinavica.* Oct 1996;67(5):479-481.

119. Bridgeman JT, Zhang Y, Donahue H, Wade AM, Juliano PJ. Estrogen receptor expression in posterior tibial tendon dysfunction: a pilot study. *Foot Ankle Int.* Dec 2010;31(12):1081-1084.

120. Liu SH, al-Shaikh R, Panossian V, et al. Primary immunolocalization of estrogen and progesterone target cells in the human anterior cruciate ligament. *J Orthop Res.* Jul 1996;14(4):526-533.

121. Bryant AL, Clark RA, Bartold S, et al. Effects of estrogen on the mechanical behavior of the human Achilles tendon in vivo. *J Appl Physiol (1985).* Oct 2008;105(4):1035-1043.

122. Pardes AM, Freedman BR, Fryhofer GW, Salka NS, Bhatt PR, Soslowsky LJ. Males have Inferior Achilles Tendon Material Properties Compared to Females in a Rodent Model. *Ann Biomed Eng.* May 5 2016.

123. Fryhofer GW, Freedman BR, Hillin CD, et al. Postinjury biomechanics of Achilles tendon vary by sex and hormone status. *J Appl Physiol (1985).* Nov 01 2016;121(5):1106-1114.

124. Malfait F, Coucke P, Symoens S, Loeys B, Nuytinck L, De Paepe A. The molecular basis of classic Ehlers-Danlos syndrome: a comprehensive study of biochemical and molecular findings in 48 unrelated patients. *Hum Mutat.* Jan 2005;25(1):28-37.

125. Steinmann B. The collagen family: structure, assembly, and organization in the extracellular matrix. *Connective Tissue and Its Heritable Disorders*. New York: Wiley-Liss; 2002:431-523.

126. Malfait F, Wenstrup RJ, De Paepe A. Clinical and genetic aspects of Ehlers-Danlos syndrome, classic type. *Genet Med.* Oct 2010;12(10):597-605.

127. Connizzo BK, Freedman BR, Fried JH, Sun M, Birk DE, Soslowsky LJ. Regulatory role of collagen V in establishing mechanical properties of tendons and ligaments is tissue dependent. *J Orthop Res.* Jun 2015;33(6):882-888.

128. Zhu CQ, Popova SN, Brown ER, et al. Integrin alpha 11 regulates IGF2 expression in fibroblasts to enhance tumorigenicity of human non-small-cell lung cancer cells. *Proc Natl Acad Sci U S A.* Jul 10 2007;104(28):11754-11759.

129. Shen H, Grimston S, Civitelli R, Thomopoulos S. Deletion of connexin43 in osteoblasts/osteocytes leads to impaired muscle formation in mice. *J Bone Miner Res.* Apr 2015;30(4):596-605.

130. Gnocchi VF, Scharner J, Huang Z, et al. Uncoordinated transcription and compromised muscle function in the lmna-null mouse model of Emery- Emery-Dreyfuss muscular dystrophy. *PLoS One.* Feb 22 2011;6(2):e16651.

131. Ahmadzadeh H, Connizzo BK, Freedman BR, Soslowsky LJ, Shenoy VB. Determining the contribution of glycosaminoglycans to tendon mechanical properties with a modified shear-lag model. *J Biomech.* Sep 27 2013;46(14):2497-2503.

132. Heber-Katz E. The regenerating mouse ear. *Semin Cell Dev Biol.* Aug 1999;10(4):415-419.

133. Heber-Katz E, Leferovich J, Bedelbaeva K, Gourevitch D, Clark L. The scarless heart and the MRL mouse. *Philos Trans R Soc Lond B Biol Sci.* May 29 2004;359(1445):785-793.

134. Fitzgerald J, Rich C, Burkhardt D, Allen J, Herzka AS, Little CB. Evidence for articular cartilage regeneration in MRL/MpJ mice. *Osteoarthritis Cartilage.* Nov 2008;16(11):1319-1326.

135. Donnelly DJ, Popovich PG. Inflammation and its role in neuroprotection, axonal regeneration and functional recovery after spinal cord injury. *Exp Neurol.* Feb 2008;209(2):378-388.

136. Sereysky JB, Flatow EL, Andarawis-Puri N. Musculoskeletal regeneration and its implications for the treatment of tendinopathy. *Int J Exp Pathol.* Aug 2013;94(4):293-303.

APPENDIX A: EXPERIMENTAL PROTOCOLS

APPENDIX A: EXPERIMENTAL PROTOCOLS

TABLE OF CONTENTS

AFM Protocol

T:\Protocols\AFM

Ben Freedman; Biao Han; Lin Han

Making Tips

1. Wash tip with DI H_2O after use

2. Open software, load experiment

3. Put blank tip on

4. Stage | Initialize
    a. Brings scan head all the way up

5. In setup,
    a. Zoom to 0x
    b. Move focus controls so see reflected cantilever
    c. Adjust laser to cantilever tip,
        i. Zero horiz + vert deflections
        ii. Maximize sum
    d. Return to zoom of real image + put crosshair over tip
        i. Move focus up 1mm from optics
        ii. Remove air holder metal piece

6. Navigate (to operate xy stage)
    a. Position glue on mica under tip (with micropipette)
    b. Lower jog until about 1mm (focus + wheel mouse) (use lock feature)

7. Scan head down until hit glue, then up slowly ~1mm (crash protect and move up a little to remove cantilever bend and can drag tip in X-Y direction to confirm attached
    a. So colloid moves toward tip end

8. Put 10um spheres down
    a. Tip reflection, find sphere, then return to "sample"
    b. Push down on sphere for a <u>couple minutes</u>, then move up and remove tip
    c. Can check sphere attached by brighten up 1mm then switch to "tip reflection"

9. For next tip, use Biao's method to max the sum by adjust up/down arrow knob
    a. Setup, move focus up 1mm, navigate… (repeat)

<u>Notes</u>:
The 0.3N/m tip is the middle one that is longest.

Calibration

1. Before use fluid holder, make sure it is clean (DI H_2O)
    a. Want holder with bridge to push spring

2. Focus laser on cantilever tip
    a. Remove scanner head (loosen set screw)
        i. Make sure lens clean
        ii. Put fluid skirt
        iii. Head back on
        iv. Push display for 3 seconds, so it stays on)

    b. Put tip on AFM

    c. Initialize stage

    d. Put fluid bar for fluid holder

    e. Zoom to see reflection of the tip (see laser)
        i. Top adjuster- adjusts laser diode to tip
        ii. Side adjusts- adjust detector (set to zero) {max sum}
        iii. If illumination is off, can adjust on screen or with knob

    f. Bring focus back to real tip (not reflection)

3. Calibration Steps with Mica
    a. Peel of layer of Mica (with tape) (If no mica, glue it to a magnet with superglue)

    b. Check parameters; expanded mode; deflection setpoint to 1V

    c. Keep deflections within 0.15 of 0

    d. If click engage, tip crashes, need to move head up

    e. Ramp- For air calibration, go to expanded mode
        i. Plot unit: volt
        ii. Trigger thresh (3V (~~for soft tips~~); go back to metric
        iii. 1000nm rampsize for calibration
        iv. 5 um/s forward/reverse
        v. Turn Z-closed loop on
        vi. If air doesn't work, withdraw and add fluid
        vii. Get about 175-190 nm/V for 0.3N/m tips

    f. Thermal Tune
        i. Withdraw tip
        ii. Thermal tune (X2);
            1. (do this b/c can't always do in fluid; fluid attenuates (<6kHz)
        iii. Take screen shot; change full capture and save as ds_air (deflection sensitivity) OR create text file with this information.

    g. Add 1xPBS,
        i. Setup + refocus tip

1. Zero deflections
2. Only adjust ←→ knob off tip, then zero deflections

ii. Navigate- click autocompensate for fluid (know distance is 1mm; can't see surface clearly because it is transparent)

iii. Check parameters

iv. make sum zero using top left knob so just on tip, then raise sum; zero horizontal and vertical;

v. Ramp (1um)- update sensitivity (do a few times); keep z-closed loop on (doesn't matter as much for indentation)
   1. **Get about 216 nm/V**
   2. **Deflection sensitivity (ds) fluid < ds air**

vi. Withdraw tip

h. Thermal Tune

i. Thermal tune (repeat twice) (calib | thermal tune)

ii. Simple harmonic oscillator (fluid→changes index of refraction→changes sensitivity)
   1. Range- 1-100kHz
   2. Acquire data, zoom in (control + drag box), select each side, calculate spring constant; → can change spring K by manually enter in box under "thermal tune"

iii. Turn off crash protection transiently- before place specimen because sum will decrease
   1. Alt+ ~ | stage control |crash protect off <<because fluid meniscus breaks>>
   2. Then turn back on (add fluid b/w tip and specimen, then turn crash protect on)

4. Actual stiffness of cantilever is 0.3 N/m; range: 0.1-0.6 N/m
   a. Freq should be ~20kHz (resonance freq); range: 15-30kHz
   b. Deflection sensitivity in fluid should be < air

<u>Other</u>:
3rd plot set as deflection error v. time
Screen shot thermal + sensitivity

Test a specimen

1. Lower tip
2. Navigate
3. Engage
4. With specimen,
    a. Check horiz/vert deflections zeroed, deflection set point → 1V

    b. If adjust ramp size, velocity must be changed back **
        i. Want 80-20% to not be in contact; code needs part of curve to be baseline
        ii. Set to 5um/s
        Note: Forward and reverse velocity related to ramp rate and ramp size

    c. Change both folders to desired paths (_p1 (position 1))

    d. Height sensor = piezo
    For stiff → piezo movement = cantilever
    For soft → all piezo movement by sample deformation

    e. Calculate Sample Deformation

    Piezo movement (height sensor) = sample deformation (indent depth) + cantilever bending (deflection error); we calculate the sample deformation

        i. Want indentation 100nm→1500nm; ideally around 1000nm
            1. Adjust trigger threshold so sample deforms 1000nm
            2. Hesitant to go < 0.5 V
            3. Can adjust X offset for lateral motion of piezo prior to indent if weird curve

        ii. Also plot deflection error v. height in metric, not volts

        iii. If force doubled, depth → 1.5x ($F \sim d^{1.5}$)

$$F = \frac{4}{3} E^* R^{1/2} d^{3/2}$$

5. Each position → 3 pokes; total of 12 positions (10-15 for each region)
6. For next position, select | highlighted 1.003, and enter in 2
    a. Default 2.000

Other Notes:

- *if retracted → tip down
- Extended → tip up

- **may have range in section thickness, be careful**
- **if have weird curves, replace PBS>**

- Sample deformation= piezo (height) – defelction error = 1000nm – 585 nm = ~400nm; want at least 100nm and <1500nm

AFM Data Export Protocol

T:\Protocols\AFM

Ben Freedman (2017-01-19)

Steps

1. Open Nanoscope Analysis
2. Look for browse files tab on RHS and click it

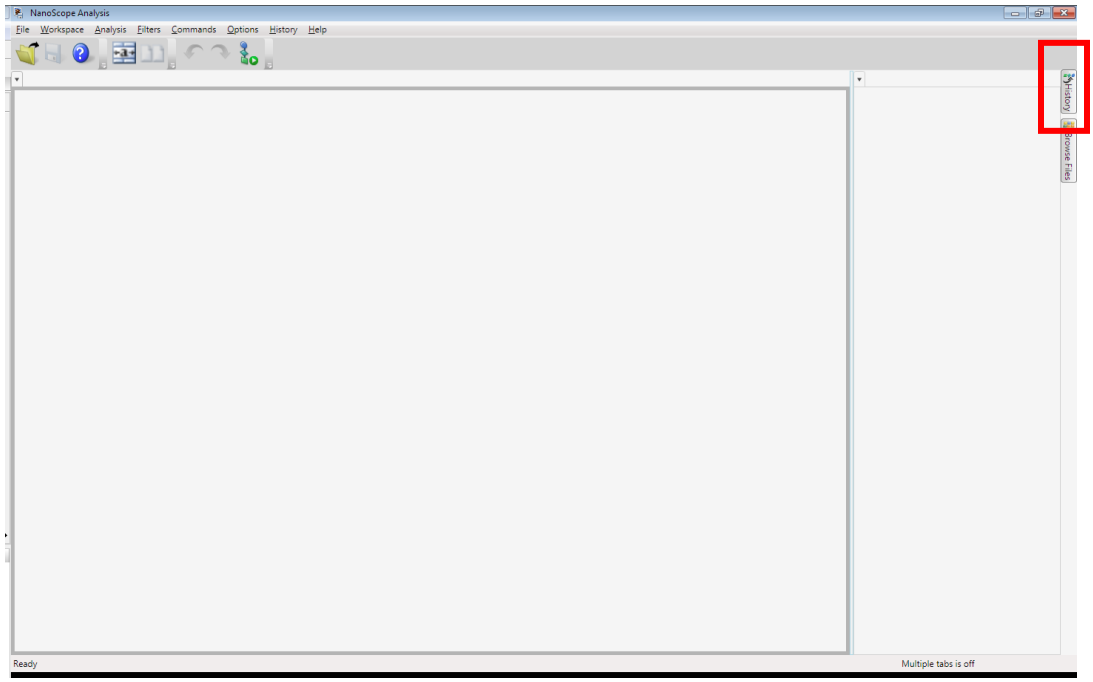

   a. Find the date you want to export and click OK

3. Select all force plots (ctrl+A)

4. Right click, export ASCII
   a. Export channels 1+2
   b. Units- natïve; uncheck display
   c. No header

5. Save As
   a. In each folder, create txt folder

Other random notes from 2/22/16 meeting:

6. Look up poisson ratio
7. If do 5um thick, put 5 instead of zero
8. Assumes indentation depth is <1/10 thickness

AFM Analysis Code

T:\Protocols\AFM

Biao Han; Ben Freedman (Updated: 3/17/2016)

1. The main program is the “ComputeAFMHertzRepulsiveModulusAgg”. In the parameters, first one is path(absolute path). Usually I copy all the codes I need to the same folder as the data so I can leave the path with a blank string: ‘’.
2. Then the filename is the main filename excluding the position and repetition indices. For example if your file names are like sample_p1.000 then the filename input should be ‘sample’.
3. Then the pos_indx is a matrix that contains all position indices. For instance if you did it from p1 to p12 then this can be [1:12], or if you want to exclude position 6 then it could be [1:5,7:12].
4. Then the start_indx and end_indx are the start and end of the repetition. Usually if you did 000 to 002 then start_indx is 0 and end_indx is 2.
5. Then k is the measured spring constant of the probe
6. def_sens is the deflection sensitivity.
7. Tip_shape is 1 for spherical tip or 2 for pyramidal tip.
8. Rt is the radius of the tip.
9. Niu is the Poisson ratio of your sample this you would have to go through literature.
10. Plot_figure is 1 or 0 determining whether it would plot the fittings and let you examine. Usually we put 1 there to examine the fittings.
11. H_c is the thickness of the sample for finite thickness correction (substrate effect). If you don’t want to do this correction just put 0 there.
12. The last one is_raw is whether you want to use golden section method to find the contact point. Keep in mind that if is_raw is 0 then golden section method would be used and vice versa.

Crimp Analysis Protocol

T:\Protocols\CP

Ben Freedman – 2016-09-21

X:\software cooker-freezer\crimpycrimp\beta\v1.2.0- BRF Thesis (X = Maxine)

1. Type in crimpycrimp;

2. Choose image file (from "Align folder")

3. Enter min alignm maps (default 27 for thesis work)

4. Skip 1st image? [No]

5. Was this a fatigue test? [No]

6. Select all maps for processing

7. Input for almap and image number
    a. Almap number corresponds to the alignment map number
    b. Image number corresponds to the number of the image within the particular alignment map (1:30 usually); basically this number is proportional to the angle of the polarizer rotation. If there are 30 images/map over 180 deg, each image increments at about 6º. Usually, the best setting is image number of 21, but this should be checked against all alignment maps

8. Check crimp visibility

9. Before you click "OK"; resize the image for viewability; then adjust image number + almap number. Once satisfied; click "cancel" to exit the while loop.

10. In "Figure 1¨Image" ; in the dropdown menu, select the first image. Note, this is different than the first image that appeared (first image in the first map) as these were specifically indexed from the image num + almap num settings you just selected.

11. Now, position the ROI (which has dimensions: rows:150; col:20) to be the "center" and "lateral" regions. For injured, there may be no crimp visible at the injury site.

12. Click "batch"; save the output fig at the end and save the data to the right place.

13. Repeat for ROI; just click "FFT ROI" and move the ROI then hit "batch"

CP Image Analysis Protocol

T:\Protocols\CP

Updated: 2017-01-23
Author: Ben Freedman BS

Flow Chart of Steps

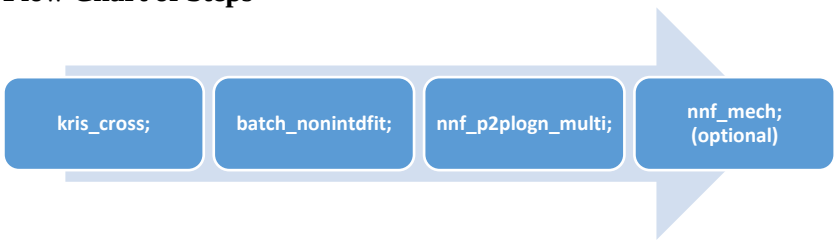

kris_cross; (Output: _intd.txt files—for each alignment map gives bundle intensity v. motor position)

---

a. Set working directory to:
   X:\software cooker-freezer\cross_polar\beta-Ben-v5 (x = max)

b. Type in **"close all; clear all; clc; kris_cross;"**

c. ***Dialogue box:*** Set Bundle width (pixels) as 10 and bundle spacing (pixels as 20. Note: this is the default. This setting was determined based on slight motion artifact of the image during CP rotation.
   i. Click OK

d. ***Dialogue box:*** Choose Sample Image File: Navigate to where your images were saved. Note: if you didn't click "appending motor data" you'll get an error since you have no motor output.txt file.
   i. Click Open for any of the images.

e. ***Dialogue box:*** Enter the minimum number of images/alignment map as 15.
   i. Click OK

f. ***Dialogue box:*** Skip 1st image?
   i. Click NO

g. ***Dialogue box:*** Was this a fatigue test?
   i. Yes/ No/ Cancel ← based on what you tested.

h. A box will appear asking you to choose what alignment map series to analyze.
   i. After the specimen ID, image time stamps for the start and end of each map are listed.
   ii. Navigate to the **excel spread sheet** that has times at which the specimen failed. **Only select images prior to this point** and **do not select duplicates to save processing time**. For example, for some times 2 maps were taken. Just select the first one.
   iii. Once the desired maps are selected, click "OK"

i. Select a **region to crop**. Click OK

i. Move the ROI to contain the tendon and region above it. Note: A smaller ROI is better to reduce computational time, but make sure you consider that the tendon will elongate during the test.
ii. Once the ROI is selected double click on it.
iii. The maps will start analyzing.

j. After the first map was processed, it will ask you for a location to save.
   i. Ben created folders for you to save your data in:
   Josh|Data Analysis | Imaging |10x20 | Testing
   1. Within each genotype/age listed there are folders for specific specimens. Within those folders there is one for tendon and one for the wave plate.
   2. Save the tendon .intd files to tendon and waveplate .intd files to waveplate.
   3. Click "save"

k. kris_cross; will loop through all alignment maps and save them accordingly. Be careful to save all maps to the right folders.

l. Repeat for each specimen/wave plate.

Batch_nonintdfit- (generates _nnf.txt file file- fits $\sin^2$ function to each bundle)

a. Type: "**close all; clear all; clc; batch_nonintdfit;**"
b. navigate to saved locations of .intd files. Click one and they all run.

nnf_p2plogn_multi; - applies threshold to all . nnf files. – generates nnf_sum.txt file.

1. Type: "**close all; clear all; clc; nnf_p2plogn_multi;**"

nnf_mech- current usage for fatigue data at multiple loads.

1. Type: "**close all; clear all; clc; nnf_mech;**"

New: 2016-10-10 – Polymask using same ROI from crimp image.

For thesis-specific analysis of regional variation, three functions were constructed:

- nnf_polymask;
- nnf_crimp_polymask;
- nnf_crimp_polymask2;

Notes to user: All read in an NNF.txt file. The first allows you to manually construct a polymask around the tendon. The latter two read in the f50.txt files from the crimp analysis (which had already been created/processed). The benefit of these is that the ROI was drawn on the original images. Note, to do this, the header information regarding ROI placement was saved and used to position the same ROI on the NNF.txt images. The software will ask you to specify which ROI you want to analyze (left, center, right). Once the mask files are created/saved, you run "nnfmsk_p2plogn_multi" to create the .nnfsum.txt files. You later merge the .nnfsum.txt files with mechanical data to create an nnfmech.txt file, that can then be probed at various time points with nnf_spec_thesis1.m.

<u>Detailed steps:</u>

1. type "**nnf_crimp_polymask2;**"

2. Navigate to the NNF.txt file (i.e. alignment map) you want to process (any is fine as the same ROI will be applied across all NNF files).

3. Navigate to the crimp output file (_f50.txt) for the same specimen;
    a. Note, it will automatically filter the list of specimens for it

4. Select the ROI you want to process

5. Double click on the ROI drawn (note, it should look like it's in the midsubstance for either the left, center, or right sides.

6. Save the mask in the particular CP analysis 10x20 for the specimen of interest

7. Run "**nnfmsk_p2plogn_multi**;" for the ROI and NNF.txt file for the particular specimen for EACH ROI (i.e. process it three times per specimen (left, center, right).

8. Then, run nnf_mech_slrp → pick 1 load, then follow instructions

Additional notes:
-save nnfsum.txt file as "_Center_nnfsum.txt", etc depending on ROI chosen
-use copy_csv.txt files when possible as part of the nnf_mech file saving.

Cryopillar Protocol

T:\Protocols\Cryofilm
Freedman Thesis- Updated 2017-01-06

I. Materials Needed

	1	Sheet of cryofilm (Type 2C(10) 3.5cm used for this protocol)
	1	Scalpel (11 blade)
	1-2	Pairs of fine forceps
	1	Weigh boat
	1	Dissection mat
	1	Roll of scotch tape
	1	Pair scissors
	1	Ruler
	1	Bottle 70% EtOH

II. Protocol

a. Spray and wipe down dissection mat with 70% EtOH.
b. Cut strips of cryofilm along width of sheet at marked intervals with scalpel. Use ruler to ensure a straight cut.

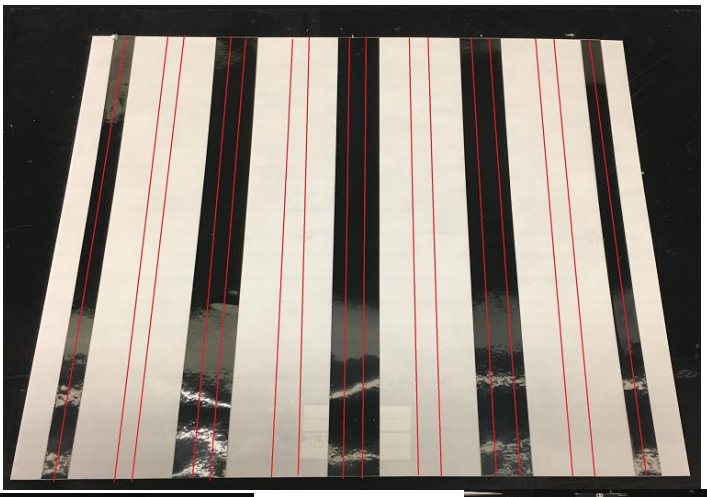

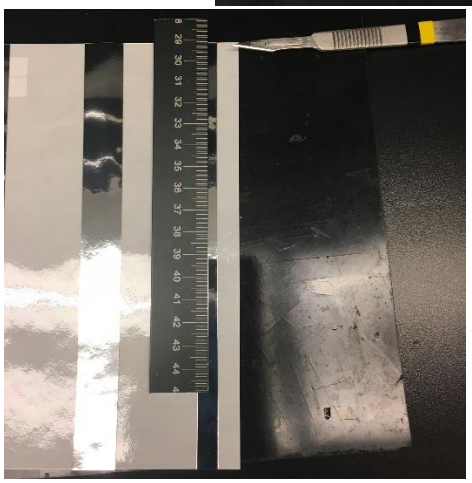

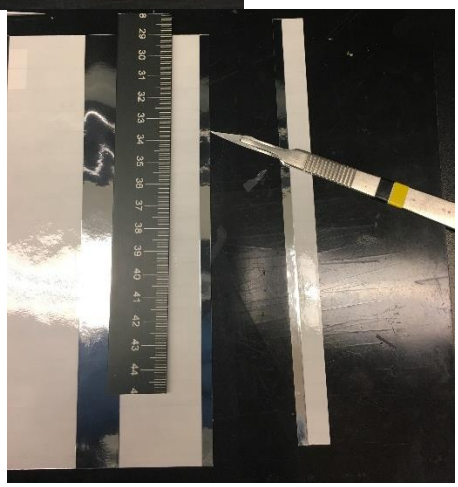

c. When removing excess white film and metal in between strips, save the white strips, and trash metal.
d. Height of strips will vary. These are rough estimates and do not have to be exact.
    1) Metal should be around 5mm.
    2) White film strip should be between 10mm - 15mm.

e. Cut strips with scissors along blue lines.

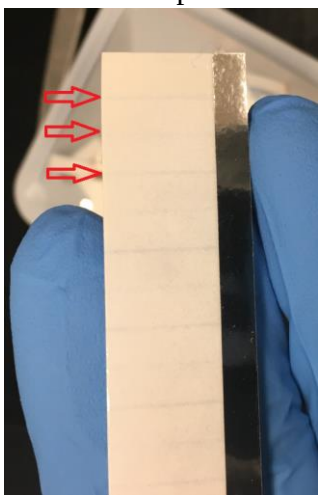

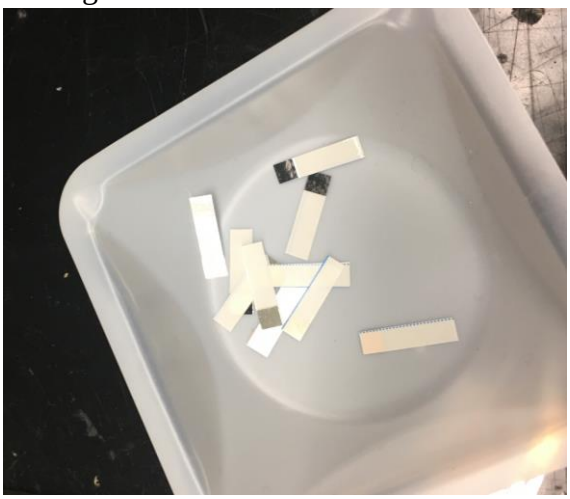

Get roughly 5cm – 6cm of scotch tape and place on mat with sticky side up.

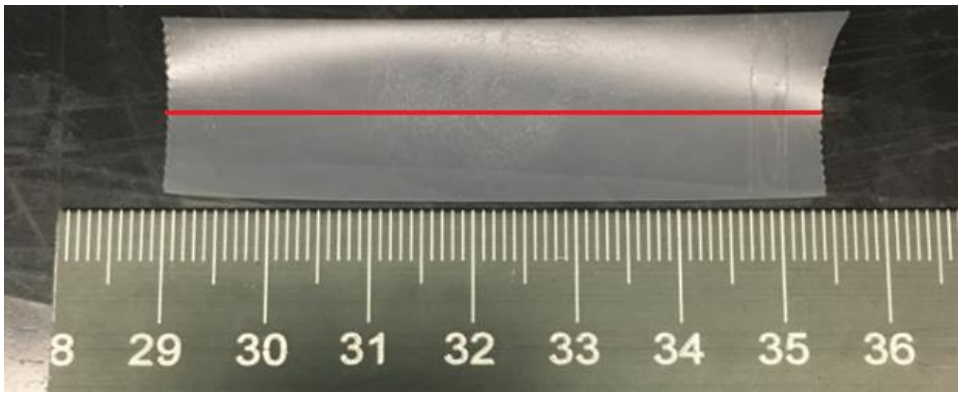

f. Cut tape lengthwise into two strips with scalpel.
g. Pick up cryopillars with fine forceps, and place on tape with laminated side up. Final product should look like:

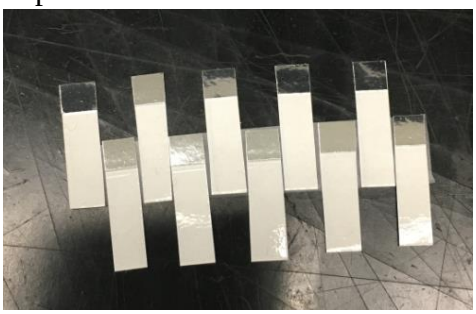

h. Try to minimize the amount of exposed tape, this will prevent cryopillars from sticking to each other while they're in storage.
i. Store cryopillars in box or weighboat. If done correctly, they should stack without issue.

Section Fixing Protocol

T:\Protocols\Cryofilm
Freedman Thesis – Updated 2017-01-19

---

*Video saved on Maxine.

I. Supplies Needed

a. Sectioned samples
b. Chitosan
c. 10 mL - 4% PFA
d. 20uL Pipette
e. Fine forceps
f. Kim wipes
g. Ice
h. Large dissection scissors
i. Fume hood
j. DI H_2O

k. Weigh boats (labelled – DI H_2O and 4% PFA)
l. Timer
m. 70% ethanol

II. Procedure

a. Fume hood setup
    i. Take frozen, pre-allocated 4% PFA out of freezer and allow ~10-15min to thaw in a small weigh boat on ice
        1. PFA should be in a closed container unless under the hood.
        2. Leave 4% PFA on ice
    ii. Fill weigh boats with ~10 mL DI H_2O
b. Set pipette to 17uL
c. Section Fixing
    i. Fetch sample from the freezer
    ii. Use fine forceps to peel off cryofilm sections from the glass slide and place in the 4% PFA with the silver tape of the cryofilm facing up
    iii. Set the timer to 3 min for the film to "fix" in the PFA
    iv. While film is fixing in PFA, clean off the glass slide of any excess OCT with the 70% ethanol and Kimwipes
    v. Once slide is clean, use pipette to place 3-4 equally spaced dots (depending on how many cryofilm sections per sample) of chitosan on the slide (~6ul chitosan/dot)
    vi. After 3min in the PFA, use fine forceps to transport the cryofilm sections from the PFA to the DI H_2O
    vii. Use fine forceps to carefully grab the section out of DI H_2O and orient the sample so that the gold part of the tape is facing up. Cut around the tendon sample being careful not to cut the sample
    viii. Place the cryofilm section (face up) on the chitosan droplets. Try to keep the chitosan thin and equally distributed under the sample so that the film is fully placed and fixed onto the slide. Angle the slide to allow excess chitosan to run off (can wipe with kimwipe)
    ix. Once all sections for that sample have been fixed to the slide, place slide in black slide holder box, angled. Let dry for 24h in cold room with box cracked open slightly
    x. Repeat for all slides.
d. For AFM, DO NOT fix; follow steps vii- x and let dry at room temp for 1.5 hr, but keep hydrated with small droplet of PBS on sample.
    i.

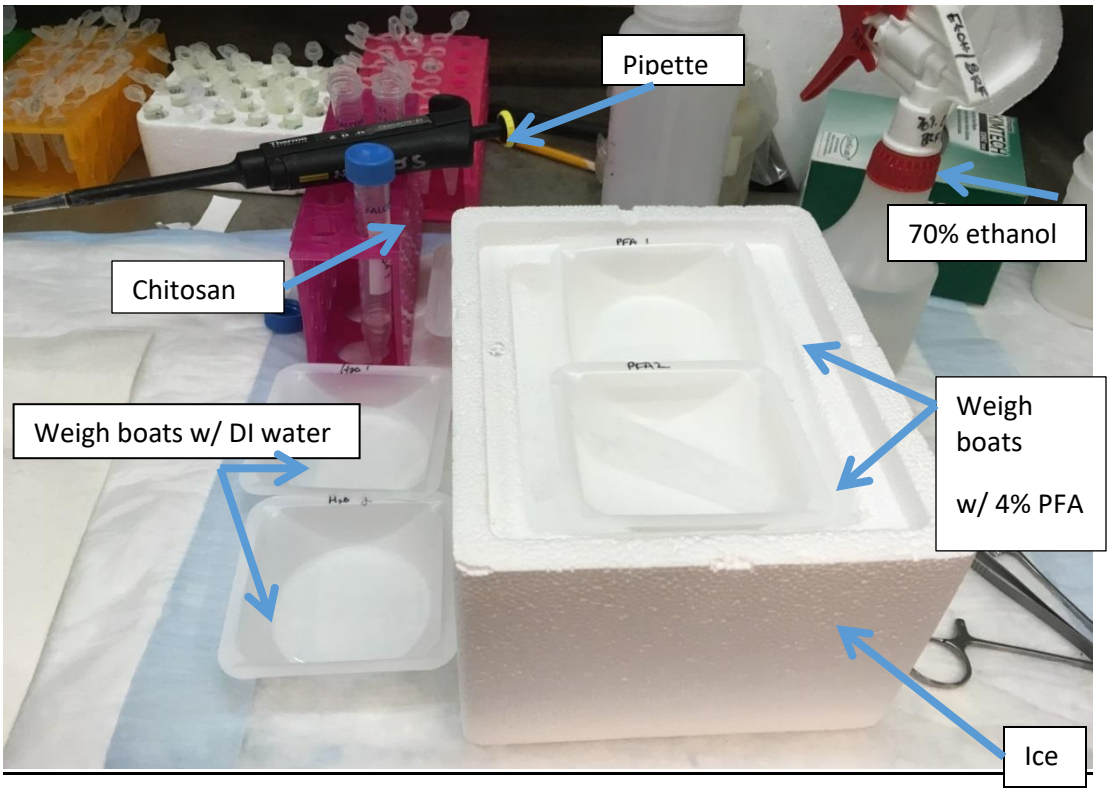
Pipette
70% ethanol
Chitosan
Weigh boats w/ DI water
Weigh boats
w/ 4% PFA
Ice

Cell Profiler Protocol

T:\Protocols\Image Analysis

Ben Freedman (Edited: 2017-01-16)

I. Download Cell Profiler

a. http://cellprofiler.org/
b. On the Website, there are many tutorials, forums, blog, support, and a full online manual
c. Full online manual: http://d1zymp9ayga15t.cloudfront.net/content/Documentation/cp2.1.0_manual_0c7fb94.pdf

II. Operation of Cell Profiler Overview

a. Double click on **Cell Profiler** icon

b. First, **open** the project
   i. This contains the settings for analysis. Note, if you are starting from scratch you can build/optimize this analysis procedure.

c. Add images (either drag in to copy of double click to add)
   i. Note, to remove, you just right click the images and select "remove"

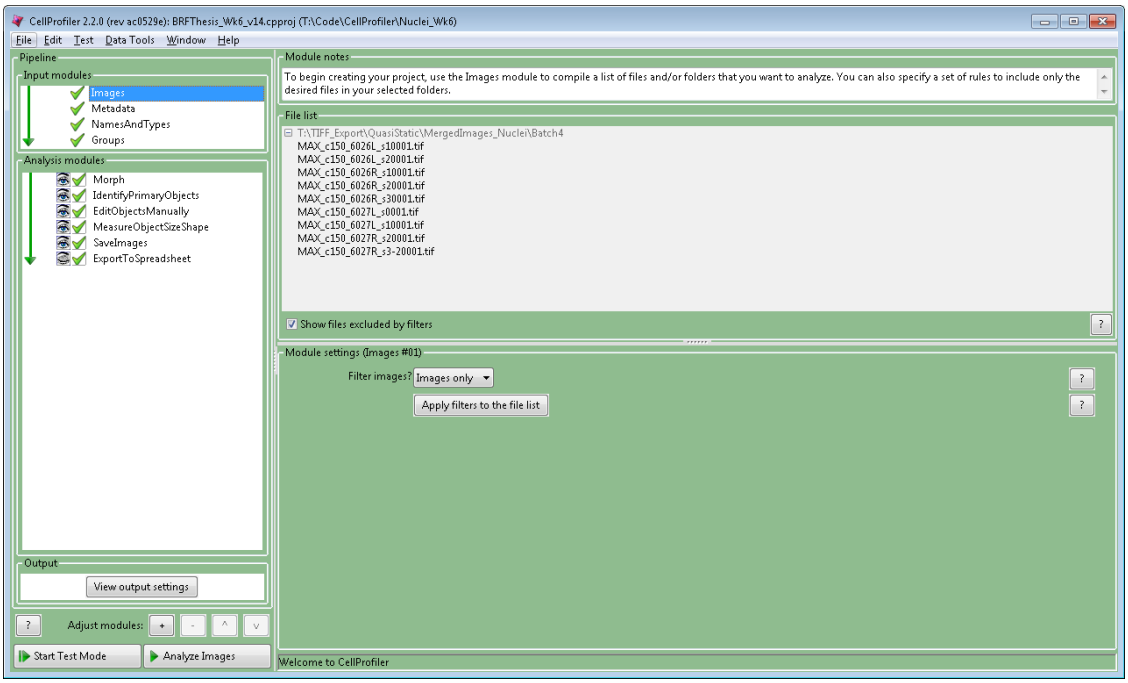

d. Set the output folder location by clicking "**View output settings**"

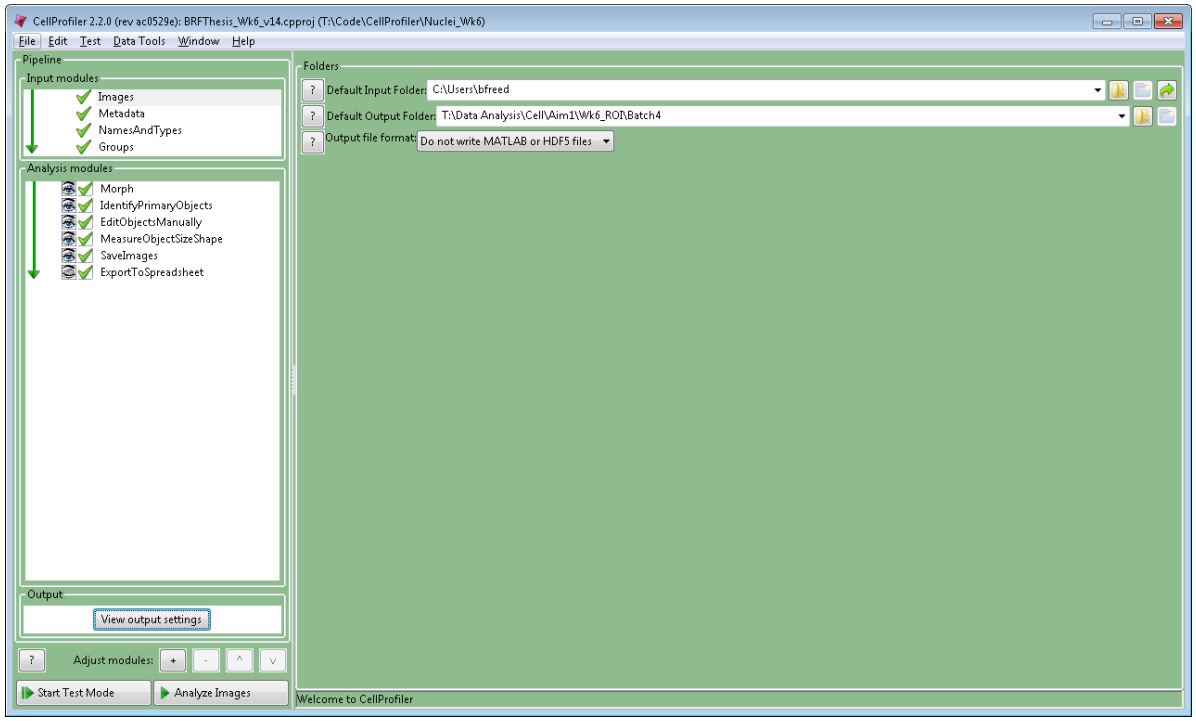

e. Click "**Analyze Images**"

i. After each image is enhanced and a first-round of object approx. is completed, the user will edit the objects manually. Once completed, click 'Done' and another image will be processed.

ii. There are **SEVERAL** key hot keys to make ROI adjustment faster.

1. **C**: Join all selected objects into one that forms a convex hull around them all. The convex hull is the smallest shape that has no indentations and encloses all of the objects. You can use this to combine several pieces into one round object.
2. **D**: Delete the control point nearest to the cursor.
3. **F**: Freehand draw. Press down on the left mouse button to draw a new object outline, then release to complete the outline and return to normal editing.
4. **J**: Join all the selected objects into one object.
5. **M**: Display the context menu to select a command.
6. **N**: Create a new object under the cursor. A new set of control points is produced which you can then start manipulating with the mouse.
7. **T**: Toggle between fill and outline mode for objects.

8. **X**: Delete mode. Press down on the left mouse button to start defining the delete region. Drag to define a rectangle. All control points within the rectangle (shown as white circles) will be deleted when you release the left mouse button. Press the escape key to cancel.

iii. **Editing the objects**

1. Using the mouse
    a. (**R**) Click – Allows editing of a single object
    b. (**L**) Click – Toggles an object depending on overall toggle mode (outlines or fill) set by hitting "**T**". Note, if an object is being edited, you cannot toggle.

2. Using the keyboard
    a. See above commands.

3. Return to original view, pan, and zoom. <u>If any one of these is clicked, you cannot edit objects on the image.</u>

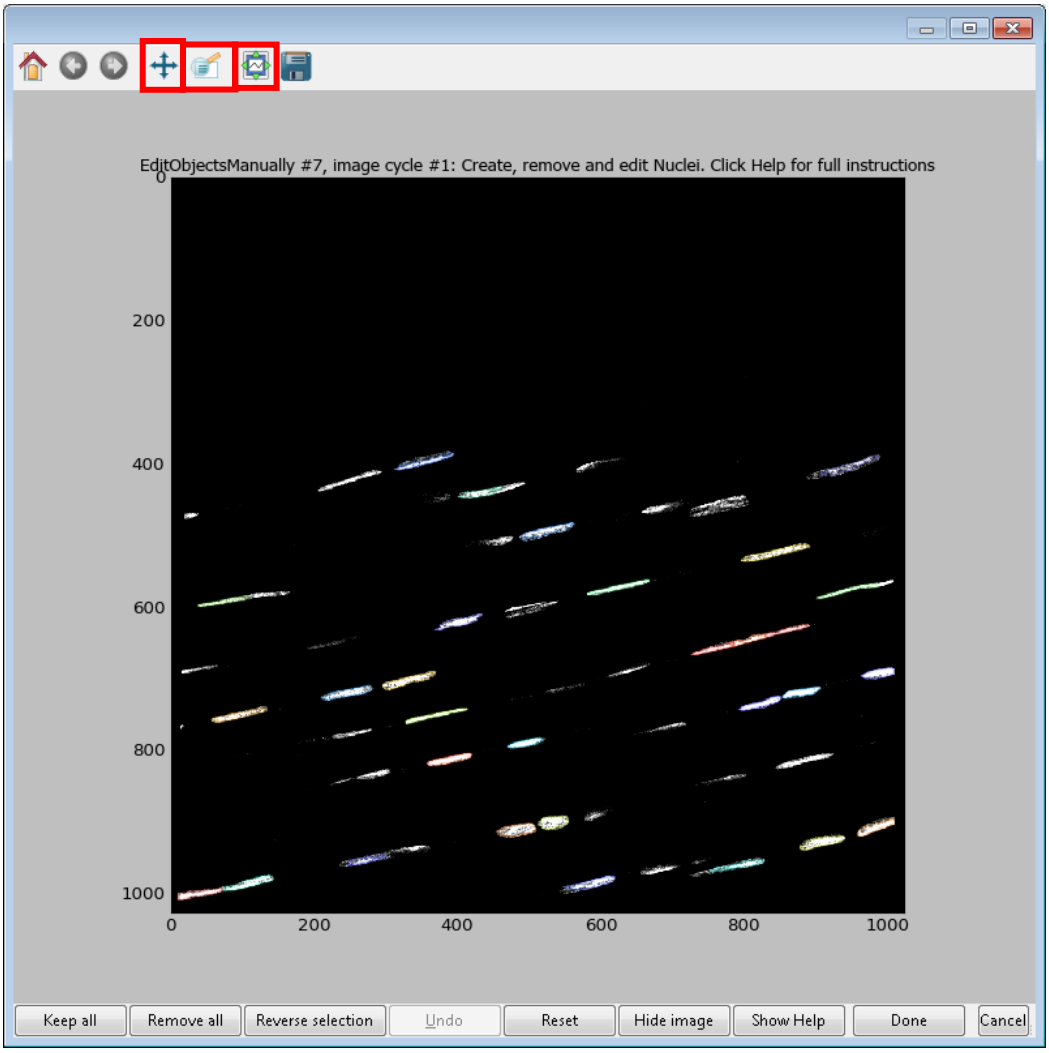

****You may need to click "undo" at times. After you click "undo' you must draw an ROI for other settings to work again. Type "F" to freedraw.**

III. Example for editing objects.

a. Here is an example of control tendon. Note how spindle-like the nuclei are.

   i. Zoom in on the point you want to edit.

   ii. Toggle between outline and fill mode by hitting "T"

      1. Note, if you have zoom or pan selected you cannot toggle or edit.

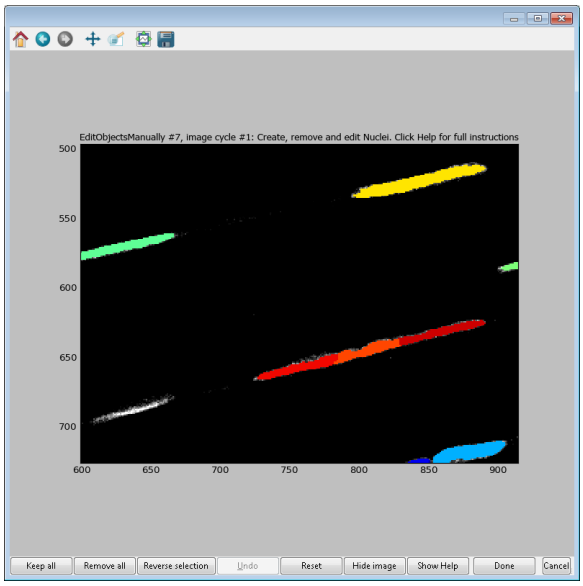

b. To selected a ROI, **(R) CLICK;** you will notice dots appear around the perimeter.

c. To delete a dots, type "**X**", then draw the box over the dots you want to delete. For each deletion, you must type "**X**". (Before: left; After: right)

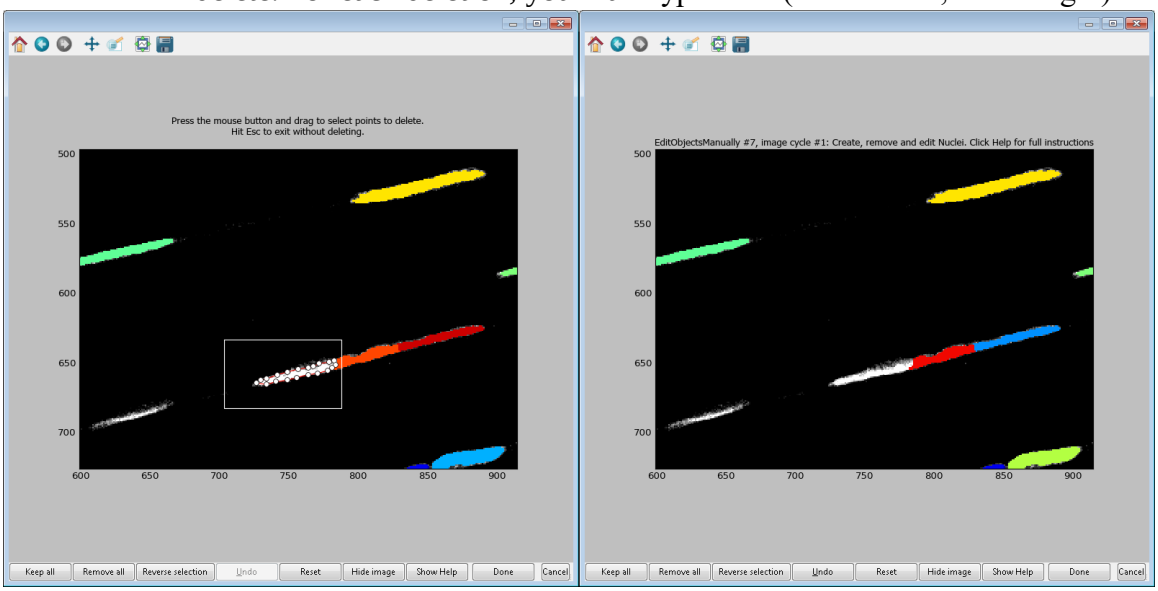

d. To draw a new ROI, type 'F", then left click to draw at the cursor around the nucleus. Once completed, you will see the area you drew outlined in dots. Again, these can be edited by moving them individually or deleting (X).

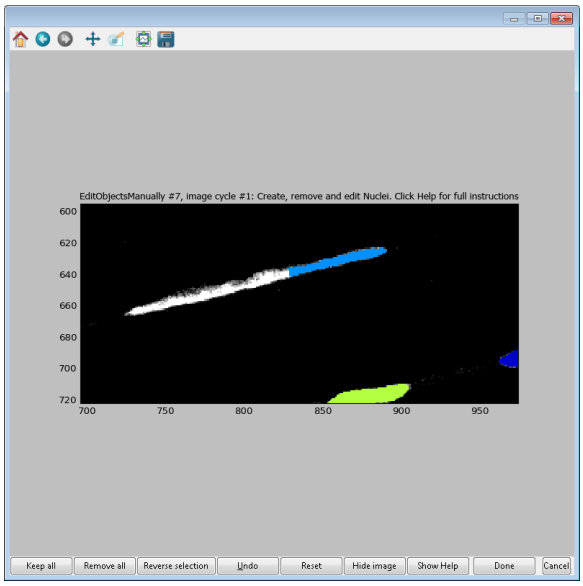

e. In addition, to moving the dots or deleting (X), you can type "C" which forms a convex hull around the dots drawn. This makes them appear more organized (Right image)

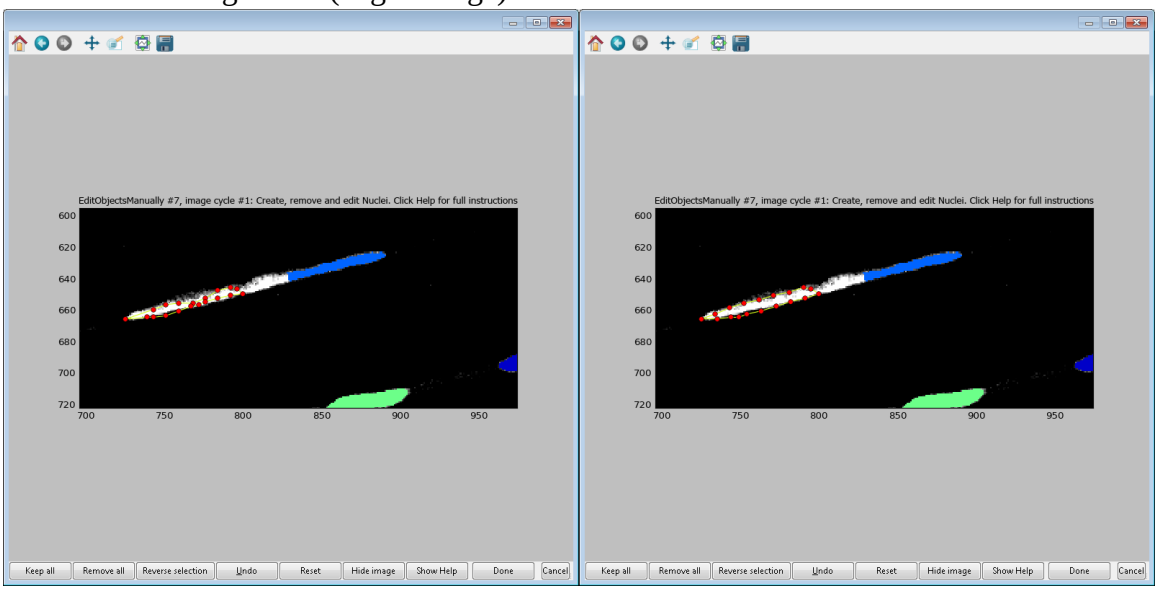

f. Suppose you have two ROIs that really should be joined,
   i. Select each by **(R) clicking** on the individual ROIs and then press "**J**" (for join)
   ii. This merges the nearest ROIs.
      1. You can also type "C" if you wanted a convex hull around them, but that can change the overall geometry.

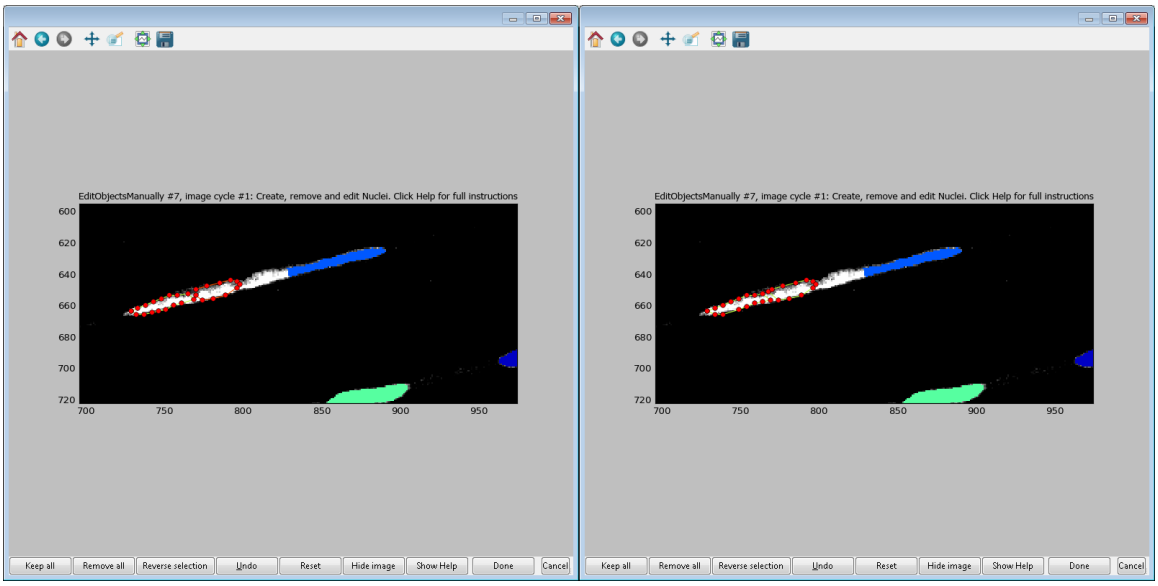

g. Once you are set, deselect the ROI by **R CLICK**ing on it (dots go away). You will see the object shaded in. Note, this can be toggled to outline view by hitting "**T**" as long as zoom or pan are not selected.

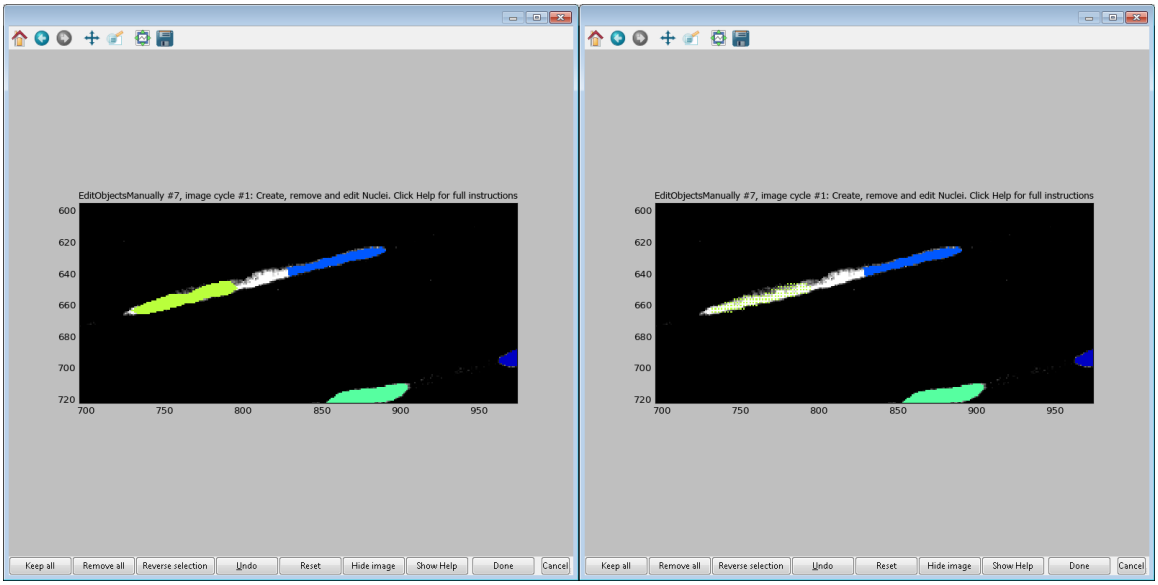

h. Another example of toggle mode fill v. outline. Note the nuclei without outlines/fill that were not detected.

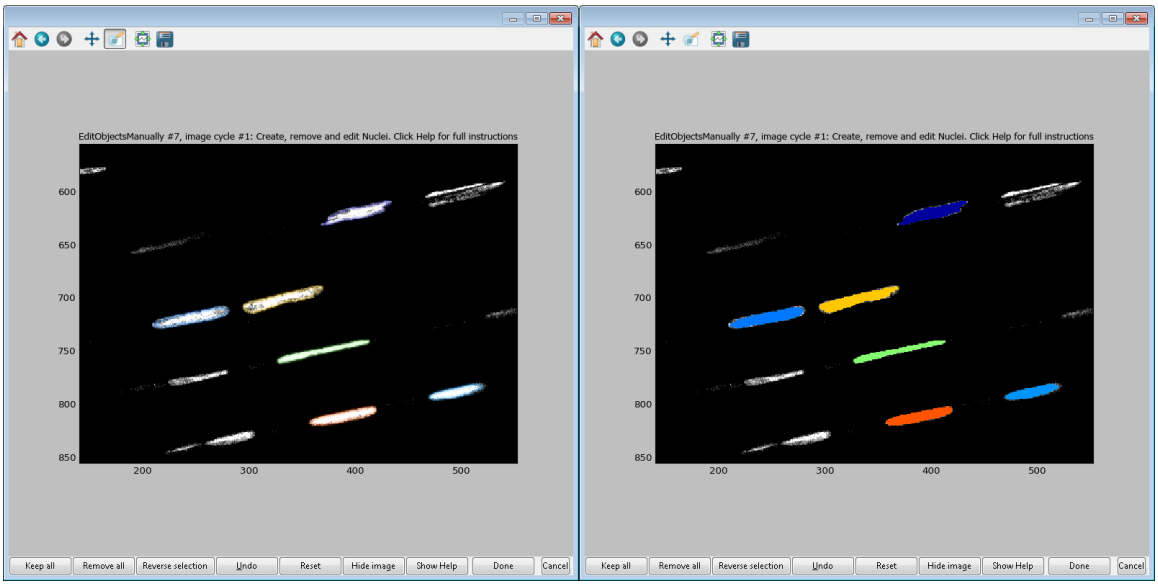

i. Once an object (i.e., nucleus) is set, move onto the next on until all are complete. Please be thorough and toggle to confirm ROI accuracy.

j. Once completed click **'Done'** and another image will load.

FIJI Analysis Program (MACRO)

T:\Protocols\Image Analysis

Ben Freedman; 2017-01-09

Programs needed to be installed:

1. FIJI-
2. Place the following macros within the plugins folder in FIJIapp
    a. analyzeNuclei.ijm
    b. batch_lif2tif.ijm
    c. batch_zPro.ijm
    d. batch_zPro2.ijm
    e. editSaveTif.ijm
    f. readSaveTif.ijm
    g. wait_for_user.java

Steps

1. Open FIJI

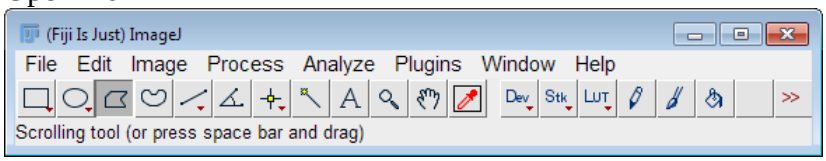

2. Go to Plugins | Macros | Run (or edit)

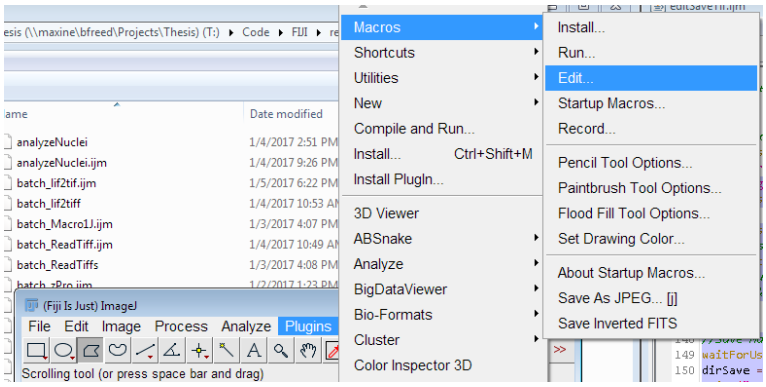

    a. **Open <u>editSaveTif.ijm</u>** <<Note, this is within the plugins folder in FIJIapp. The FIJIapp folder is located wherever you saved FIJI to on your computer.

3. Click "**Run**" ; do not edit any of the code.

4. Find the folder of interest that contains images. You only need to click the folder (ie don't need to enter the folder). After you click OK, this will happen. Note the following:

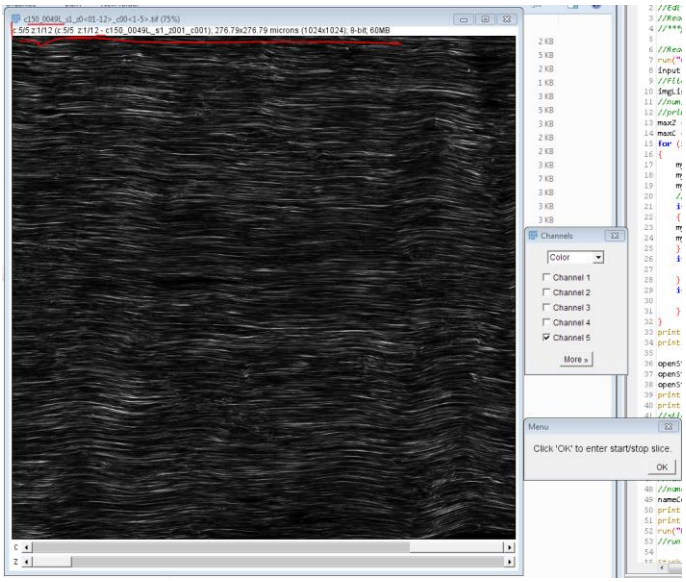

a. This image has **two scroll bars**
   i. C: Channels (1-5)

   ii. Z: Number of Z-stacks, which will vary per specimen. Note, in the top left corner of the image (highlighted in red), it says how many of each there are.

b. The Menu bar indicates: “click OK to enter start/stop slice” . Only click OK when you know what the start/stop is. This means you need to scroll through the Z-stacks to determine.

c. Channels Tool: Allows you to click what you want displayed. If you want a composite image, under the dropdown menu, click “composite”.

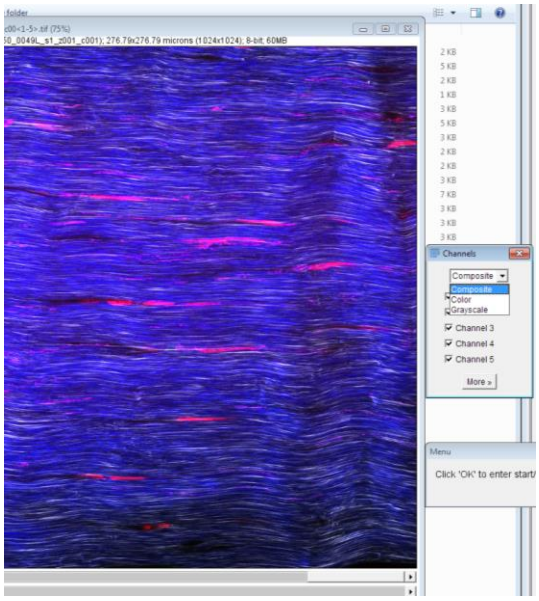

5. MENU: “ Click “**OK**” to enter **start/stop** slice.

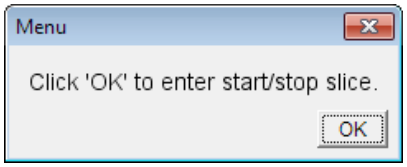

a. Scroll through Z-stacks to determine.
   i. For example,

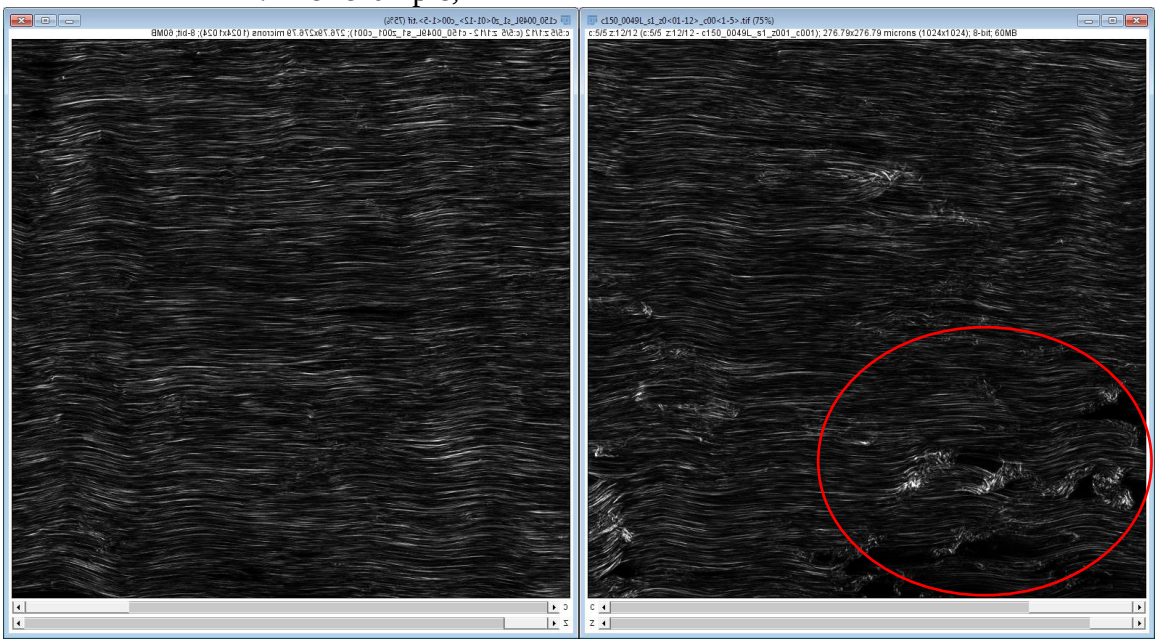

Image 1 **Image 12**

ii. Note, in image 12 the scredding of the section. AVOID this. Thus, pick something more like image 1→8 or 1→5

b. Once determined, click OK, this screen will pop up. Under slices, enter in the range.

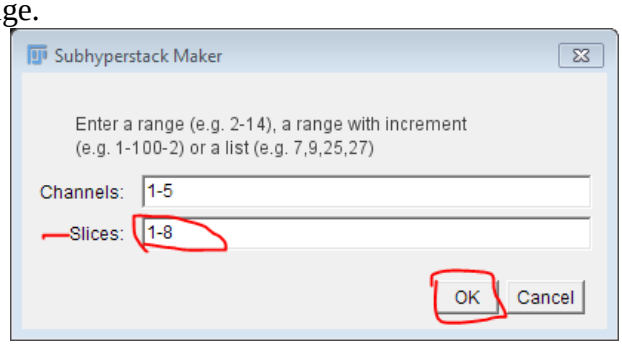

6. Crop ROI using Polygon (pop up)

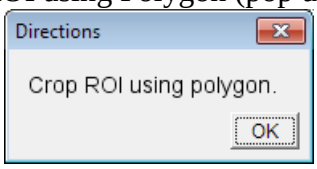

a. Click "OK"

i. The polygon tool will default, draw a ROI, then click "OK"

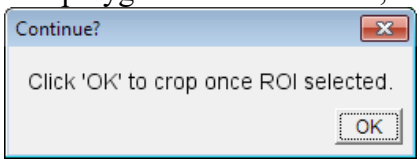

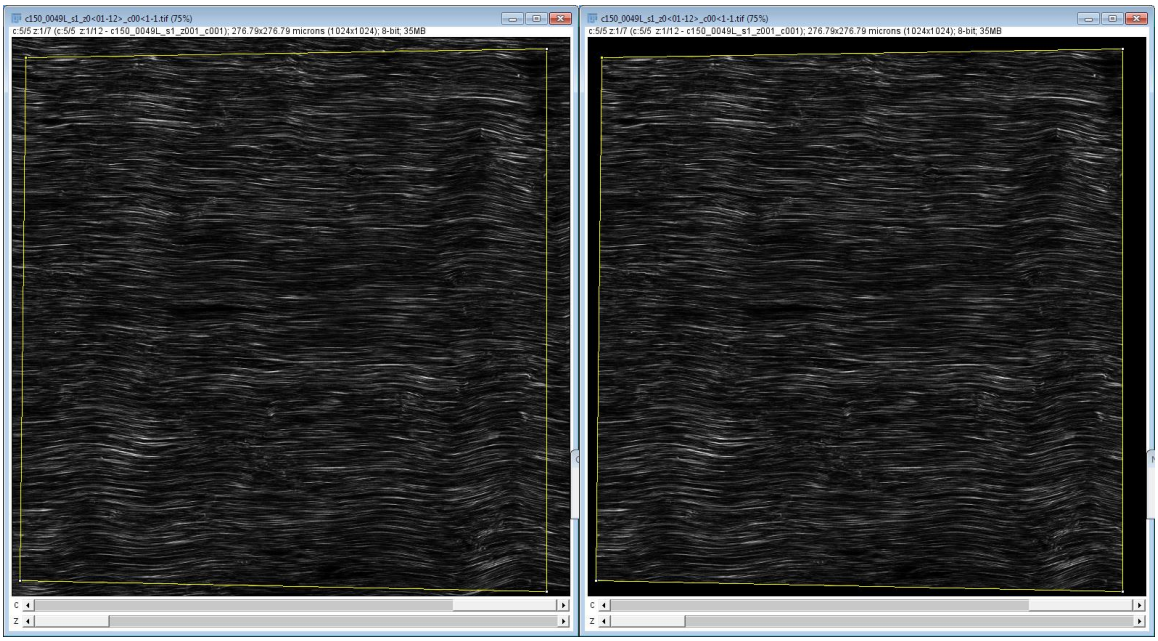

Pre-crop **Cropped**

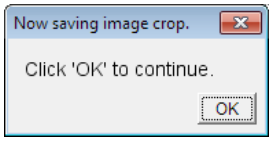

7. Select Output director → Just hit enter unless you want it elsewhere

    a. Folder Name: Cropped1 (Hit ENTER again). If you wanted multiple different crops, you could use the dropdown to select Cropped2, etc.

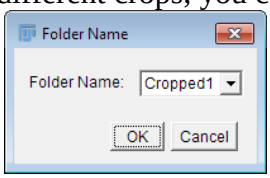

The cropped images will save. Then it will let you know it will run a Z-projection.

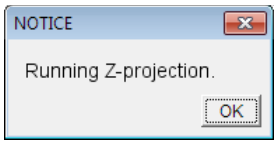

8. Adjust colors: DO NOT CLICK OK UNTIL YOU ARE SET. IT IS ESSENTIAL THAT YOU CLICK "APPLY" AFTER EACH COLOR IS SET

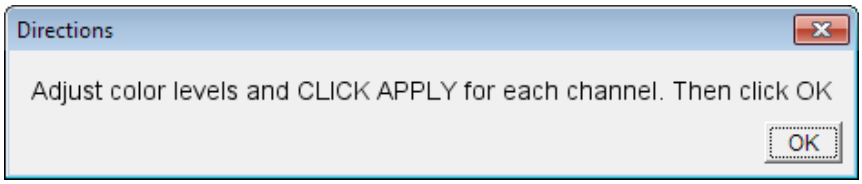

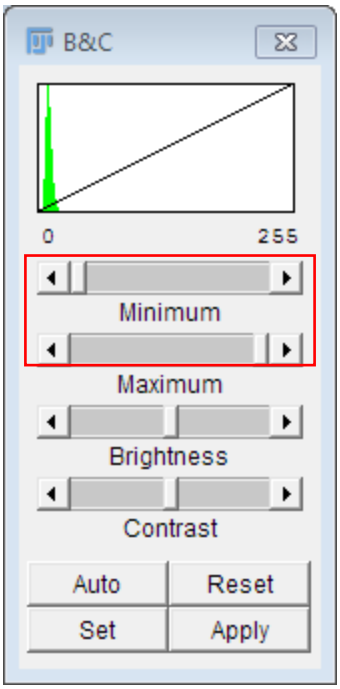

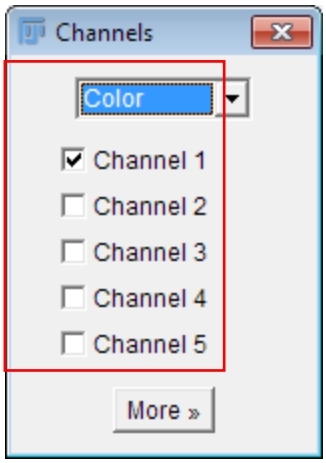

9. Step through each channel, and adjust min/max accordingly. For all, except channel 1, best to start w/ Auto before fine tuning min/max. THEN YOU MUST CLICK APPLY FOR IT TO KEEP THE SETTING.
    a. ONCE THIS IS DONE, CLICK "OK" IN THE DIRECTIONS BOX

    b. For example, for CHP (Ch1)

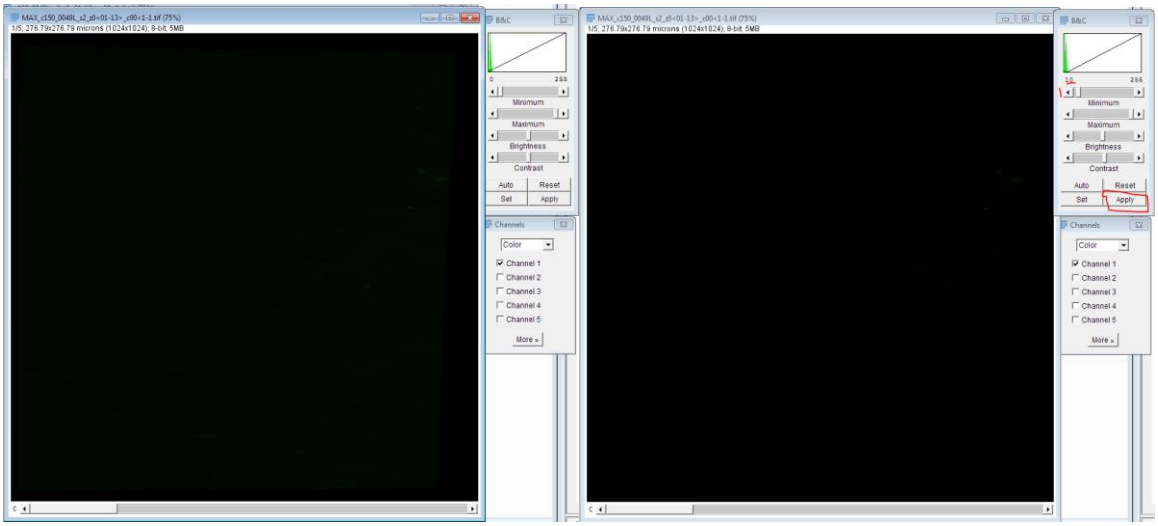

Before After

<Note, adjusted min from 0→10, then click Apply> Very little CHP signal, just removed background. **<u>. Click apply</u>**

    c. For example, for nuclei (Ch2)

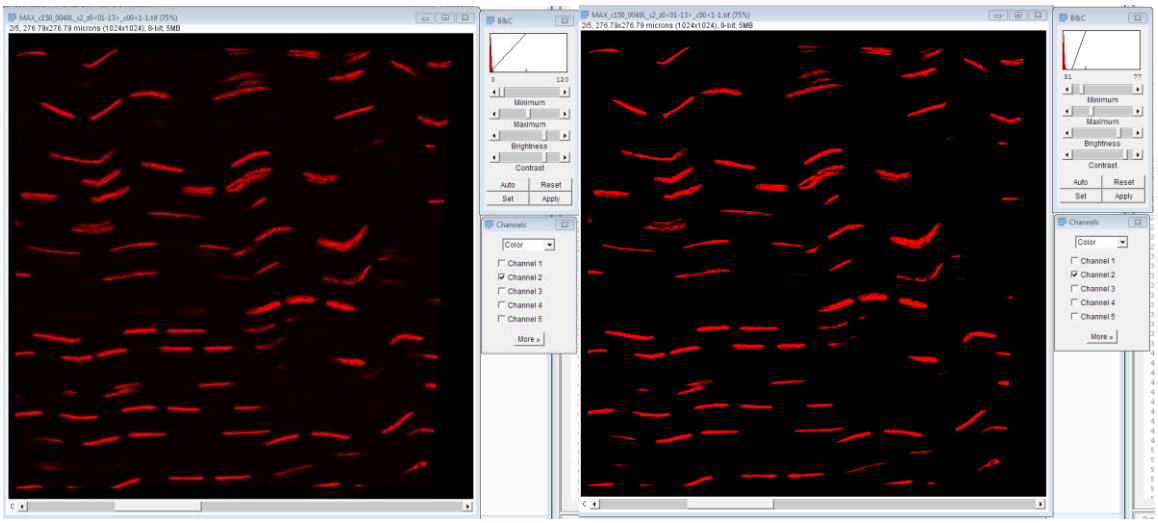

Before **After**

<<Hit auto, then adjusted min/max. Once you click "apply", min/max will go to extremes.>> . **Click apply**

d. For example, for actin (Ch3)

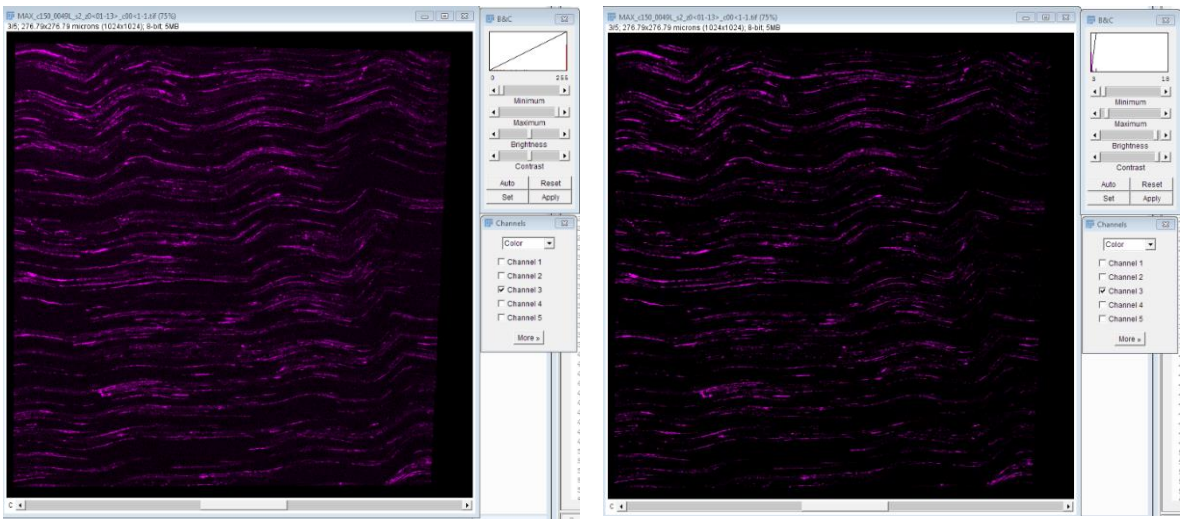

Before **After**

<<Clicked auto, then again, adjusted min/max to remove background. **Click apply**

e. For example, for backward scatter collagen (Ch4)

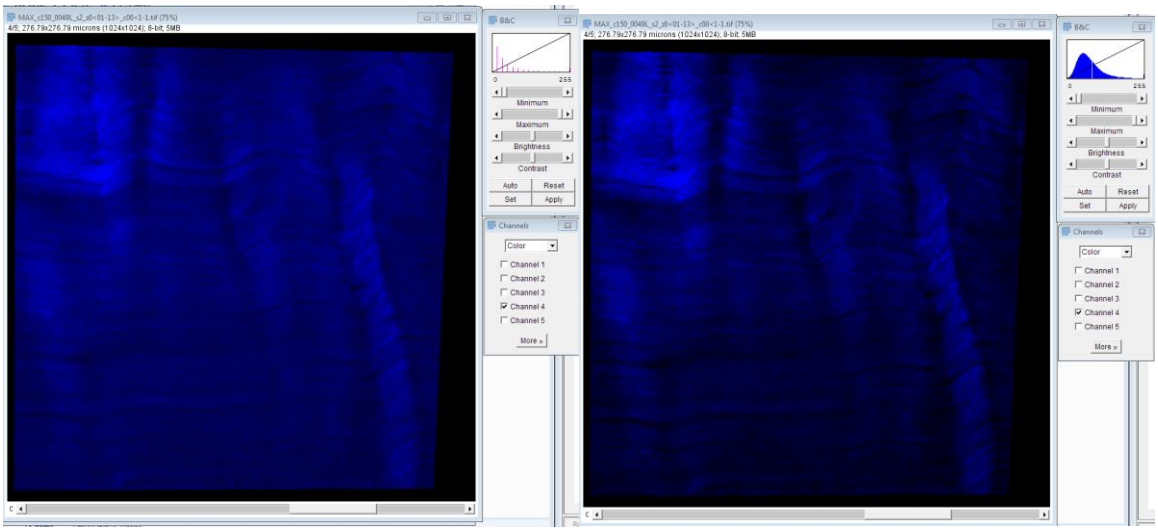

Before **After**

<just click auto> . **<u>Click apply</u>**

f. For example, for forward scatter collagen (Ch5)

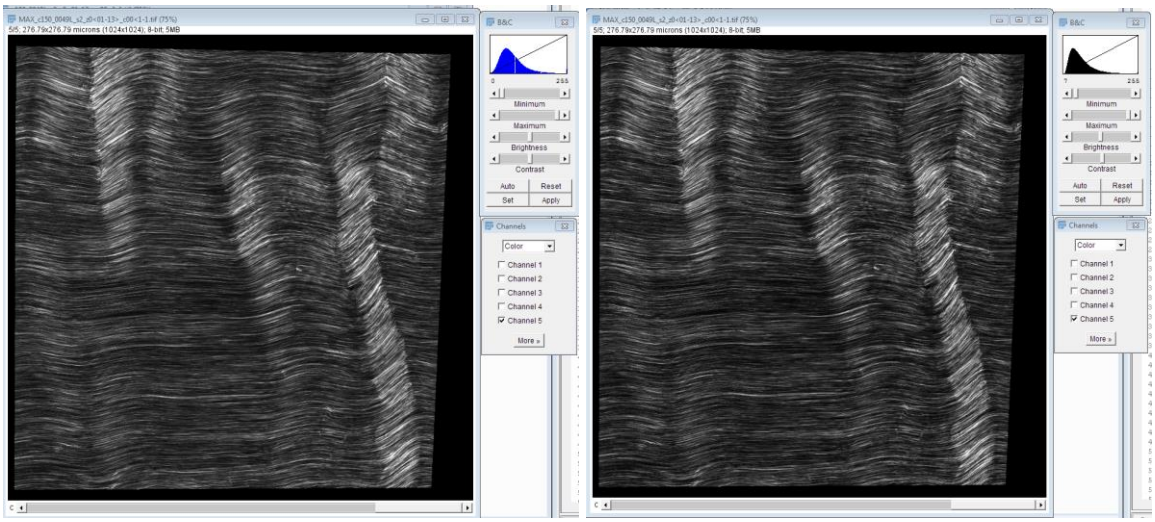

Before **After**

<just click auto> **<u>. Click apply</u>**

10. Apply subtract background.

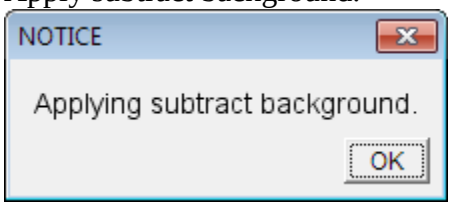

11. Hit enter as Save; Save as Max1 unless you run this more than once. (puts in Max1 folder)\

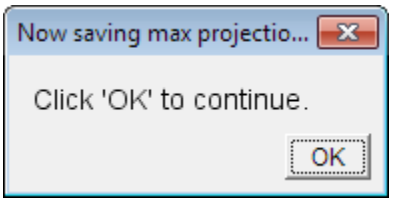

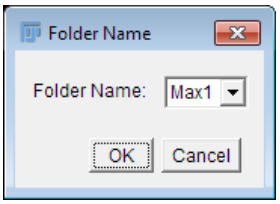

12. Click "**OK**" to **close** images

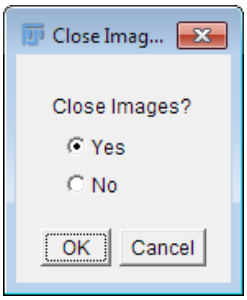

13. Click "**run**" to **repeat** above steps for next specimen.

ImageJ IHC Batch Process ROI Protocol

T:\Protocols\Image Analysis
Freedman Thesis

---

1. Download the plugin to set ROIs all the same size-- http://rsb.info.nih.gov/ij/plugins/roi.html
2. Loaded into imageJ using Plugins | instal…
3. Then it appears in the plugins menu
4. We opened up 4x IHC images as an image seq and had the 4x or 2x H&E next to it to easily see the scar- verify this is correct/ROi is in the midsub
5. Then you can add a rect ROI and use Specify ROI
6. Dimensions are TBD based on image res. Note, you must determine this from the pix: mm conversion
7. Note, that the ROI will propagage through all images
8. Move the ROI to the right spot; then click Edit | clear outside; note: DO Not apply to all images (answer no to dialogue box that pops up)
9. Once repeat for all images
10. Then change to 8-bit image (image/adjust). Enhance contrast, normalize, 0.5% saturated.
11. Then save reduced images as image seq. (so you can adjust/try diff thresholds)
12. Then set thresholds
13. Particle analysis
14. Note that we are interested in the ratio between area thresholded (#pix) div by the size of the ROI (xx by xx pixels). This requires a small additional calculation. eThe software %area in output window is the thresholded region divded by the entire window of the full image.

Protocol: How to save images on the Eclipse: The Right Way

T:\Protocols\Image Analysis

Last Edited by: Ben Freedman (2015-03-02); Contact: freedman.br@gmail.com; 413-537-3369

Forward

- We hold these truths to be self-evident, that all images are created equal, that they are endowed by their Creator with certain unalienable Rights, that among these are exposure time, LUTs, and the pursuit of auto-white balance.

Translation:

- It is very important that identical image settings are applied when saving images.
- Changing exposure, gain, voltage, AE compensation, filters, zoom, magnification, auto white balance (AWB), and the look up tables (LUTs) will change the way the image appears on the screen.
- When saving images, you MUST click the "Apply LUTs" button and then save the image. Simply clicking the camera does not apply the AWB or LUT settings.
- The software that you open the images (e.g., Windows Image Viewer or Image J) will affect image appearance.
- Different monitor settings on computers will also influence image appearance.

Protocol

Summary:

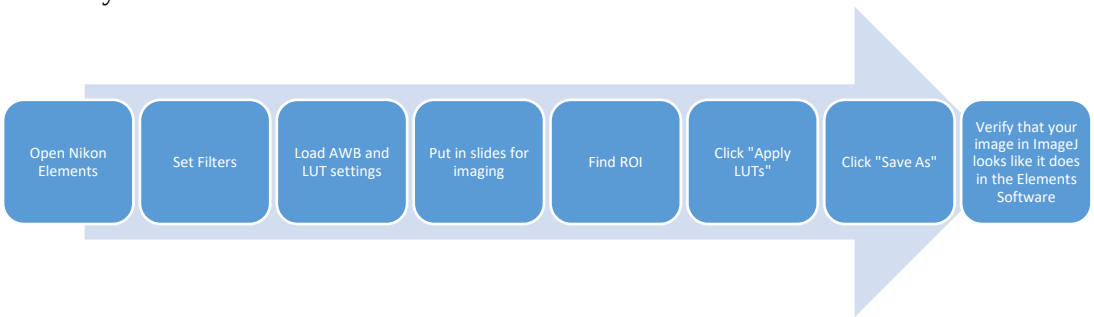

Detailed Steps (with pictures ☺):

1. Open NIS Elements

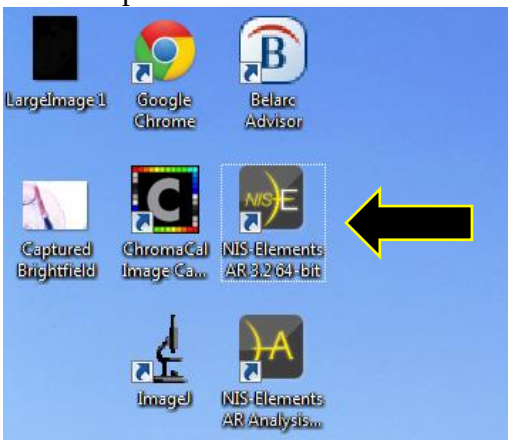

2. Select **Nikon Camera**
3. Press “Escape” on the left side of the Eclipse, place slide on stage, hit “Escape” again.
4. Click “**brightfield**” in the top toolbar. Click “**Play**” button to visualize image, go to ROI (may need to zoom), then continue on with the protocol.
5. Set filters (Manual). These are on the side of the Eclipse.
    a. ND8: Out
    b. ND32: In
    c. NCB11: Out

6. Under **DS-Fi1 Settings**, set the AWB settings. Click Command, Load Setting, e.g., LJC_10x, etc.
   ***Note:** The settings will depend on magnification. Settings for 4x and 10x have been created. (i.e., AWB_LJS_10x , or AWB_LJS_4x)
    a. For example, for LJS_10x, the following settings will load from top to bottom:
        i. Mode: Normal
        ii. Resolution
            1. Fast: 1280x960
            2. Quality (Capture): 2560x1920
        iii. Exposure
            1. Mode: Manual Exposure
            2. AE Comp: 0.0 EV
            3. Exposure: 25ms
            4. Gain: 1.00x
        iv. Color
            1. Contrast: Enhanced
            2. AWB:
                a. R: 1.25, G:1, B: 2.37 <<note, these will vary based on setting for magnification chosen above>> You can find these settings by going to camera options.
    b. Enter these settings manually:
        i. Voltage: 8
        ii. Zoom: 1x
        iii. Condenser: BF
    c. These are dependent on the objective; you can leave them alone. E.g.,
        i. Field Stop: 30.6 mm
        ii. EpiField Stop: 8.9 mm
        iii. Aperature Stop: 30.5mm
        iv. Filter Block Changer: DIA

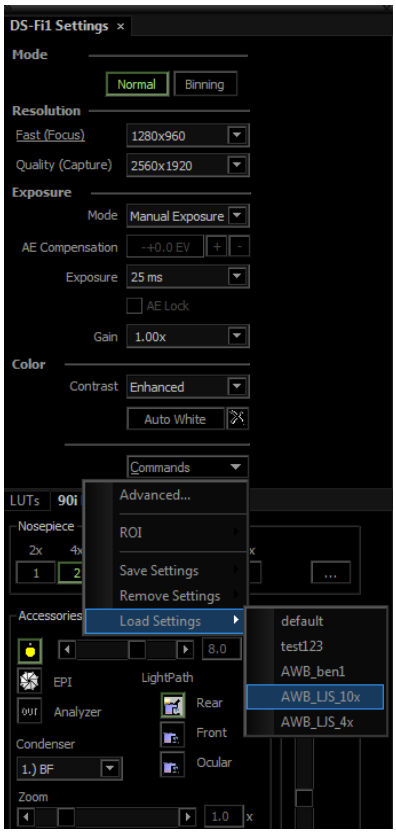

7. Set the LUTs: (Next to 90i Pad, you will see LUTs)
    a. Click LUTs
    b. Click the Disk "Save/Load LUTs"

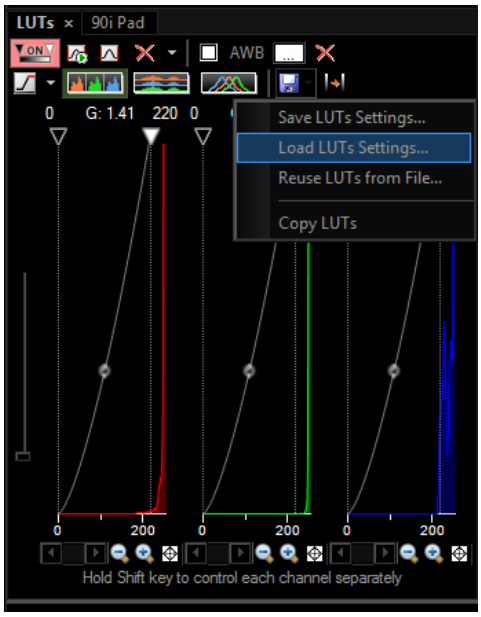

    c. Click "Load LUTs"

i. Navigate to MAX: \\max\soslowskylab\Protocols\Eclipse\LUT Settings

d. Again, depending on what you are imaging & magnification, these will vary. The options that have been created are:

i. IHC 4x, 10x
ii. H&E 4x, 10x

e. Click the setting you want

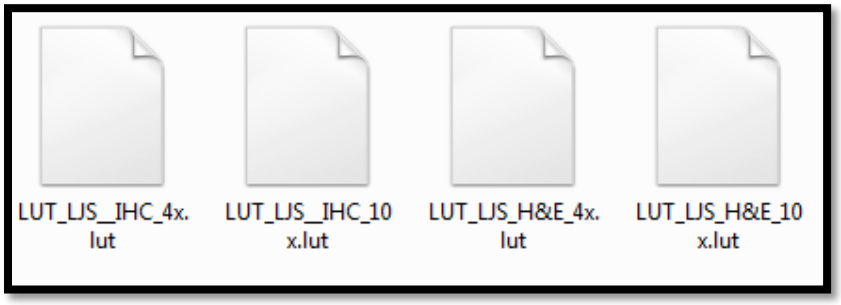

8. Confirm that the ROI on the screen is in focus and that you are interested in imaging it.

9. To take an image
   a. Go back to the LUTs tab
   b. Click the "Modify Image through LUTs" button

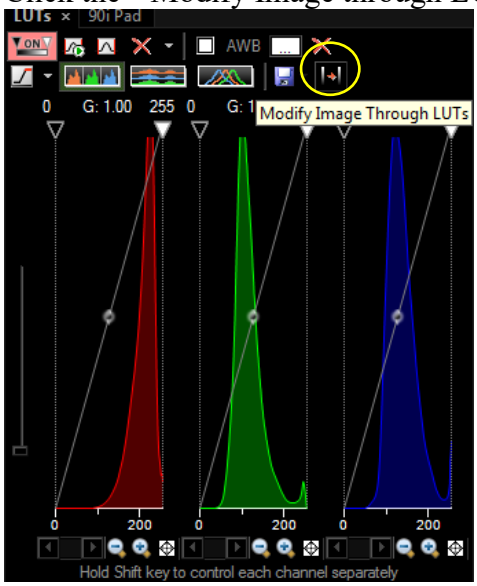

c. This dialogue box will appear. Click "OK"


Process LUTs
Image data will be modified and lose the quantitative information.
Do not ask again in this session (Always apply).
OK
Cancel

d. Note, image header says “Frozen” ♫ Do histo…do histo…

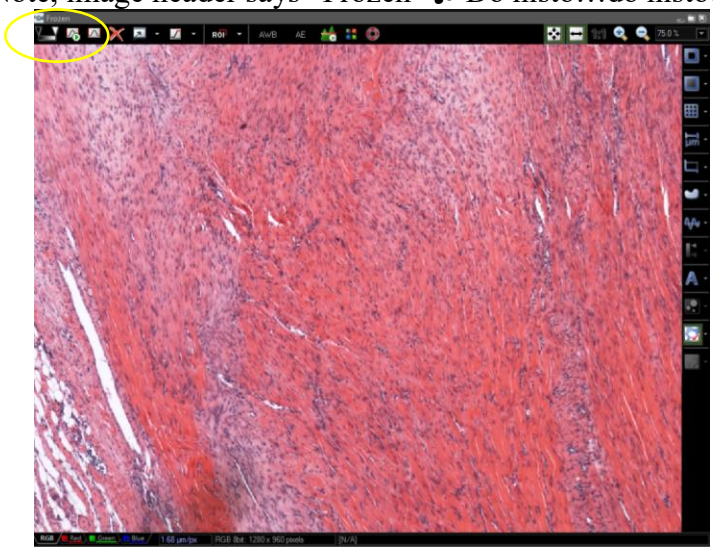

e. Go to file | Save as, etc. and save the image. Any image type is fine.

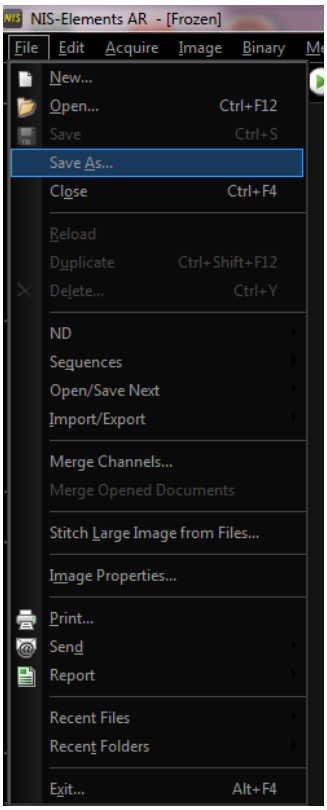

f. Open in imageJ to confirm it looks right. For comparison, this is what it looks like in Windows Viewer. Always use ImageJ.

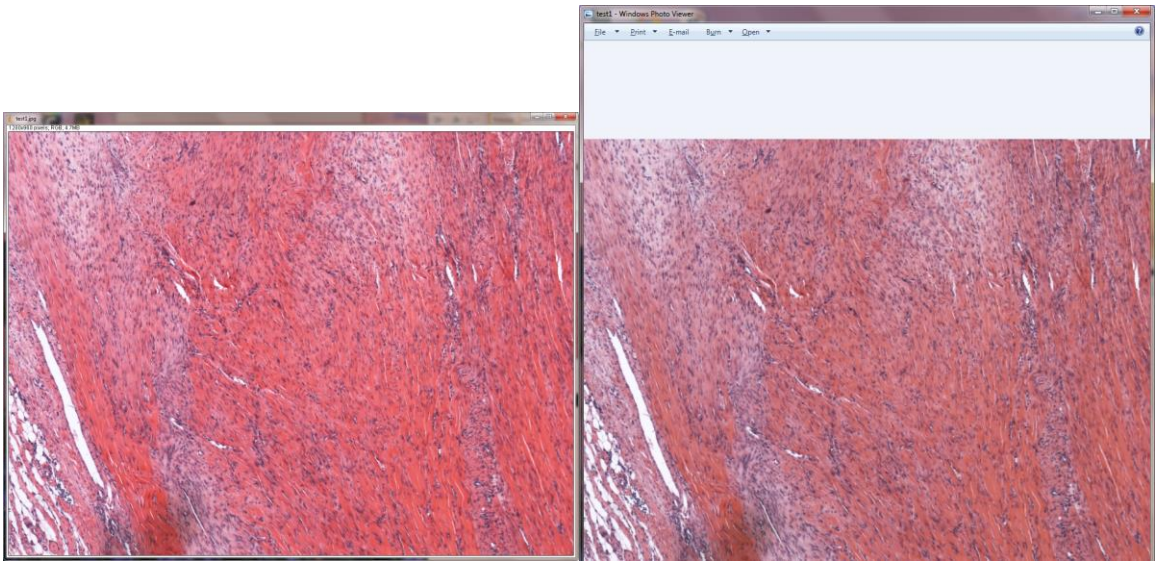

ImageJ ☺
Windows PhotoViewer ☹

g. For comparison, if you DID NOT click “apply LUTs”, and just clicked the camera, your image would look like this in imageJ. Note, the difference.

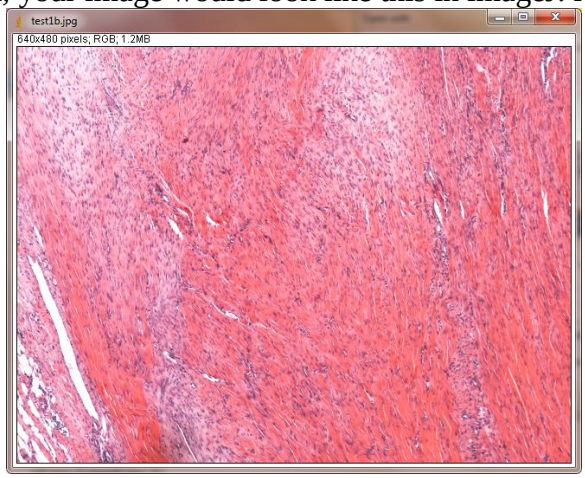

Catch the subtly in color?

h. Here is a more extreme case. I’ve adjusted the LUTs to make the image look bad on purpose.

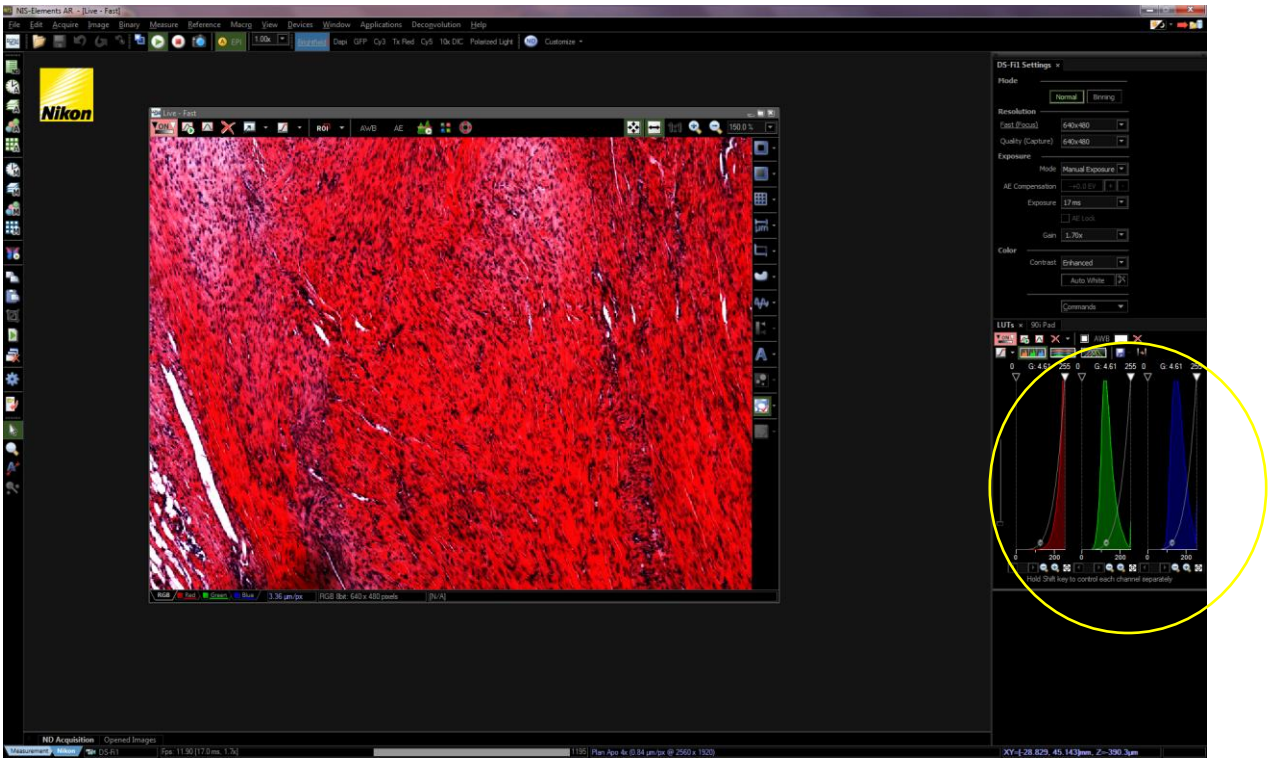

Now, if I click “camera”, watch what happens versus what saves.

How the image looks in Elements:

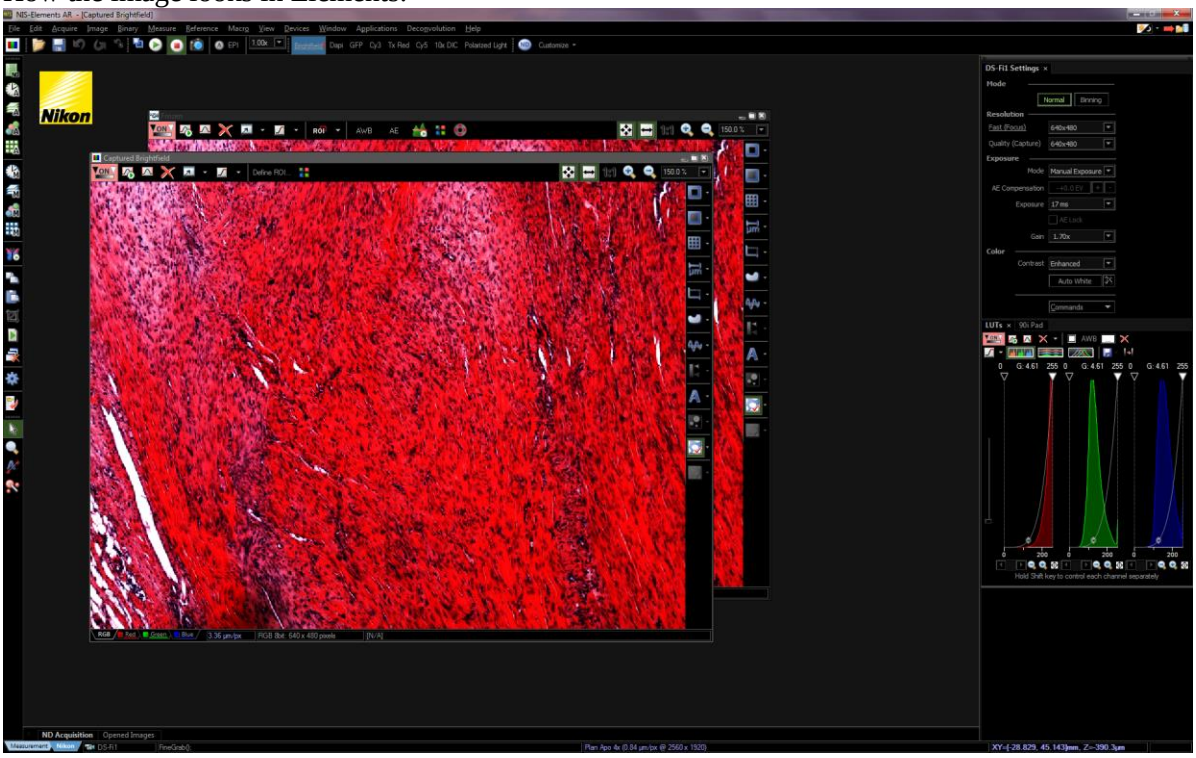

How the image looks in imageJ:

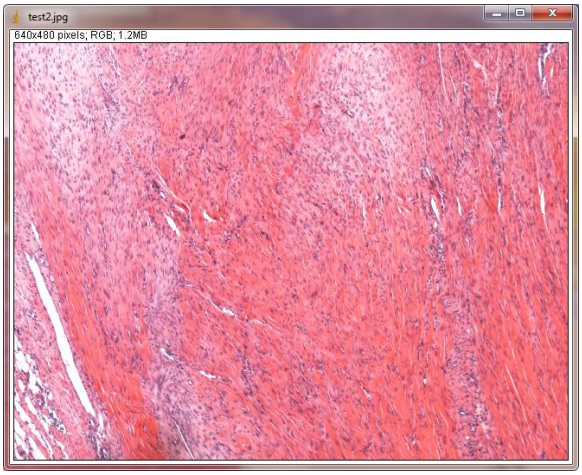

The altered “LUT” was not applied when clicking the camera alone.

However, when we click “apply LUTs,” (AS WE SHOULD ALWAYS DO) and then save, watch what we get:

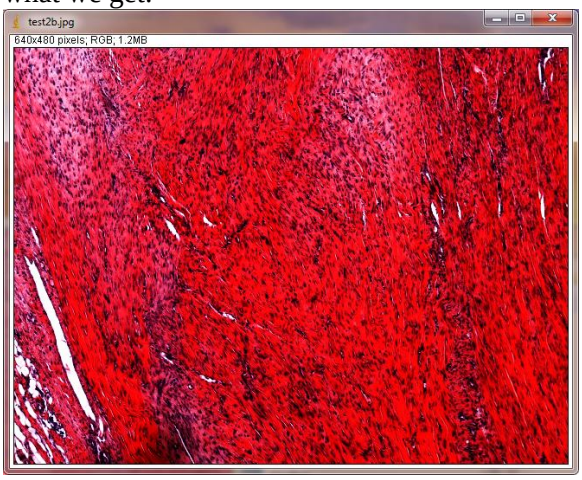

Which is what we wanted from the Live viewer in Elements.

If this mistake was applied to your data, it would be very very bad.

Patellar Tendon Live Testing Protocol

T:\Protocols\Mechanics

Freedman Thesis- Updated 2016-03-12

Videos available on Maxine

I. Supplies Needed

a. Fixturing
   1) Liquid metal
   2) Pipette tips (cut)
   3) Pipette
   4) 3 pots
   5) Hot plate
   6) 1 50 mL Falcon tube of liquid metal
   7) Cup of ice
   8) 3 50mL falcon tubes with water

b. Dissection
   1) Eppendorfs (with BM)
   2) Mouse waste bags in freezer
   3) Scalpel blades (#11)
   4) Gismo powered ON
   5) Tools: scalpel, fine forceps, pickups, hemostat (for foot), microscissors
   6) Stereomicroscope for fine dissection of DEAD tissues
   7) Stamper (dog bone)
      1. 2mm biopsy punch
      2. 3D printed thing
      3. Black mat for transferring tissue
   8) Black mat for entire dissection
   9) Gauze + paper towels

c. Freezing
   1) Liquid N_2 in a Styrofoam container
   2) Metal plate
   3) Plastic OCT containers (labeled)
   4) OCT
   5) Large hemostat
   6) Fine forceps
   7) Scalpel blade + holder
   8) Freeze spray (box of 12)
   9) Tin foil (labeled)

d. Instron
   1) Crosshead set to proper height (inches = XX)

1. Torque wrench

2) Biopuls bath (set to 37ºC)
    1. Temperature gauge
    2. Power plugged in
3) Inner chamber of biopuls with flat piece
    1. Elmer's gel stix glue
4) Fixture installed
    1. Bottom dovetails + top patellar tendon grip (with lip)
5) WaveMaker opened
6) Imaging- DigiVlepo_trigger (Labview)
    1. Teleconverter
    2. gigE camera
    3. light source
    4. inverted camera stand
    5. AF MICRO-NIKKOR 200MM F/4D IF-ED
7) Waste
    1. Bleach stock
    2. Vacuum flask
8) Allen wrenches (4 with yellow tape to mark)
9) 10N load cell (+ calibrate it)

e. Sacrifice
    1) Specimens in pre-labeled bags (if dead) or dissected immediately
    2) IF dead tests, put bags in -20ºC freezer

f. Media (basal media) (5% FBS)
    1) Aliquot 150mL in 250mL bottles (autoclaved) (Grav 60)
        1. 5% FBS
            a. 950mL DMEM (high glucose)
            b. 50mL FBS

II. <u>Procedure</u>

a. Instron setup
    1) Install inner cylinder of biopuls bath 12 hours before testing using Elmers glue stix gel
    2) Raise crosshead to proper height
    3) Install biopuls bath
    4) Add DI water to inner part and about 1" on bottom.
    5) Insert thermometer
    6) Turn on bath to warm and stabilize at temperature. Once the temperature has been reached, basal media can be added immediately before the test (siphon out DI water in inner part)

7) Open Wavemaker twice and make sure load cell is calibrated. If correct, “load” should appear on right figure axis label

b. Media aliquot + warming
   1) Remove 50mL of DMEM and replace with 50mL FBS (to make 5% FBS basal media)
   2) Aliquot 150mL into 250mL bottles
      1. Note, bottles should be rinsed, dried, and autoclaved prior to use
   3) An hour prior to testing, place 150mL of media in incubator on 5th floor with lid unscrewed. 10 min prior to testing, tighten lid and place in warm water bath maintained at 37C.

c. Dissection
   1) Euthanize animal for 10 min in CO_2
   2) Aliquot basal media into a 1.5 mL Eppendorf tube
   3) Clamp foot in hemostat (so it doesn’t move around) and make incision through skin around knee
   4) Remove skin like a sock
   5) Using the blade, cut on either side of the patellar tendon, and start to tease away connecting points where the patella rests on the femur **BE EXTREMELY CAREFUL NOT TO TOUCH THE ACTUAL TENDON AS IT MAY RESULT IN MATRIX DAMAGE AND CELL DEATH**
   6) Once the patellar tendon is free, pull it back and use blade to cut between femur + tibia
   7) Hydrate patellar tendon
   8) Cut off foot at ankle
   9) Remove surrounding musculature + fibula using scalpel + scissors
   10) Hydrate patellar tendon
   11) Place entire tissue in basal media Eppendorf

d. Gismo (pre-stamp)
   1) Place tendon with anterior surface up on custom black mat jig.
   2) Click “RUN” | “Start” | zero x, y, and z | Click |Capture mode
   3) Make 3 passes in midsubstance region, each 0.1mm apart
   4) Click “STOP” and save to proper place (suggest date folder yyyy-mm-dd, and individual specimen folders)
   5) Place entire tissue in basal media Eppendorf

e. Stamping
   1) Make sure liquid electrical tape backing surface is replaced daily
   2) Carefully place tendon in stamping device, anterior surface up

3) Patella is inserted beneath forward clamp
4) Tighten down patellar clamp
5) Once tendon is straightened (sometimes tibia can curl), place wax over tibia and underneath tibia clamp. Tighten tibia clamp
6) Insert new sterilized 2mm biopsy punch + tighten set screw
7) Position punch in center of tendon/defect (in event defect is not centered)
8) Move micrometer adjustment 1.35 mm in either direction (essential 2.7 turns from center position) + push to stamp out struts of tendon
9) Loosen clamps for patella and tibia
10) Place entire tissue in basal media Eppendorf

f. Gismo (post-stamp)
    1) Place tendon anterior surface up on custom black mat jig
    2) Click “RUN” | “Start” | zero x, y, and z | Click |Capture mode
    3) Make 3 passes in stamped region, each 0.1mm apart
    4) Click “STOP” and save to proper place (suggest date folder yyyy-mm-dd, and individual specimen folders)
    5) Place entire tissue in basal media Eppendorf

g. Fixturing
    1) Aliquot liquid metal (if not done already) into a falcon tube
    2) Heat in a water bath on hotplate
    3) Also heat 50mL falcon tubes filled with 50mL of DI water on hot plate (to eventually remove fixture tibia)
    4) PMMA tubes were fabricated and reduced in diameter from 0.75” to fit into 0.75” diameter fixture. These can be held by the paradromic orthogonal technology 3D printed setup.
    5) Before adding metal, remove 37ºC DI water from biopuls and add 150mL of media.
    6) Using the end of a 1000uL pipet tip that has been trimmed to create a larger diameter, pipet out liquid metal (under the hood) and add into hole in PMMA pot. Quickly position tibia so that anterior tendon faces towards to shorter end (note: hole is not centered)
    7) Maintain tendon hydration
    8) Quickly move to 5848b. Position pot in fixture with shorter end opposite to side set screw, tighten set screw, then position with set screw up (note: posterior tendon will face up.)
    9) Take patellar grip and put in patella. Carefully tighten screws and then place into Instron. Note, the anterior face should be closest to

the camera.

h. Installation to Instron + image capture
    1) Once in place, tighten the set screw in the bottom fixture to prevent bottom fixture motion
    2) Raise the biopuls to submerge the tendon in media
    3) Use the XY position to center the tendon and minimize the load
    4) Preload to 0.02N
    5) Open Wavemaker Editor and select the protocol you want to use. Update the file saving path and click "apply current to all blocks" 2-3 times. Then click the save icon to save the protocol.
    6) Now, make sure image capture is working. Go to digiVlepoTrigger on the imaging PC (after opening Labview 2013). Set the file path and name, make sure the "~" is present after the file name.
    7) Open the protocol that was just saved by going to file| open. Always do this, even if you see it in the recent protocols area. Focus lens, aperture, distance of lens to specimen, and adjust light source to optimize image.
    8) Click "Start" and "Zero time" simultaneously (both Instron + imaging computer)
    9) Set a timer for 25 min, the length of each test (note a hold is added at the beginning to standardize the length of each test.
    10) At end of test,
        1. Lower biopuls bath
        2. Dry tendon gently with a Limwipe
        3. For flash freezing, spray tendon with freeze spray and then cut patellar end parallel to long axis of top fixture.
        4. Freeze spray again
        5. Loosen bottom grip set screw with Allen wrench
        6. Place bottom grip on lab bench + spray again
        7. Position pot/fixture unit over plastic piece for OCT sectioning with the posterior part of the tendon up and CAREFULLY use a scalpel blade to cut the tendon off the tibial tuberosity. Note, the blade is angled down so tendon ends up in plastic dish.
        8. Move tendon to desired spot/orientation and add OCT, then emerge into liquid N2. Once frozen, wrap in labeled tin foil piece and keep tissues in -20ºC freezer.

III. <u>Order of events</u>

a. Install biopuls, calibrate 10N load cell, heat up bath with DI water, power up camera, Wavemaker, Digivlepo, prep OCT, freeze spray, blade holder+blade (Person 2)

b. Put aliquoted media in incubator with lid loose (Person 2)
c. Warm up liquid metal (Person 1)
d. Get sacrifice pre-labeled bags
e. Set up dissection area (Person 1)
f. Sacrifice 1 mouse (Person 2)
g. Get liquid N2 (Person 2)
h. REPEAT
    1) Dissect/gismo/stamp/gismo/prep left limb (Person 1)
    2) Add/replace DIWater with media when putting fixturing in liquid metal (Person 2)
    3) Test left limb (Person 1)
    4) Dissect/gismo/stamp/gismo/prep right limb (Person 1)
    5) Freeze left limb (Person 1)
    6) Put/remove pot in warm water falcon tube + replace blade (Person 2)
    7) Sacrifice 1 mouse (Person 2)
    8) Test right limb (Person 1)
    9) Freeze right limb (Person 1)
    10) Check liquid N2 supply (Person 2)
i. Clean up (Person 1 + Person 2)

Area Analysis Protocol

T:\Protocols\Mechanics

---

1. Open MATLAB R2012a
2. Type into the command line: gismo_area;
3. A gui will appear as shown on the right.
4. Click Load. Select the .txt file you want to analyze.
5. Click Mark GisMo and use the cursor to select the sides of each peak going from left to right. When all the peaks are marked click enter.
    a. Note, the below images are an example and are not from this thesis work.

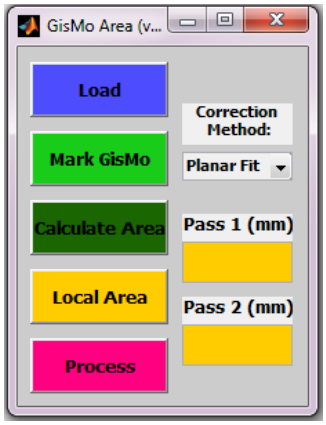

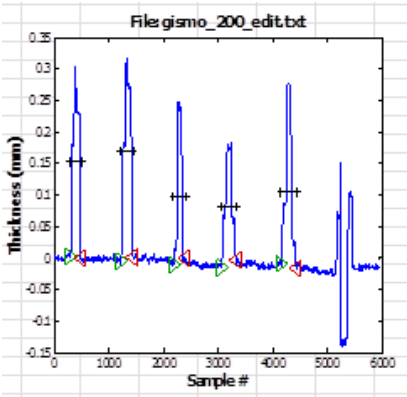

6. An area vs. length bar graph will pop up. It is good practice to save these graphs so you can review any outliers later without having to redo the analysis.
7. Other features include selecting local area.
8. Record the output in the spreadsheet under unstamped and stamped area, respectively.
9. Additionally, the thickness can be computed by using Gismo in the cooker folder and the function, plot_ythick.

Bilinear Fit Protocol (For Force-Displacement Data)

T:\Protocols\Mechanics
Freedman Thesis- Updated 2017-01-03

III. Setting the Directory

a. Directory: X:\software cooker-freezer\Fatigue\BRF_Thesis\Released\Version3.09-5848-BenThesis (Maxine)
b. M-file: Bilin_MRB_BRF_5848;
c. Data located here: T:\Experimental Data\Mechanics\Testing
   1) (T = Thesis folder in bfreed)

IV. Protocol

a. Open MATLAB 2012a or later

b. Type: Close all; clear all; clc; in the command window

c. Type: "Bilin_MRB_BRF_5848;" in the command window

d. Please decide: "What blocks should be analyzed"

   1) Select "RT Strain"; Note, others are for recovery protocols in "**dead**" / frozen tissue. We may analyze these later.

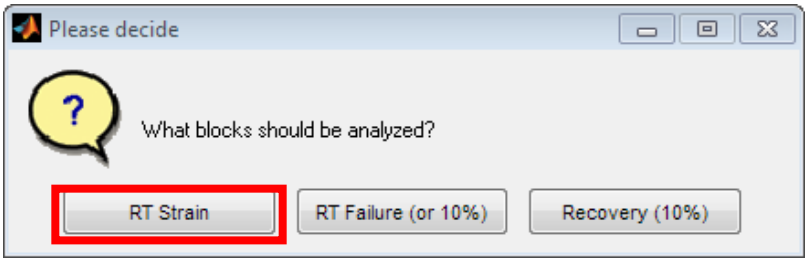

1) Run the analysis for the **LIVE** specimens only. Lists can be found on Maxine/BRF Thesis
   2) Navigate to the folders with data to open a *_csv.txt file. Note, only open these if the name is <<indicates **10% strain ramp**; otherwise 1%>>
      1. odd + R
      2. even + L

e. **Note, figures should plot on x-axis to **0.25mm**** If not, wrong file.

f. Click on the minimum force for your range of interest

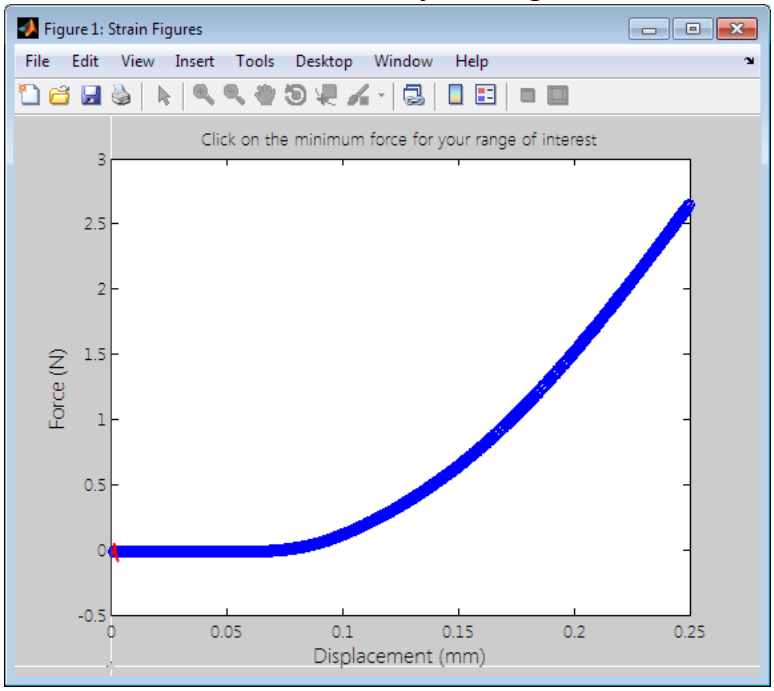

g. Click on the max force for your range of interest

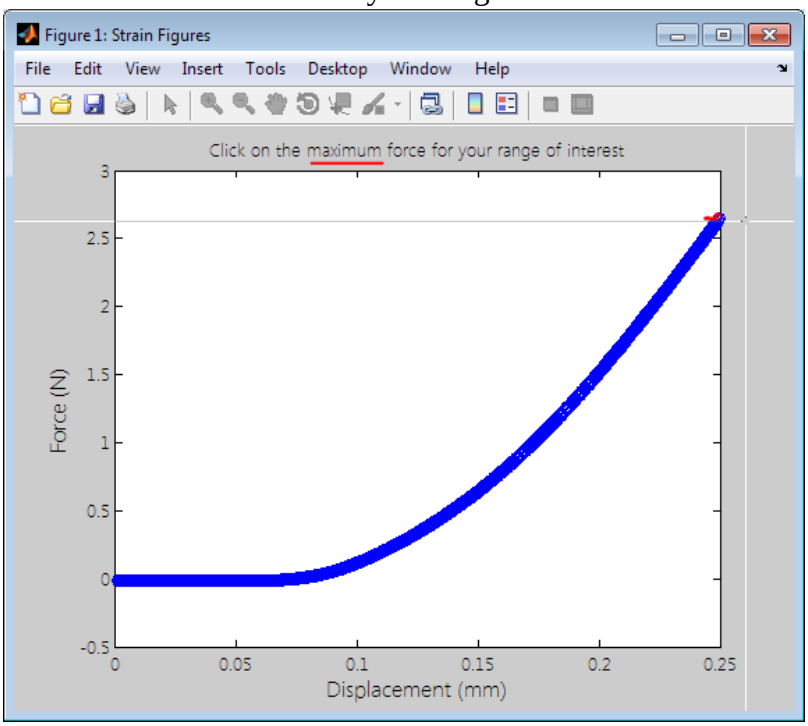

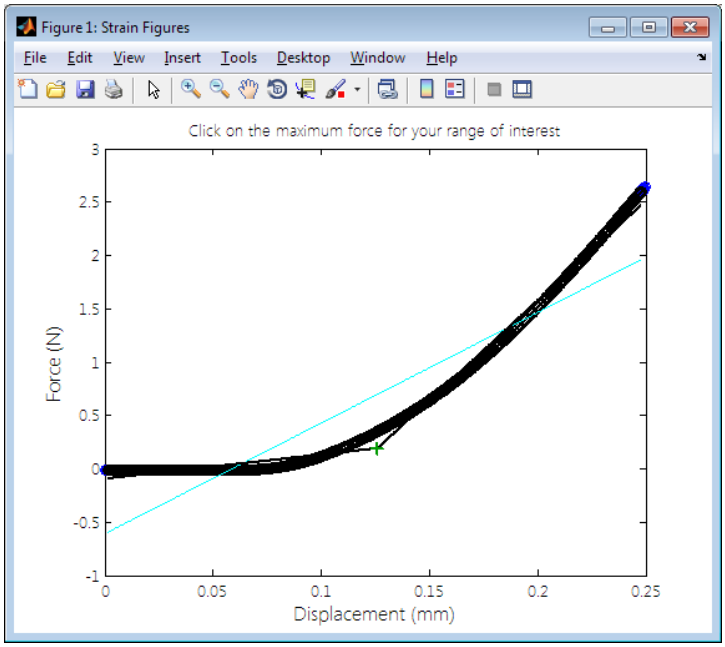

Bilinear Fit plotted as well as transition. Overall fit is also included (cyan)

h. Copy outputs from command window to Excel

```
%Filename     BPx(mm)     BPy(N)   ToeStiff(N/mm)   LinStiff(N/mm)   RMSE
c150_0083r - Copy_csv.txt     0.126   0.189    2.267    18.713    0.062
>>
```

1. **Filename**: the name of the file
2. **BPx** (mm)- Transition displacement (BP = breakpoint)
3. **BPy**(N)- Transition force
4. **ToeStiff**(N/mm)- slope of first fit in toe region
5. **LinStiff**(N/mm)- slope of 2nd fit in linear region
6. **RMSE**- root mean sq error of fit

- Note, you can compute modulus by the stiffness data by multiplying by gage length and dividing by CSA to give N/mm² or MPa.

- Also, we can compute "stretch" $\lambda = l/L$ outside of normal outputs here from the transition displacement as (BPx+Gage)/gage.

Protocol: **Fatigue Analysis Protocol** (MATLAB)

T:\Protocols\Mechanics

Author: Ben Freedman
Contacts: freedman.br@gmail.com; 413-537-3369

1. Where Files are Kept:

X:\software cooker-freezer\Fatigue\BRF_Thesis\Released\Version3.09-5848-BenThesis

2. Flow Chart of Steps:

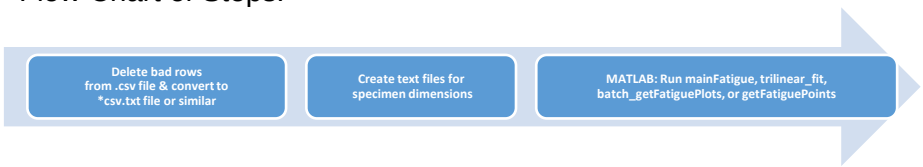

   a. Create specimen dimension file; there is a new function that can do this with instructions provided within the header. Essentially requires 3 cols, 1st is specimen name and the other two are gage length and area.
   b. Make everything into a csv.txt file for faster read-in. Note, sometimes the 5848s output data weird with an extra space or miss a comma which messes everything up. This can usually be caught by eye. You can also search through the text file with ctrl+f for certain combinations of letters, spaces, and characters to find errors in output.
   c. Benware function- I always meant to change the colors. Maybe I will do this in the future.
   d. Batch processing is possible by typing in certain functions individually, such as “LoadAndFitSine_v5;” and EqForce_brf5848;

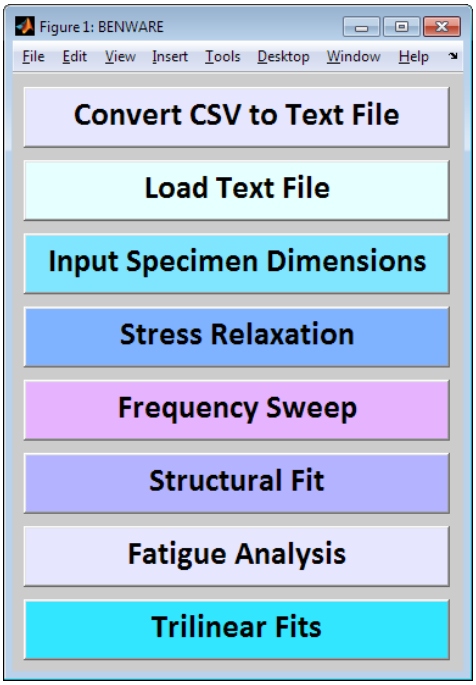

If a csv.txt file has already been created (usually faster this way since convert CSV to Text does not operate in batch) (faster to use batch_csv2txt_csvread), just click “Load Text File.” Then, input specimen dimensions (only necessary if you are planning to run the fatigue analysis for laxity and peak strain calculation).

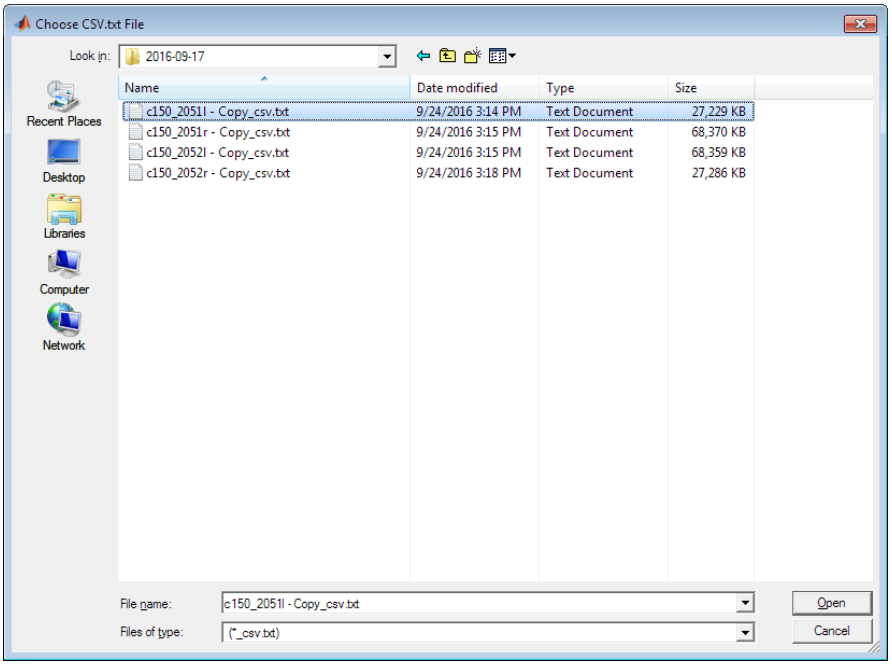

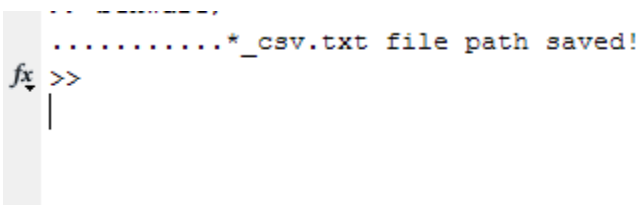

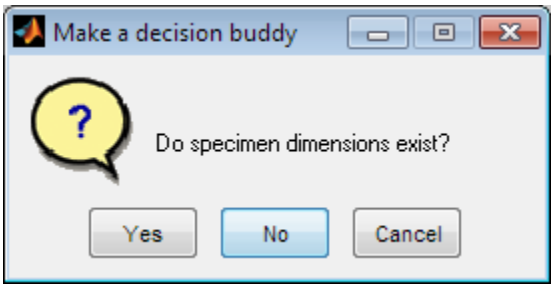

Click “Yes” and go to the .txt file containing them.

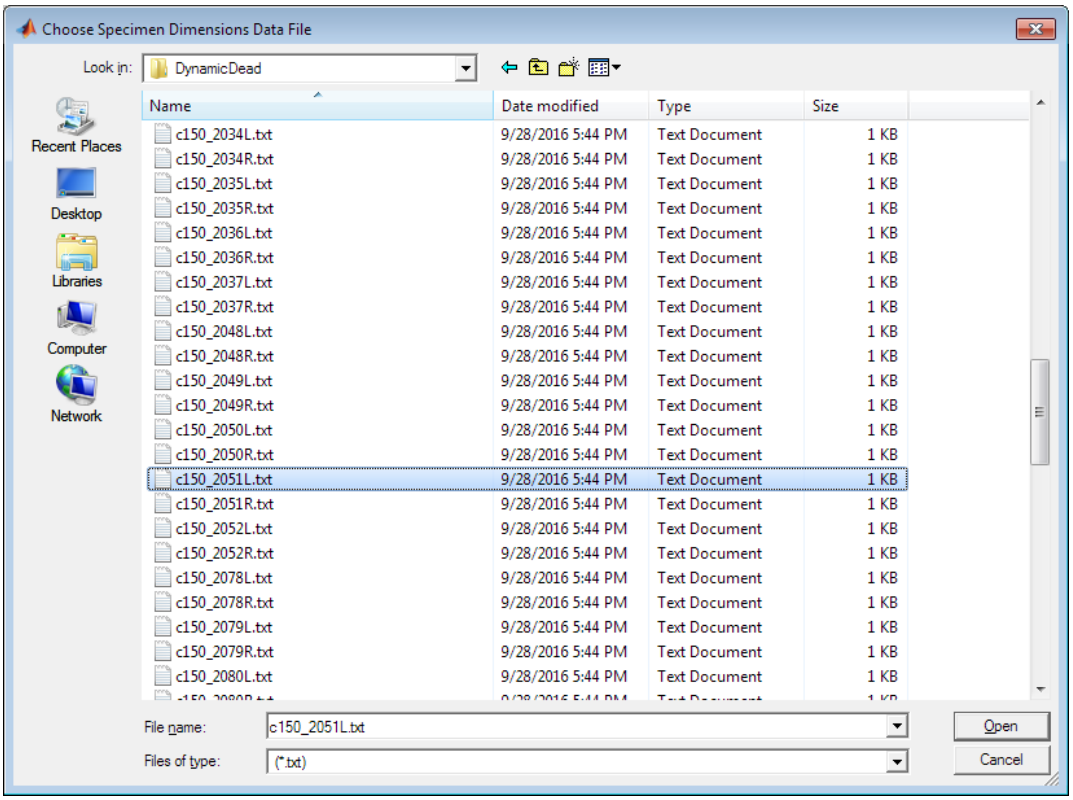

Click “Stress Relaxation”

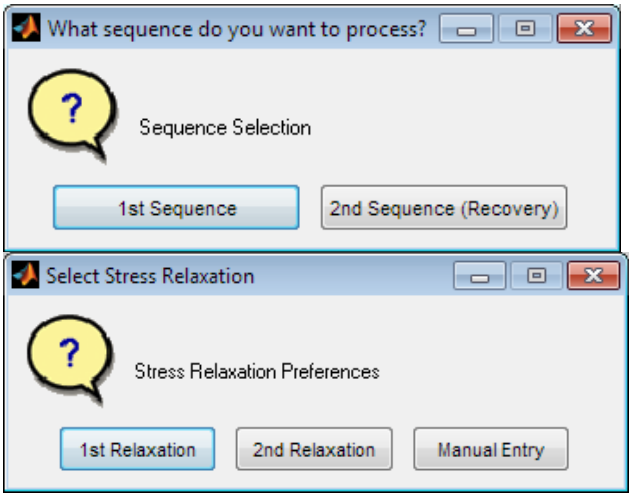

<This is here for the dynamic dead loading case where there are two sequences and two strains evaluated unlike in the live testing where we processed one sequence and a single strain>

Example output:

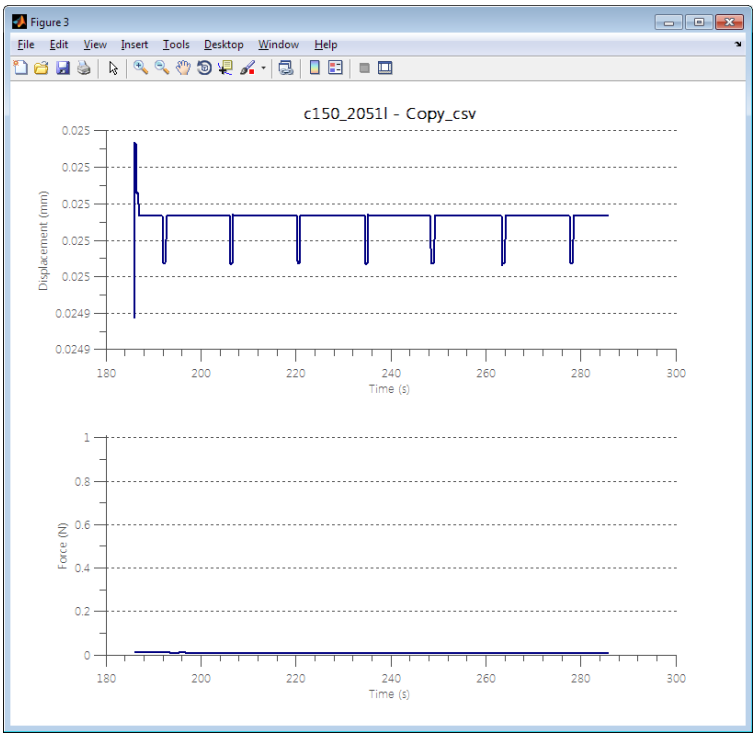


```
..........Analyzing Stress Relaxation Data.
........1st Sequence.
........1st Relaxation.
%Fpk      Tpk      Feq      Teq      Relaxation(Percent)
c150_2051l - Copy_csv    0.012    186.061     0.007    286.000     41.298
..........Stress Relaxation Analysis Complete!
fx >>
```

Now click “Frequency Sweep”, note, this can be done in batch for all samples in the folder. For this, just click the specimen of interest.

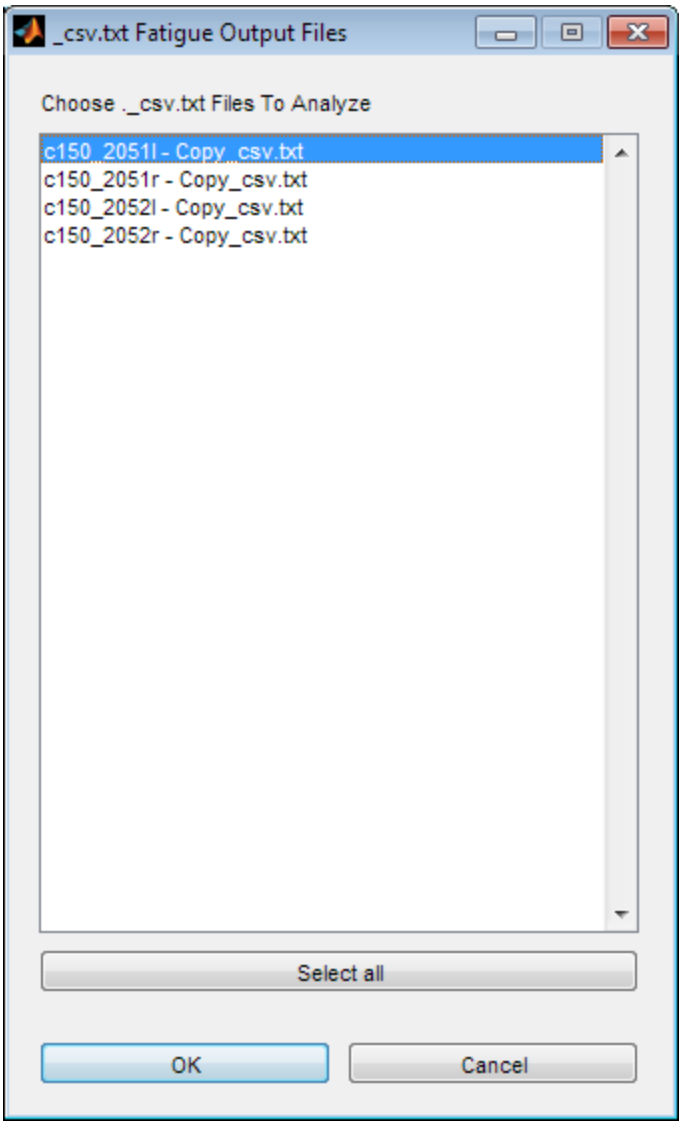

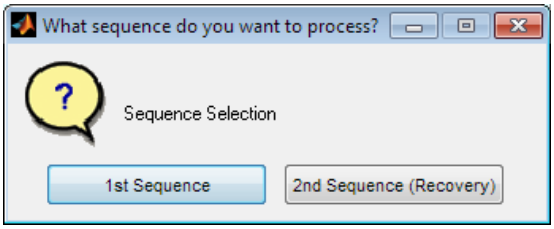

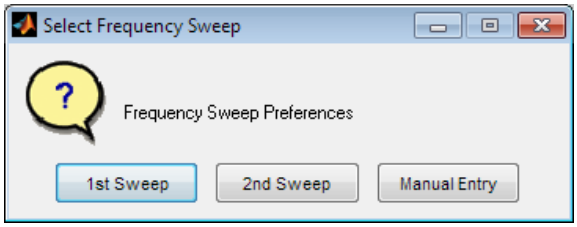

Same as before

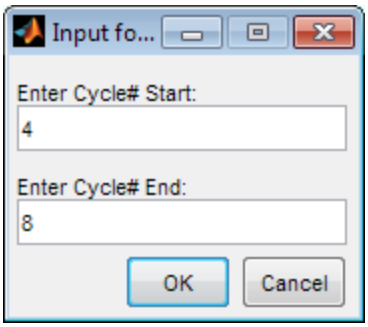

This just limits the cycles processed. It was a bigger deal for better fits with the electropuls than the 5848s, but it is fine.

Use output2 (a single row). Output1 is what Buckley + Dunkman used and requires the “PowerTransposer” excel spreadsheet to reformat the data. It is bulky. Use output2.

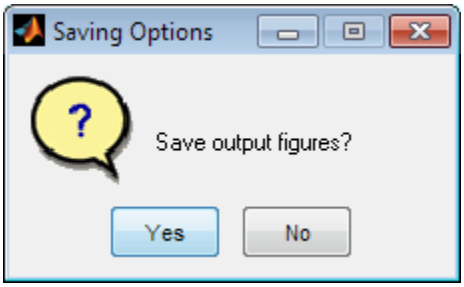

Copy/pasting figs to .ppt is not necessary with this. It saves the figures output to the same folder they are read in from.

Example output for Extension v. time figures. Note, these were originally coded by Mark Buckley (I believe).

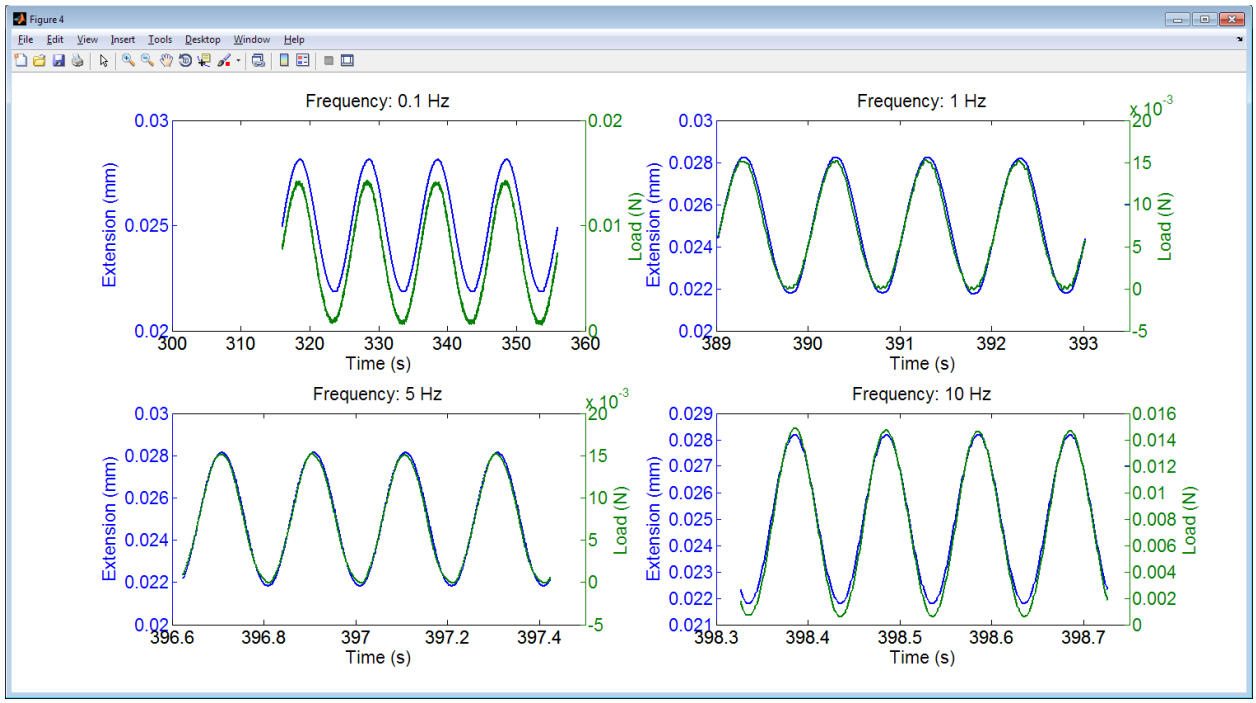


```
........1st Sequence.
........1st Sweep.
.......Output 2.
..........Not saving figures.
%Filename     u_Amp (0.1Hz)    u_Amp (1Hz)      u_Amp (5Hz)      u_Amp (10Hz)    F_Amp (0.1Hz)     F_
c150_20511 - Copy_csv     0.003131     0.003263     0.003182     -0.003192   0.006639      0.007649
..........Frequency Sweep Analysis Complete!
>>
```

(note I did not save the figs here)

Now, structural fit. Details regarding this are also in a separate structural fit protocol.

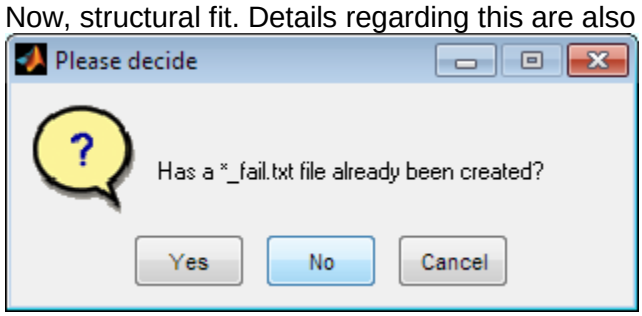

Click NO

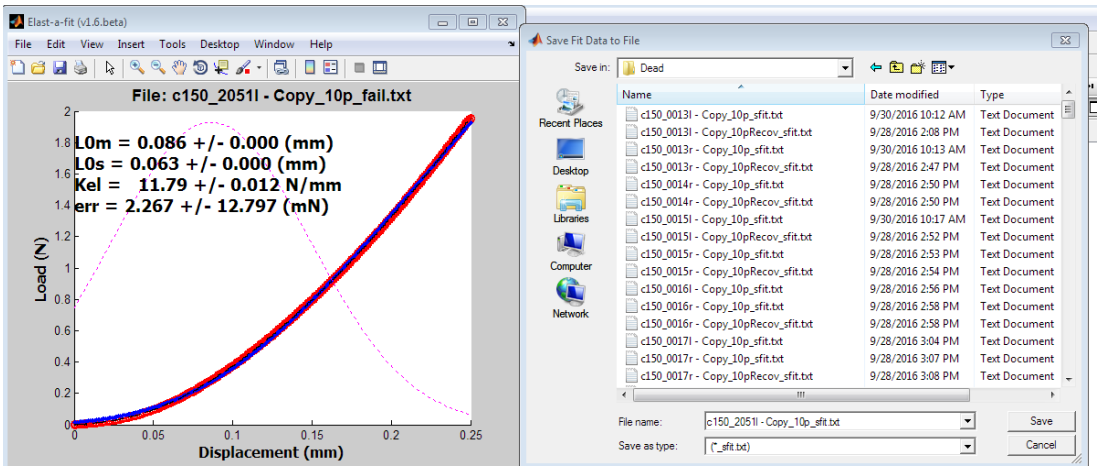

Example output (copy out command window) and save file to a Structural fit folder in data analysis. Note, this is used for Optikos later.

```
%File    DispFmax(mm)    Fmax(N)  sL-mn(mm)    sL-sd(mm)    Kel(N/mm)    CI sLmn(%)   CI sLsd(%)
c150_2051l - Copy_10p_fail.txt  0.2500  1.9560  0.086   0.063   11.789  0.2 0.2 0.1 9.353
>>
```

Now, click “Fatigue Analysis”
For these, you must go unblind to know what target loads are needed/pre-programmed for computing stiffness, etc.

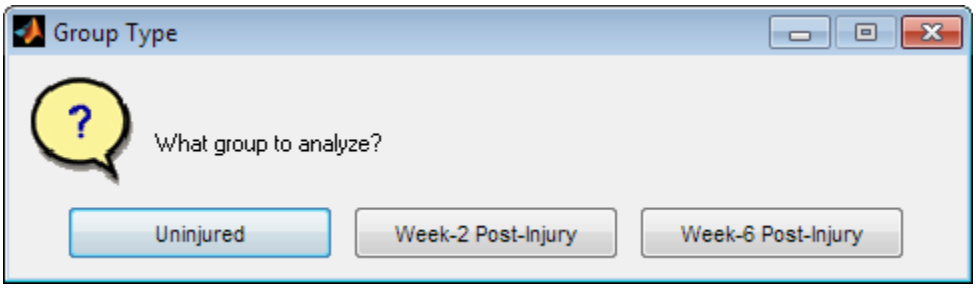

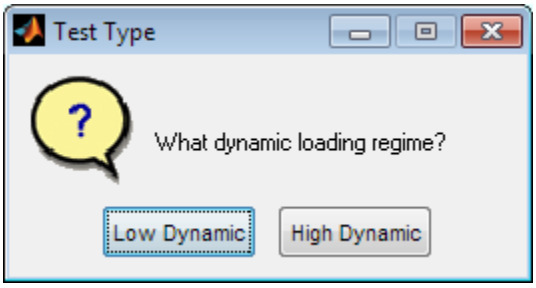

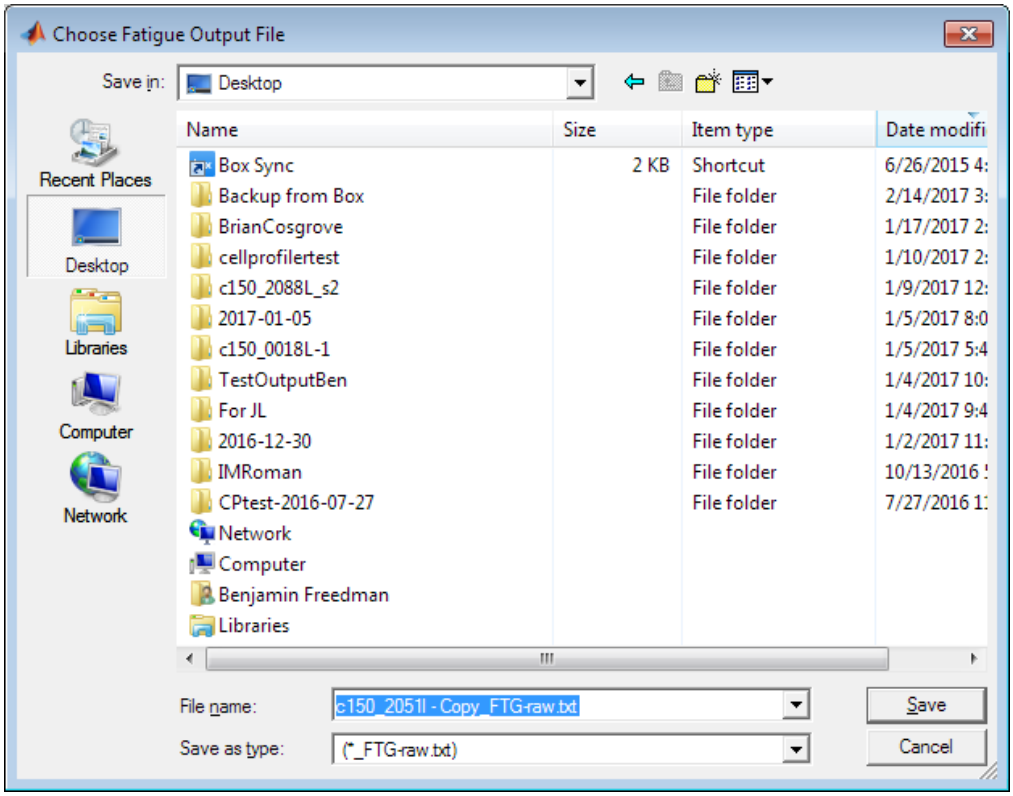

Two types of files are saved. An *_FTG-raw.txt and a FTG_spec.txt. The first contains all data and the 2nd contains the data probed at 5, 50, and 95% fatigue. There are other functions that can probe by cycle number too (getFatiguePoints…).

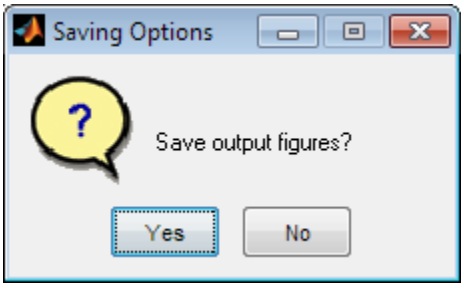

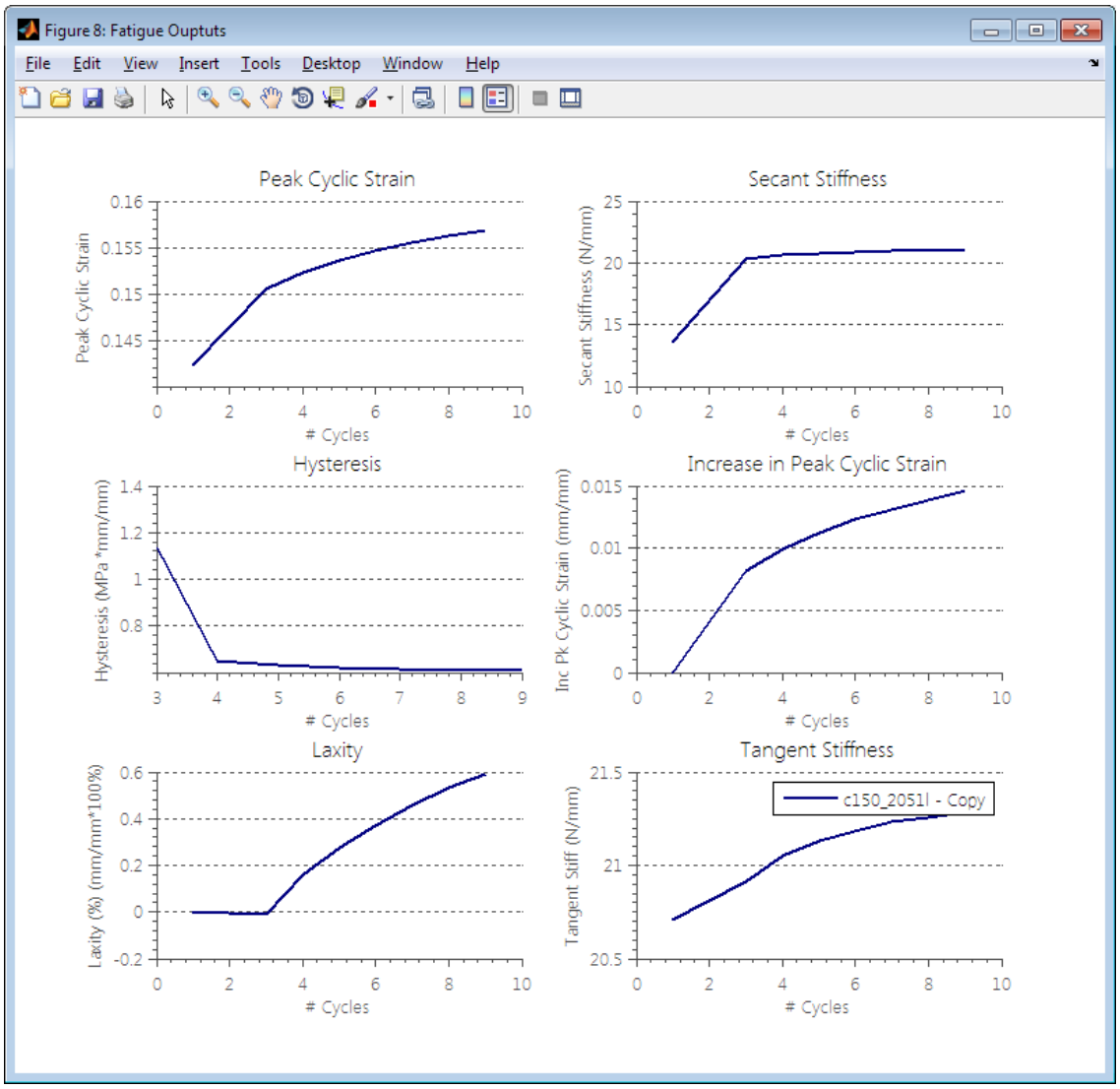

Note, data looks jagged because it only 10 cycles. For 1000 cycles it is smoother.

i. Specimen Dimensions File

1. Measure the gage length from optical data

2. Measure cross sectional area from GISMO

3. Create a Specimens Dimensions File that contains information from (1) and (2)

4. You can do this easily using notepad.

5. Name the file “YourSpecimenID.txt” , then enter data similar to below: **note, hit “tab” between data entries

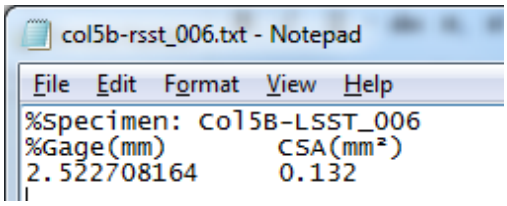

e. With regard to data output, the following columns are output
    i. Filename
    ii. Gage length
    iii. CSA
    iv. Cycles to failure
    v. Peak Strain at cycle 1
    vi. Peak Strain at cycle 5
    vii. Peak Strain at cycle 10
    viii. Peak strain at 5% fatigue life
    ix. Peak Strain at 50% fatigue life
    x. Peak strain at 95% fatigue life
    xi. Secant Stiffness at 5% fatigue life
    xii. Secant Stiffness at 50% fatigue life
    xiii. Secant Stiffness at 95% fatigue life
    xiv. Tangent Stiffness at 5% fatigue life
    xv. Tangent Stiffness at 50% fatigue life
    xvi. Tangent Stiffness at 95% fatigue life
    xvii. HysteresisF (force definition (N*mm/mm) at 5% fatigue life
    xviii. HysteresisF (force definition (N*mm/mm) at 50% fatigue life
    xix. HysteresisF (force definition (N*mm/mm) at 95% fatigue life
    xx. HysteresisS (stress definition (MPa*mm/mm) at 5% fatigue life
    xxi. HysteresisS (stress definition (MPa*mm/mm) at 50% fatigue life
    xxii. HysteresisS (stress definition (MPa*mm/mm) at 95% fatigue life
    xxiii. Laxity/Damage at 5% fatigue life
    xxiv. Laxity/Damage at 50% fatigue life
    xxv. Laxity/Damage at 95% fatigue life
f. For modulus, compute from stiffness, CSA, gage length
g. For fatigue properties at set cycle numbers, use “getFatiguePoints”
    i. Note, this can run in batch
h. For fatigue plots either use
    i. batch_getFatiguePlots;
    ii. getFatiguePlots;

3. Key Points if Need to Edit:
    a. Cycle numbers grabbed for fatigue loading blocks

    b. Load thresholds used to compute the tangent stiffness and laxity/damage(Ds); note, they should be approx. the lower and upper

bounds of what looks “linear” during cyclic fatigue loading.

c. Potential data saving things such as formatting decimal places and matrix sizes

d. Be cautious if you change the type of protocol that might affect the quadrant that fatigue loading cycles start since they may alter the algorithm that detects peaks and minimums.

e. The larger program, benware; uses many functions in addition to fatigue loading analysis, so please be cautious when editing.

Optikos Protocol

T:\Protocols\Mechanics

2015-06-18

---

1. Located here: Y:\Software- Released\optikos
   Better version: \\Max\soslowskylab\software\optikos\v1.5.0 (beta)

2. First, separate ramp to fatigue and fatigue images to separate folders. Also, you'll want to run the structural fits in benware.

3. Type "optikos;"

4. Find images

5. Contrast & filter the images

6. Click "Choose ROIs" Draw a box in the midsubstance only, draw bottom left, top left, then click "track" When completed, click "Text Output" and save as "**L**_roip.txt" (L for left) in the same folder as the images
   a. **Pay attention to ROI tracking and image correlations! If it doesn't look like it is tracking, write that down!!**

7. Now, repeat step 6 for the right, then save as "R_roip.txt"

Note, it is likely easiest to repeat #s 3-7 for all specimens before moving onto steps 8 & 9.

8. Once you have tracked your two stain lines (and generated trk.txt files). You create an element & strain file by running

   trk2element;

   (choose the two trk.txt files, and then save it to a new output file)

9. To analyze the stiffness, run

   el2d_stiffness;

   The output from the screen which you will copy and past into excel has:

   Kstrn(N/%), which you divide by area to calculate modulus
   Kopt(N/pix), which you multiply by the resolution pix/mm to get
   stiffness (N/mm)

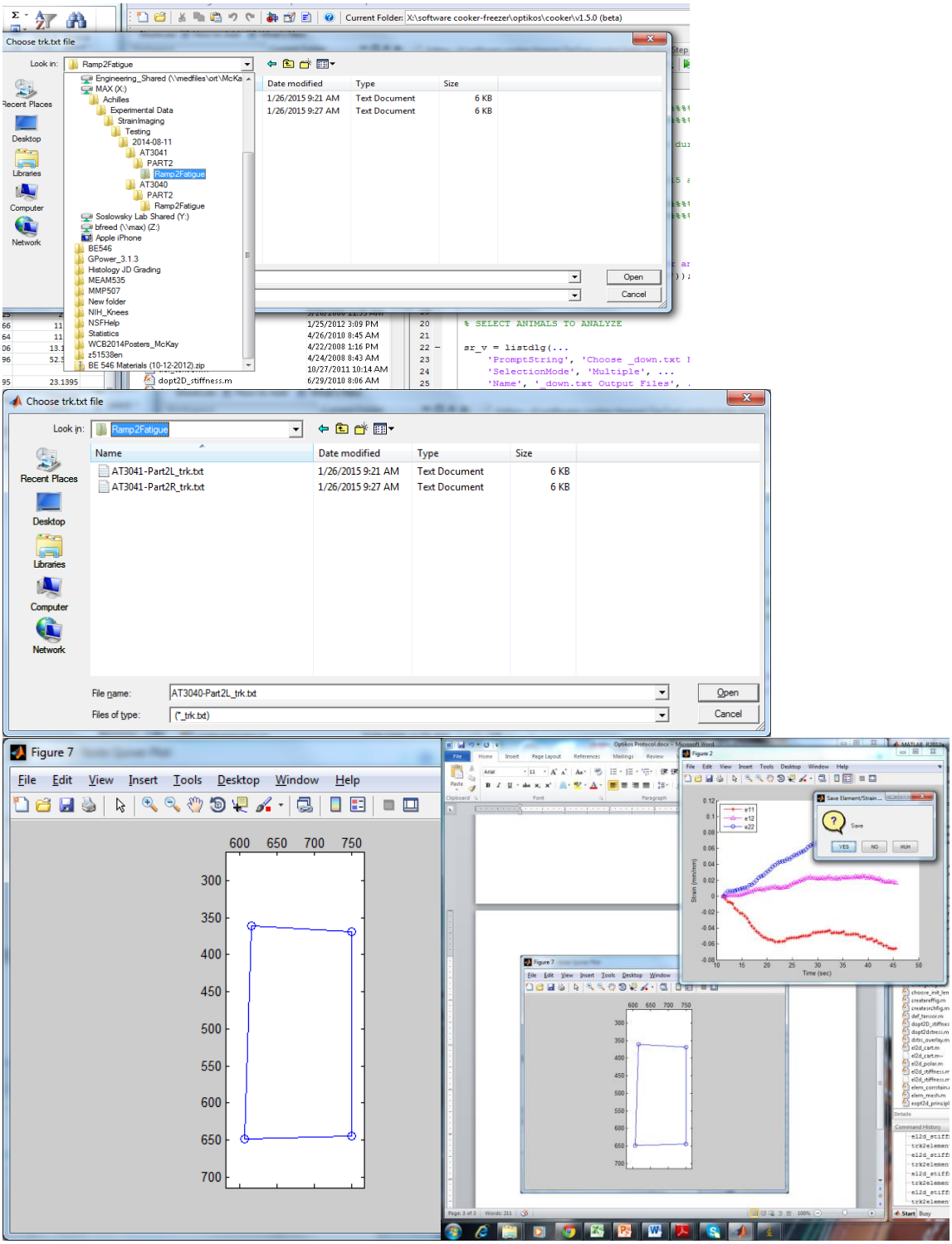
Current Folder: X:\software cooker-freezer\optikos\cooker\v1.5.0 (beta)
Choose trk.txt file
Look in: Ramp2Fatigue
Date modified
Type
Size
1/26/2015 9:21 AM
Text Document
6 KB
1/26/2015 9:27 AM
Text Document
6 KB
Open
Cancel
% SELECT ANIMALS TO ANALYZE
sr_v = listdlg(...
'PromptString', 'Choose _down.txt
'SelectionMode', 'Multiple', ...
'Name', '_down.txt Output Files',
Choose trk.txt file
Look in: Ramp2Fatigue
Name
Date modified
Type
Size
AT3041-Part2L_trk.txt
1/26/2015 9:21 AM
Text Document
6 KB
AT3041-Part2R_trk.txt
1/26/2015 9:27 AM
Text Document
6 KB
File name: AT3040-Part2L_trk.txt
Files of type: (*_trk.txt)
Open
Cancel
Figure 7
File Edit View Insert Tools Desktop Window Help
600 650 700 750
300 350 400 450 500 550 600 650 700

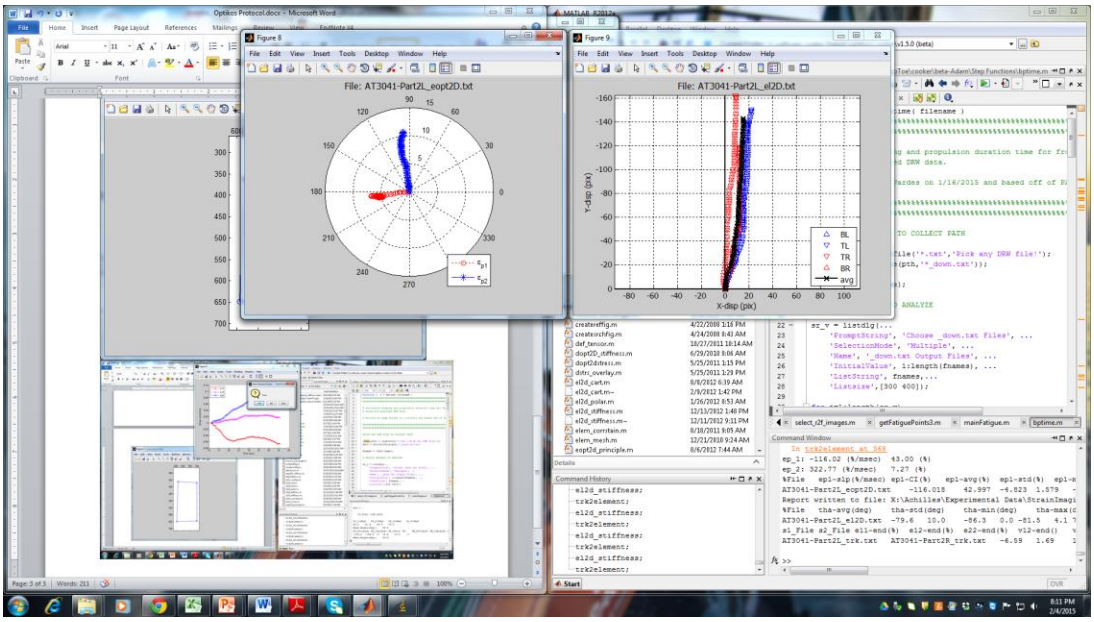

Now el2d_stiffness;

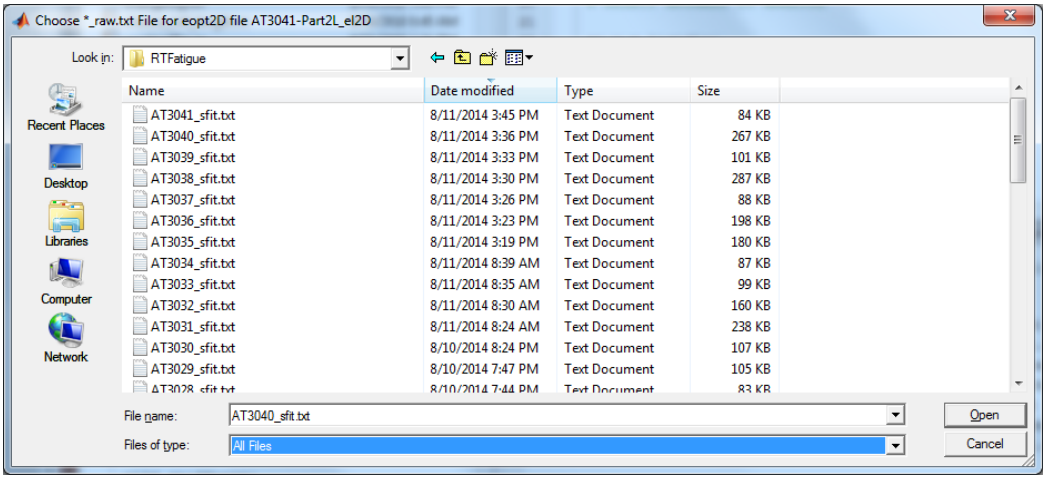

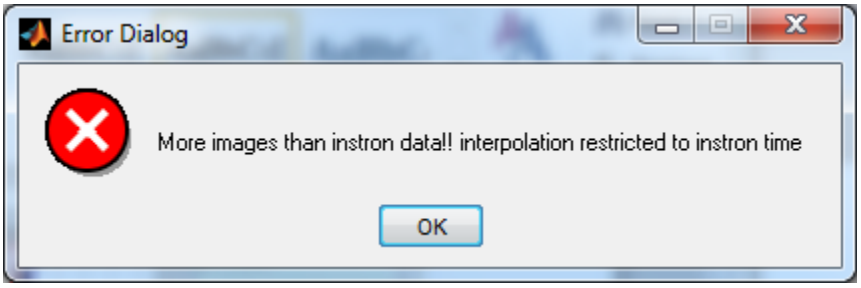

Normal

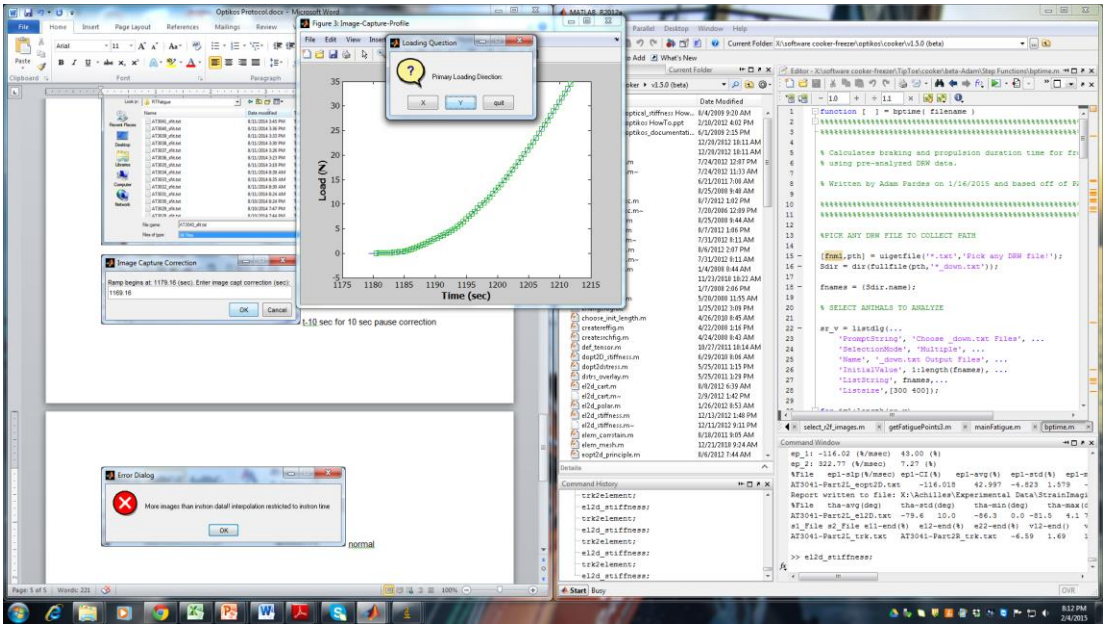
Figure 3: Image-Capture-Profile
Loading Question
Primary Loading Direction:
X
Y
quit
Load (N)
Time (sec)
Image Capture Correction
Error Dialog
More images than instron data!! interpolation restricted to instron time
OK
normal

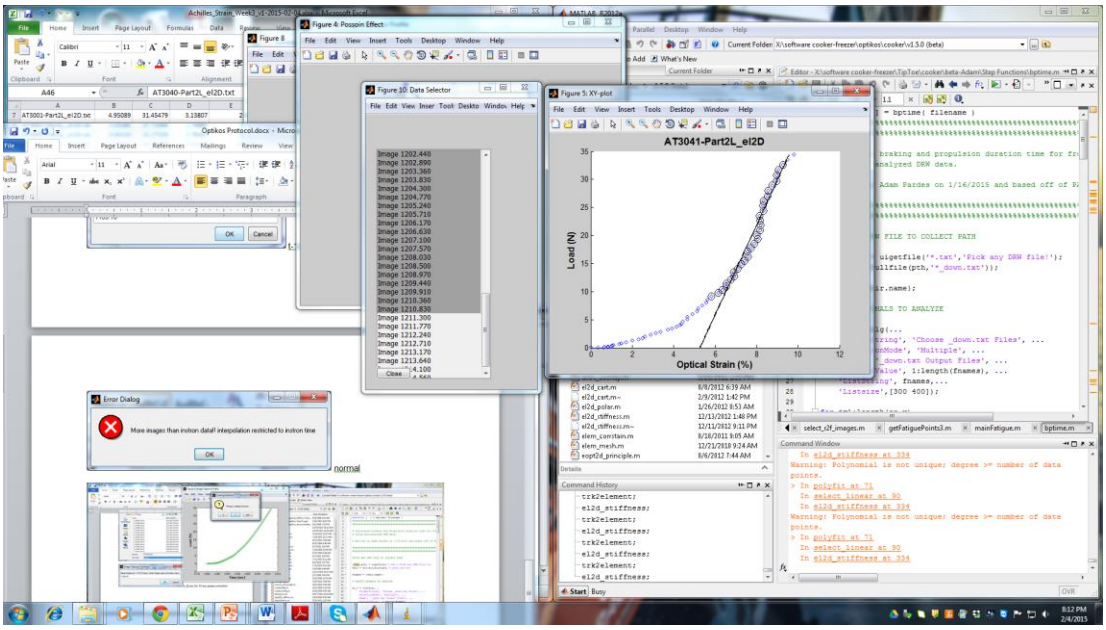
Figure 4: Poisson Effect
Figure 10: Data Selector
Figure 5: XY-plot
AT3041-Part2L_el2D
Load (N)
Optical Strain (%)
Error Dialog
More images than instron data!! interpolation restricted to instron time
OK
normal

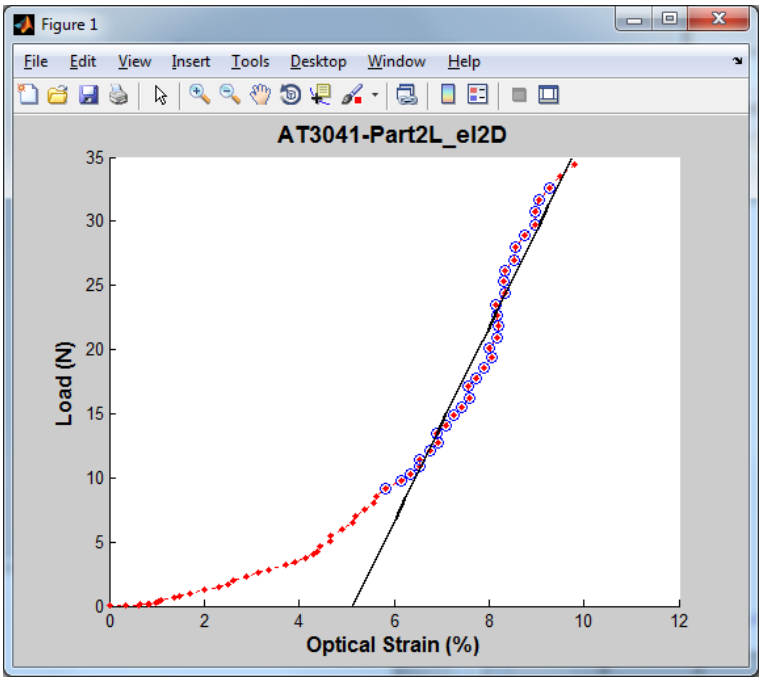
Figure 1
File Edit View Insert Tools Desktop Window Help
AT3041-Part2L_el2D
Load (N)
Optical Strain (%)
0
5
10
15
20
25
30
35
0
2
4
6
8
10
12

Protocol for the Structural Fit Model Program for Fiber Recruitment Analysis

T:\Protocols\Mechanics

RUNNING THE PROGRAM

1. Open MATLAB (v7.0 or later).
2. Set a new path to Y:\Software\TendonMechanics\cooker.
3. In the command prompt, type "r2f_structfit;"
4. Choose the file you want to analyze (should be a *raw.txt file extension).
5. The program will then prompt you to choose a failure/yield strain. Normally we would choose this at the peak of the load-displacement curve, but this program will work better if you choose a point that is still in the linear region. For example, Figure 1.

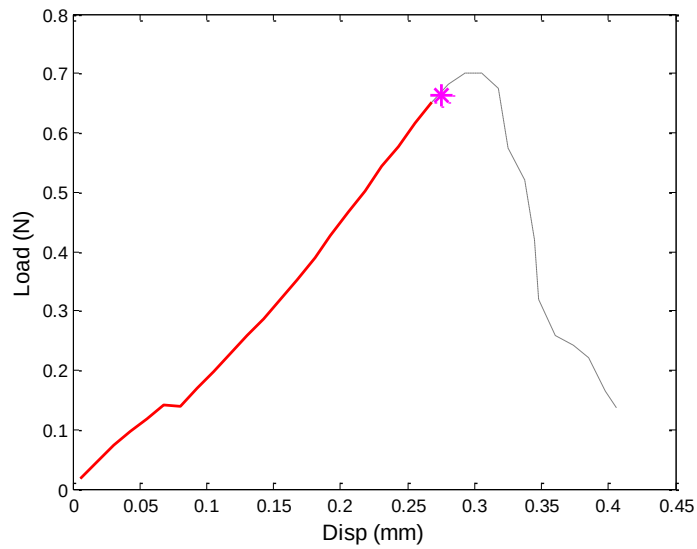

Figure 1: Load-Displacement curve that has the yield/failure strain marked with a magenta star. Note that this is still in the linear region.

6. Let the program run and it will fit a structural fiber recruitment model to the data.
7. The program will prompt you to save a *_sfit.txt file. This will contain the fit parameters for the whole model. Choose to save by clicking "save" or cancel.
8. Repeat for all samples.

ANALYSIS OF THE PROGRAM OUTPUT

Figure 2: Two examples of a structural fit model output. BugsBunny is a bad fit, but TigerLily is a good fit.

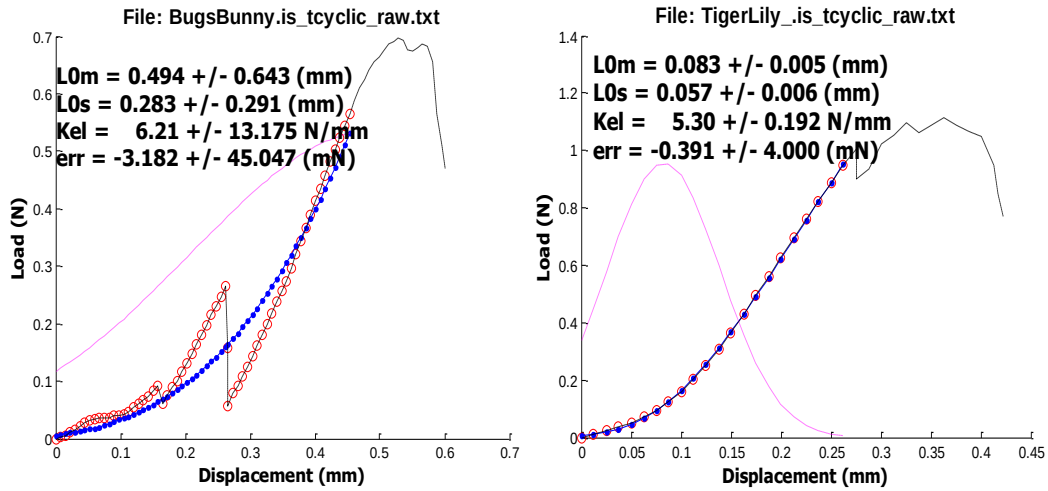

1.
2.
3. A plot of the data and the structural fit is outputted. You can use this figure to determine whether the model has fit the data well or not. See Figure 2 – On the left is a bad fit since there is a discontinuity in the plot and on the right is a very good fit. These plots also write the L0m, L0s, Kel and err of the fit. These parameters are also given in the MATLAB output.
4. In addition to the plots, the program will output a *_sfit.txt file that contains the fit parameters for the entire data set.
5. Finally, text is outputted into MATLAB that is required for analysis.
    a. Copy and paste the output in the MATLAB command window into an Excel file. The file should have the following headings:
        i. %File, dFmax(mm), Fmax(N), sL-mn(mm), sL-sd(mm), Kel(N/mm), CI sLmn(%), CI sLsd(%), CI Kel(%), err-mn(mN), err-sd(mN), rmse(mN)
    b. If the confidence interval (CI) of any of the three parameters is greater than 50, than that parameter is considered a bad point. These points are up to the discretion of the user as to whether they should be discarded or not. If all three CIs are greater than 50, that point should be discarded.
    c. Next you must calculate the displacement at each percentage of fiber recruitment.

i. To do this, create a matrix in MATLAB by typing “dt1 = []”.

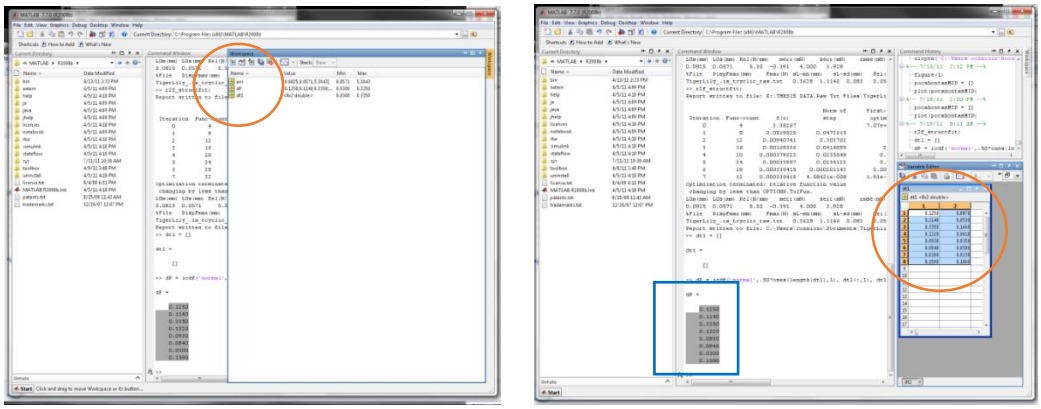

Figure 3: Screenshots showing (left) where to find the variables in the workspace (Double-click on the variable to open it), and (right) how to input the data columns into the variable matrix. Both shots also showing the output of the command used in item iii for 50% fiber recruitment (blue rectangle).

ii. Then go into the command workspace and copy and paste the columns “sL-mn(mm)” and “sL-sd(mm)” into the variable matrix. See Figure 3.

iii. In the command prompt, type “dP = icdf('normal'**,.50***ones(length(dt1),1), dt1(:,1), dt1(:,2)).” The “0.50” is the percentage of fiber recruitment so for each percentage, you will change this number. Typically, 50% is for the transition strain and 75% is in the linear region.

iv. This prompt will output one column of data; this is the displacement for the 50% fiber recruitment mark. In order to get the strain, simply divide by the gauge length.

**Note: A template for this analysis exists in Y:\Software\TendonMechanics.

Viscoelastic Mechanics Analysis Protocol

T:\Protocols\Mechanics

1. Open MATLAB.
2. Set working directory or set a path to:
   \\maxine\software cooker-freezer\SLRP\Cooker\v1.0.1_Matlab M files combined
3. Type into the command line: csv2txt;
4. Select the Instron .csv file. The program will create a new file in the same location with the same name but with .txt after. To streamline the process, you can type the same command for as many specimens as you have and run them all in a row.
5. Next, we'll analyze the mechanics. Type into the command line: LoadAndFitSine_KAR;
6. Navigate to the instron file for the specimen, which should be a '_csv.txt' extension.
7. **Dialog Box:** Input the proper vector of block numbers and frequencies for this protocol. For Mouse PT (SLRP2), the block numbers and the frequency vectors are to the right. Also input the seconds to subtract from position time stamp, which is 0.002.
8. **Dialog Box:** Enter the starting cycle and ending cycle. As default, this is 1 and 10.
9. The program will then run the mechanical evaluation for all frequencies and strain levels (should be 27 for this protocol). The images should look like this:

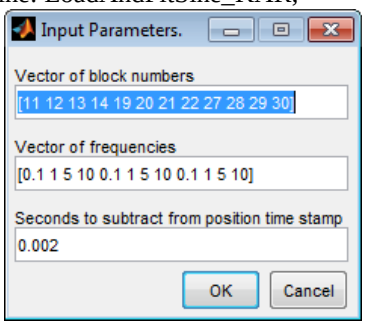

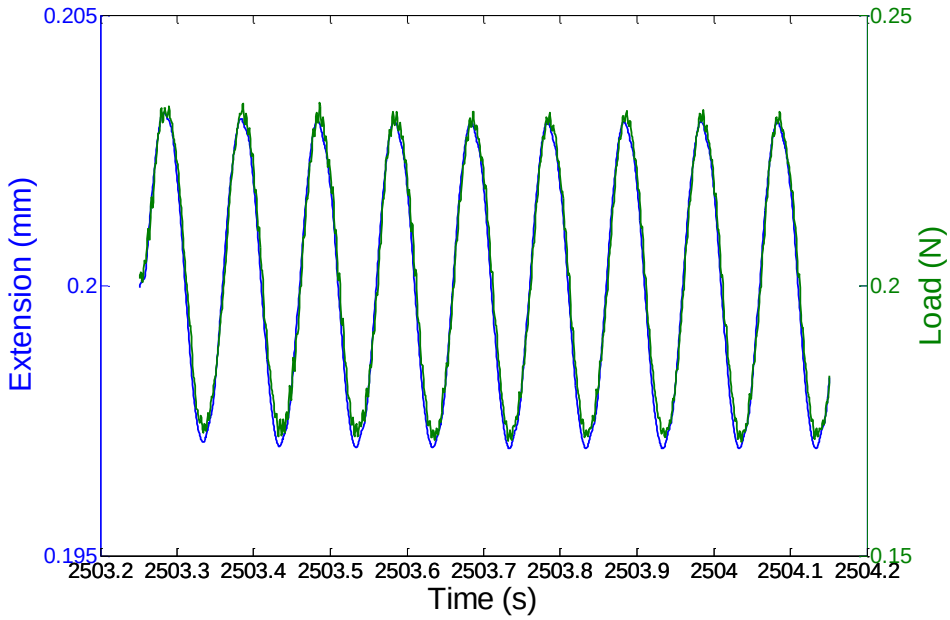

10. Copying and pasting these graphs into excel is inconvenient, but, again, very helpful when it's time to eliminate outliers.
11. Copy and paste the data from the MATLAB into the viscoelastic tab of the spreadsheet.

Abaqus Modeling Protocol

T:\Protocols\Modeling
Ben Freedman

I. Sync Abaqus with Visual Studio and Fortran Compiler

II. Setting up a simple model
   a. Map Workstation 3 to BRF thesis folder on maxine
   b. Open Abaqus CAE
   c. Start Session
      i. Create Model Database
         1. With Standard/Explicit Model
   d. Click "Create Part"

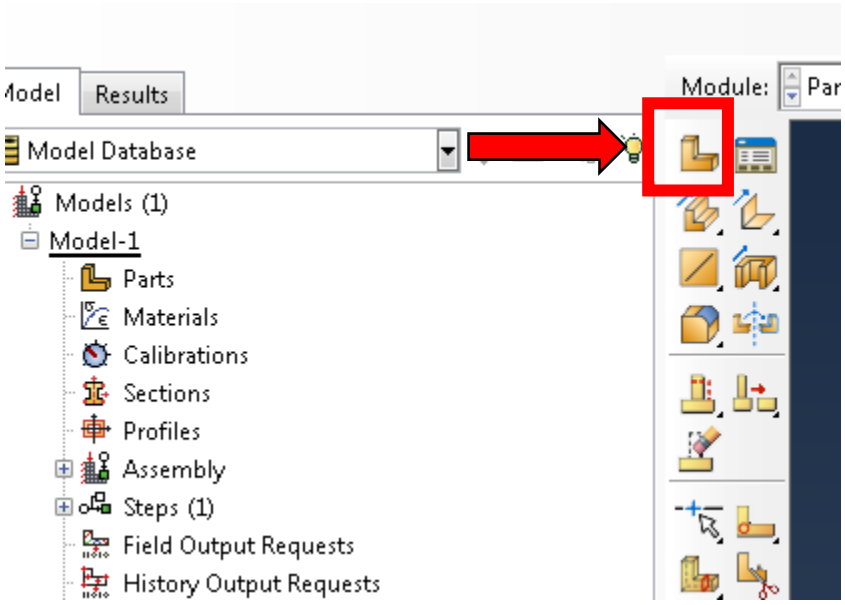

      i. Name the part (eg Matrix)
         1. Settings
            a. Modeling space: 3D
            b. Type: Deformable
            c. Shape: Solid
            d. Type: Extrusion
            e. Approx size: 200
      ii. Click Continue

Protein Extraction Protocol

T:\Protocols\Protein

Carrie Barnum (modified by Ben Freedman 2016-09-22)

Protein Isolation Solution: Made 20mL (500uL/Eppendorf)

1. 7 M Urea
2. 2 M Thiourea
3. 75 mM NaCl
4. 50 mM Tris-HCl pH 8.3

*Protease inhibitor → in 4º refrig in Rm 412
*Pestles- SAMPLE PESTLE WITH TUBE, RNASE, DNASE FREE, 1.5ML, 50/PKG 199226
Clean all tools with methanol and dry before beginning.

Make sure bench is clean

1. Measure out buffer (ie protein isolation solution), usually for using 500uL.
2. Add protease inhibitor which is 100X (for 300uL of solution, add 3uL of protease inhibitor)
3. Transfer buffer with phosphate (ie protease) inhibitor to eppendorf with sample.
4. Use tools such as scissors to cut sample into pieces while sample is on ice (regular ice) and in the buffer
5. After cutting tissue use plastic pestle to further homogenize the tissue
6. Once tissue is homogenized, sonicate in the cold room (or on ice if you cannot sonicate in cold room). Sonicate off and on for about 5-10 minutes by sonicating for only around 5-10 seconds with a 5-10 second break. **Remember that DNA is sticky so you must homogenize until the DNA becomes disrupted, you will know that the DNA is lysed when the solution becomes less viscous <<in 5th Floor Stemmler or Smilow>>
    a. Remember to clean off tip of sonicator w/ DI H_2O and Kimwipe
7. Spin cold (at least at 14000 rpm or MAX speed) for a half hour (in cold room)<<in Smilow or Dodge lab>>
8. Once the lysate is finished spinning, collect the supernatant and run the Bradford assay in order to get the concentration.

In chemicals area:
Urea molar mass: 60.06g/mol
Fisher Chemical Part Number U15500 Cost $27.90 for 500g
Thiourea molar mass 76.12g/mol
Fisher Chemical Catalog Number: 138915000 Cost $35.70 for 500g
NaCl molar mass 58.44g/mol
Fisher Chemical Catalog Number: S640500 Cost $30.38 for 500g

At lab bench
Tris-HCl (ordered at 1M)
Teknova Inc. Catalog Number T1083 $52.39 for 1000mL
**Physically hand specimens to Dr. Cao or leave in -20 freezer; send Dr. Cao labeling info and date of isolation

Using the MP/Confocal in CRB Genetics

T:\Protocols\SHG

Edited by: Ben Freedman (2017-01-23)

Background from Carrie at UDel here; T:\Protocols\SHG\Background\From U Delaware

Scope Details: Sequential scans on an upright laser-scanning multiphoton confocal microscope (Leica TCS SP8; Wetzlar Germany; 1024x1024 pixel resolution, fov: 277µm x 277µm, scan speed: 400Hz) were completed to evaluate stains for denatured collagen, collagen, F-actin, and nuclei in tendon sections. Denatured collagen and nuclei fluorescence were captured simultaneously with excitation using 488nm and 638nm wavelength lasers, followed by F-actin with a 552nm wavelength laser (all with PMT detectors). Second harmonic generation (SHG) imaging was achieved a Coherent Chameleon Vision II Ti:Sapphire laser tuned to 880nm. For all imaging, a 40x oil immersion objective (HC PL APO 40x/1.30 oil CS2) was used for focusing the excitation beam on slides mounted on the stage with the longitudinal axis of the tendon aligned with the horizontal axis of the visual field. Transmitted and reflected SHG signals were collected using 440/20 emission filters on PMT NDD and PMT-RLD detectors. Z-stacks were taken at 1.5µm intervals to capture the tendon midsubstance or injury site. Images from 2-3 tendon sections were taken per specimen.

SETUP:

1. Unplug TLD cables and plug in SHG TLD so we detect the forward scatter.

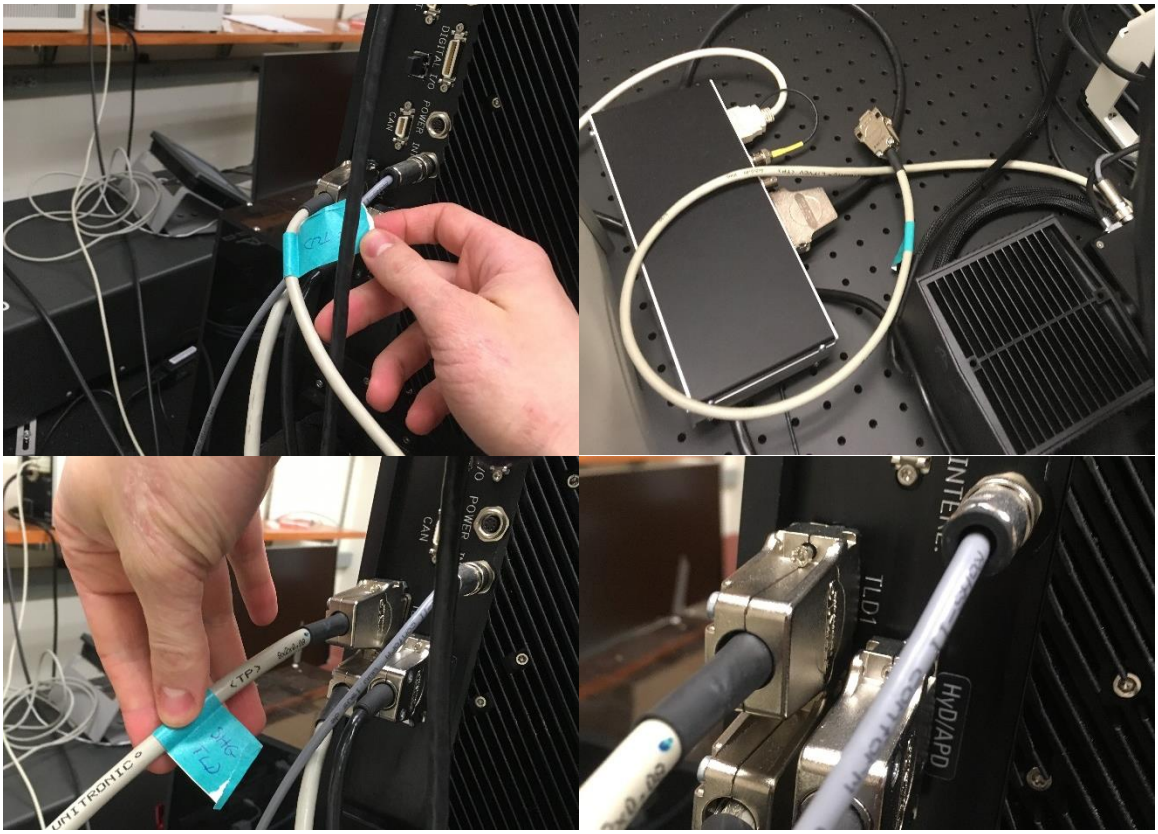

Figure 1: (**Top**) Unplug (**Right**) Plug in cable for forward scatter.

2. Turn on Box 1 and Box 2, turn key on MP laser (standby→ON), turn on powerstrip

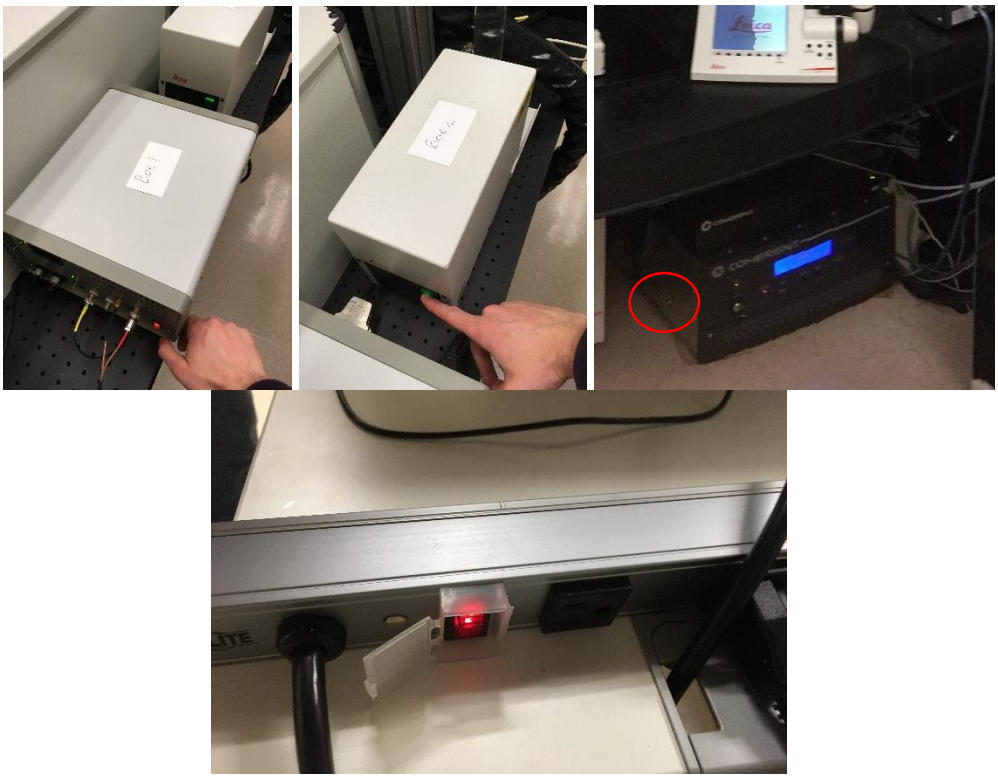

Figure 2: (**Top Left**) Turn on Box 1 + 2, (**Top Right**) Turn key to ON, and (**Bottom**) Turn on PowerStrip.

3. Put black box on for SHG imaging. Andrea will instruct you on how to do this.

Figure 3: (**Left**) Black box off (**Right**) Black box on

4. Move condenser into correct positioning for forward scatter and push the knob to the left to direct light through it. There is a knob on the underside that you can turn. Note that it is hidden under the stage in the image on the left, but is in the bottom right.

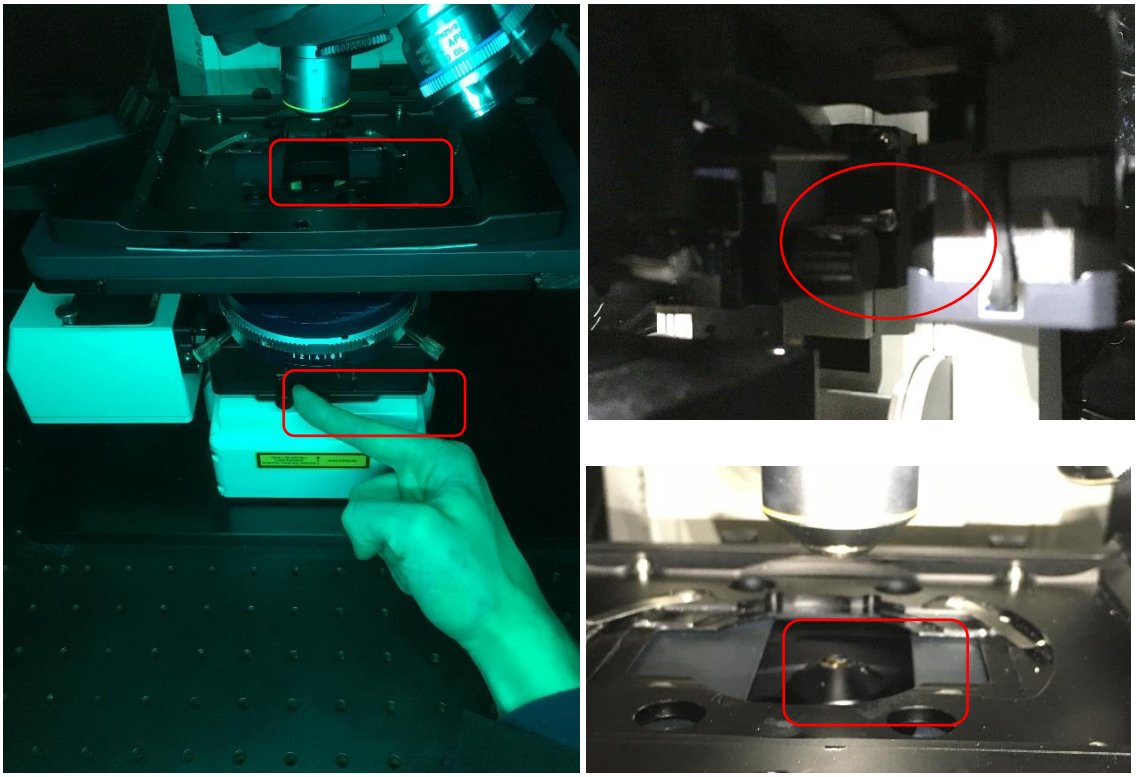

Figure 4: (**Left**) Push knob to left to activate condenser light path. (**Right**) Turn knob to raise/lower condenser until it is all the way up.

5. Operate the control panel. Not shown are the focus (fine/coarse) and x-y stage controls. These take some practice in getting used to. There are several buttons to push. Note, if you push "Focus", the objective is brought to the "0" position. This can make it much faster to adjust lens position.

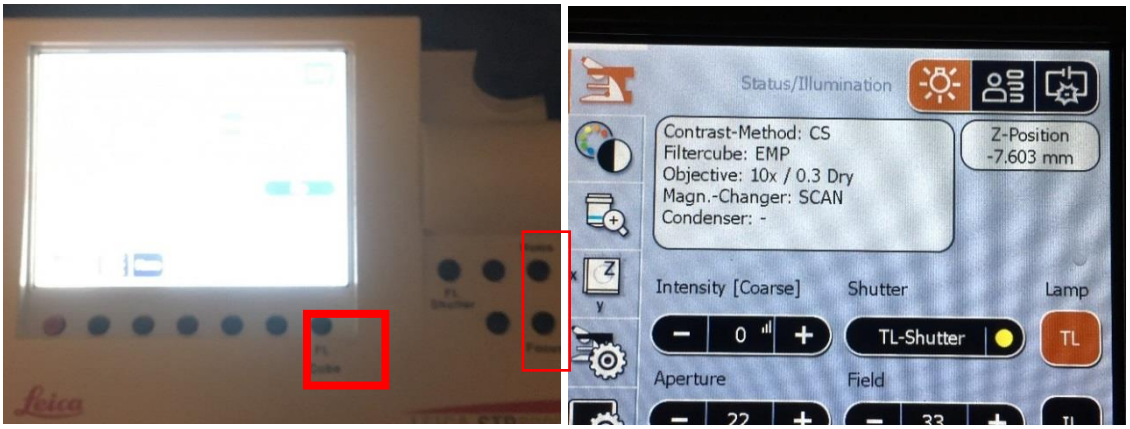

Figure 5: (**Left**) Raise/lower lens. (**Right**) Microscope panel. Can adjust shutter of brightfield by pressing TL-Shutter. Intensity can also be adjusted in the "intensity" module.

6. In the light module, you can select if you want to view a bright field image (BF) or fluorescence. The shutter is opened through "TL-Shutter". You can adjust the fluoro filtercubes by touching "UV", "GFP", or "RFP".

In the objective module, you can select the objective of interest. Note, that the 40x, 63x, and 20x are oil immersion. To switch, push the desired magnification once (objective will raise), then push again to switch (objective will lower to same position). For new users, it is best and safest to move the objective to the max height from the stage before switching.

Figure 6: (**Left**) Light module. (**Right**) Objective module.

7. The height of the objective from your sample is viewed here. You can set the home and zero position. Best to not adjust the home position, but only the zero if necessary.

   The instrument panel contains many adjustments including gain, offset, rotation, pinhole, zoom, and z-position.

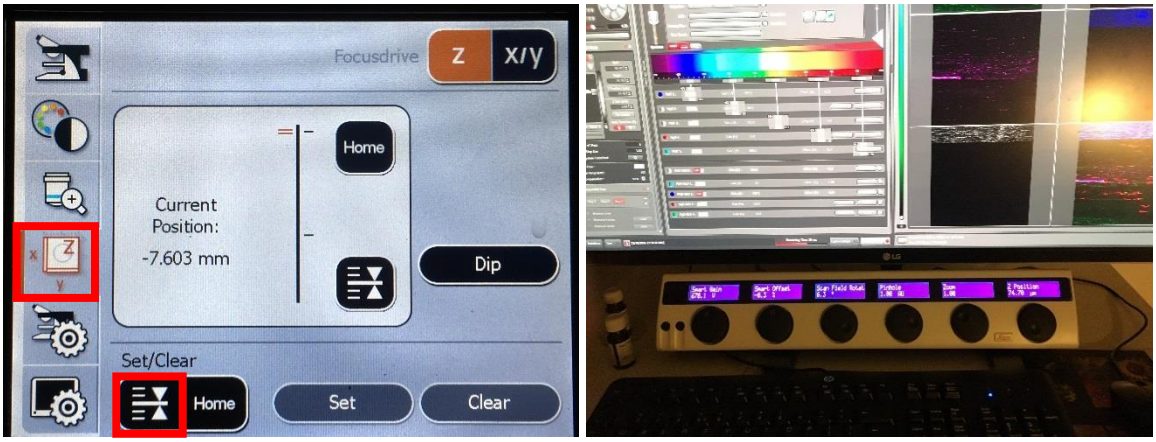

Figure 7: (**Left**) Z-position. (**Right**) Instrument panel.

8. **Start the Software** (Click "LAS X" on the Desktop)
   a. Select machine_MP_Laser_ON_SP.xlhw (for MP imaging including SHG)

b. In the main screen, first open your sequence file. If you don't have one, make one with Andrea Stout. Click "Seq" to make the sequential scan panel appear, then click load and select your sequence. Leica will ask you to turn on certain lasers.

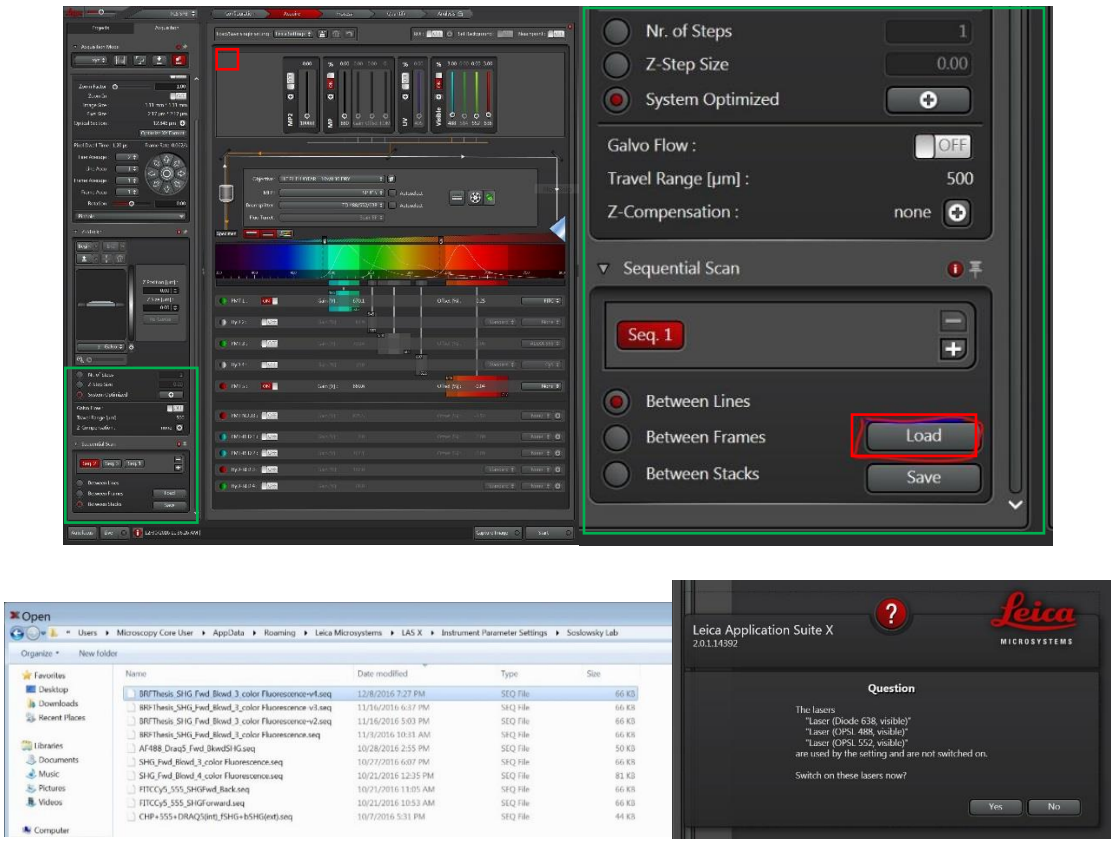

Figure 8: Loading a sequential file.

9. To **open** the **MP laser shutter**, first click the "+" button in the MP area (green box).
    a. Then, **click and <u>hold</u>** the MP shutter button until the dot becomes red. You will hear a "click" sound and it will say "pulsing"

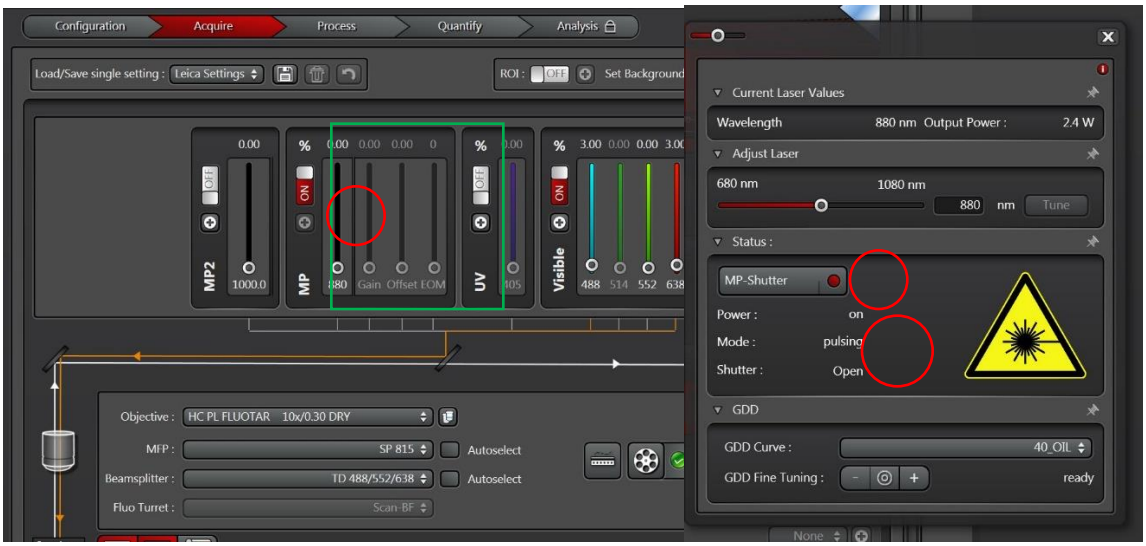

Figure 9: (**Left**) Open MP laser shutter settings. (**Right**) Open the shutter.

10. Under **acquisition mode**, set
    a. Image Format: 1024x1024
    b. Speed: 400Hz
    c. Bidirectional X: ON

*For higher-res images, you can click "optimize XY format", but note that this will increase imaging time.

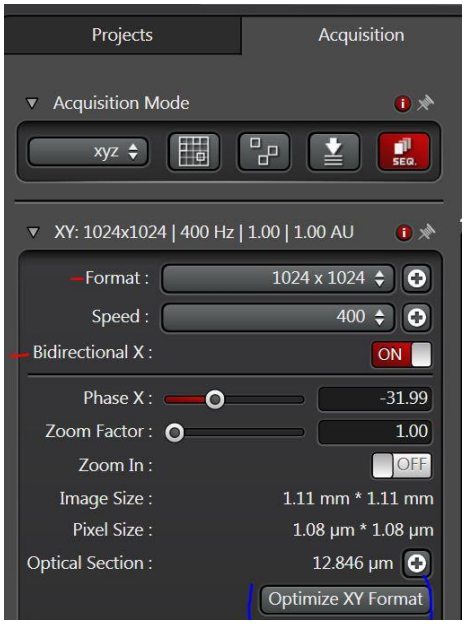

Figure 10: Set acquisition properties.

TAKE IMAGES!

1. Click "**LIVE**" to view a live image for a particular sequence.
    a. To image a sequence completely, click "**Start**"

    b. To image a Z-stack, first click "**LIVE**", then find the top/bottom of the stack and set the limits accordingly. Then click "**Start**" to image the full sequence + Z. If you are not stitching together panels, set this to "between stacks" rather than "between frames"
        i. Set step size to be 1.5um

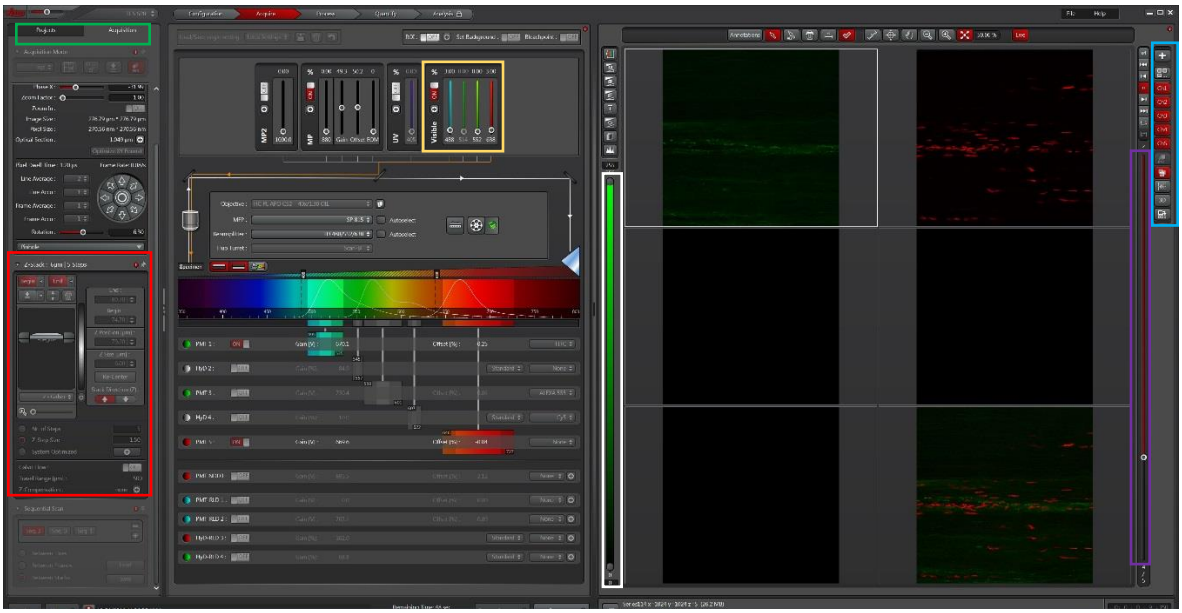

Figure 11: Additional operations. (**Red**) Set Z-stack. (**White**) Set LUTs (**Purple**) Set Z-position to view (after imaging a Z-stack) (**Yellow**) Set/view active lasers for a sequence. These can also be adjusted as needed. (**Green**) Acquisition/Projects tab.

    c. To name an image after you take it, go to the "projects" tab and relabel it. Press "F2" as a hotkey to adjust labeling.
        i. Note, the new project name should be set as "project" to avoid random labeling to persist.

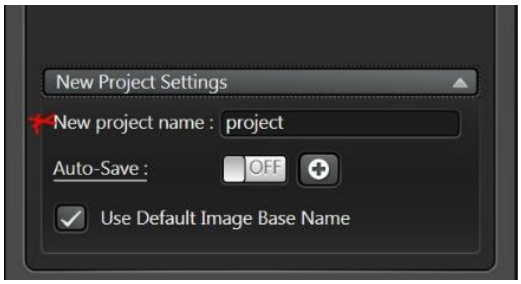

2. To save, in the "Projects" tab, click the disk and locate the folder with which you want to save. Recommend backing up images on an external hard drive. Export from .lif to .tif can easily be done in FIJI. I have MACROs developed that can do this.

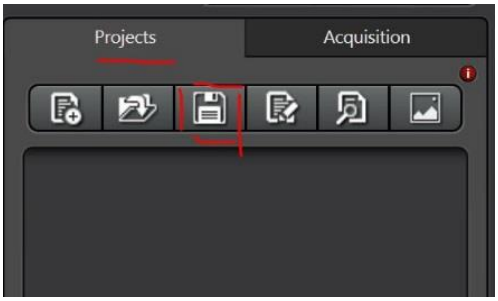

CLEAN-UP:

1. Remove slide

2. Wipe oil immersion lens with lens paper

3. Make sure .lif image file is saved and backed-up on external HD.

4. Click "X" in top corner to close.
    a. Click "Yes" to turn the Chamaeleon laser to standby.

5. Importantly, you must now shut the system down in the reverse order it was turned on (Shut down computer → Turn off power strip → MP laser key (to standby) → box 2 + 1 off → switch TLD cables back)

6. Remove the Black box, lower the condenser, make sure area is clean.

7. Fill out time sheet and note any problems, laser used, objective used.

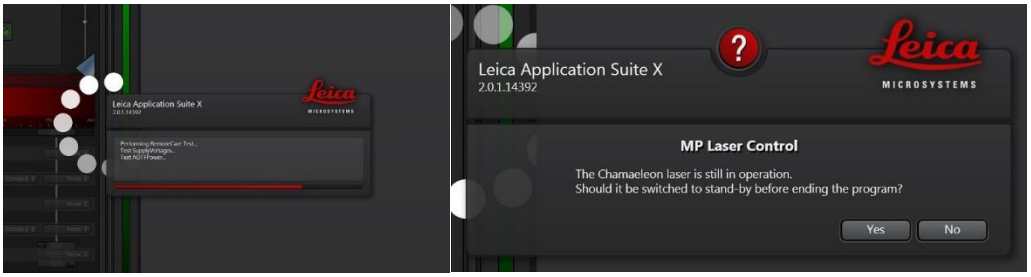

Figure 13: Shutdown

SHG fiber alignment analysis Protocol

T:\Protocols\SHG
Updated: 2017- 01-13
Author: Ashley Rodriguez

I. Open up MATLAB (compatible with 2012a-2015a)
II. Set current folder to X:\software cooker-freezer\SHG_Align\Cooker\SHG_align
    a. X: is \maxine
III. Type "close all; clear all; clc; FFT_align_msk" into the Command Window
IV. ***Modal Dialogue Box***: Navigate to where your images are located. Choose first image
    a. Cropped folder for uninjured specimens (e.g. T:\TIFF_Export\QuasiStatic\c150_**0**0XXL-1\Cropped1)
        i. T: is Ben's thesis folder
    b. Max (maximum projection) folder for injured specimens (e.g. T:\TIFF_Export\QuasiStatic\c150_**2**0XXL_s1\Max1)

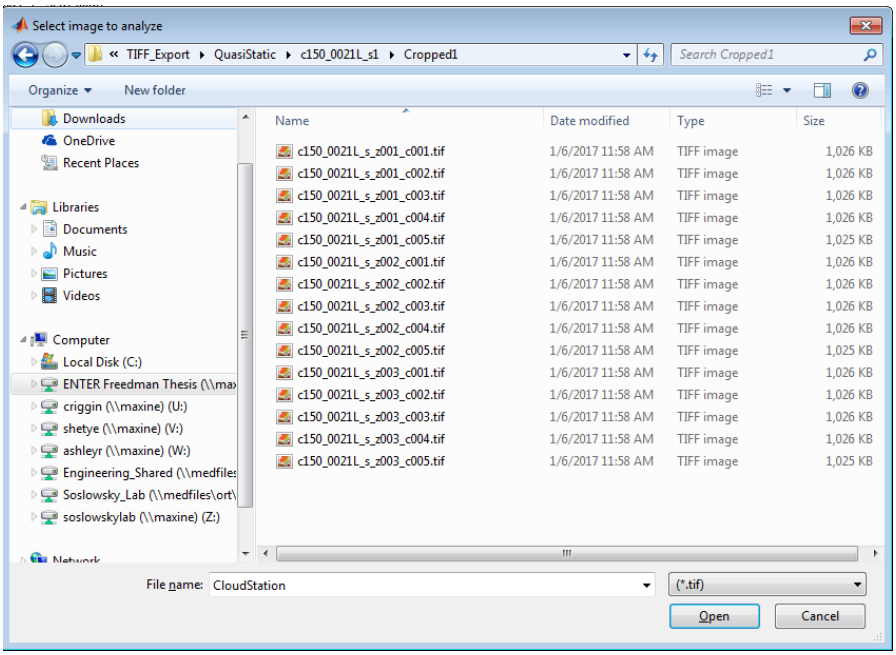

V. ***List Dialogue:*** Select the images you wish to analyze.
    a. Choose all *c005.tif for uninjured specimens (from the cropped images folder)
    b. Choose *0004.tif for injured specimens (from the maximum projection folder)
VI. ***Dialogue Box:*** "Do you need to create a mask?"
    a. Click "That sounds great"

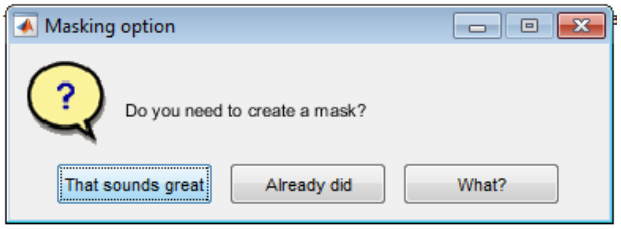

VII. ***Dialogue Box:*** "Sharpen and enhance all images?"

a. Click "Yes" for uninjured specimens. These samples have not been contrasted and enhanced yet.

b. Click "No" for injured specimens. These samples have been contrasted and enhanced.

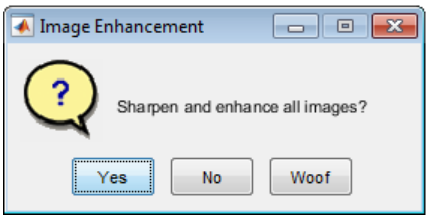

VIII. ***Dialogue Box:*** "Enter Bundle Width and height"

a. Enter 15 for width and 15 for height

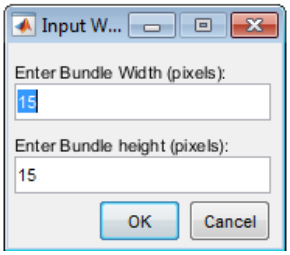

IX. ***Dialogue Box:*** "Would you like to save figures?"

a. Click "Yes". Histogram and quiver plots will save to the same output file location you choose in the following step.

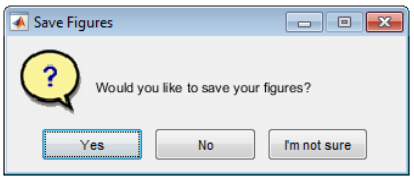

X. ***Modal Dialog Box:*** "Choose Collagen Fiber Organization Output File"

a. Within the specimen's folder, create a new folder called "SHG_mask" to save all output files to

b. Click "Save" (No need to change the name of the output file)

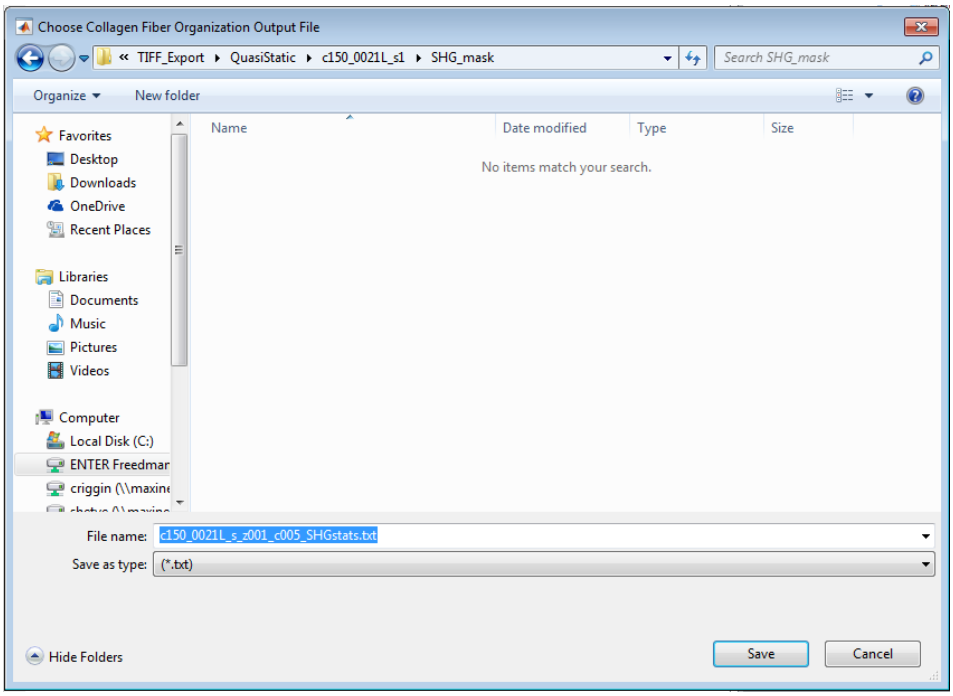

XI. ***Dialogue Box:*** "Draw border around the ROI"

a. The image has already been previously cropped in FIJI using the macro, "editsaveTiff.IGN. The image in this program needs to be outlined for the processing to work properly.

b. Draw along the edges of the ROI and double click once as you connect the last vertices

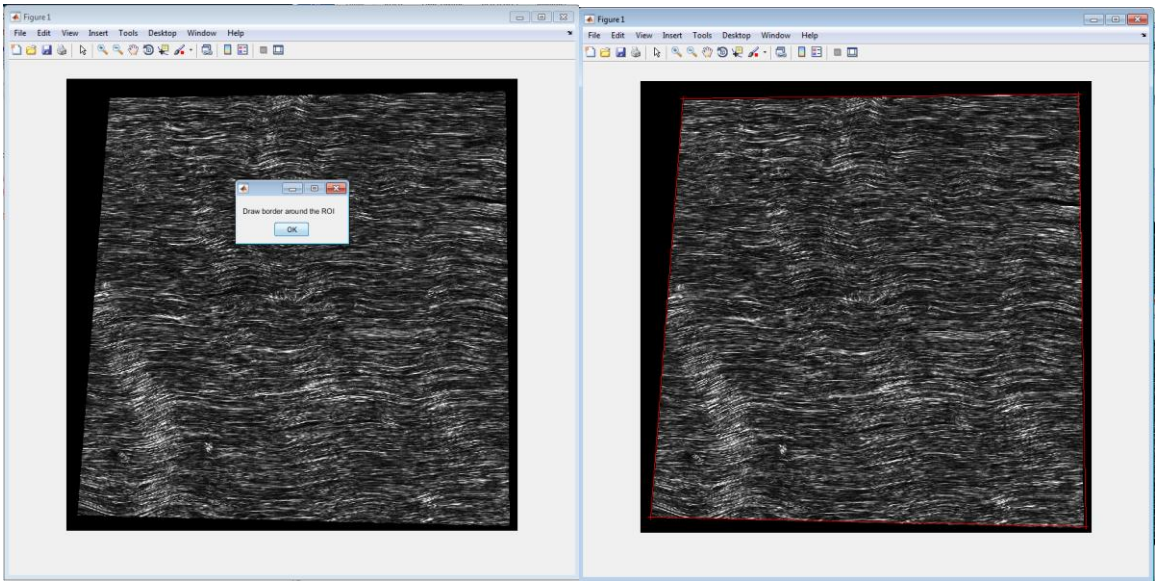

XII. MATLAB will process and output figures should pop up

a. The first time running the program will take longer to process to begin the parallel loop. After running the first time, the program will run very quickly.
b. ***Quiver plots***: Displays the quiver for angular orientation of the fibers overlaid on the SHG image. The green arrows indicate healthy fibers. Red arrows indicate damaged fibers, determined by adjacent fiber angles greater than 30° or eccentricity between 0 and .90.
c. ***Angular histogram fit***: plots all angles in a histogram with a distr. fit

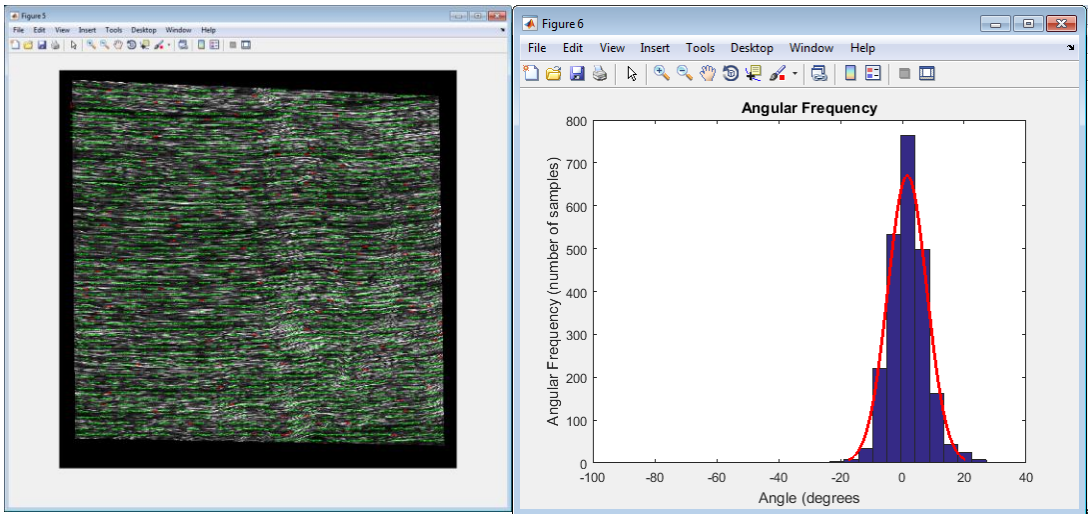

d. The histogram and quiver plots are saved to the output file location

XIII. Copy and paste the output from the Command Window to an excel file. The program will save all output .txt's to the folder you previously navigated for output files.

a. Command Window
b. **_SHGstats.txt* – saves the circular statistics for all images that were processed
c. **_SHGangles.txt* – saves all calculated angles with their respective position in the image
d. **_SHGmask.txt* – saves the coordinates of the vertices of the mask that was draw over the ROI.

XIV. Repeat for all specimen.

Protocol: **Phalloidin + Draq5 + CHP for Mouse Patellar Tendon- Version 1 (EDITED: 2016-12-12)**

T:\Protocols\Staining\Cell\Actin and Nuclei
Author: Ben Freedman

- Part of this protocol was adapted from Sarah Rooney Laminin/Dapi methods.
  - X:\SIR Thesis\Protocols\Histology

Reagents + Supplies:

Name	Location in Lab	Purpose
BSA	401 Refrig	Blocking
Triton	401 shelf	Blocking
1x sterile PBS	401 Shelf	Wash steps
Phalloidin **Alexa Fluor 555 Phalloidin (A34055)**	-20º Freezer	Stain for F-Actin
Draq5 **DRAQ5 Fluorescent Probe Solution (5 mM) (62254)**	4º Refrig	Stain for Nuclei
Coverslips	Bioassay supplies	Protect tissue
Black immunoassay boxes	Pankti's bench	Darkness and holding slides
ProLong Gold Antifade without DAPI	Bioassay supplies	Mount/adhesive for coverslip
Kimwipes	Supply closet	Dry slide + maintain box humidity so slides do not dry out
Nail Polish	Bioassay supplies	Seal coverslip to slide edges
1.5 mL Eppendorf tubes	Bioassay supplies	Make 5% BSA/triton; Mix Phalloidin + Draq5 with BSA
Methanol	Fire cabinet	Add 1.5mL to Phalloidin powder initially

Phalloidin, DRAQ5, CHP Protocol:

1. Circle each section with a PAP pen (and sharpie underneath slide)

2. Wash twice with 1x PBS

3. Block with 5% BSA in PBS and 0.1% triton for 1 h at room temperature in a humidity chamber at 4ºC
    a. To make 5% BSA, first make 10% BSA (dissolve 1g BSA in 10ml of 1xPBS)
        i. To make 1000ul, add 500ul of the 10%BSA to 499ul PBS and 1uL triton (very viscous, make 100x → 10x (100ul))
        ii. Make a few eppendorfs worth (initial incubation, primary antibodies)
    b. (wet KimWipes and place them in the black immunoassay slide box)

4. Use a vacuum system to remove excess vehicle solution from sections.

5. Incubate with primary antibody solution for 12 hour at 4ºC in dark box (if new, add in 1.5mL of methanol) (**20ul/ section**)
    a. 1x PBS (1000 ul total)
        i. 1000ul – 50ul – 1ul– 100ul = 849 ul

    b. 1:10 CHP (1000ul total)
        i. 100ul CHP
            1. **Prior to using, add CHP to PBS and heat at 80ºC for 5 min. Then place tube directly into ice water to cool.

    c. 1:20 Phalloidin (1000ul total)
        i. 50ul phalloidin

    d. 1:1000 DRAQ5 (1000ul total)
        i. 1ul DRAQ5

6. Wash 3 times 5 minutes each with PBS; then 1 wash with molecular water

7. Mount coverslips on slides with ProLong Gold Antifade without DAPI. Avoid air bubbles.

8. Let sit in 4ºC overnight prior to step #10

9. Seal edges of coverslip with clear nail polish. Store at 4ºC in a dark slide box.

Example calculation:
-Want 50uL per section; for 8 sections, need 400uL

- To make 1200uL containing 5% BSA and 0.1% triton,
----we started with 10% BSA. So, to make 1200uL, add 600uL BSA to 558.8uL PBS (remove 1.2uL)

----Add 1.2uL Triton (0.001x1200uL)

- When adding in Phalloidin/DRAQ5 mixture for dilutions above; we made 1000uL total. Hence, for the ratios of 1:500 and 1:1000, we get the necessary amounts above.

MTT Experimental Protocol-----Ben Freedman----2016-01-21

T:\Protocols\Staining\Cell\MTT

Updated: 2016-03-12

https://www.thermofisher.com/us/en/home/references/protocols/cell-culture/mtt-assay-protocol/vybrant-mtt-cell-proliferation-assay-kit.html

---

Vybrant® MTT Cell Proliferation Assay Kit

Actual protocol:

1. Prepare a 12mM MTT stock solution that can last up to 4 weeks at 4ºC.
    a. Get 12mM by adding 1mL of sterile PBS to a 5mg vial of MTT.
    b. Note, the MTT should be made under sterile conditions in the TC hood to keep the reagent sterile. The stock can also be stored at -20ºC to last longer.
2. For labeling viable cells, add 100uL of stock solution to 1000uL of DMEM. Keep the mixture at 37ºC before dissection.
3. After dissection, leave eppendrof tubes open in incubator (to ensure proper CO2 and pH levels)
4. Transfer to PBS for 30 min at room temp
5. Then fix with 4%PFA at 4ºC overnight
6. Rinse in PBS, then freeze + section+rinse again

Mouse Patellar Tendon Surgery Protocol

T:\Protocols\Surgery

Supplies

- Sterile drape
- Sterile surgical instrument pack
- 2x 0.75mm punch biopsies per mouse (1 per leg)
- 5-0 Prolene suture
- Fine dissection pickups and large needle driver
- Plastic coated scalpel for backing each punch

Procedure:

1. In preparation for the surgical procedure, mice are anesthetized with a mixture of isoflurane (2-5%) and oxygen, and both hind limbs are shaved and cleaned with alcohol and betadine. Animals will be placed on a sterile surgical table with a water circulating warming blanket under the drape.
2. Anesthesia is maintained via nose cone at the level of 1-2% isoflurane to ensure the proper surgical plane of anesthesia.
3. Mouse is placed is a supine position with the knee flexed
4. Place a midline incision (cheat medially) over the knee joint through the skin. Following the skin incision, two cuts parallel to the tendon are made in the retinaculum on each side.
5. Use fine dissection pickups to lift the patellar tendon off the knee and place a plastic coated blade underneath the patellar tendon.
6. With the coated blade serving as support, a 0.75mm diameter biopsy punch is used to create a full thickness partial width transection in the patellar tendon.
7. The skin wound is closed with 5-0 prolene suture
8. Repeat on other leg if bilateral surgery is required.
9. The mouse is recovered under a heat lamp in a cage with apha-dri bedding and allowed to resume normal activity.